FTD-MT- 64-15

TRANSLATION

NONFERROUS METALLURGY

COPY 1 OF 1	cat
HARD COPY	$. 6.00
MICROFICHE	$. 1.25

FOREIGN TECHNOLOGY DIVISION

AIR FORCE SYSTEMS COMMAND

WRIGHT-PATTERSON AIR FORCE BASE

OHIO

FOREWORD

This document is a machine translation of Russian text which has been processed by the AN/GSQ-16(XW-2) Machine Translator, owned and operated by the United States Air Force. The machine output has been fully post-edited. Ambiguity of meaning, words missing from the machine's dictionary, and words out of the context of meaning have been corrected. The sentence word order has been rearranged for readability due to the fact that Russian sentence structure does not follow the English subject-verb-predicate sentence structure. The fact of translation does not guarantee editorial accuracy, nor does it indicate USAF approval or disapproval of the material translated.

EDITED MACHINE TRANSLATION

NONFERROUS METALLURGY

English Pages: 205

S/0149-063-000-004

PREPARED BY:

TRANSLATION DIVISION
FOREIGN TECHNOLOGY DIVISION
WP-AFB, OHIO.

Ministerstvo
Vysshego i Srednego Spetsial'nogo
Obrazovaniya SSSR

Izvestiya
Vysshikh Uchebnykh Zavedeniy

TSVETNAYA METALLURGIYA

4

1963
6-y god izdaniya

Izdaniye Severokavkazskogo
Gornometallurgicheskogo Instituta
g. Ordzhonikidze

Pages 1-151

NON-FERROUS METALLURGY

USSR

/Following is the translation cover-to-cover of the Russian-language publication Izvestiya vysshikh uchebnykh zavedeniy -- Tsvetnaya metallurgiya (News of the Higher Educational Institutions -- Non-Ferrous Metallurgy), No 4, 1963, Ordzhonikidze, pages 1-151./

CONTENTS

Metallurgy

Metals and Metal Working

Reviews and Bibliography

EFFECT OF FORM OF SHOT BIT MAGAZINE ON DRILLING RATE

M. A. Chorikashvili

(North Caucasus Mining and Metallurgical Institute,
Faculty of Special Lecture Courses on Mining.)

In shot drilling one of the factors influencing the drilling rate is the form of the bit magazine supplying shot to the face. There is as yet no common viewpoint as to what should be the form of the shot bit magazine and how this form depends on the drilling and operating conditions.

The most diverse forms of shot bit magazines exist. In practice square-edged and the triangular types are used, being the simpler, although they are not the most profitable.

In the process of drilling the bit magazine fulfills the role of feeder, i.e., assures the striking of the shot on the working face of the bit. In addition, a large portion of the washing liquid entering the columnar annular space passes through the magazine. Increase in magazine width establishes favorable conditions for retention of the shot between the bit face and the rock face due to decreased effect on the shot on the outgoing stream of washing liquid, and, at relatively low revolutions per minute of the drilling shell, leads to a reduction in the drilling rate due to the decreased working area of the bit face. Therefore, the magazine should be of such a shape which would permit the most intensive entrance of the shot under the bit face, and its dimensions would assure stability in performance and a maximum drilling rate.

It is also necessary to take into account that with increasing performance the body of the bit wears out as to height, but the magazine changes its own form and size. This last fact adversely affects drilling productivity. Thus, for instance, as wear increases in the bit with a triangular magazine its working area (its face) is increased, and the specific pressure decreased.

To sustain the required specific pressure it is necessary gradually in the course of drilling to increase the axial force on the rock face. However, the adjustment of specific pressure with specific accuracy is difficult to achieve, since a frequent change of load adversely affects the drilling rate. Accordingly, the triangular form of the magazine, which had been recommended by S. A. Volkov, V. M. Soltysh /1,2/ and other investigators has lately been increasingly replaced by the square-edged magazine. Such a magazine has both a parallel axis (straight arm) as well as an axis inclined to the bit axis.

N. I. Blinov /3/ has suggested a right-angled magazine positioned parallel to the axis of the bit, 150-200 mm in height, and with a width equal to 1/4 - 1/8 of the length of the circumference. He however has noted that at the identical specific pressure and peripheral velocity an increase in the magazine width produces a slowdown in drilling rate. However, he does not present the magazine width as definite functions of the drilling parameters in his studies.

In a manual /4/ it is recommended that the shot bits with an arc-shaped magazine of constant cross section be used, suggested by A. N. Kirsanov /5/. In the same source (Table 201, page 332) are offered specific peripheral velocities of shot bit rotation depending on the category of the ores being drilled. And in addition, the peripheral rates of bit rotation appear to decrease with increase in ore category.

The width of the magazine is selected as constant and equal to 1/4 - 1/5 of the length of the external bit circumference. At the same time, as results of experimental studies of many investigators have shown (I. A. Ostroushko, L. A. Shreyner, S. A. Volkov, V. M. Soltysh, A. N. Kirsanov, etc.) the drilling rate increases with increase in the revolutions per minute of the boring shell, and consequently also with increase in peripheral velocity. A greater working area of the shot bit face also entails increase in drilling rate. If this is so, then the width of the shot bit magazine in our opinion depends on the peripheral velocity of rotation.

When deep geological survey holes are drilled, when the durability of the boring instrument does not permit high rates of rotation of the boring shell, in practice it is usual to use standard shot bits with wide magazines that lowers the drilling rate significantly.

I. A. Ostroushko correctly points out that when a steady feed shot is supplied to the internal annular space of the bit it is possible to successfully drill even without a magazine /6/.

Since the selection of the optimal forms and dimensions, depending on the operating conditions, is of significant practical and theoretical interest, during 1961-1962 a series of experiments

was conducted on the boring stand of the North Caucasus Mining and Metallurgical Institute using bits of various forms and magazine sizes. During the course of experiments in drilling into ores of category IX bits with triangular, trapezoidal, and right-angled (parallel to the axis) magazines were used, and a right-angled incline (at various angles to the face) magazines as well.

During the laboratory experiments the specific pressure for all the bits was held constant (35 kg/cm^2). The magazine width during comparative tests varied and was equal to 1/3, 1/4, 1/5, 1/6 and 1/8 of the circumference. All the bits had the same diameter, equal to 91 mm. Drilling was carried out using steel shot--chopped straw /sechka/ 3.5 mm in size.

Studies revealed that the best choice is the inclined magazine which has a constant right-angled cross section, providing good feeding of the shot at relatively high peripheral velocities of the bit rotation (Table 1). This phenomenon apparently is due to the fact that the slope of the incident side of the magazine favors direction of the shot to the face part of the bit.

Since the shot bit when functioning constantly changes its center of rotation, and its rotation rate is higher than the speed of the pellets along the circumference, the leading side of the magazine will capture the pellets.

When a direct-line magazine is used, the pellet colliding with the edge of the leading side of the magazine has a high probability of striking again in the radial clearance between the bit and the wall of the slit, while with an inclined magazine the pellet will head downward in the direction of the bit face, insuring the best supply of shot to the face as compared with the direct-line magazine. In drilling it is necessary that the shot be always on the face of the well. This condition is observed for limited washing (with a feed rate up to 1.0 m per one cm of the bit diameter) and low peripheral velocities of shot bit rotation < 0.6 m/sec.

But to attain high passage rates drilling must be carried out under forced conditions, i.e., at high peripheral velocities of bit rotation, high specific pressure, and intensive washing. Under such conditions, the pellets between the bit and the wall are moved by centrifugal forces (in exiting from under the face) and with rotation of the washing liquid lagging somewhat from the bit.

It is logical to assume that the form of the magazine will be the most acceptable if it affords prolonged, at definite drilling conditions, residence of the shot in the magazine slits, i.e., during its fall the shot is found between its front and rear edges, but the trajectory of the fall of the shot does not have to cross the trajectories of all the points of the leading edge of the magazine. Thus, proceeding from these conditions it is possible to establish a relationship between the form of the magazine

Results of Laboratory Tests of Bits from Magazines of Several Shapes and Widths. Drilling Done on Rocks of Category IX with the ZIF-300 Rig at about 700 rpm. Water Rate = 20 li/min. Specific Pressure = 35 kg/cm^2.

Table 1

(a) Форма магазина	(b) Ширина магазина	(c) Скорость бурения (в *мм/мин*) при окружных скоростях, *м/сек*				(d) Износ коронок по высоте, *мм/пог. м*	(e) Возможная проходка в ремонтах при износе магазина по высоте от 110 до 10 *мм*, *м*
		0,38	0,68	0,89	1,8		
(f) Треугольный магазин	$\frac{1}{3}\pi D$	2,6	5,3	8,9	19,8	54,3	2,4
(g) То же	$\frac{1}{4}$ •	3,1	6,5	10,1	17,3	49,1	2,6
•	$\frac{1}{5}$ •	3,8	7,5	12,1	16,1	47,0	2,77
•	$\frac{1}{6}$ •	4,4	8,8	13,2	15,4	43,5	2,99
•	$\frac{1}{8}$ •	5,1	8,7	12,4	15,3	38,7	3,36
(h) Трапецеидный магазин	$\frac{1}{3}$ •	2,7	5,4	9	20,3	54,0	2,4
То же	$\frac{1}{4}$ •	3,2	6,5	10,4	18,2	48,5	2,68
•	$\frac{1}{5}$ •	3,8	7,6	12,3	16,8	47,3	2,75
•	$\frac{1}{6}$ •	4,4	8,7	13,6	15,7	44,2	2,94
•	$\frac{1}{8}$ •	5,2	8,4	12	15,3	39,0	3,34
(i) Прямоугольный магазин	$\frac{1}{3}$ •	2,7	5,2	8,7	18	53,0	2,83
То же	$\frac{1}{4}$ •	3,0	6,1	9,2	17	49,0	3,06
•	$\frac{1}{5}$ •	3,8	7,0	9,8	14,8	47,1	3,2
•	$\frac{1}{6}$ •	4,4	8,5	11,7	14,3	45,2	3,32
•	$\frac{1}{8}$ •	5,0	8,3	10,1	13,2	40,1	3,73
(j) Наклонный магазин	$\frac{1}{3}$ •	2,8	5,6	9,3	24,4	51	2,94
То же	$\frac{1}{4}$ •	3,2	6,8	10,2	22,7	44,6	3,36
•	$\frac{1}{5}$ •	3,9	7,9	12,9	20,6	44,1	3,4
•	$\frac{1}{6}$ •	4,4	8,8	14,1	18,5	42	3,57
•	$\frac{1}{8}$ •	5,2	8,5	13,2	17,1	38	3,95

Legend to Table 1: a) Form of magazine; b) Width of magazine; c) Drilling rate (in mm/min) at the peripheral velocities listed, m/sec; d) Wear of bit in height, mm/linear meter; e) Possible passage per run when magazine is worn in height from 160 to 10 mm, meters; f) Triangular magazine; g) As above; h) Trapezoidal magazine; i) Square-angled magazine; j) Inclined magazine.

and drilling conditions.

Let us consider the movement of pellets occurring in the bit magazine. The pellet is under the influence of several forces. Gravity causes the fall of the pellet at definite velocity, which can be determined by the Rittinger /7/ formula

$$U = K_f \sqrt{\frac{2(\gamma_1 - \gamma_2)}{\gamma_2 (\gamma_1 g \delta)}},$$

where U = rate of pellet drop, cm/sec;
K_f = coefficient of shot form;
δ = average diameter of shot, cm;
γ_1 = specific gravity of the shot material;
γ_2 = specific gravity of the washing liquid.

However, the ascending flow of the washing stream moves at the velocity

$$S = \frac{Q}{F},$$

where Q = pump productivity, cm^3/sec;
F = area of annular bit well walls.

Then, the dropping velocity of the shot decreases to the value C = U - S.

Under steady-state drilling conditions shot hitting the magazine will advance downward at a constant velocity.

The washing liquid in the bore hole due to the influence of the revolving bit, is given, simultaneously with a translational movement a movement along its circumference, and carries away the shot in the magazine at a peripheral velocity of w. The peripheral velocity of the shot will depend on the viscosity of the liquid, the kind of flow motion, the form of the shot, and the rotation rate of the bit itself. At certain operating conditions the peripheral velocity of the shot as an approximate function can be rep-

resented as follows:

$$w = K v_{\kappa}.$$
$$(b,r)$$

where K = variable coefficient taking the above factors into account ($K < 1$);

$v_к$ = peripheral velocity of bit rotation.

Based on the foregoing, the trajectory of shot motion in the magazine can be approximately represented as the inclined line AB (Fig 1) coinciding with the direction of the resultant velocity.

From Fig. 1 it is clear that the shot A when falling will be in the magazine only for the case in which any point of its trajectory does not emerge beyond the limits of the cut.

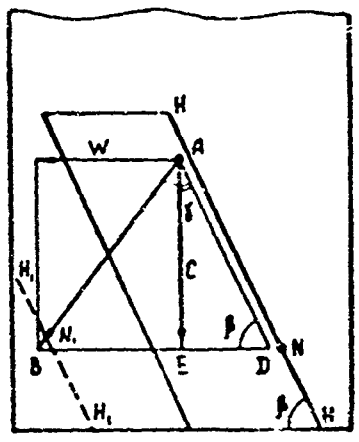

Fig. 1. Scheme of movement of shot in the bit magazine.

Let us consider the combined position of the shot A and the cuts of the magazine over a certain interval of time t. If for simplicity of calculation we take t = 1 sec, then the shot will appear at point P, after this interval of time. The leading edge of the magazine HH shifts to the position H_1H_1. To observe the condition of mutual movement of shot and cut (Fig. 1) it is necessary that the shift along the periphery of the point N of the leading edge of the magazine not exceed a certain value. In 1 second the point N moves to the point N_1 where $NN_1 = v_к$. In Fig. 1 NN_1 = BD. Then the condition for shot being always in the magazine

slots can be expressed mathematically by

$$BE + E\Pi \leq v_k; \tag{1}$$

but BC = w and from Δ AED ED = C · tg γ . After substitution of the corresponding values in equation (1) we have

$$w + C \cdot \operatorname{tg}\gamma = v_k,$$

and since w = Kv_k, Kv_k + C·tg γ = v_k. Hence $\operatorname{tg}\gamma = \frac{v_k(1-K)}{C}$.

The function derived allows us to see that the angle of inclination of the magazine slits to the bit axis is directly proportional to the peripheral velocity of rotation and inversely proportional to the falling velocity of the shot.

Thus, with increase in the number of revolutions per minute of the boring shell, the angle of inclination of the leading edge of the magazine should decrease, since $\gamma = 90 - \beta$, i.e., the angle β must be different for the various rotation rates, other conditions being equal.

For verification, a series of experiments were performed using bits with various angles of inclination (90°, 65°, and 45°) of the leading side of a magazine of right-angled cross section (Fig. 2). With increase in the number of revolutions per minute of the boring shell from 30 to 140 rpm, a signficant difference in the drilling rate for bits at various angles of inclination of the leading side of the magazine was not observed. And with further increase in the number of revolutions per minute in the drilling rate the difference in the drilling rates was clearly revealed. For bits with $\beta = 65^\circ$ an increase i the drilling rate was observed (at n = 378 rpm) as compared with bits with $\beta = 90^\circ$ amounting to 40%, and to 27% for bits with $\beta = 45^\circ$. Thus, the best suitable angle of inclination is 65°.

Since operations under laboratory conditions are close to those observed in practice, it is possible to recommend for practical use magazines with an angle of inclination of the incident edge to the face equal to 65°. Here, the optimal dimensions of the magazine width as a function of the peripheral velocity and the bit are as follows:

$0{,}4 - 0{,}6$ м/сек $\frac{1}{8}\pi D$;

$0{,}61 - 0{,}8$ м/сек $\frac{1}{6}\pi D$; $0{,}81 - 1{,}2$ м/сек $\frac{1}{5}\pi D$; $1{,}21 - 1{,}6$ м/сек $\frac{1}{4}\pi D$;

$1{,}6$ м/сек $\frac{1}{3}\pi D$.

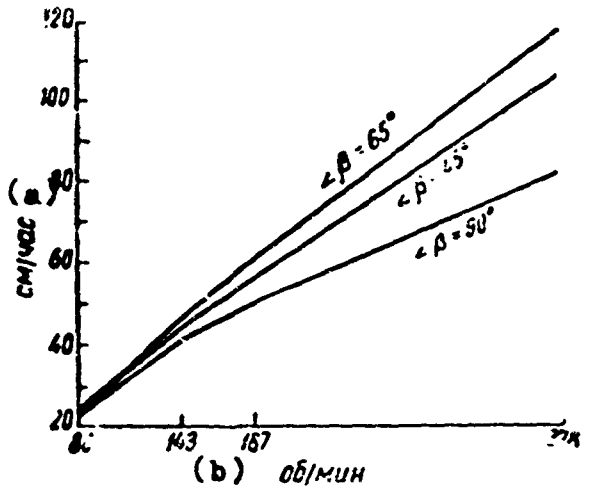

Figure 2. Mechanical drilling rate (in cm/hr) as a function of the rpm of the drilling shell (rpm) for different slopes β of the leading edge of the magazine. The bit diameter = 91 mm, magazine width = 0.2 π D.
LEGEND: a) cm/hr; b) rpm

The magazine dimensions suggested refer only to bits with a flat working face and an outer diameter equal to 91 mm.

The height of the magazine, in our opinion, must be chosen as related to the category of the ores being drilled. From the results of industrial tests (Table 2) it is clear how the bit wear with height increases and the passage per run decreases as a function of the category of ores drilled. Therefore, in drilling ores of category IX and higher shot bits with a magazine height of 200 mm should be used. Here the length of the run should be increased significantly. And when drilling ores of categories lower than IX a magazine height of 160 mm fully insures normal passage after the run.

The investigations conducted with bits of various magazine widths confirmed the relationship that with increase in working area of the face the drilling rate rises (Cf. Table 1). This effect, in our opinion, is explained by the fact that with decrease in magazine width the area of the face increases, i.e., and the number of simultaneously effective shot and duration of contact of the bit with the shot is increased.

TABLE 2

Results of production tests of bits for various forms of magazines.

(a) Форма магазина	(b) Время чистого бурения, *час*	(c) Проходка за рейс, *м*	(d) Механическая скорость бурения, *м/час*	(e) Износ коронки за рейс, *мм*	(f) Износ коронки по высоте, *мм/пог. м*	(g) Примечание
1	2	3	4	5	6	7
(l) **Породы VIII категории**						
(h) Треугольная	4,7	4,5	0,96	135	29	P = 550 *кг*, окружная скорость коронки 1,3 *м/сек*. Ширина магазина $\frac{1}{5}\pi D$, глубина скважины 190 *м*. Станок ЗИФ-650-А (o)
(i) Трапециевидная	4,3	4,4	1,02	118	27	
(j) Прямоугольная ‖ оси	4,5	3,6	0,81	73,4	20,4	
(k) Наклонная	4,25	4,9	1,16	92,2	18,9	
(m) **Породы IX категории**						
(h) Треугольная	5,76	2,48	0,13	129	52	p = 30 *кг/см*^{2}, окружная скорость коронки 0,61 *м/сек*. Ширина магазина $\frac{1}{6}\pi D$, глубина скважины 370 *м*. Станок ЗИФ-1200А (p)
(i) Трапециевидная	5,43	2,55	0,17	125	49	
(j) Прямоугольная ‖ оси	5,36	2,20	0,41	90	41	
(k) Наклонная	5,55	2,72	0,49	103,4	38	
(n) **Породы X категории**						
(h) Треугольная	5,64	0,76	0,135	74	98	p = 35 *кг/см*^{2}, окружная скорость вращения коронки 0,61 *м/сек*. Ширина магазина $\frac{1}{6}\pi D$, глубина скважины 440 *м*. Станок ЗИФ-1200А. (q)
(i) Трапециевидная	5,37	0,79	0,147	72,8	92	
(j) Прямоугольная ‖ оси	5,54	0,72	0,13	63,4	88	
(k) Наклонная	5,57	0,87	0,156	69,5	80	

LEGEND: a) Form of magazine; b) Time of straight drilling, hr; c) Passage per run, meters; d) Mechanical drilling rate, m/hr; e) Wear on bit per run, mm; f) Wear on bit in height, mm/linear meter; g) Remarks; h) Triangular; i) Trapezoidal; j) Rectangular, parallel axes; k) Inclined; l) Category VIII rocks; m) Category IX rocks; n) Category X rocks; o) P = 550 kg/peripheral bit velocity = 1.3 m/sec. Magazine width 1/5 πD, well depth = 190 m. Rig -- ZIF-650A; p) ; = 30 kg/cm^2, peripheral velocity of bit -- 0.61 m/sec. Magazine width 1/6 πD, well depth - 370 m. Rig ZIF-1200A; q) p = 5 kg/cm^2, peripheral velocity of bit rotation - 0.61 m/sec. Magazine width 1/6 πD, well depth - 440 m. Rig ZIF-1200A.

CONCLUSIONS

1. Bits with inclined magazine of constant cross section have the best boring qualities compared to other forms of magazines. The angle of inclination of the magazine slots depends on the peripheral velocity of the bit.

2. The width of the shot bit magazine must be selected in relationship to its peripheral velocity, but the height--as a function of the category of ores drilled within the 160-200 mm limits.

LITERATURE

1. Volkov, S. A., Vremennaya instruktsiya po drobovomu bureniyu (Provisional Instructions on Shot Drilling), Gosgeolitizdat, 1950.
2. Soltysh, V. M., Razvedka i okhrana nedr (Surveying and Conservation of Mineral Resources), No 4, 27 (1955).
3. Blinov, N. I., et al., Razvedka i okhrana nedr, No 12, 24 (1958).
4. Avrutskiy, A. L., Volkov, S. A. et al., Spravochnik mastera kolonkovogo bureniya (Handbook of Ore Drilling Foremen), State Scien.-Tech. Publ. House of Liter. on Mining, 1960.
5. Kirsanov, A. N. Razvedka i okhrana nedr, No 6, 19 (1957).
6. Ostroushko, I. A., Zabornyye protsessy i instrumenty pri bureniy gorny perod (Stope Processes and Instruments in Drilling Rock), Gosgortekhizdat, p 226, 1962.
7. Vozdvizhenskiy, B. I., Vasil'yev, M. G. Burovaya mekhanika (Drilling Mechanics), Gosgeoltekhizdat, 1954.

Received by Editor
28 March 1963

LEVEL TRENCH IN THE SYSTEM OF LAYER CAVING

Ye. N. Bakhrushin

(North Caucasus Mining and Metallurgical Institute,
Faculty of the Exploitation of Mineral Deposits.)

(Article written under the supervision of
Prof. N. S. Demin.)

The system of layer caving has several advantages over other systems of exploitation, which consists of its high extraction rate and low impoverishment of ore, relative fire-safety, etc. However, this system is characterized by several shortcomings, the chief of which is the low productivity of the face worker. The main reasons for this lower productivity are the additional amounts of labor spent in secondary scraping of broken ore, which represents 15 - 20% of the total outlays in working the block.

In 1939-1940 a variant was proposed using as the stope a level open-cut trench. This trench, extended to the height of the block, completely removed the necessity of double scraping of broken ore, improved the working conditions of the scraper winch in the washed layer and assured continuity in cleaning operations in the transition from the overlying layer to the underlying. The correctness of the direction chosen in the designing of the layer stoping system was entirely confirmed by experimental studies conducted on several copper-pyrite mines of the Urals and Zolotushinskiy Polymetallic Mines. The intensity of block working here was 130-140 tons per 24 hours, which exceeded by approximately two fold the twenty-four hour output at the existing method of block exploitation with accumulated workings. The productivity of the face worker in the system of layer caving using the level trench was 3.5-4.5 m^3 per shift, or 30-35% higher than the previously applied variants. In particular blocks the face worker productiv-

ity rose to 7.0 m^3 per shift /1,2/. Thus, one of the essential advantages of the level trench is the high labor productivity as the trench is being dug through.

However, in spite of the fact that calculations confirmed the economic value of using level trenches at an angle of incidence of ore deposits as high as 30% /3/, they have thus far not found broad use in practice. The application of the variant of the layer stoping system with level trench in the mines of the country is purely random. Thus, for 1962 not a single block was worked with level trenches at the mines Zolotushinskiy and Degtyarskiy by the mine managements. This is explained mainly by the fact that the method of bracing level trenches has until now been insufficiently developed. When applied to the mine "III Internatsional" the method of supporting the trenches with a crib proved to be a failure. Due to the difficulty in disassembling the arrays of crib at the working layer, in most cases they were left in the worked out spaces. As a result, under the pressure of the caved country rock, crushing of the underlying arrays of trench support occurred. Moreover, the arrays of supports left in the caved space frequently led to accidents in the block.

The use of level trenches was practiced at the Zolotushinskiy mine entirely without bracing. The role of the crib in this case was played by the trench-stored ore which was exposed as the layers were worked. However, in spite of the stability of the ore, in this case rupture in the trench walls were observed that hampered further cleaning of the excavation area.

At different times methods for bracing the level trenches with square lining, metallic and reinforced concrete crib have been proposed, however the methods found no practical use because of their complexity and laboriousness.

One of the reasons for the limited acceptance of the level trenches in the practice of the layer caving system is their limited discussion and popularization in scientific and technical literature. Therefore, we believe it important in this article once again to dwell on this question, considering mainly the method of bracing the trench.

Bracing of level trenches should satisfy the following main requirements: sustaining of the lateral pressure of the trench walls with a 1.5-2-fold strength margin; to be simple in manufacture, installation, and disassembly.

For the proper selection of the form and design of the level trench supports approximate calculations of rock pressure on its crib will be carried out. For this purpose we used the data of Prof. R. M. Tsimbarevich /4, page 67/, which defines the lateral pressure on the excavation wall as the value of the effective pressure on the supporting wall of the slipping prism klm loaded from above (Fig. 1). The height of the prism in this case is equal to the height of the trench, and the slipping angle of the prism

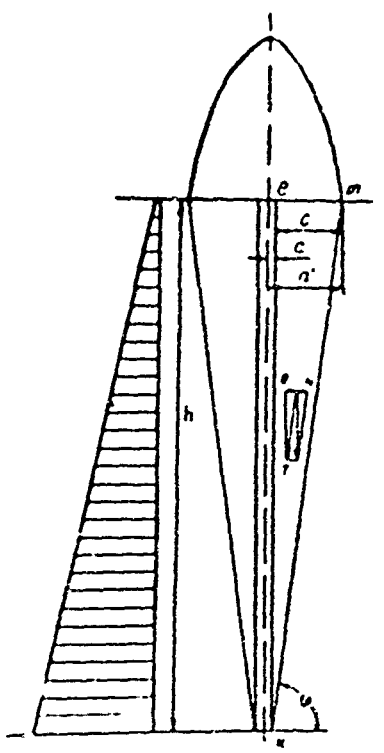

FIGURE 1. Scheme by which rock pressure on the crib of the level trench is determined.

$$\theta = \frac{90^\circ + \beta}{2},$$

where β = angle of internal rock resistance, degrees.

The value of the effective pressure on the side of the slipping prism per linear meter of trench length is

$$R = \frac{\gamma}{2}(2h_0 + h)h \cdot \operatorname{tg}^2 \frac{90^\circ - \beta}{2}.$$

where R = effective pressure on the side of the slipping prism, ton/m;

γ = weight by volume of the ore in which the trench was cut, ton/m^3;

h_c = height of the prism loaded from above, reduced to the weight by volume of the ore γ, m;

h = trench height, m.

In turn, the quantity

$$h_{\text{к}} \quad \frac{\gamma_1}{\gamma} \cdot \frac{a + h \cdot \operatorname{ctg} \frac{90^\circ + \beta}{2}}{\operatorname{tg} \beta_1},$$

where γ_1 = weight by volume of the caved rock, tons/m;
a = half width of trench, m;
β_1 = angle of internal friction of caved rock, degrees.

Values of effective pressure per 1 m^2 trench applied tc center of gravity of the trapezium in the stress-strain diagram

$$P = \frac{R}{h}.$$

Let us determine the values of the effective pressure per 1 m^2 of trench wall as a function of ore thickness under the following conditions: trench height = 45 m; trench width = 1.6 m; weight by volume of ore = 3.8 tons/m^3; weight by volume of caved rock = 2.0 tons/m^3; angle of internal friction of caved rock = 22°15'.

The results of the calculations are presented in the table and depicted in Fig. 2. As we can see, the pressure on 1 m^2 of trench wall is a very small quantity even under lean ore conditions.

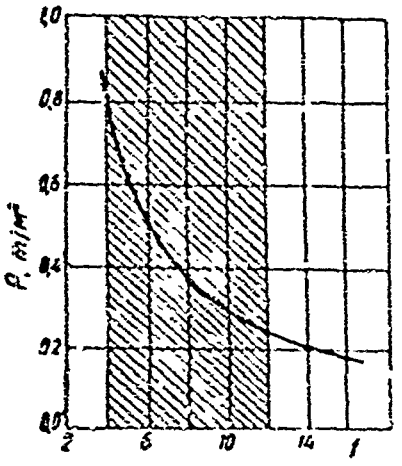

(a)

FIGURE 2. Pressure on crib of layer trench as a function of thickness f of the rock. Cross-hatched portion = region of rational use of the layer caving system. LEGEND: a) P, t/m^2.

The stress-strain diagram in Fig. 1 reveals an increase in the load at the trench base, but even a maximum load at the level of the haulage horizon does not exceed 1.0 - 1.5 tons/m^2. For comparison we will determine the permissible load on a cross bracing using the formula suggested by Prof. R. M. Tsimbarevich /4,

page 237/ for mining cribs

$$p = \frac{\sigma_{kp} F}{k},$$

where p = permissible load on cross bracing, kg;
σ_{kp} = critical compression stress, kg/cm^2;
F = area of cross bracing cross-section, cm^2;
k = safety factor (k = 1.5 - 2).

The critical compression stress is

$$\sigma_{kp} \text{ (кг/см}^2\text{)} = 220 - 1{,}5\,\frac{l}{i},$$

where l = length of cross bracing, cm;
i = radius of inertia, which for a circular cross section is taken equal to $d/4$;
d = diameter of cross bracing, cm.

If we take $i = 15/4 = 3.75$, $\sigma_{kp} = 220 - 1.5\,(160/375) = 156$ kg/cm^2, and $F = 177$ cm^2, then the permissible load on the cross bracing is p = 13.8 tons.

It is natural that with such a relationship of the actual and permissible loads on the cross bracing, the use of continuous cribs for reinforcing the level trench can by no means be justified. As it is known, the use of this form of support is advisable under conditions of intense rock pressure. Under conditions we are considering, when even for low ore thickness the pressure on 1m^2 of trench is less than 1/8 of the permissible pressure of the cross bracing, the use of cribbing will inevitably entail much extra outlay in labor and mine timber, but also, as was indicated above, will lead to additional complications in block working. Therefore, we believe that cribbing is not practical in supporting level trenches and cannot be recommended for practical use in the system of layer stoping.

When we consider the relative simplicity in the raising of beam supports, we cannot avoid dwelling on the question of the possibility of its use in bracing trench walls. From Fig. 1 it is clear that beam cribbing can resist pressure from the side of the slipping prism only in the case when the lock of the beam emerges beyond the slipping line km. To observe this condition the average length of the beam must lie within the limits of 3 m, and for the first layers excavated -- 6 m. It is natural that bracing of walls by beams of such length for a trench with 1.6 m will prove to be wholly impossible. Thus, the beam cribbing can be used only in bracing separate local breakdowns in the trench walls.

In bracing level trenches under conditions of low rock pressure we believe it possible to use a cross bracing with wooden frames. The distances between the frames in the vertical row is 1 m, judging from the normal height of measuring tape. The distance between the supports of one frame is taken as 2 m. The frames forming ore chute sections of the trench are strengthened with additional supports in order to prevent breakthrough of the ore, and are covered from within and without by boards. The distance between the ore chute sections is taken as equal to 6 m (Fig. 3). In this case, the largest area per single stand is 3.3 m^2 and the pressure on it at a thickness coefficient 4 according to the scale of Prof. M. M. Protod'yakonov is equal to 4-6 tons, which is considerably below the permissible. As we can see, such a form of bracing proves to be reliable enough under level trench conditions and is the simplest and most feasible.

TABLE

:sure Per One m^2 of Trench Wall as a Function of Ore Thickness

(c)

(a) f	(b) β	Давление на стенку траншеи, $т$	
		(d) на 1 пог. $м$	(e) на 1 $м^2$
4	80°	36,2	0,80
7	82°30′	18,6	0,41
12	84°15′	11,3	0,25
16	85°	9,0	0,20

LEGEND: a) f, thickness; b) angle of internal friction of caved rock; c) pressure on trench wall, tons; d) per one running liter; e) per one meter^2

Cutting of the trench is done by the usual method according to the diagram with the storing of broken ore (Fig. 4). To protect the cross cut of the haulage horizon, a pillar 2.5 m high is left above it, through which 6 m of ore-recovery ramps are cut.

In the cutting one should give special attention to producing smooth trench walls unbroken by the effects of explosion. This can be achieved by a certain increase in the number of shaping blast holes with a simultaneous decrease in the weight of charge in each blast hole. For this purpose the horizontal location of blast holes in the face of the broken layer is recommended. It is natural that this will result in a certain lowering of the labor productivity in the cutting of the trench. However, one should remember that the trench is not a cleaning face (although it resembles such), and in this case a lowered productivity will be justified by the high reliability of trench use during the en-

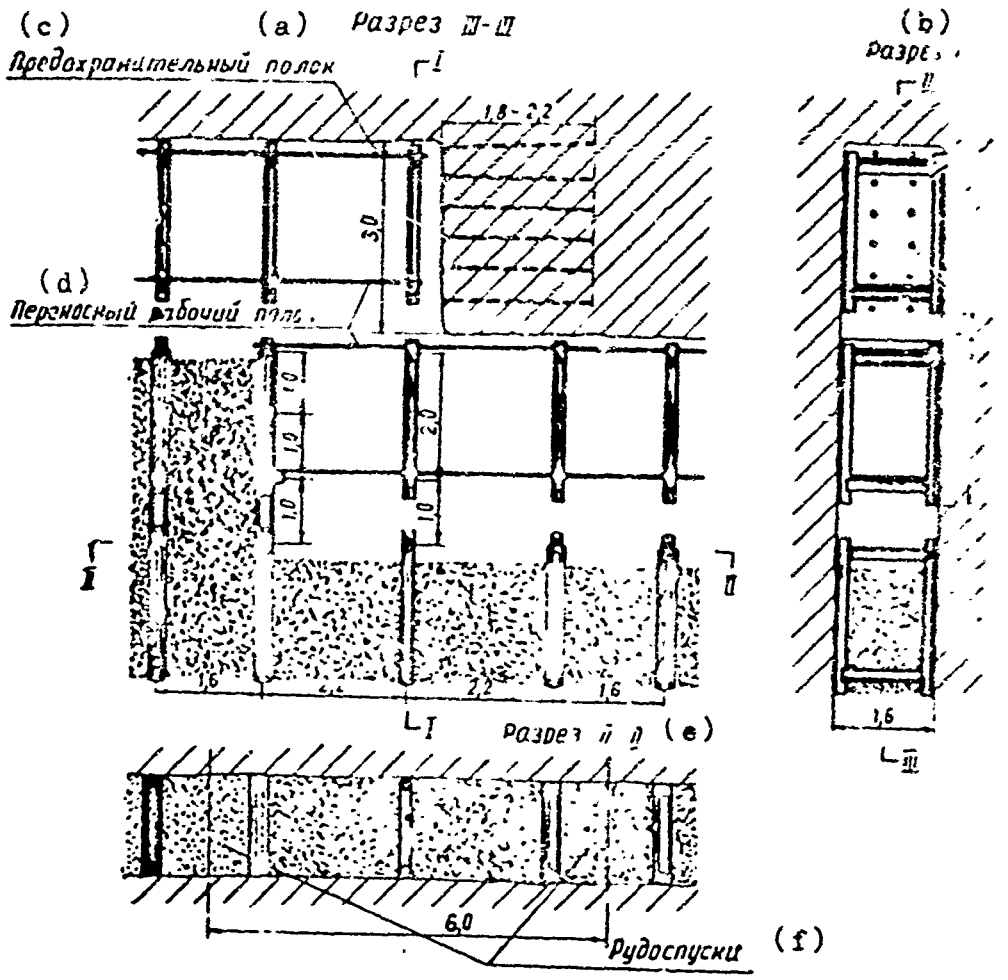

FIGURE 3. Design of level trench crib. LEGEND: a) Section III-III; b) Section I-I; c) Protective shelf; d) Tramming level; e) Section II-II; f) Ore chutes

tire period of the block working.

Drilling is carried out by squads of workers positioned on the cross bracing supports shielded by a protective shelf. During operations it is necessary to regularly check the verticalness of the trench walls with a plumb. The bracing of the trench is carried out as it is being cut. The crib elements of necessary sizes are prepared at the surface. Assembling the cross bracing with the supporting beam (which in this case is understood to be the vertical element in the crib frame) is done on the one hand "in mortise" and on the other--"in corral". The verticalness of the crib installation is checked by a plumb line.

When the trench is being cut its extreme section is equipped as the passageway and is used for access to the main haulage horizon. The ore broken in the cutting of the trench remains stored

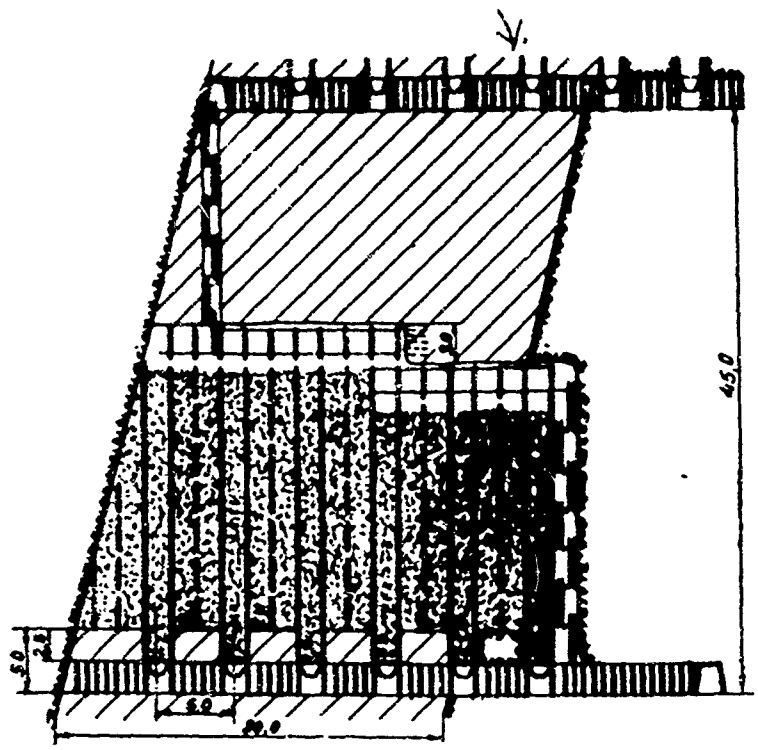

FIGURE 4. General scheme of passages of level trench

and receives some of the pressure from the trench walls. As the layers are worked the excesses of this ore are sent through the ore-recovery sections.

The proposed method of bracing was tested in the working of molybdenum veins at the Davendinskiy deposit using the system of stored ore and cross bracing, and the method completely justified itself /5/.

Let us determine the productivity of the face worker in the cutting of the trench. For this we will use the well known formula

$$Q = \frac{1}{\frac{1}{Q_{бур}} + \frac{1}{Q_{кр}}},$$

where Q = productivity of face worker in cutting the trenches, tons/shift;

$Q_{бур}$ = productivity of drillman, tons/shift;

$Q_{кр}$ = productivity of timberer, tons/shift.

Using the numerical data in /6/: $Q_{бур}$ = 29.6 tons per shift, $Q_{кр}$ = 196.0 tons per shift, productivity of face worker is found

to be 2.56 tons per shift.

The actual productivity will be somewhat lower due to the restricted cross section of the face and the increased number of spurs. Taking the reduction in productivity tentatively as 15%, we obtain a productivity of the face worker in cutting the trench of 21.8 tons per shift, which is more than twice as high as in the cutting of accumulating workings.

Conclusions.

1. The reinforcing method of level trenches using cribbing applied earlier under low rock pressure conditions is plainly unadvisable.
2. The beam bracing of the trench walls cannot be recommended since it is not sensitive to the load of the slipping prism.
3. Cross bracing in the variation proposed is a fully reliable form of level trench cribbing.

LITERATURE

1. Spravochnik po gornorudnomu delu (Handbook on Mining), Vol 3, page 194, 1961.
2. Seledkov, Yu. V. et al, Sistemy podzemnoi razrabotki rudnykh mestorozhdeniy (System of Underground Working of Ore Deposits), Metallurgizdat, page 357, 1958.
3. Demin, N. S., Belyaev, V. G., Trudy SKGMI (Works of the SKGMI), No 15, 114 (1957).
4. Tsimbarevich, P. M., Kurs rudnichnogo krepleniya (Course in Mine Timbering), Ugletekhizdat, 1951.
5. Dobrovol'skiy, N. D. et al , Gornyi zhurnaya (Mining Journal), No 2, 1957.
6. Sbornik edinykh norm vyrabotki na podzemnye pornye raboty rudnikov tsvetnoi metallurgiy (Handbook of Individual Exploitation Norms in Underground Mining for Nonferrous Mines). 1960.

Received by Editor
20 April 1963

THERMAL CALCULATIONS OF LOCAL COOLING OF AIR IN CLEANING FACES USING MOBILE AIR CONDITIONERS

G. V. Duganov and V. N. Kukharev

(Dnepropetrovsk Mining Institute,
Faculty of Mine Ventilation.)

Stemming from the increased depth of mining operations in several metal mines, as for example, at the Sadonskiy polymetallic pits, a need has arisen to regulate the thermal conditions in cleaning and preparatory faces. One of the most effective and universal methods of such control is the use of artificial cooling of fire damp by means of mine refrigerating equipment.

However, this method is best applied only in the case when further increase in volume and flow of the air entering the workings becomes economically unprofitable, or when the measures do not achieve the required effect of cooling the mine atmosphere. In several cases, natural sources of cold have been used with success in cooling fire damp, as for instance, the air-cooling installation Sadonskiy pit, working on the basis of the cold melted waters of glaciers /1/.

Analysis of the methods and means for conditioning fire damp used in mines of the USSR and abroad shows that in the great majority of cases the most economic method is the local cooling scheme using underground refrigerating installations /2/. Scientific studies conducted by the Dnepropetrovsk Mining Institute /Dnepropetrovskiy gornyy institut; DGI) revealed that in a large number of cases the cooling air entering to air out the cleaning faces (blocks, lava, chambers) can be expeditiously produced by mobile refrigerating installations (mine conditioners) of KPSh type, of the Dongiprouglemash design /5/. These installations are used for lowering the air temperature in the faces of preliminary workings, but as proven by calculations and materials of mining measurements, they can be successfully applied also in cleaning faces of metallic pits and coal mines.

Use of the mine mobile conditioners is envisaged, for example, in cooling air at deep levels of the Sadonskiy mine, where the potential reserve of a natural source of cold in melted glacier waters will be insufficient. Studies in this direction were conducted in the Sadonskiy mine by DGI in 1962. A similar scheme of fire damp conditioning in cleaning faces (lavas) is also planned by the Institute Dneprogiproshakht for the mines imeni Artem, imeni Dzerzhinskiy, and others in the Tsentral'nyy Rayon of the Donets Basin /2/.

The scheme of local conditioning using mobile conditioners has significant advantages as compared with the central and semicentral scheme of the distribution of refrigerating installations in mines which have a great dispersion of mining operations, since in the use of mobile conditioners the necessity of carrying out ventilation diggings is eliminated--for collectors used in the concentrated supply of air to the cleaning faces of several blocks (recovery sections).

The essentials of the scheme of local cooling of firedamp mobile conditioners consists of the following. A conditioner is placed in a broadened area of the haulage drift near a cleaning block (Fig.) and as the cleaning face continues to be advanced to more than 150 m away, the conditioner is shifted to a closer location.

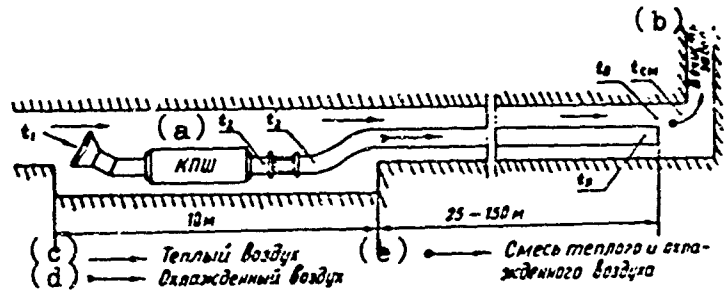

FIGURE. Design scheme for air cooling in a cleaning face. LEGEND: a) Moveable air conditioner; b) To cleaning face; c) Hot air; d) Cooled air; e) Mixture of hot and cooled air

For a smaller change in distance from conditioner to the face the length of airline through which the cool air passes to the cleaning block or longwall is extended. Only part of the air admitted to the face is cooled (namely the portion which passes through its air cooler), and is compressed by an auxiliary fan through the flexible airline to the lower part of the blind pit of the block or the recovery furnace of the longwall. Then the cooled air is mixed with its incooled part so that the temperature of the air mixture corresponds to the given air temperature at the face.

The authors of this article have developed a method for calculating the required cold-productivity of the installation for local cooling of air, taking into account the variation of parameters of the ventilation stream as various factors act on it, which should above all include: difference in temperatures of the rock massiv and the ventilation stream; heat emission in the functioning of the equipment; heat exchange between the cooled and uncooled air; heat increases due to friction of the air in the pipes; heat emission in the operation of the fan and from other sources. The method of calculation is marked by simplicity and fully satisfies the requirements of accuracy in engineering calculations.

The cold-productivity of the installation Q_0 is determined from the formula

$$Q_0 = G_{тр}(i_1 - i_2), \qquad (1)$$

where $G_{тр}$ = given quantity of air subject to cooling in the conditioner, kg/hr (usually 6000-10,000 kg/hr);

i_1 and i_2 = enthalpy of the air before and after cooling, corresponding to the temperatures t_1 and t_2, kilocalories/kg;

t_1 = temperature of air in the stope in front of the air cooler, determined by the method of direct thermal calculation, ° C /2/;

t_2 = temperature of cooled air upon leaving the conditioner, ° C.

The value of t_2 can be calculated from the following expression:

$$t_2 = t_3 - \Delta t_{в.у} - \Delta t_{тр} - \Delta t_{т.о}, \qquad (2)$$

where t_3 = air temperature at end of airline, °C;

$\Delta t_{в.у}$ = increase in temperature of firedamp in the fan, °C;

$\Delta t_{тр}$ = increase in temperature due to friction of air against the walls of the airline, °C;

$\Delta t_{т.о}$ = increase in temperature due to heat exchange between the cooled air in the pipeline and the uncooled air in the stope, °C.

The temperature of the air t_2 entering into expression (2), is found from the heat balance equation

$$t_3 = \frac{G_{см}\ t_{см} - G_в\ t_в}{G_{тр}},$$

where $G_{см}$ = total amount of air admitted for ventilation of the longwall (cleaning block), kg/hr;

$G_в$ = amount of air passing through the stope (bypassing the conditioner), kg/hr;

$t_{см}$ = temperature of the mixture of air cooled in the conditioner and admitted for ventilation of the cleaning face; determined by the method of inverse thermal calculations /2/, the temperature applicable to conditions of the Sadonskiy mine is taken as equal to +25° C;

$t_в$ = temperature of air in stope (before mixing) /See Note/, °C.

(/Note/ The air temperature in the excavations ventilated for up to one year was determined by thermal calculations using the method of O. A. Kremnev /2/, while for excavations in which the length of the ventilation pipeline was short (up to 25 m), is taken as equal to t_1.)

The increase in temperature $\Delta t_{в.у}$ of the air in the fan is determined by the formulas /3/:

For axial fans

$$\Delta t_{в.у} = 9{,}8 \frac{H}{\gamma}\left(\frac{1-\eta}{\eta}\right)10^{-3} + 7{,}5 H_{ст} \cdot 10^{-3},$$

For centrifugal fans

$$\Delta t_{в.у} = 9{,}8 \frac{H}{\gamma}\left(\frac{\eta_{дв}}{\eta} - 1\right)10^{-3} + 7{,}5 H_{ст} \cdot 10^{-3},$$

where H = total pressure of the fan, mmH_2O;

γ = specific gravity of the air, kg/cm^3;

$H_{ст}$ = static pressure of the fan, mm/ng;

η = overall efficiency of fan;

$\eta_{эл}$ = efficiency of electric motor.

The increase in air temperature due to friction against the walls of the airline is about one degree and can be calculated from the formula

$$\Delta t_{тр} = \frac{860 R_1 v^2}{102 \times 3600 \gamma C_v} l, \qquad (3)$$

where R_1 = resistance of 1 linear meter of airline, $kg \cdot sec^2/m^3$;

v = amount of air passing through the airline, m^3/sec;

γ = specific gravity of air, kg/m^3;

l = length of airline, m.

The quantity $\Delta t_{тр}$ calculated according to formula (3) has some additional value in the air temperature increase, since here the cooling action of air seeping through the leakages in the airline connections. However, the error in this case does not exceed 5%, which is quite permissible for ventilation calculations.

The increase in temperature due to heat exchange between the cool air in the pipeline and the uncooled air in the workings is determined by the formula

$$\Delta t_{т.о} = \frac{F_{тр} \kappa}{G_{тр} c_p} \left(\frac{t_1 + t_в}{2} - \frac{t'_2 + t_3}{2} \right),$$

where $F_{тр}$ = heat-transfer surface of airline, m^2;

κ = heat-transfer coefficient from the wall of the airline to air, kilocalories/$m^2 \cdot hr \cdot deg$ (taken from handbook data in special literature, for example, /4/, etc.);

$t'_2 = t_2 + \Delta t_{в.у}$ -- air temperature in airline after passing through the fan, °C.

Placing the values of the quantities obtained t_3, $\Delta t_{в.у}$, $\Delta t_{тр}$, and $\Delta t_{т.о}$ in formula (2) and carrying out simple transformations, we obtain the final formula for determination of air temperature after passage through the air cooler

$$t_2 = \frac{1}{1 - Б} \left[t_3 (1 + Б) - Б (t_в + t_1) - \Delta t_{тр} \right] - \Delta t_{в.у},$$

where $Б = \frac{F_{тр} \kappa}{2 G_{тр} C_p}$.

If the value of Q_0 calculated by formula (1) exceeds the cold-productivity of 1 KPSh conditioner (Q_0 = 90,000 kcal/hour), then in this case coupled operation of two conditioners on a single air conduit can be carried out; here a series of parallel scheme of conditioner operation is possible.

Under otherwise equal conditions preference must be given to the scheme with parallel arrangement of conditioners, since in this case the aerodynamic drag of the installations and the extent of air cooling is considerably reduced, compared with the series operation of conditioners.

The series performance of conditioners can be recommended for a relatively small amount of air entering the cleaning face (2.5 - 4.0 m^3/sec) and in the presence of a higher high-pressure auxiliary fan.

LITERATURE

1. Duganov, G. V., DAN USSR (Reports of the AS UkSSR), No 12, 1958.
2. Shcherban', A. N., Kremnev, O. A., Zhuravlenko, V. Ya., Spravochnoye rukovodstvo po teplovym raschetam i proyektirovaniyu ustanovok dlya okhlazhdeniya vozdukha (Handbook on Thermal Calculations and Designing of Equipment for Air-Cooling), Gosgortekhizdat, 1960.
3. Merkulov, V. A., Krasuntsev, E. M., Arakelyants, A. K., Trudy seminara po gornoy teplotekhnike (Works of the Seminar on Mining Heat Engineering), No IV, 1962.
4. Mikheev., M. A., Osnovy teploperedachi (Fundamentals of Heat Transfer), Gosenergoizdat, 1953.
5. Duganov, G. V., Kukharev, V. N., Baratov, Ye. I., Trudy seminara po gornoy teplotekhnike, No IV, 1962.

Received by Editor
23 April 1962

APPLICATION OF THE TEMPLATE AND GRID FOR TRANSFER OF INDICATOR DIAGRAMS RECORDED BY THE MAI-2 INSTRUMENT TO THE SYSTEM OF P-V COORDINATES

N. M. Barannikov

Moscow Institute of Steel and Alloys,
Faculty of Mining Mechanization

The MAI-2 stroboscopic indicator permits the recording, with high accuracy, of indicator diagrams in investigating piston machines, and in particular, piston compressors as the function of the angle of rotation of the compressor crankshaft in the coordinates P - φ (Figure 1). For analysis of compressor operation it is necessary to have indicator diagrams in the coordinates pressure - stroke (P - V).

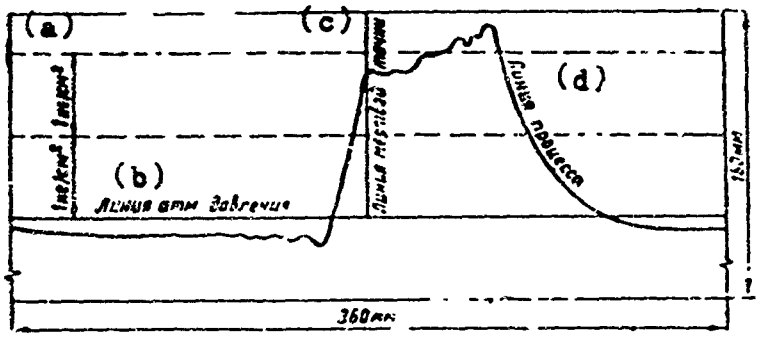

FIGURE 1. Indicator diagram of compressor in the coordinates P - φ .
LEGEND: a) 1 kg/cm^2; b) Atmospheric pressure line; c) Dead point line; d) Process line

Therefore, in the present article /See Note/ we consider the question of how to reconstruct indicator diagrams recorded by the MAI-2 instrument from P - φ coordinates to P - V coordinates using specially prepared template and grid.

/NOTE/ Scientific leader, Professor V. I. Kiselev, (Doctor of Technical Sciences).

For this, it is first of all necessary to calculate the piston displacement as the function of the angle of crankshaft rotation. /See Note/. According to Figure 2, the piston displacement has the function of angle of crankshaft rotation can be determined by the formula

$$s = R\left[(1-\cos\varphi) + \lambda\left(1 - \sqrt{1 - \frac{1}{\lambda^2}\sin^2\varphi}\right)\right],$$

where s = piston displacement, mm;
R = radius of crank, mm;
λ = ratio of length of connecting rod to radius of crank
φ = angle of rotation of crank, measured from upper dead point in the direction of rotation;
L = length of connecting rod, mm.

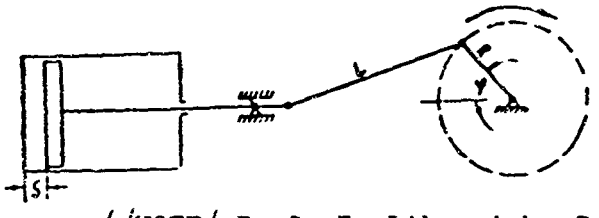

FIGURE 2. Scheme of compressor for determination of s = f (φ).

(/NOTE/ B. G. I. Librovich, S. N. Poznyakov, Teplovoznyye dvigateli /Diesel Locomotive Engines/, ONTI, 1937.)

The piston displacement as a function of the angle crankshaft rotation for the compressors most widely used in mining is shown on the table.

Movement of Piston as a Function of Angle of Rotation of Compressor Crankshaft

(a) φ, grad	(b) S, mm			φ, grad	S, mm		
	200B-10 S	B-300-2K	B-55 и 2BГ		200B-10 S	B-300-2 K	B-55 2BГ
0	0	0	0	100	129,67	193,00	353,10
10	1,89	2,80	5,16	110	145,39	216,70	396,60
20	7,49	11,00	20,20	120	159,49	238,20	4 5,90
30	16,54	24,40	44,60	130	171,68	256,70	468,80
40	28,60	42,20	77,20	140	181,80	272,00	498,70
50	43,12	63,80	116,50	150	189,74	284,00	520,80
60	59,49	88,10	161,00	160	195,43	292,90	5 7,00
70	76,99	111,00	208,50	170	198,85	298,30	546,70
80	94,95	140,60	257,60	180	200,00	300,00	550,00
90	112,70	167,50	306,20	—	—	—	—

LEGEND: a) Degrees; b) mm

For reconstruction of the indicator diagrams it is necessary to prepare a template and grid. The template can be made most conveniently from transparent organic glass 360 x 180 mm in size. The template dimensions are determined by the diameter and width of the indicator drum of the MAI-2 instrument. The diameter of the indicator drum is prepared so that its circumference is equal to 360 mm, i. e., each millimeter of the diagram corresponds to one degree of

crankshaft rotation. The width of the indicator drum is 130mm. The pattern is carried out as follows: Along its center (Figure 3) the lines ab is drawn, then on both sides of it lines are drawn at equal intervals (N Figure 3, each 10^{o}) parallel to lines ab all along the template. The line I - I is drawn perpendicular to lines ab at a distance of 10 mm from the lower margin of the template, and 70 mm from line I - I line II - II is drawn.

The extension of two lines on the template is dictated by the following fact. The MAI-2 indicator is designed simultaneously to record the diagram from the cylinder interior at the first and second compression step in different scales. For diagrams recorded from the cylinder interior at the first step a scale is used in which the line of atmospheric pressure is approximately 60 mm from the edge of the diagram (see line of atmospheric pressure in S Figure 1), and for diagrams recorded from cylinder interiors at the second step, the atmospheric pressure line is located almost along the margin of the diagram. Hence it is obvious that the template line I - I is used in transferring diagrams from cylinder interiors at the second step, and line II - II in transferring diagrams from cylinder interiors at the first step.

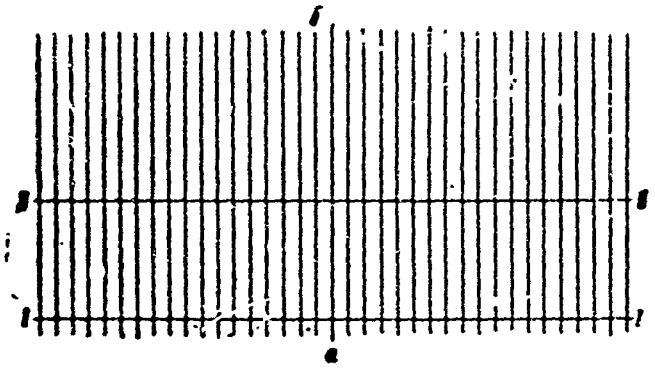

FIGURE 3. Pattern for rearranging diagram from the P - φ coordinates to the P - V coordinates.

Here one should note that this template is useful in dealing with indicator diagrams recorded from any piston compressor irregardless of type and method of action. The grid, however, should be prepared for each type of compressor studied. It is most suitably made from tracing paper. The construction of the grid shown is suitable for the 200 B-10/8 compressor (Figure 4). For this compressor, according to the table, a stroke is 200 mm.

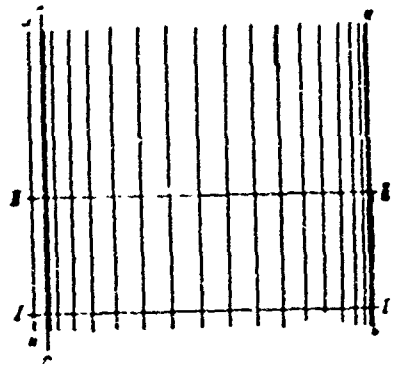

FIGURE 4. Grid for rearranging the diagram from P - φ coordinates to P - V coordinates.

Let us assume that we wish to have the length of the indicator diagram in the P - V coordinates equal to 100 mm (scale in reconstructing indicator diagrams from the P - φ coordinates to P - V coordinates can be chosen by the experimenter as desired). On a sheet of tracing paper (see Figure 4) we extent on the left the vertical line cd, which will correspond to the position of the piston at the upper dead point. Then from the line cd we draw a second vertical line ek 100 mm to the right, which will correspond to the position of the piston at the lower dead point. The intermediate lines between cd and ek are drawn at the base of the table, reducing all values down to one half, since the total length of the indicator diagram was selected to be less than one half of the compressor stroke.

Measured off from line cd to the left is a distance corresponding to the dead space of the cylinder (see Figure 4, line hn). For the compressor in question the dead space amounts to 4%. Then, the extent of the dead space in the diagram scale is 100X 0.4 = 4mm. The lines I - I and II - II are plotted in exactly the same way as was done on the template. Hence, the line I - I will be used in transferring diagrams recorded from cylinder interiors at the second step, and the line II - II -- from cylinder interiors at the first step. With this the plotting of the grid for the 200 B-10/8 compressor is completed.

Further on the sheet of paper on which we wish to record the indicator diagram in P - V coordinates, we plot an axis of P - V coordinates draw the axis of P - V coordinates, and plot the atmospheric pressure line (Figure 5). Then, we place the grid on this sheet of paper so that the line hn coincides with the axis of pressure P, and the line II - II with the line of atmospheric pressure, if we are transferring a diagram recorded from the cylinder interior at the first step. In transferring diagrams recorded from the cylinder interior at the second step, the line hn is combined

with the axis of pressures P, and the atmospheric pressure line with the line I - I.

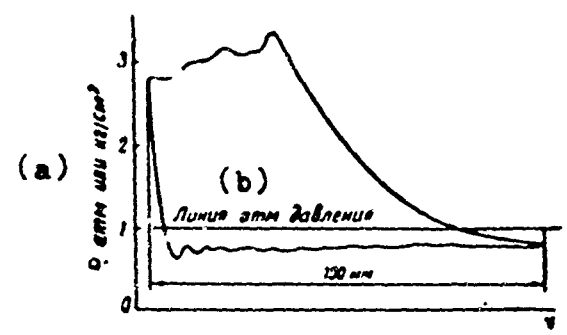

FIGURE 5. Indicator diagram of the compressor in P - V coordinates. LEGEND: a) P, atm. or kg/cm^2; b) line of atmospheric pressure.

Transfer of the diagram is carried out as follows: On the template superimposed on the diagram recorded measure the distance from the atmospheric pressure line to its crossing with the process line of the diagram (See Figure 1) and mark (perforate) this section through the grid onto the sheet of paper. Then using the measure thus obtained successively transfer all points of the diagram(in our case every 10^0), the grid is removed from the sheet of paper, and from the prickholes on it the indicator diagram of the compressor is outlined in P - V coordinates (See Figure 5).

Received by Editor
5 January, 1963

EXPERIENCE IN MODELING A FLOTATION PROCESS

A. D. Pogorelyy, M. A. Sartayeva, and A. S. Malyugin

(North Caucasus Mining and Metallurgical Institute
Chair of General Metallurgy)

The principle of the flotation of real pulps is very complex even for a simple instrument -- the periodic-action laboratory machine. The analytic expression of the principle of the process, the function extraction versus time, depends on a numerical coefficient characterizing the hydrodynamic properties of the applied flotation machine -- the amount of "aeration", and also depends on a very complex functional parameter characterizing the pulp.

Investigators of the flotation process have long noticed a very simple regularity in the behavior of monomineral and monodisperse pulp. This is the well known formula of the kinetics of periodic flotation

$$\lg \frac{\lambda}{\lambda - \varepsilon} = \frac{\varphi t}{2{,}303}, \qquad (1)$$

which is called the K. F. Beloglazov formula in our literature.

At the basis of this expression, lies the differential function

$$dC = -C\varphi\, dt, \qquad (2)$$

where C = concentration

φ = constant of flotation rate
t = time.

For the particular case of the periodically operating laboratory machine integration leads to the formula (1) for the case of the multiple-cell machine, functioning under steady-state conditions /1/, to the formula

$$C_{\substack{\text{tailings}\\ \text{(crude)}}} = C_{\substack{\text{output}\\ \text{(crude)}}} \left(\frac{w}{w + \varphi V}\right)^n, \qquad (3)$$

where w = rate of feed supply
V = volume of machine cell
n = number of cells ..

In the function (2) and its particular cases (1) and (3) it is postulated that the rate of the process is proportional to the concentration C and that the flotation rate constant is not dependent on time.

By virtue of the assumptions lying at the basis of the differential function (2), all particular regularities are valid for pulp composed of identical hard-grains, with φ unchanging with time, and with the invariable observance of "free flotation" conditions. "Free flotation" requires but little filling of the surface of air bubbles with mineral particles. In the study (2) it is shown that during the filling of air bubble surface to the extent of 20 %, deviations from the regularity (1) become very significant For a complex pulp, the relationship extraction-time is arrived at by summation of extractions for all sizes of particles differing in φ since very particle size obeys the simple relationship (2). The forms of such relationships, upon assigning the properties of the pulp by the function of the distribution of hard masses based on floatability $\frac{dM}{d\varphi} = \theta(\varphi)$, are presented in the study (3).

In constructing the regularities of continuous fluctuation /1, 5/, additional conditions beside the assumptions related to the differential regularity (2) were introduced, whose justification can be proven only by experiment.

Valid analytic relationships are very valuable, since they permit calculations to do much of what earlier would require experimentation. Therefore, it is very essential to know as precisely as possible what the main relationships for identical particles are, and above all, formula (1).

An experimental check of formula (1) has been the subject of a large number of studies dealing with narrow size classes of pure natural materials and with artificial materials: electrographite

/4/, glass beads, etc., which yielded a relationship close to formula (1).

In flotation practice, it has been difficult to accurately maintain the conditions of the relationship (2): identity of all floatable articles and invariability of flotational properties with time. Therefore, it is very useful to have a model of the flotation process with precise compliance with the conditions of the differential relationship (2).

In this study, flotation is modeled according to the process of evaporation of dissolved volatile substance in a current of air bubbled through a layer of the solution, if the solution is governed by Henry's law. The partial pressure of the vapor of the volatile substance above such a solution is proportional to its concentration in the solution. If the rate of the entering bubbling gas, the dispersity of its bubbles, the height of the column of solution, and the temperature are stabilized, then the rate of removal of the volatile substance will be proportional to its concentration in the solution. Consequently, this process of removal of the volatile substance obeys the differential relationship (2), i.e., models the flotation process. By virtue of the identity of all the particles of the dissolved substance -- its molecules, the causes complicating the simple relationship (2) for flotation are eliminated.

The process can be carried out in a model of a pneumatic flotation machine. Inasmuch as it contains no impeller all the causes of changes in "aeration" due to the number of revolutions and the extent of impeller wear are eliminated. Chosen as the pulp model is a solution of elemental bromine in water at concentrations close to 0.03 mole/liter Br_2 (5g/liter). When dissolved, the bromine remains as diatomic molecules at chemical changes upsetting the Henry's law agreement of the solution do not appear. The advantage of working with bromine is simplicity and accuracy in determining its concentration by the iodometric method, a disadvantage is the need for working under forced current. The bubbling of the solution will be done by oxygen, which is inert to bromine and water.

A model of the pneumatic machine for study of flotation is represented in Figure 1. The instrument is constructed from plexiglas sheets of 3 mm thickness and from the top view represents a square cornered chamber with a double bottom. The upper bottom is built of perforated sheets along which a layer of filtration glass cloth is placed.

The lower sheet has 0.35 mm-diameter holes situated in the junctions of the grid of 5.6 mm squares. The upper sheet includes 4 mm diameter holes located above the holes of the lower sheet, serving as a screen securing the filtration cloth. In the space between the upper and lower bottom, oxygen is admitted, passing through the pores of the glass cloth into the filling cell of liquid as bubbles 3-5 mm in diameter. The top-exposed cell has on its long sides vertical slots for installing 11 detachable partitions, not reaching to the bottom,

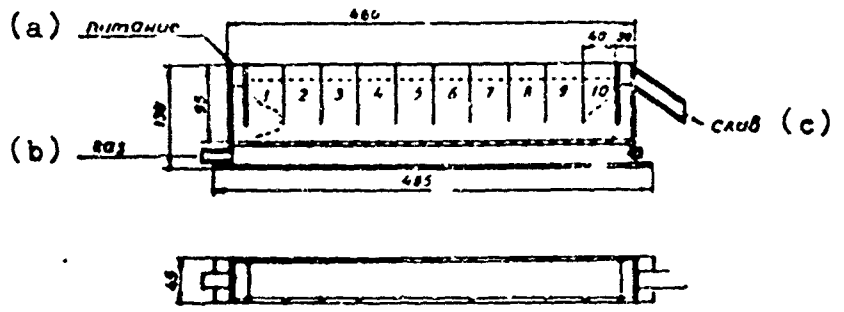

Figure 1. Model of pneumatic flotation machine. Dashed line shows path of air bubbles along the machine faces. LEGEND: a) feed; b) gas; c) overflow.

dividing the cell into 12 smaller sections. The extreme partitions are made of sheets 3 mm in thickness and will form the receiving and mixing cell of the equipment for working under continuous process conditions. The lower bottom has no holes on the sections under the receiving and mixing cells of the equipment. Openings are drilled into the right, mixing cell in its facing wall, determining the filling level of the cell along with a groove for release of spent liquid. The remaining 9 partitions are made of nitrocellulose film of 1.5 mm thickness and are used for breaking down the long chamber into a desired number of shorter sections.

The oxygen for boiling is fed into the equipment from a steel "oxygen" cylinder through a reducing valve, to gas heaters arranged in parallel, and a diaphragm fuel gauge. The consumption of oxygen is controlled by the gauge cock of the reducing valve on the fuel gauge and is governed by the gas meter readings.

The solution is prepared from elemental bromine and water containing 20 g/liter KBr. The addition of the KBr was intended to lower the bromine vapor pressure above the solution in order to increase the duration of the experiments and to avoid overfrequent readings. During the experiments under continuous process conditions, the solution was fed into a special pressure tank with a constant solution level (level regulator), and from there through glass tubes through the regulating cock in the receiving section of the machine. The rate of solution supplied was determined by the measurements of the volume of solution flowing from the machine. The cylinder containing the bromine, the level regulator, and the machine were located in a hood.

The determination of bromine in the solutions was carried out by the volumetric iodometric method. A volume of solution removed by

pipette was poured into a beaker containing 15 ml of 20 % KI solution, and the liberated iodine was back-titrated by a solution of sodium hyposulfite with the addition of starch before the end point.

Preliminary experiments with pure water determine the capacity of the machine under various working conditions for the continuous process use and established that it was best to work with a 960 ml volume of liquid and a consumption of 10-25 liters/minute of oxygen. During experiments under the condition of the periodically operating laboratory equipment, all the partitions were removed, the overflow openings were closed, and the following operations performed. 970 ml of the initial bromine solution was accurately poured into a porcelain jar. Oxygen was fed into the empty machine at a given rate. 10 ml of the initial bromine solution was removed for analysis, a stop watch was started, and as fast as possible, the bromine solution was poured into the machine, which took 2-3 seconds. Then samples of the solution for analysis were removed by pipette from the machine cell at equally spaced intervals of time, compensating for the decreased volume of the liquid in the cell by submersion of the plexiglas plates of the corresponding volume at the left face of the cell. Upon completion of the experiment, liquid was poured from the cell, and only then was the stream of oxygen turned off. The results of analyses made of the chamber contents are plotted on the graph in the coordinates lg C_{Br} versus time.

During experiments under continuous process operations, at least two of the extreme partitions were left in the machine, in order to form a receiving and overflow cell, and the outlet hole of the machine was open. The feeding installation was set at the desired rate of bromine solutions supplied. The porcelain jar was filled with the original solution, the oxygen was admitted, the chamber filled, the supply of the feed solution was begun, and the stop watch started. The solution flowing out was periodically analyzed and collected in a receiver for volume measurements. Analyses showed that the bromine concentration in the solution had been lowered to a definite limit. After three identical bromine concentrations were obtained, it was assumed that a steady state of the process had been achieved and the needed measurements made. A beginning was also made in investigating the performance of the multiple-cell machine, after the necessary number of thin partitions had been installed in it.

Inasmuch as the partial pressure of the bromine vapor above the solution depends on temperature, this quantity was stabilized at an accuracy of up to 0.5°.

The first group of experiments had the purpose of checking the maintenance of the general relationship of periodic flotation (1) for various conditions. Table 1 includes the results of 3 experiments, and Figure 2 presents the three corresponding graphs of change in solution concentration with time.

As can be seen from Figure 2, the graphs of the process using coordinates lg C_{Br} - time are straight lines, fitting well the experimental points. For each of the lines, the value of the constant of the bromine removal rate from the solution is shown calculated from experimental data; it is an analog of the flotation rate constant in the equation of K. F. Beloglazov. We emphasize that in the experiments, 3 bromine concentrations decreased down to more than one-thirtieth, although the relationship maintained its rectilinearity. The experimental data presented indicates that the process of removal of elemental bromine described from the solution by currents of oxygen bubbles does model the process of the flotation of uniform particles.

In order to evaluate the results of the continuous process in this particular machine we will need to know the value of the constant of bromine removal rate φ calculated from experimental data for the periodic process. This data showed that the rate of bromine removal at constant temperature and solution concentration is proportional to the rate of bubbling oxygen supplied. In this equipment, the dispersion of the air bubbles rising to the surface of the solution only under the action of gravity and their residence in the liquid are constant.

TABLE 1

Results of Experiments on the Removal of Bromine from Solution Under Periodic Process Conditions

(a) Время от начала опыта, мин	(b) Опыт 1 (c) Расход газа 11,5 л/мин, t = 17°		(b) Опыт 2 (d) Расход газа 22,4 л/мин, t = 17°		(b) Опыт 3 (e) Расход газа 20 л/мин, t = 21°	
	C_{Br}, г/л	lg C_{Br}	C_{Br}, г/л	lg C_{Br}	C_{Br}, г/л	lg C_{Br}
0	2,80	0,447	4,29	0,632	4,57	0,66
1	2,14	0,330	—	—	—	—
2	1,55	0,190	1,40	0,146	1,43	0,155
3	1,18	0,071	—	—	—	—
4	0,91	$\bar{1}$,959	0,53	$\bar{1}$,724	0,457	$\bar{1}$,66
5	0,71	$\bar{1}$,851	—	—	—	—
6	0,54	$\bar{1}$,732	0,18	$\bar{1}$,233	0,148	$\bar{1}$,17
7	0,42	$\bar{1}$,623	—	—	—	—

LEGEND: a) time from beginning of experiment, minute; b) experiment 1; c) consumption of gas = 11.5 liters/minute, t = 17°; d) consumption of gas = 22.4 liters/minute, t = 17°; e) consumption of gas = 20 liters/minute, t = 21°.

Then, the mass of bromine removed per unit volume gas should be proportional to the partial pressure of the bromine above the solution, which by virtue of Henry's law, is proportional to the concentration of bromine in the solution and to the pressure of the saturated bromine vapor. At the room temperatures at which the experiments were conducted, the pressure of the saturated bromine vapor is increased by approximately 15 % during a 5° change in temperature, which points to

the need to calculate the temperature dependence. Based on the known function relating pressure of the saturated bromine vapor with the temperature, and using the experimental data of the investigation of the periodic process, the following formula is obtained.

$$\varphi = 0{,}000\,146\,Q\,(30 + 7{,}88\,t), \tag{4}$$

describing the variation in the constant of bromine removal rate for the machine considered, depending on the feed rate of the bubbling oxygen Q (liters/minute) and the temperature t.

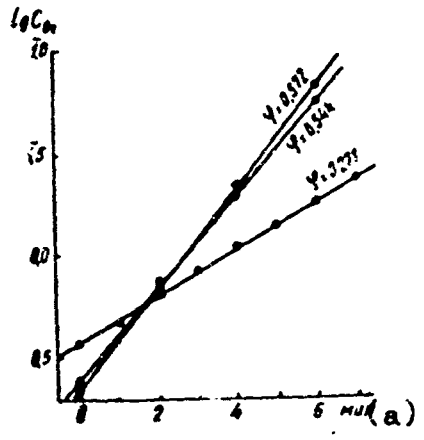

Figure 2. Graph change in composition of the bromine solution as a function of the duration of the experiment under periodic-process conditions. LEGEND: a)minutes.

We must dwell here on the peculiarities in the movement of the gas bubbles through the liquid in the machine. As can be seen from Figure 1, at the machine faces, the flow of bubbles at first deviates from the wall, and then, describing a steep arc, again approaches the machine faces at the surface of the liquid. Thus, a volume of liquid significantly free of bubbles is obtained, in which strong eddy flow of liquid will arise. During the installation of the partitions, this peculiarity in the movement of the bubble flow is retained, but is less clearly pronounced.

The second group of experiments had the purpose of investigating the continuous process in the machine fitted with extreme partitions, forming a receiving and overflow cell. Figure 3 shows the results of three experiments in the sublimation of bromine during a constant

consumption of oxygen and at fixed rates of bromine solution supplied until the steady state was arrived at.

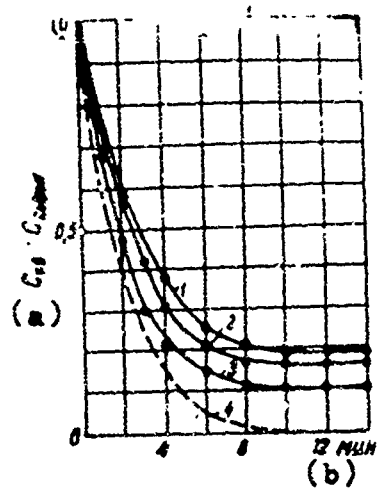

Figure 3. Graph of variation and the composition of the bromine solution under continuous process conditions up to stabilization of the process. t = 18°, consumption of gas = 20 liters/minute, volume of cell = 960 ml, rate of solution supply (in ml/min); 1 - 130; 2 - 100; 3 - 69; 4 - periodic process. LEGEND: a) $C_{tlgs} : C_{raw\ material}$; b) -minutes.

Plotted on the abscissae axis is the time elapsed, on the ordinate axis -- the ratio $C_{tlgs} : C_{raw\ material}$, since this quantity does not depend on the composition of the solution supplied. In 10-12 minutes, the composition of the solution flowing from the cell no longer changes, which points to a steady state. Observation of the intensity of the color of the bromine solution showed that in the head part of the machine a very decided fading of the color of the solution flowing from the entrance cell is observed, then it is steadily fainter along the direction of flow. In this cell, whose length exceeds the width by ten times, the mixing action of the gas bubbles does not equalize the composition of the solution and an appreciable drop in concentration is established in the direction of the flow. A sample of solution measured at a distance of one-third of the machine length from the entrance chamber showed that the bromine concentration was 0.97 g/liter at a composition of the tailings of 0.63 g/liter and of the feed composition equal to 6.47 g/liter.

Table 2 shows the characteristics of the action of the machine under steady state conditions and the results of calculations made for five experiments.

TABLE 2

Characteristics of the Process of Bromine Removal from Solution in a Single-cell Machine Functioning in a Steady State Condition

(a) Экспериментальные данные							(i)	(b) Расчетные данные	
(c) Температура, °C	(d) Расход газа, л/мин	(e) w, мл/мин	(f) v/w, мин	(g) при C = 1, г/мин	(h) $C_{сырья}$, г/л	$C_{хв}$, г/л	Технологическое действие процесса $w \lg \frac{C_{сырья}}{C_{хв}}$	(j) $C_{хв}$ периодического процесса (5), г/л	(k) $C_{хв}$ непрерывного процесса (3), г/л
16	20	33	26.6	0,155	4,0	0,237		0,000	0,31
18	20	69	12.7	0,501	6,47	0,630	70	0,011	0,85
18	20	100	8,8	0,501	5,24	0,870	78	0,053	0,97
18	20	130	6,7	0,501	4,00	0,770	93	0, 39	0,92
18	22	130	6.7	0,551	4,00	0,534	--	0,099	0,85

LEGEND: a) experimental data; b) calculated data; c) temperature, °C; d) gas consumed, liters/min; e) w, ml/min; f) v/w, minute; g) at C = 1, g/min; h) $C_{raw\ material}$, g/liter; i) technological action of the process $w \lg C_{raw\ material} / C_{tlgs}$; j) C_{tlgs} of periodic process (5), g/l; k) C_{tlgs} of continuous process (3), g/l.

Listed are: temperature, rate of oxygen supplied, composition and rate of feed, the quantity φ calculated according to formula (4), the value of the formal residence of the solution through the working cell of the machine V/w in minutes, composition of tailings (capacity of cells taken as 880 ml, since of the 960 ml in the machine 80 ml are in the receiving and overflow cells, where the solution is not aerated and does not change in its composition), and the special characteristics of "technological action of the process," equal to the product of productivity w by the logarithm of the extent of tailings depletion.

$$w \lg \frac{C_{сырья}}{C_{хв}}.$$

In the study /5/ is presented the value of such a characteristic in the analysis of the performance of the machine during continuous-process conditions, since a similar characteristic of this machine operative under the same value of the constant φ, under periodic-process conditions does not depend on the composition of the tailings and has a maximum value. In the next to the last column in Table 2 is presented the composition of the tailings calculated by the formula

$$2,303 \lg \frac{C_{сырья}}{C_{хв}} = \varphi \frac{V}{w}, \qquad (5)$$

describing the operation of a hypothetical machine in which mixing in the longitudinal direction is wholly excluded /5/. Such a tailings composition in this machine would be found during periodic-process operating conditions for a period of V/minutes. Presented in the last column are the tailings compositions calculated by formula (3) describing the operation of the machine under the condition of complete equalization of the composition of the cell contents. Such operating conditions correspond to mechanical flotational machines with a short cell.

Comparison of the experimental values of the bromine concentration in the machine tailings with the calculated values for these quantities for the two limiting performance cases (next to the last and last column in Table 2), it is shown that at the machine length considered, the effect of mixing is very great, but is still far from maximum, since the experimental values of the concentrations are very far from the upper limit (next to the last column) but differ substantially from the lower limit (last column). Comparison of the values of the "technological action of the machine" shows that increasing the supply rate, other conditions being equal, increases process efficiency.

The third group of experiments was designed to estimate the influence of partitions forming a row of identical sections on the results of steady-state processing. In Table 3, are included the results of the experiments for various numbers (1, 2, 5, 10) of identical sections in the machine. Presented are the observed concentrations of bromine in the machine tailings and the calculated concentrations, according to formula (3) for a unit composed of n consecutively linked machines. In the calculation of the value of V, the section volume equal to the volume of a machine 860 ml in volume is used divided by the number of sections.

Comparison with experimental data shows that the insulation of partitions is useful, since the roaming content in the tailings invariably decreases with increase in number of partitions. Machines with 2, 5, and 10 sections produce richer tailings than aggregate units of the same number of flotation cells, i.e., the sections considered are not equivalent to the theoretical cells of a flotation machine which has intensive mixing. The reason for lower indices of the machine in question is the imperfect separation of its sections formed by the partitions falling shy of the machine bottom by 6 mm. Actually, under each partition there will be formed a free opening extending the entire width of the cell occupying about 10 % of its transverse working cross section.

TABLE 3

Concentration of Bromine in the Tailings of a Machine Functioning Under Steady-State Conditions for the Listed Number of Partitions Forming Identical Cells, Temperature = 18°, Rate of Gas Feed = 20 liters/minute

(a) Характеристика процесса	(b) Ед. измерения	(c) Число отсеков в машине 1	2	5	10
(d) $C_{сырья}$ 5,24 г/л Br, φ 0,501	(g)				
(e) Скорость подачи питания	мл/мин	100	80	—	—
(f) Концентрация Br в хвостах (h)					
опытная	г/л	0,87	0,64	—	—
расчетная	"	0,96	0,41	—	—
(i) $C_{сырья}$ 6,47 г/л Br, φ 0,501					
(j) Скорость подачи питания	мл/мин	69	69	53	53
(k) Концентрация Br в хвостах:					
опытная	г/л	0,63	0,34	0,19	0,12
расчетная	"	0,88	0,52	0,049	0,015

LEGEND: a) process characteristics; b) units of measurement; c) number of sections in machine; d) $C_{raw\ material}$ = 5.24 grams/liter Br, φ = 0.501; e) rate of feed; f) concentration of Br in tailings: experimental, calculated; g) ml/min; h) g/liter; i) $C_{raw\ material}$ = 6.47 g/liter Br; j) and k) as in e and f, respectively.

Through these openings the exchange of mass takes place in both directions with the neighboring sections that results in a lower efficiency of the machine. It is obvious that improving the partition construction to limit exchange between sections should improve the indices of machine performance.

Results of the investigation showed that the process of bromine removal from the solution by the current of oxygen in the described model of the flotational machine under periodic-flotation conditions, obeys the relationship (1) only for the flotation of ideal, monomineral and monodisperse pulp. From this follows the validity, for the process of bromine removal, of the differential relationship (2) and also other relationships at the basis of which this differential dependence lies.

Experiments with solutions of bromine under continuous-process conditions demonstrated the justification for the propositions derived from the theoretical calculation for machines with a long cell, carried out in the study /5/. The experiments permitted an estimate of the role of longitudinal mixing in the long cell, the value of the partitions dividing the long machine into a number of sections, and the positive benefit from increasing the feed rate on the process indices.

Experiments with bromine solutions under continuous-process conditions can be used in investigating the various models of machines and the various constructions of partitions in order to select the best variants. It is possible to experimentally study by means of model machines transient conditions, whose calculation is very laborious. With a model of the process, these studies can be carried out with much less effort and with higher accuracy than with real pulps. Bromine is not the only material useful in modeling the flotational process. Any volatile substance inert to oxygen and which is soluble, obeying Henry's law, can serve for this purpose. Bromine tempted us by the simplicity and precision of its analytic determinations, which are the most laborious part of any technological study. Undoubtedly, the arsenal of chemistry will include other, more convenient materials for modeling flotation, with which it will be possible to investigate industrial equipment as well.

It must be emphasized that from the viewpoint of the theory of similarity, in this study we are talking about similarity of processes governed by the relationship (2) at constant φ, but not about similarity of the solution of the volatile substance of an ideal pulp. Producing a solution modeling pulp under any conditions of the flotation process would be very tempting, since it would open up the way for obtaining an objective and reproducible quantitative evaluation of such characteristics as the quantities "aeration" and "flotation activity" of the mineral in the pulp. However, available experimental material is inadequate to resolve the question of the presence or absence of more profound analogies in the processes compared.

CONCLUSION

It has been shown that the process of removing a volatile substance by currents of gas bubbles from an aqueous solution obeying Henry's law models the process of the flotation of an ideal, monomineral, and monodisperse pulp. Experiments on models shows the validity of all the relationships stemming from the differential equation

$$dC = -C\varphi\, dt,$$

describing the relationship of ideal pulp flotation under "free flotation" conditions.

LITERATURE

1. A. D. Pororelyy, N. M. Demido, I. M. Matveyev, Izvestiya vysshikh uchebnykh zavedeniy -- Tsvetnaya metallurgiya, No 6, 16 (1961).
2. A. D. Pogorelyy, ibid, No 1, 33 (1962).
3. A. D. Pogorelyy, ibid, No 5, 59 (1961).
4. K. F. Beloglazov, Zakonomernosti flotatsionnogo protsessa (Relationships in the Flotational Process), Metallurgizdat, 1947.
5. A. D. Pogorelyy, Izvestiya vysshikh uchebnykh zavedeniy -- Tsvetnaya metallurgiya, No 2, 1963.

SUITABILITY OF AN AQUEOUS ACETONE SOLUTION FOR MODELING THE FLOTATIONAL PROCESS

The inconvenience of working with elemental bromine forced us (the study was carried out with the participation of Engineer G. F. Kochetova) to search for substitutes avoiding the necessity for working under pressure. Acetone, CH_3COCH_3, boiling at 56°, soluble without limit in water, and easily and accurately determined quantitatively by the iodometric method, can serve as such a substitute. Experience in the evaporation of acetone from aqueous solutions containing 4 grams/liter of CH_3COCH_3 in stabilized current of air bubbles at room temperatures showed that the rate of acetone removal is proportional to its concentration in solution. It follows from this, that such solutions can be used for modeling the process of flotation of an ideal pulp, instead of bromine. Working with such solutions can be conducted without special precautions taken, in the usual laboratory setting with normal ventilation. For the determination of acetone in solution, it is possible to use the Messinger method (Berl' Lunge, Khimiko-tekhnicheskiye metody issledovaniya (Chemical-Technical Research Methods), Vol III, No 2, page 267, GNTI, 1941). According to this methods, 50 ml of 1 IN KOH solution and 50 ml of 0.1 N iodine solution is added to 10 ml of the acetone solution to be analyzed which has been poured into a conical flask fitted with a ground glass stopper, the acetone is combined with the iodoform according to the reaction

$$CH_3COCH_3 + 6I + 4KOH = CHI_3 + CH_3COOK + 3KI + 3H_2O$$

The excess iodine in the alkaline medium is converted into a mixture of iodide and iodate. To complete the reaction and to coagulate the iodoform, the mixture is kept in the flask for 30 minutes with periodic agitation. Then, 50 ml of 1 NHCl solution is accurately poured into the

flask. Here, the iodide and iodate form elemental iodine, which is back titrated with thiosulfate in the presence of starch; the iodoform here remains unchanged. The difference between the amount of iodine introduced into the sample and the excess iodidine back titrated with thiosulfate gives the amount of iodine reacting with the acetone. One ml of an 0.1 N iodine solution is equivalent to 0.9667 mg CH_3COCH_3.

Received by editor
6 February 1963

MECHANISM OF ACTION OF POLYACRYLAMIDE FLOCCULANTS

S. F. Kuzkin, V. P. Neber, I. A. Yakubovich, S. N. Zolin

(Moscow Institute of Steel and Alloys, Chair of Rare Metal Ore Beneficiation.)

At present there does not exist a unified unanimous concept of the mechanism of action of polyacrylamide flocculants. This is due not only to the complexity and variety of the composition of the solid and liquid phases of the suspension, but of the flocculants themselves. Also, a unified opinion does not exist as to the optimum composition of polyacrylamide flocculants. The flocculants produced presently are not pure polyacrylamides, but the copolymer acrylamide and acrylic acid of various compositions and molecular weights (in the following, products containing polyacrylamide and its derivatives will be noted by the symbol PAA).

Authors studying the adsorption of PAA on minerals /1,2/ assumed that its molecules are attached due to hydrogen bonds through the amide and undissociated carboxyl group simultaneously on two or more particles, forming "bridges" uniting them into aggregates. The dissociated carboxyl groups, due to electrostatic repulsion, induce the straightening of the polymer chain in solution and increase its length, promoting adsorption of the macromolecules simultaneously on several particles. The possibility of bonding by means of the carboxylate ion is not precluded.

Several investigators established that in the presence of PAA the ζ-potential of mineral particles is lowered as the result of their coagulation /3-5/. Binding of the particles by PAA macromolecules (flocculation) intensifies this effect. However, the opinion does exist /6/ that the ζ-potential does not have decisive significance in the aggregation of a PAA suspension.

In our investigations, in addition to the sedimentation experiments we measured the ζ-potential by the flow and adsorp-

tion method /5/ using specially synthesized labelled PAA of several molecular weights and extensive hydrolysis (See Tables 1 and 2). The labelled PAA was produced from ethylene chlorohydrin and labelled with C^{14}-sodium cyanide. Determination of the molecular weight was carried out according to the formula in /7/. Measurements of viscosity were performed using a capillary medical viscosimeter. Precipitation of pure minerals (quartz, microcline, muscovite, calcite, and others) and mixtures was carried out both with industrial as well as with specially synthesized samples of PAA of various molecular weights and degrees of hydrolysis. The minerals were crushed in porcelain mortars to a coarseness of -44 microns. The sedimentation experiments were carried out at room temperature and a solid:liquid ratio of 1:10.

Unlabelled samples of hydrolyzed PAA were produced from the unhydrolyzed sample 1, and the labelled samples -- from sample 4. Hydrolysis was performed by heating equal volumes of a 1% solution of PAA and 1N sodium hydroxide on a waterbath at 60 - 70° for various intervals of time. The degree of hydrolysis was determined by Kjeldahl combustion and colorimetric determination of the ammonium salts.

In the adsorption measurements a mineral sample weighing 1 - 2 grams was mixed with a solution of labelled PAA in a test tube with a solid: liquid ratio of 1:5. After filtration of the suspension, the precipitate was repulped with distilled water at a S:L ratio of 1:10, and was filtered once again. Drying was conducted at a temperature not above 40°, after which the powder was mixed thoroughly and part of it was transferred into a cassette. The activity was measured by an end-window counter fitted with a thin mica aperture.

It was found /5/ that PAA strongly aggregates particles of positively charged minerals (calcite, fluorite), lowering their electrokinetic potential. On negatively charged minerals--quartz and microcline in distilled water or in alkaline medium and in the absence of reagents lowering the negative ζ-potential, PAA does not adhere to surfaces of minerals, does not change their ζ-potential, and does not aggregate the suspension. Flocculation can occur only during preliminary lowering of the -potential of minerals down to less than 30-40 millivolts. The carboxyl groups PAA act not only toward the extension of the polymeric chain, but also toward preventing adsorption of the flocculant on surfaces, which fact proves to be decisive for negatively charged particles of quartz and microcline. At the same time, carboxyl groups promote adsorption of the reagent on positively charged surfaces.

It was also established that in spite of the negative ζ--potential of natural minerals--quartz and microcline, PAA is adsorbed on them, lowers their ζ-potential, and flocculates suspensions of these minerals (Fig. 1). This is accounted for by

TABLE 1

Characteristics of Samples of Unhydrolyzed PAA.

(a) № образца	(b) Характеристическая вязкость, пуаз	(c) Молекулярный вес в млн. O_2 ед	(d) Активность, мс/г
1	5,1	1,82	—
2	3,2	0,91	—
3	2,6	0,68	—
4	1,9	0,43	ок. 0,6
5	1,3	0,23	ок. 0,6

LEGEND: a) Sample No.; b) Characteristic viscosity, poises; c) Molecular weight in millions of O_2 units; d) Activity, mc/g.

TABLE 2

Characteristics of Hydrolyzed Samples of PAA.

(a) № образца	(b) Продолжительность нагрева, мин	(c) Содержание орган. азота, %	(d) Степень гидролиза, %
6	10	17,2	12,7
7	20	15,1	23,2
8	30	11,7	40,7
9 (меченый) (e)	20	15,7	20,3

LEGEND: a) Sample No.; b) Duration of heating, minutes; c) Content of organic nitrogen, %; d) Extent of hydrolysis, %; e) Labeled.

the natural activation of the minerals by polyvalent ketones. After treatment of the mineral surfaces with hydrochloric acid and washing, the ζ-potential of quartz and microcline remained almost unchanged. However, thereafter PAA did not adhere to minerals, did not reduce their ζ-potential, and did not flocculate. In the attachment of PAA on the ketone centers of the minerals, which have a total negative charge, the charge was reduced to the coagulation threshold (-30 millivolts).

If PAA adheres to particles with a positive ζ-potential, then full compensation of the charge on the internal facing of the double electric layer occurs; the particle becomes electrically neutral (for low amounts of PAA), or actually acquires a low common negative ζ-potential (for large amounts of PAA).

As the result of experiments conducted it was established that with increased molecular weight of PAA flocculation of minerals rises (Fig. 2), and that the higher the molecular weight of PAA, the more of it is adsorbed on minerals, but the monomers are not adsorbed.

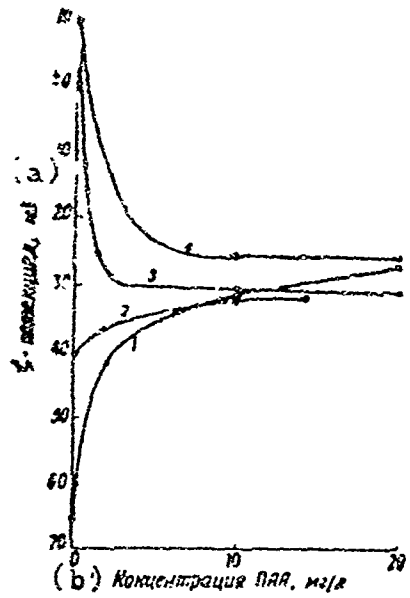

FIGURE 1. Effect of PAA on the ζ-potential of the following minerals: 1 - quartz; 2 - microcline; 3 - calcite; 4 - fluorite. LEGEND: a) ζ-potential, mv; b) Concentration of PAA, mg/l

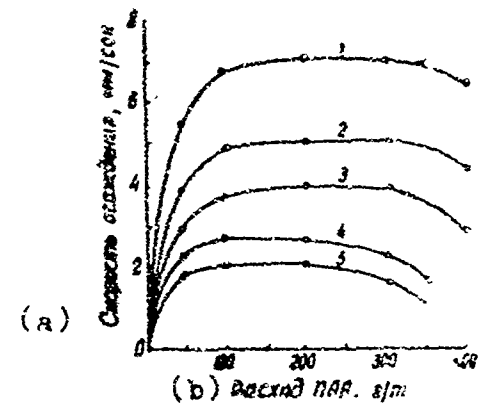

FIGURE 2. Effect of molecular weight of PAA on the precipitation of SiO_2 (pH = 2). Molecular weight in millions: 1 - 1.8; 2 - 0.91; 3 - 0.68; 4 - 0.43; 5 - 0.23. LEGEND: a) Precipitation rate, mm/sec; b) Consumption of PAA, g/t.

Study of the effect of the pH of the medium showed that pure silicic acid, whose surface is completely free of cations, does not aggregate PAA independently of the extent of hydrolysis and molecular weight in neutral and weakly alkaline media; for pH values lower than 3, strong aggregation is observed (Fig. 3). In accordance with this, PAA independently of the extent of hydrolysis is adsorbed strongly in an acid medium (Fig. 4). In contrast to pure silicon dioxide, natural quartz, and also microcline and muscovite, are readily flocculated with PAA in acidic and neutral media; accordingly, adsorption in a neutral medium is almost equal to adsorption in an acidic medium.

It was additionally established that with an increase in the effect of the extent of PAA hydrolysis flocculation of silicate minerals is worsened independently of the medium pH, here the adsorption of hydrolyzed PAA is somewhat weaker. PAA adsorbed

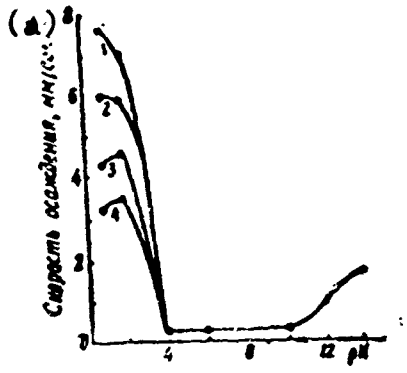

FIGURE 3. Effective pH of the medium on the precipitation of SiO_2 with PAA. Extent of hydrolysis of PAA (in %): 1 - < 1; 2 - 12.7; 3 - 23.2; 4 - 40.7

LEGEND: a) Sedimentation rate, mm/sec

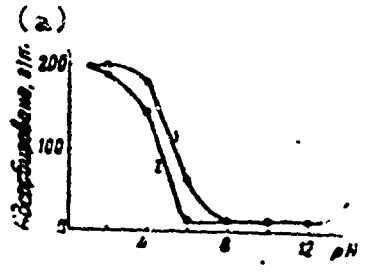

FIGURE 4. Effective pH of the medium on the adsorption of PAA on SiO_2. Extent of hydrolysis of PAA (in %): 1 - < 1; 2 - 20.3.

LEGEND: a) Adsorbed, g/ton

in an acidic medium, both when hydrolyzed and when unhydrolyzed, can be removed by simple rinsing with distilled water almost completely from the surface of pure silicon dioxide, and to a significant extent from the surface of natural silicate minerals. Moreover, hydrolyzed PAA is more rapidly eliminated (Fig. 5). A similar picture is also observed in strongly alkaline medium (pH = 12-14), where certain increase in flocculation is observed as compared with a weakly alkaline medium (Fig. 3). In contrast to silicate minerals, flocculation of salt-like minerals depends little on these pH (calcite, apatite, barite), and adsorption is significantly greater and is irreversible. An increase in the extent of hydrolysis lessens their flocculation with PAA in a neutral medium only for increased concentrations of the flocculant. Adsorption changes little with increase in extent of PAA hydrolysis.

These facts suggest the thought that the mechanism of attachment and flocculation with PAA in acidic, neutral and alkaline media is dissimilar. If in neutral and alkaline media, where strong dissociation of carboxyl groups takes place, the action of the PAA is satisfactorily explained by a reduction in the ζ-potential of the minerals when PAA is adsorbed on them (at the carboxyl groups), and also is accounted for by the binding of the particles by PAA molecules, than in an acidic medium where the carboxyl groups do not dissociate, and the ζ-potential of minerals is near zero, such an explanation is unsatisfactory. Favorable conditions exist in an acidic medium for formation of hydro-

gen bonds between the mineral surface and the amide and undissociated carboxyl groups of the PAA, also ketonic bonding through the dissociating amide groups. Therefore, the action of PAA in an acidic medium is due only to the formation of bridges of PAA molecules uniting the particles into aggregates, but the ζ -potential and mechanism of usual coagulation do not play a significant role.

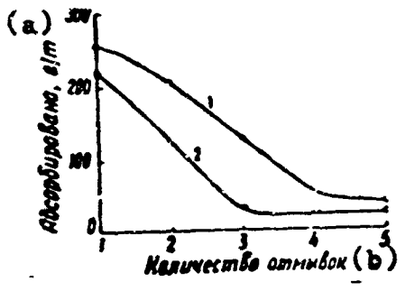

FIGURE 5. Desorption of PAA from the SiO_2 surface in rinsing with water (after adsorption in an acidic medium). Extent of PAA hydrolysis (in %): 1 - <1; 2 - 20.3. LEGEND: a) Adsorped, g/ton; b) Number of rinsings

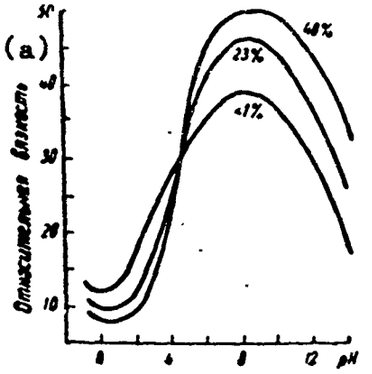

FIGURE 6. Viscosity of 0.5% solutions of PAA as function of pH and extent of hydrolysis. LEGEND: a) Relative viscosity

Study of the viscosity of solutions of various PAA as a function of pH revealed that PAA had a minimum viscosity at pH = 1.2, however, with further increase in the acidity of the medium the viscosity begins to rise, confirming the existence of weak dissociation of the amide groups (Fig. 6). Thus, in a strongly acidic medium PAA manifests the properties of a weakly cationic polyelectrolyte. The minimum viscosity in the acidic medium is accounted for by the strong intramolecular interaction of undissociated carboxyl groups, causing the coagulation of PAA molecules. This apparently is caused by the weakening of the flocculation of the suspensions with increase in extent of hydrolysis (in an acidic medium).

The maximum viscosity is observed in a weakly alkaline medium due to the dissociation of PAA in the anionic mode due to the carboxyl groups. With increase in extent of hydrolysis, i.e., the content of carboxyl groups, the viscosity is increased, while in an acidic medium it is lowered.

In neutral and weakly alkaline media pure silicon dioxide does not adsorb PAA and is not flocculated, since the negatively charged carboxylate ions do not adhere to its surface. Upon the

addition of iron or calcium cations pure silicon dioxide begins to attract PAA and is strongly aggregated in neutral and alkaline (Figs.7,8). However, with increase in extent of hydrolysis of PAA flocculation deteriorates, in spite of the increase in the length of the flocculant molecules in the solution. Such behavior is caused by the fact that the increase in the number of dissociated carboxyl groups in the PAA molecules increases the negative charge of the particles after PAA is attached to them, and on the other hand, this increase in the number of dissociated carboxyl groups prevents adsorption of the groups on negatively charged surfaces.

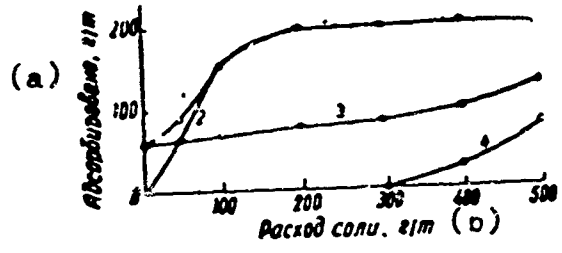

FIGURE 7. Effect of inorganic salts on adsorption of PAA on SiO_2 in a neutral medium; 1-$FeCl_3$ - unhydrolyzed PAA; 2-$FeCl_3$ + PAA, 20.3% hydrolyzed; 3-$CaCl_2$ + unhydrolyzed PAA; 4-$CaCl_2$ + 20.3% hydrolyzed PAA.
LEGEND: a) Adsorbed, g/ton; b) Salt consumed , g/ton;

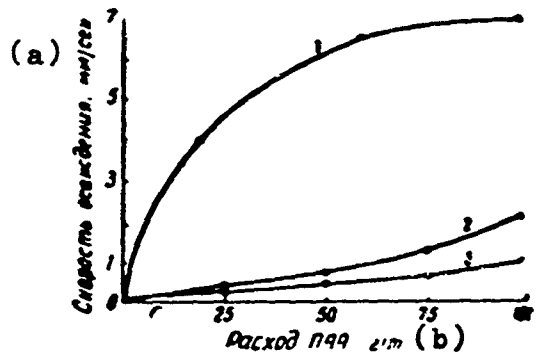

FIGURE 8. Effect of extent of PAA hydrolysis on the precipitation of SiO_2 activated with iron salts. Extent of PAA hydrolysis (in %): 1 - 1; 2 - 12.7; 3 - 23.2
LEGEND: a) Sedimentation rate, mm/sec; b) Consumption of PAA, g/tons

With an increase in the number of positively charged centers on the surfaces (which for instance is always achieved on salt-like

minerals), the distinction in attraction as between hydrolyzed and unhydrolyzed PAA disappears, while the difference in the aggregating action is diminished. This can be explained as due to a decrease in the ζ-potential of the particles in the presence of cations, but also by the facilitation of bridge-formation due to the association of macromolecules through cations and carboxyl groups with the formation of more durable and longer bridges. It is known that, however, when the salt content is too high the aggregating action of PAA diminishes. Thus, in real pulps, depending on the pH, salt concentration, diameter and composition of the solid phase, the consumption of the flocculant, the size, form, and adsorption of macromolecules, their association and bridge-formation will fluctuate. In agreement with this variability, the optimal extent of hydrolysis in neutral and alkaline media will be dissimilar and each case must be approached individually.

In an acidic medium, in all cases the carboxyl groups cause the coagulation of PAA molecules and these hinder the formation of connecting bridges between the particles. Therefore, in an acidic medium, it is necessary for all ore pulps to use unhydrolyzed PAA. A study of the effect of mixing has on the action of PAA revealed that with increased duration of mixing with the flocculant, independently of its composition and pH, flocculation of suspensions is deteriorated, although the amount of reagent adsorbed for a small consumption of flocculant remains unchanged, while for large amounts consumed, the amount of reagent adsorbed in some cases is even increased. This suggests that during flocculation, geometric configuration and mutual location of molecules in the adsorbed state play important roles in addition to adsorption.

For all the minerals studied, when the consumption of PAA was raised above a certain value, depending on the mineral and the conditions of the medium, deterioration of PAA flocculating action set in.

This data leads to the conclusions that during flocculation partial non-uniform covering of the mineral grain surfaces occurs. Upon total covering being achieved stabilization begins. In flocculation with high-molecular weight macromolecules bridges will be formed between the particles, binding them into a stable aggregate. The existence of such bridges is proved by direct observations with the electron microscope /8/. This feature differentiates their action from the action of other compounds and is caused by the specific properties of the polyelectrolyte molecules: high molecular weight, flexibility, sharply asymmetric structure, and the presence of ionogenic groups capable of forming various kinds of bonds, both strong and weak.

Upon addition to the suspension of a PAA solution, its molecules as a result of thermal motion arrive at the particle surfaces and given the presence of the appropriate centers are held

there. The remaining part of the macromolecule remains in solution in the form of the waving tail or tentacle. When continuous collision of particles is in effect, these tentacles are fastened to other particles. The probability of such cohesion of particles is increased with greater tentacle length; this cohesion is possible only in the case when their length is not less than the thickness of the double electrical layers surrounding the particles.

Thus, for the most effective bridge formation the macromolecule should include in its composition ionogenic groups in small numbers. Weakly hydrolyzed PAA satisfies this requirement, having a small number of carboxyl groups in neutral and alkaline media, but in strongly acidic medium--a small number of dissociating amide groups.

The situation is however complicated by the fact that the macromolecules in solution have a great tendency toward association /9,10/. The size and nature of these associates depends on the concentration of the polymer, salts, on the pH, molecular weight, and other factors. The effective cohesion of two or more particles can be achieved as the result of the association of macromolecules already adsorbed at one end. Durable associates will most frequently be formed as the result of the action of hydrogen bonds, however, in the presence of polyvalent cations they can be formed also between ionogenic groups united through cations. Association is promoted by the heterogeneity of the surface of the solid particles, as a result of which local increase in the macromolecular concentration occurs (both those attached to one particle as well as those attached to two at the same time). The association of macromolecules after adsorption leads to an increase in the durability of the cohesion of particles by virtue of the formation of polymolecular bridges, which under certain conditions take on the character of a separate phase of the gel type, exhibiting mechanical durability and elasticity /10,11/.

With increase in PAA concentration its adsorption on surfaces increases. If the PAA has many dissociating carboxyl groups (as in the case of strongly hydrolyzed PAA in neutral medium), then as a result the ζ-potential of the particles increases and their stability is greater. However, stabilization during increased consumption of weakly hydrolyzed PAA flocculants cannot be explained by the increase in the ζ-potential, since the flocculants do not bring about a significantly higher ζ-potential.

As was shown by B. V. Deryagin and co-workers /12/, during adsorption of polymers the thickness and stability of the wedging hydrate layers increases. A similar effect is revealed also with PAA: by means of flotation experiments /13/ and measurement of the boundary angles of wetting /14/ it was revealed that PAA increases the hydrophilization of the surface, especially at high concentrations.

Initially, with increased consumption of PAA a two-dimensional strongly hydrated film will be formed, giving the particles additional stability /12/. With still higher consumption an independent phase will be formed in the form of a thick gel-like film, and with sufficient amount of PAA a mechanically strong gel-like structural network will be formed at distances exceeding the dimensions of separate grains and their aggregates all throughout the bulk of this suspension or of a significant portion of it /11/. As a result, precipitation of particles and their units is greatly retarded or halted completely.

Conclusions.

1. Aggregation of suspensions by polyacrylamide flocculants is caused by strong adsorption of the macromolecules simultaneously on several particles with the formation of durable bridges between them. This effect can be intensified as a result of a reduction in electrical charge on the particles.

2. Stabilization of suspensions at increased concentrations of the polyacrylamide flocculants is caused by an increased attachment of the polymer molecules on the particles. As a result of the significant surface covering by these macromolecules the charge of the particles is increased, along with an increase in the thickness and durability of the wedging hydrate layers up to the formation of a mechanically stable gel-like structure throughout the bulk of the suspension.

3. To accelerate thickening and filtration of ore pulp in an acidic medium it is necessary to apply weakly hydrolyzed polyacrylamide flocculant, and in neutral and alkaline media--hydrolyze. The optimal extent of hydrolysis in a neutral medium should be selected individually for each pulp together with reagents containing polyvalent cations.

LITERATURE

1. Michaels, A. S., Morelos, O., Ind. Engng. Chem., 47, No. 9, 1955.
2. Maslenkova, G. L., Kolloidnyy zhurn. (Colloidal Journal), No 5, 1961.
3. Tsun-chien, Ch'an, K issledovaniyu mekhanizma osazhdeniya ugol'ny shlamov i osvetleniya shlamovykh vod s dobavleniem polnakrilamida (Investigation of the Mechanism of Sedimentation of Coal Sludges and Clarification of Sludge Water by Addition of Polyacrylamide), Moscow, 1960.
4. Healy, T. W., Journal Colloid Science, 16, 609 (1961).
5. Kuz'kin, S. F., Nebera, V. P., Tr. Mintsvetmetvolota (Works of the Ministry of Nonferrous and Gold Metallurgy), No 33, 1960.

6. Gorlovskiy, S. I., Khaymman., V. Ya., Obogashcheniye rud (Beneficiation of Ore), No 4, 1961.
7. Amer. Cyanamide Co., New Product Bull., No. 34, 1955.
8. Beutelspacher, H., Z. Pflanzenernahr., Dung., Badenkunde, 69, 108 (1955).
9. Kargin, V. A., Bakeev., N. F., Kolloidnyy zhurn, 19, 133 (1957).
10. Voyutskiy, S. S., Rastvory vysokomolekulyarnykh soyedineniy (Solutions of High-Molecular Compounds), Moscow, 1960.
11. Rebinder, P. A., Aron, Ya. B., DAN SSSR (Reports of the Academy of Sciences, USSR), 52, No 3, 1946.
12. Deryagin, B. V., Kusakov, M., Izv AN SSSR, OMYeN (News of the Academy of Sciences USSR, Math-Phys. Division), No 5, 1936.
13. Kuz'kin, S. F., Zolin, S. N., Izv vUZ, Tsvetnaya metallurgiya, No 4, 24 (1961).
14. Zelenov, V. I., Intensifikatsiya protsessa sgushcheniya pul'p na zolotoiz-vlekatel'nykh fabrikakh putem primeneniya sinteticheskikh flokulyantov (Intensification of the Process of Coagulation of Pulp at Gold-Recovery Plants by Using Synthetic Flocculants), author's abstract of candidatorial dissertation, Moscow, 1962.

Received by Editor
20 February 1963

DETERMINATION OF THE OPENNESS OF MINERAL GRAINS USING AN ANALYTICAL METHOD

V. M. Galich

(Mekhanobr Institute)

For quantitative evaluation of the relationships between free mineral grains and their concretions at present the gravitational method of determining the nature of impregnation by means of separation of graded material in gravity solutions (1,2) is used. With this method the total content of inclusions is determined and not solitary inclusions, therefore the data obtained is more reliable in predicting the behavior of ore during beneficiation.

An advantage of the gravitational method is also the possibility of operating with comparatively large batches, which is particularly important in appraising ores with uneven impregnation and with a low metal content, where the application of other analytical methods proves to be not very effective.

Comparison of the results of gravitational analysis of similar size classes of ore samples for various degrees of crushing showed that the increase in extraction of ore minerals in the heavy fractions with increasing extent of crushing of the samples is due in the main to an increase in the yield of the finer classes, affording increased extraction as compared to the coarser material.

The research methods developed and treatment of results made it possible to establish, in studying various ore types, with sufficient accuracy the relationship of the freeing molybdenite from concretions and revealed the character of the concretion of minerals in molybdenum and copper-molybdenum ores of the Kavzhidinskiy, Shakhtominskiy, and Syrygichinskiy deposits.

A preliminary microscopic study of the samples produced a general picture of the mineralogical composition and impregnation of molybdenite. The samples studied can be divided into three types:

The first type is characterized by a comparatively large sulfide separations; the main size of the molybdenite scales associated with the sulfide aggregates are as long as 0.32-0.48 mm, and 0.01-0.03 mm in thickness (samples of the Dzhidinskiy and Shakhtominskiy deposits);

The second type is represented by thin non-uniform impregnation of molybdenite and sulfide. The main size of the molybdenite inclusions amounts to a length of 0.22-0.36 mm, a thickness of 0.01-0.02 mm (sample from the Kadzhidinskiy deposit);

The third form is distinguished by very fine non-uniform impregnation with intimate mutual intergrowth of sulfides and rock. The size of the molybdenite inclusions varies from 1/1000th millimeter to 0.21 mm (samples from the Shakhtominskiy deposit).

Below the Dzhidinskiy and Shakhtominskiy deposits are considered in detail, which differs sharply from each other both as to actual composition as well as impregnation.

Each of the samples investigated was crushed over different periods of time, the unloading of the grinding mills and also the flotation products underwent dispersion-screen analysis with subsequent chemical analysis of each class. This data was compared with the results of the separation of narrowly classified material in gravity solutions(Tables 1 and 2, Figure 1).

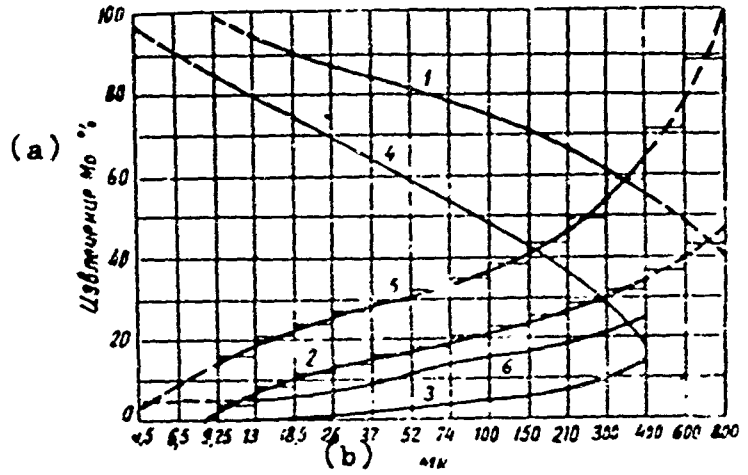

Figure 1. Results of separation in gravity liquids of pulverized or of the Dzhida fraction: 1 -- heavy; 2 -- light; 3 -- average. Syrygichiy fraction: 4 -- heavy; 5 -- light; 6 -- average. Time of pulverization = 10 minutes. LEGEND: a) Recovery of Mo, %; b) microns

In so doing, relationships were obtained between the molybdenite in the form of free grains or rich concretions (heavy fractions) and molybdenite

TABLE 1

Results of Separation in Gravity Fluid of Size Classes of Dzhidinskiy Deposit Ore

(a) Крупность класса, мк	(b) Тяжелая фракция, уд. вес > 2,89					(c) Промежуточная фракция, уд. вес < 2,89 > 2,70					(d) Легкая фракция, уд. вес 2,70				
	(e) Выход, %		(h) Содержание Mo, %	Извлечение от содержания Mo в классе, %	Извлечение от содержания Mo в руде, %	Выход, %		Содержание Mo, %	Извлечение от содержания Mo в классе, %	Извлечение от содержания Mo в руде, %	Выход, %		Содержание Mo, %	Извлечение от содержания Mo в классе, %	Извлечение от содержания Mo в руде, %
	от класса (f)	от руды (g)		(i)	(j)	от класса	от руды				от класса	от руды			
−400+300	1,91	0,034	0,550	57,90	0,98	4,24	0,076	0,026	11,58	0,18	93,84	16,893	0,092	20,52	0,53
−300+210	5,74	0,026	0,214	64,08	2,18	3,68	0,169	0,043	8,51	0,28	90,58	4,166	0,058	27,41	0,91
−210+150	8,93	0,071	0,656	69,23	6,94	2,99	0,356	0,117	6,24	0,61	91,08	10,839	0,015	24,53	2,45
−150+100	9,58	0,145	0,612	72,86	10,42	2,21	0,334	0,190	5,09	0,74	88,21	13,320	0,020	22,05	3,14
−100+74	11,75	0,149	0,421	76,25	9,00	1,80	0,229	0,161	4,27	0,51	86,45	10,979	0,015	19,48	2,29
− 74+52	11,19	0,108	0,438	79,78	8,70	1,61	0,156	0,118	3,11	0,35	87,20	8,458	0,011	17,11	1,85
− 52+37	16,44	0,145	0,249	82,60	7,27	1,33	0,117	0,075	2,06	0,18	82,23	7,236	0,009	15,34	1,35
− 37+26	17,78	0,151	0,209	85,45	6,56	1,05	0,089	0,057	1,02	0,11	81,17	6,899	0,071	13,53	1,03
− 26+18,5	21,21	0,140	0,167	88,69	6,28	0,67	0,044	0,030	0,79	0,04	78,12	5,156	0,005	10,92	0,78
− 18,5+13	21,62	0,091	0,122	92,24	4,70	0,46	0,019	0,043	0,51	0,04	77,92	3,273	0,003	7,25	0,37
− 13+9,5	25,50	0,084	0,078	96,25	3,56	0,21	0,007	0,047	0,32	0,02	74,23	2,450	0,001	3,43	0,12
(k) Исходный материал	1,250	3,140	0,328	78,82	66,59	1,730	1,590	0,308	3,63	3,07	97,02	89,670	0,0093	17,55	14,85

TABLE 2

Results of Separation in Gravity Fluid of Size Classes of Syrygichinskiy Deposit Ore

(a) Крупность класса, мк	(b) Тяжелые фракции, уд. вес > 2,89					(c) Промежуточные фракции, уд. вес < 2,89 > 2,7					(d) Легкие фракции, уд. вес < 2,70				
	Выход в % (f) от класса	(g) от руды	Содержание Mo, % (h)	Извлечение от содержания в классе, % (i)	Извлечение от содержания в руде, % (j)	Выход, % от класса	от руды	Содержание Mo, %	Извлечение от содержания в классе, %	Извлечение от содержания в руде, %	Выход, % от класса	от руды	Содержание Mo, %	Извлечение от содержания Mo в классе, %	Извлечение от содержания Mo в руде, %
—400+300	0,56	0,044	2,570	20,24	0,92	8,46	0,661	0,196	23,01	1,05	90,98	7,105	0,015	56,75	2,58
—300+210	1,22	0,137	2,557	29,33	1,95	8,01	0,899	0,272	20,52	1,36	90,77	10,184	0,0 0	50,15	3,37
—210+150	3,11	0,411	1,987	38,63	3,87	7,67	1,015	0,381	18,13	1,83	89,22	11,800	0,078	43,24	4,38
—150+100	4,02	0,546	2,139	45,42	5,35	7,12	0,968	0,435	16,60	1,97	88,26	12,090	0,080	37,98	4,10
—100+74	6,08	0,762	1,727	50,63	6,54	6,58	0,821	0,488	15,11	2,00	87,34	10,940	0,082	31,26	4,50
—74+52	8,57	1,429	1,833	56,50	9,81	5,09	0,949	0,599	12,09	2,13	85,74	14,300	0,102	31,11	5,70
—52+37	10,98	0,827	1,047	62,71	7,2	4,87	0,367	0,349	9,28	1,07	84,15	6,345	0,0 1	28,01	3,19
—37+26	12,59	0,601	0,563	66,12	4,43	4,24	0,202	0,193	7,76	0,50	82,57	3,929	0,031	36,12	1,74
—26+18,5	15,27	0,492	0,380	68,83	3,63	3,18	0,102	0,220	7,59	0,44	81,55	2,626	0,025	23,58	1,25
—18,5+13	14,10	0,338	0,192	74,39	1,69	2,25	0,054	0,089	5,12	0,12	83,65	2,007	0,008	20,19	0,44
—13+9,25	16,83	0,146	0,208	82,02	2,16	1,80	0,015	0,055	4,86	0,06	81,37	0,708	0,009	16,18	0,42
—9,25+6,5	18,68	0,232	0,123	87,49	1,43	1,56	0,019	0,064	4,21	0,06	79,76	0,989	0,001	10,95	0,18
—6,5+4,5	21,23	0,222	0,088	91,97	1,17	1,22	0,013	0,025	3,92	0,02	77,55	0,811	0,01	7,81	0,06
Исходный материал (k)	6,44	6,187	1,302	52,83	50,15	6,34	6,089	0,33	13,27	12,55	87,22	83,820	0,06	33,90	32,05

thinly interspersed in the country rock mineral in the form of very lean concretions containing empty ore (light fractions).

Used as the gravity liquid was bromoform with a specific gravity of 2.89 and bromoform, diluted with alcohol, with specific gravity of 2.7.

The operation of separation in gravity solutions for the size classes was carried out by means of standing in separatory funnels, for the fine classes -- by centrifuging in special plexiglas ampules. The fractions separated were rinsed free of the gravity solution, dried in a thermostat, and subjected to chemical analysis.

The results of the analysis (cf Tables 1 and 2) revealed that with reduced class size in each sample, the extraction of molybdenite into heavy fractions with increased, while in the intermediate and light fractions -- this extraction rate was reduced.

It is known that a high value of mineral openness leads to an increase in the extent of extraction in flotation given a favorable ratio of openness and overpulverization, i.e., when the first factor predominates over the second. Therefore, the optimum fineness range of ore pulverization is of undoubted interest.

LEGEND TO TABLE 1: a) Class size, microns; b) Heavy fraction, specific weight >2.89; c) Intermediate fraction, specific weight $<2.89>2.70$; d) Light fraction, specific weight <2.70; e) Yield, %; f)of class; g) of ore;h) Mo content, %; i) Recovery of Mo content in the class, %; j) Recovery from Mo content in the ore, %; k) Original material.

LEGEND TO TABLE 2: As for Table 1

According to the flotation experiments conducted followed by classification of the beneficiation products an evaluation was made and curves of the molybdenum extraction in the concentrate from the narrow classes of the original ore (Figure 2) were plotted. The curves show that the maximum molybdenite extraction from the products of the crushed Dzhidinskiy sample (at the optimum extent of pulverization) can be obtained from the size classes of -100 + 18.5 microns. For the corresponding products of the Shakhtominskiy sample the maximum extraction is obtained from size classes of -52 + 9.25 microns.

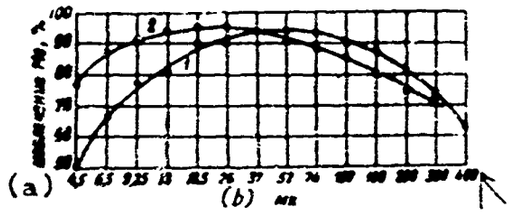

Figure 2. Recovery of molybdenum from narrowly classified material of grinding mill loads. 1 -- Dzhida; 2 -- Syrygichi. LEGEND: a) Recovery of Mo, %; b) Microns.

The results obtained (cf Table 1 and 2) give us a graphic picture of the limits of optimal openness of minerals, where the negative effect of overpulverization worsening the floatability of the mineral particles is not yet in evidence.

During the investigations it was found that the distribution of molybdenum by size classes is quite uniform with gradual increase in mineral content as the class size is reduced and with a certain drop in content in the finest classes of the pulverization products.

For the same duration of pulverization, in spite of the identical total yield of the classes in two, samples, the molybdenum distribution differed in these two samples; the extraction in the slurry portion (-4.5 microns) is lower for the more finely impregnated of Syrygichinskiy ore, in which consequently the useful minerals are subject to over-pulverization to a lesser extent.

The curve in Figure 3 illustrates this situation. Thus, in the pulverization of samples for thirty minutes, 17.39 per cent of the molybdenite belongs to the 13 micron class for the Syrygichinskiy sample, while 40.10, for the Dzhidinskiy sample.

Upon comparing the tests made it was noticed that the extraction of molybdenite concretions in corresponding classes of the intermediate fractions is significantly increased for the finely impregnated ore of the Syrygichinskiy sample, while in the heavy fractions of this sample molybdenite extraction falls off. This indicates that the openness of the mineral grains in finely impregnated ore occurs less intensively than in

coarsely impregnated ore of the Dzhidinskiy deposit. This is confirmed by theoretical calculations made for the purpose of determining the number of molybdenite concretions containing ore in each sample pulverized to differing coarsenesses.

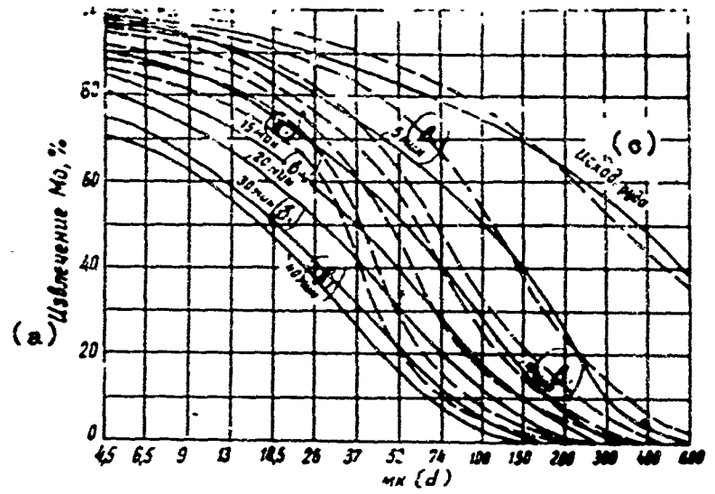

Figure 3. Distribution of Molybdenum by Size Classes in the Pulverization Products. Solid lines -- Dzhida; dashed lines -- Syrygichi. Numbers on the curves -- pulverization time in minutes. LEGEND: a) Recovery of Mo, %; b) Minute; c) Original ore; d) Microns

From Tables 1 and 2 we know the extraction in the light fraction of each class; for the calculations the average value $\varepsilon_{cp} = \frac{\varepsilon_1 + \varepsilon_2}{2}$ of extractions between classes was adopted.

The amount of concretions Q_{cp} of molybdenite in each ore class was determined from the formula

$$Q_{cp}^{(aver)} = \frac{\varepsilon_{cp} \cdot \varepsilon}{100},$$
$$(aver)$$

where ε_{cp} = average extraction in the light fractions;
ε = extraction of mineral in the narrow class.

Then, the total number of concretions Q in each class will be

$$Q_1 + Q_2 + Q_3 + \cdots + Q_n = Q,$$

where Q_1, Q_2, ..Q_n = number of concretions in each class.

The results of the calculations are presented in the form of curves in Figure 4 and Table 3.

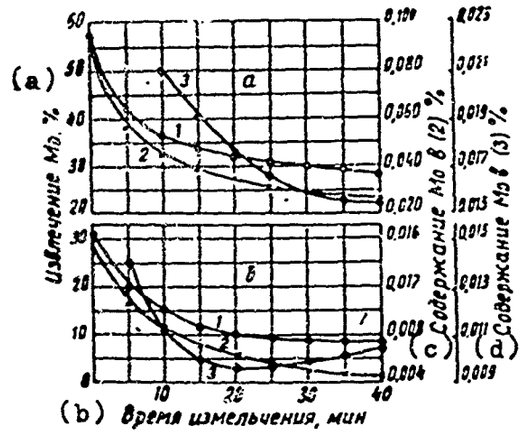

Figure 4. Comparative results of recovery of molybdenum in light fraction (1) and its content in the light fraction (2) and in the tailing (3) as a function of the pulverization time; a -- Syrygichi; b -- Dzhida. LEGEND: a) Recovery of Mo, %; b) Pulverization time, minutes; c) Content of Mo in (2), %; d) Content of Mo in (3), %

A sharp decrease in the number of concretions during the beginning moments (for pulverization lasting 5 and 10 minutes) occurrs with decreased coarseness of material, and then the opening up of the concretions takes place at this lower rate.

A practically quite complete release of molybdenum from the concretions containing country rock begins for coarsely-impregnated ore (Dzhida) for a coarseness of the order of seventy-four microns, when the content of these concretions does not exceed 8-10%, for finely impregnated ore (Syrygichi) at the same coarseness the release of molybdenum amounts to 25-30%, even for the 18.5+10 microns material -- only 20-22% of the total molybdenum content.

On comparing the data obtained with the results of flotation experiments conducted with various pulverization times, an increase in extraction is observed up to a definite point when mineral continues to be freed from the concretions, and then in spite of the fact that the opening of the minerals continues, extraction diminishes due to the slurrying of the molybdenite. It is easy to trace using curve 3 of Figure 4 that with increase in pulverization fineness the molybdenite content in the tailings is reduced due to the additional opening up of the concretions, but then increases due to overpulverization of

the free molybdenite grains.

TABLE 3

Comparative Results of the Quantitative Estimation of Concretions for Different Pulverization Times and Flotation Methods

(a) Содержание класса −0,074 мм, %	(b) Время измельчения, мин	(c) Количество сростков, %
(e) Исходная руда	(d) Джида	
0—3 мм	—	28 69
37	5	19,25
53	10	14,86
67	15	12,32
76	20	10,76
88	30	8,84
92	40	7,81
(e) Исходная руда	(f) Сырыгичи	
0—3 мм	—	57,20
28	5	38,24
41	10	32,15
52	15	29,85
64	20	27,45
80	30	24,77
88	40	22.79

LEGEND: a) Class content, -0.074 mm, %; b) Pulverization time, minutes; c) Number of concretions, %; d) Dzhida; e) Original ore; f) Syrygichi.

Conclusions

1. The dispersion-screen analysis of the pulverization products established the characteristics in molybdenite distribution into ore samples with differing Mo content and impregnation. It is shown that under identical conditions coarsely-impregnated ore of the Dzhidinskiy sample is subjected to overpulverization to a greater extent than is the finely impregnated ore of the Syrygichinskiy sample.

2. Based on the dispersion-screen and gravitational analysis a calculation was made of the number of molybdenum concretions in the

material obtained for various pulverization times that affords a clear picture of the optimal fineness in ore pulverization of differing impregnation.

3. Gravitational analysis of the products of narrowly classified samples established that with decrease in class coarseness in each sample, the extraction of molybdenite is increased in the heavy and decreased in the intermediate and light fractions; the degree of pulverization needed to liberate the minerals and concretions is achieved for the coarsely-impregnated ore (Dzhida) significantly earlier and more completely than for the finely-impregnated ore (Syrygichi). Thus, for practically opening up of molybdenum concretions containing rock, pulverization to 74 - 52 microns is sufficient for coarsely-impregnated ore, and 37 - 26 microns for finely-impregnated.

4. Preliminary investigation of ores using the gravitational-analytic method affords a possibility of obtaining a correct and sufficiently complete idea of the extent of openness of mineral components. This is of essential value both for the study of ores of new deposits as well as in the adjustment and control of technological processes at existing beneficiation plants.

LITERATURE

1. Dolivo-Dobrovol'skiy, V. V., Maslenitskiy, I. N., Forsh, D. V., Razrabotka metodiki opredeleniya vkraplennosti v syroy i droblennoy rude (Development of Methods of Determining Impregnation in Raw and Broken Ore), Mekhanobr, Leningrad, 1937.

2. Dolivo-Dobrovol'skiy, V. V., Sbornik "Teoriya i praktika obogashcheniya rud tsvetnykh i blagorodnykh metallov" (Collection: Theory and Practice of Beneficiation of Ores of Nonferrous and Noble Metals), Metallurgizdat, Sverdlovsk, 1940.

Received by Editor
18 April 1962

CALCULATION OF SURFACE TENSION OF MOLTEN HALOGENIDES AT INTERFACE WITH INERT PHASE AT MELTING POINT

O.K. Sokolov

Institute of Metallurgy of the Academy of Sciences U S S R

Knowledge of the surface tension of molten salts is highly important in pyrometallurgical processes, but also promotes advances in our ideas of the structure molten substances. In several studies /1-3/ are presented various criteria affording qualitative estimation of the surface tension of melts. In this article the problem is posed of deriving an equation for calculation of the surface tension of molten salts at the boundary with the inert phase at the melting point.

As is known /4/, the surface tension of molten salts at the boundary width the inert phase is determined by the following: interaction between the particles within the melt; crystal structure of the salt; value of the crystal lattice energy of the salt; size of the cationic radius for constant anionic radius. The surface tension of the melt itself can be defined as the Force acting on the surface layer over unit length.

As our starting point, we take the assumption that the melt consists of coordinations of ions, i. e., such a mutual orientation which corresponds to short-range orders of structure of the chrystal lattice. Thus, for instance, a melt of sodium iodide will be characterized by mutual orientation of cations with anions of iodine $Na_x I_x$, and a melt of calcium chloride -- by cations of calcium with anions of chlorine $Ca_y Cl_{2y}$, etc., in which the coordinations of the ions in the melt are not detached, but are in interaction with each other.

If, however, it is assumed that the melt consists of distinct ion coordinations, i.e., coordinations of ions not interacting with each other, and that the number of ions entering into coordination is minimum, then in this case the surface tension is

$$\sigma = \frac{F}{l}, \qquad (1)$$

where F = force of interaction between the ions of opposite sign, dyne;
l = path along which the force acts, cm.

The force then of interaction between ions of opposite sign is

$$F = \frac{Z_k Z_a e^2}{d^2}, \qquad (2)$$

where Z_k and Z_a = valencies of cation and anion;
e = charge on electron = $4.8 \cdot 10^{-10}$ absolute electrostatic unit;
d = distance between anion and cation in crystal, cm.

Calculating the force F according to equation (2), we in so doing take account of the main principles which govern the surface tension of melts.

It must also be noted that we have made certain assumption, when in equation (2) we place the value d equal to the distance between the anion and the cation in the crystal, and not in the value d equal to the distance in the anion and the cation for the melt at the melting point. This is necessitated by the fact that at present for most salts values of distance between anion and cation at the melting point are lacking. But since the value of the distance between the anion and the cation for the crystal and the melt at the melting point are close to each other /5-7/, then the error in calculating the surface tension at the melting point will be insignificant.

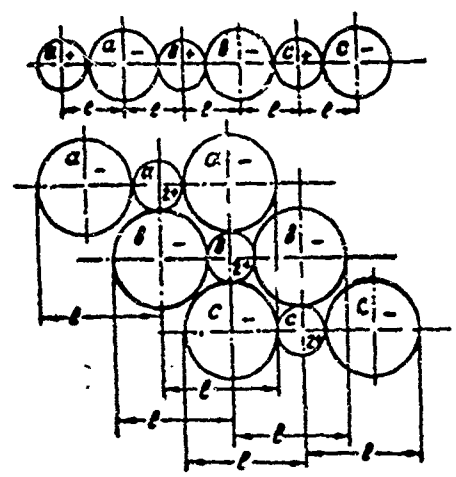

Figure 1. Minimum path along which the force acts in the melt (schematically).

The minimum path along which the force F acts (Fig 1) can be calculated from the equation

$$l = \frac{sd + ar_a}{m},$$

where R_a = radius of anion;

s = number of distances between anion and cation in the crystal for a "molecule";

a = number of anion radii in the "molecule" not entering into d;

m = number of cation radii in "molecule".

Actually, if we have a substance of the MeX type, then in this case b = 2, a = 0, m = 2, i.e.,

$$l = \frac{2d}{2} = d.$$

For a compound of MeX_2 we have: b = 2, a = 2, m = 2, i.e.,

$$l = \frac{2d + 2r_a}{2} = d + r_a.$$

As follows from Figure 1, the value of the l is that minimum distance at which the force F acts, and the entire melt will be comprised of the given minimal distances.

If the melt in reality consists of coordinations of ions that are isolated and that contain the minimal number of ions in coordination, then by placing the values of F and l in equation (1), we will obtain the value of the surface tension at the interface with the inert

phase at the compound's melting point. And in order to obtain from equation (1) the value of the surface tension expressed in dynes/cm, it must be multiplied by the coefficient $K = 10^{-2}$

$$\sigma = \frac{F}{l} K. \qquad (3)$$

In Table I are presented data on surface tension calculated according to equation (3). As follows from the data obtained, both salts have a calculated surface tension value below the experimental (Tables 1 and 2).

TABLE 1

Values of the Surface Tension Calculated from Equation (3)

(a) Соль	Расстояние между анионом и катионом в кристалле [8,9] (b) d, Å	l, Å	(c) $F \cdot 10^{-4}$ дин	(d) $\frac{F}{l} K$, дин/см
LiCl	2,56	2,56	3,53	138,0
NaCl	2,81	2,81	2,91	103,5
KCl	3,14	3,14	2,31	74,5
RbCl	3,27	3,27	2,16	66,0
CsCl	3,56	3,56	1,81	51,2
$MgCl_2$	2,59*	4,40	6,87	156,2
$CaCl_2$	2,70	4,51	6,32	140,0
$SrCl_2$	3,02	4,83	5,07	105,0
$BaCl_2$	3,18	4,99	4,56	91,5
$PbCl_2$	3,13*	4,91	4,69	95,0
$SnCl_2$	2,81*	4,64	5,75	124,0
LiF	2,01	2,01	5,72	284,2
NaF	2,31	2,31	4,33	187,4
KF	2,67	2,67	3,25	121,8
NaBr	2,98	2,98	2,58	86,5
KBr	3,29	3,29	2,13	64,7
NaJ	3,23	3,23	2,21	68,4
KJ	3,53	3,53	1,85	52,5
RbF	2,82	2,82	2,91	103,2
RbBr	3,43	3,43	1,95	56,9
RbJ	3,66	3,66	1,72	47,0
CsF	3,00	3,00	2,56	85,4
CsBr	3,71	3,71	1,67	45,0
CsJ	3,95	3,95	1,47	37,2

LEGEND: *The value of d) is taken as equal to the sum of the radii. a) Salt; b) Distance between anion and cation in the crystal /8, 9/; c) $F \cdot 10^{-4}$ dyne; d) Dynes/cm

TABLE 2

Surface Tension Values for the Halogenides at the Melting Point

(a) Соль	(b) Радиус катиона [10], Å	(c) Δ = (5), дин/см	(d) σ расчетная, дин/см	(e) Значения σ по опытным данным различных авторов			
				[4]	[11]	[13]	—[12]
LiCl	0,78	0	138,0	137,8	—	140,2	—
NaCl	0,98	21,1	124,6	113,8	116,4	114,1	109,0
KCl	1,33	30,6	105,1	97,4	98,53	97,4	91,0
RbCl	1,49	31,4	97,4	96,3	—	98,3	83,0
CsCl	1,65	27,0	78,2	91,3	—	91,3	72,0
$MgCl_2$	0,78	0	156,2	138,6	—	—	66,0*
$CaCl_2$	1,06	36,9	176,9	152,0	—	—	—
$SrCl_2$	1,27	40,5	145,5	176,4	—	—	—
$BaCl_2$	1,43	41,6	133,1	174,4	—	—	175,0
$PbCl_2$	1,32	38,9	133,9	138,0	136,5	—	—
$SnCl_2$	1,02	29,2	153,2	99,5	—	—	—
LiF	0,78	0	284,2	249,5	—	255,2	—
NaF	0,98	38,3	225,7	199 5	—	201,6	—
KF	1,33	56,3	172,1	138,4	—	143,2	—
NaBr	0,98	17,7	104,2	—	99,96	106,5	—
KBr	1,33	26,7	91,4	—	89,78	88,8	81,0
NaJ	0,98	14,0	82,4	—	87,91	88,2	—
KJ	1,33	21,7	74,2	—	79,54	78,3	72,7
RbF	1,49	49,1	152,3	—	—	132,0	—
RbBr	1,49	27,1	84,0	—	—	90,7	—
RbJ	1,49	22,4	69,6	—	—	80,3	—
CsF	1,65	45,0	130,0	—	—	107,1	—
CsBr	1,65	23,7	68,7	—	—	83,6	—
CsJ	1,65	19,6	56,8	—	—	91,6	—

LEGEND: *According to data of O. G. Desyatnikov, Zhurnal prikladnoy khimii, XXXIX, 870, 1956. a) Salt; b) Cation radius; c) dynes/cm; d) σ calculated, dynes/cm; e) Values of σ from experimental data of several authors

The deviation of the calculated data from the experimental is due to the fact that the melt consists of ion coordinations that are not isolated, but which are in interaction with each other, and that the coordinations themselves do not always contain the minimum number of ions. Therefore, in order to obtain a true value of the surface tension at the interface with the inert phase, it is necessary to add to equation (3) the quantity $\Delta\sigma$, i.e.,

$$\sigma = \frac{F}{l} K + \Delta\sigma. \qquad (4)$$

The variation in surface tension at the interface with the inert phase is accounted for by the interactions of ion coordinations with each other, such as the number of ions in coordination will probably be determined by the size of the cation. Actually (Figure 2) the smaller the cation radius, the more densely it is enclosed (screened) by the surrounding ions of the coordination itself, and consequently, the less open for action on it of ions of mixed coordinations, and the greater the cation radius, the less it is "screened" by the ions of the coordination itself and, therefore, the more accessible it is to the influence of the inner ions of its surrounding coordinations. As follows from (Figure 2), the "shielding" of the cations by the coordination anions will increase from coordination of ions c to coordination of ions a. If however the above stated requirements are valid then there probably must be some value for the cation radius at which $\Delta\sigma = 0$. Thus, assuming that when $(r_a / r'_K)\ \Delta\sigma = 0$, or (r_a / r_K) change in surface tension will be

$$\Delta\sigma = \frac{F}{l} K \left[1 - \left(\frac{r_a}{r_K} : \frac{r_a}{r'_K} \right) \right].$$

Transforming this equation, we obtain

$$\Delta\sigma = \frac{F}{l} K \left(\frac{r_K - r'_K}{r_K} \right). \qquad (5)$$

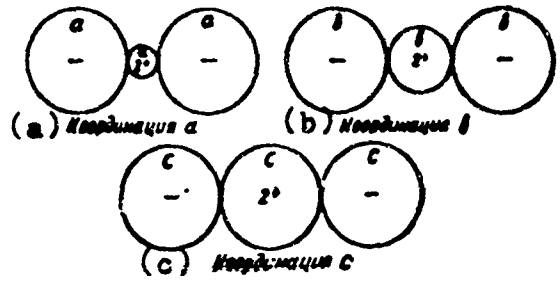

Figure 2. "Screening" of cation as a function of its size by anions of given coordination in the melt.
LEGEND: a) Coordination a; b) Coordination b; c) Coordination c.

Placing the value of $\Delta\sigma$ in the equation (4), we will have

$$\sigma = \frac{F}{l}K + \frac{F}{l}K\left(\frac{r_к - r'_к}{r_к}\right).$$

Further, assuming that $r'_к$ is numerically equal to the radius of the lithium cation (from experimental data), we get

$$\sigma = \frac{F}{l}K + \frac{F}{l}K\left(\frac{r_к - 0{,}78}{r_к}\right). \qquad (6)$$

Thus, the surface tension of melted halogens is determined by the force of interaction between ions of opposite sign as in the ion coordination itself, and also between mixed coordinations of ions per unit path.

The equation (6) is recommended for calculation of surface tension of molten halogenides at the inner phase with the inert phase. It follows from the equation that at a cation radius of the molten salt equal to 0.78 AU, the second member of the equation will be for the zero period at a cation radius of the molten salt less than 0.78 AU, the second number in the equation will have a negative sign, and in the case when the value of the cation radius is greater than 0.78 AU, -- a positive sign.

Table II presents data calculated according to equation (6) and experimental data of several authors. As follows from the data in Table II, for monovalent halogenides the experimental and calculation data are quite close to each other, while deviations of halogenides bivalent metals are somewhat greater.

In our opinion, the deviation of the calculated values of the surface tension at the interface with the inert phase from experimental values is caused mainly by the fact that our values for the cation radii are taken equal to the value of the radius in six-fold coordination, while in the melt radii can differ significantly from their values in six-fold coordination of ions.

In conclusion, it is necessary to note that the proposed equation can be used in calculating surface tension of molten halogenides at the melting point and is applicable only for those halogenides for which not more than two anions are required for one cation. This last requirement stems from the fact that the suggested equation cannot take into account the force F acting per unit path for salts in which more than two anions are necessary for one cation.

CONCLUSION

1. It is shown that the surface tension of molten halogenides at the boundary with the inert phase is determined by the force of interaction between the ions of both the coordination itself as well as of ions of adjacent coordinations per unit path.

2. An equation is derived for calculation of the surface tension of molten halogenides at the boundary with the inert phase for the melting point and good agreement is shown between the experimental and calculated data.

LITERATURE

1. Popel', S. I., Yesin, O. A., Zh. neorg. khimii (Journal of Inorganic Chemistry), No 2, 632 (1957).
2. Gerasimov, A. L., Avtoreferat dissertatsiy (Author's Abstract of Dissertation), Moscow, 1958.
3. Sokolov, O. K., Izv. VUZ, Tsvetnaya metallurgiya, No 3, 67 (1962).
4. Belyayev, A. I., Zhemchuzhina, Ye. A., Firsanova, L. A., Fizicheskaya khimiya rasplavlennykh soley (Physical Chemistry of Molten Salts), Metallurgizdat, 1957.
5. Romanov., A. V., Voprosy fiziki metallov i metallovedeniya (Problems of the Physics of Metals and Metallography), No 8, 1957.
6. Danilov., V. I., Krasnitskiy, S. Ya., DAN SSSR, Vol 101, No 4, 661 (1955).
7. Wood, R. E., Ritter, H. L., J. Amer. Chem. Soc., 75, No. 2, 471 (1953).
8. Bokiy, G. B., Vvedeniye v kristallokhimiya (Introduction to Crystallochemistry), published by the Moscow State University, 1953.
9. Ormont, B. F., Struktury neorganicheskikh veshchestv (Structure of Inorganic Compounds), Technical-Theoretical Lit. Pub. House, 1950.
10. Nekrasov, B. V., Kurs obshchey khimii (Course in General Chemistry), Goskhimizdat, 1952.
11. Bloom, H., Davis, F. G., James, D. W., Trans. Faraday Soc., 56, 1181 (1960).
12. Semenchenko, V. K., Shikhobalova, L. P., Zh. fiz. khimii (Journal of Physical Chemistry), No 6, Vo XXI, 707 (1947).
13. Jaeger, Z., Z. anorgan. und allgem. Chem., 1-3, 1917.

Received by Editor
8 January 1963

DIFFUSION KINETICS OF THE DISSOLUTION OF COPPER, NICKEL AND IRON IN MOLTEN METALS

P. M. Shurygin and V. D. Shantarin

(Ural Polytechnical Institute, Faculty of the Theory of Metallurgical Processes.)

As has already been noted /1/, investigations of dissolution kinetics from the equally accessible surface of the revolving sample /2/ can be one of the methods of determining the diffusion coefficient D in melts. Therefore, we attempted to obtain as far as possible systematic data on the rates of dissolution of copper, nickel and iron in melts of the more fusible metals, and to find the value of D for copper in several different solvents.

Information on the coefficients of diffusion are of interest in the analysis of kinetic relationships of a large number of processes of alloying, deoxidation, producing alloys, zone melting, corrosional stability, etc. Moreover, the study of diffusion aids us in discovering certain peculiarities in the structure of liquid metals. Data on diffusion coefficients in the literature are limited to a few studies by several authors, a summary of which is given in the works /3,4/.

We present in the present report results of measurements of dissolution velocities and diffusion coefficients of copper, in liquid zinc, cadmium, tin, lead, antimony, bismuth and an alloy of aluminum with copper, and also iron and nickel in molten copper.

The experimental method was described in detail in the work /1/. The molten metal was placed in a graphite crucible. The samples were reinforced with fireproof material in graphite holders. To protect the dissolved disks from possible oxidation as they were heated in a furnace to experimental temperature they were covered by a film of solder beforehand. Considering the low values of kinematic viscosity of the liquid metals, and the danger of turbulent flows caused thereby, for the experiments

small samples were used not more than 10 mm in diameter. With decrease in weight (by 300-500 mg), the surface area of the disks and the time of dissolution (up to 5 minutes) were used in calculating the rate of the process v (in $mg/cm^2 \cdot sec$).

The latter quantity, in accordance with the equation of physical chemistry hydrodynamics /2/, is equal to

$$v = 0{,}62 D^{\frac{2}{3}} \nu^{-\frac{1}{6}} (\underset{(sat)}{C_н} - \underset{(sol)}{C_v}) \sqrt{\omega} = K \sqrt{\omega}, \qquad (1)$$

where C_v and $C_н$ = concentrations of dissolved substance in bulk of solution and about sample, respectively.

The quantity v according to this equation should vary linearly with the square root of the angular velocity of disk rotation ω. Actually, for all the systems studied the dissolution rates were under diffusion conditions and within the limits of accuracy of the experiment were described at constant temperature fixed $C_н$ of the equation (1) (Figure 1).

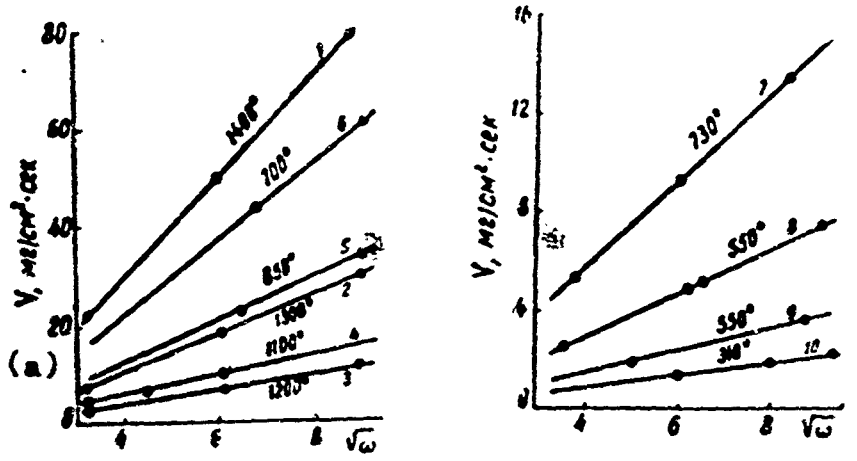

Figure 1. Kinetics of the dissolution of metals as a function of the angular rate of rotation; iron (1, 2, 3) and nickel (4) in copper, copper in aluminum (5), in antimony (6), in zinc (7), in lead (8), in bismuth (9), and in tin (10). LEGEND: a) $mg/cm^2 \cdot sec$

High values of v for copper in aluminum and nickel in copper are caused not only by the relatively high temperatures, but also by the high saturation concentrations $C_н$ of these metals. Moreover, when Cu is dissolved in Al the rate will be so high that they could not even be measured by the method used. Therefore, for a reduction in v, 50% by weight of Cu is added to the molten aluminum, thus increasing C_v itself.

As is to be expected, with increase in temperature the dissolution rate is increased, determined by the change in viscosity, diffusion coefficient, and solubility $C_н$. Therefore, when $C_v = 0$, the quantity v varies with temperature according to an exponential law. In Figure 2 the effect of temperature on the dissolution

rate of nickel and iron in copper is plotted in the coordinates $\lg v/\sqrt{\omega}$ - 1/T, and also of copper in lead.

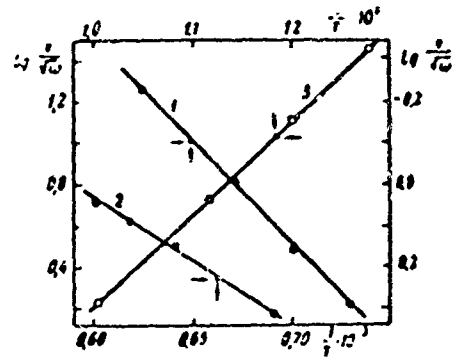

Figure 2. Temperature dependence of the dissolution rate used: 1, 2 -- nickel and iron in copper; 3 -- copper in lead.

If one were to use literature data on the viscosity of liquid metal /5/ solubility /6/ and density, then according to equation (1) it is possible to calculate the quantity D in dissolution and from it the energy of activation E of the diffusion. The results of calculations for three metals are shown in Fig. 3 in semi-logarithmic coordinates. The remaining values are shown in Table 1.

Noteworthy are the large differences in $E_д$ for various metals within limits from 5.8 kilojoules/mole for the diffusion of copper and cadmium to 50.0 kilojoules/mole in the diffusion of iron and copper, in which the lower values of the pre-exponential factor $Д_0$ in the following equation correspond to the low E

$$Д = Д_0 e^{-\frac{E}{RT}}.$$

During dissolution migration of atoms occurs through the layer with variable composition from C_v to $C_н$ and the effective coefficient of diffusion refers to some average concentration.

Knowledge of the values of the diffusion coefficients in various solvents allows us to make certain comparisons. Solubility of copper $C_н$ in metals at a fixed temperature of the 700° rises from bismuth to cadmium, i.e., with decreasing atomic number. This is accompanied by a regular reduction in the diffusion energy of activation (Fig. 4). As a rule, the high slopes of the liquidus lines correspond to the higher heats of solution, since the heat of fusion of copper remains unchanged. In other words, large $C_н$ corresponds to high heats of solution of copper in the alloy.

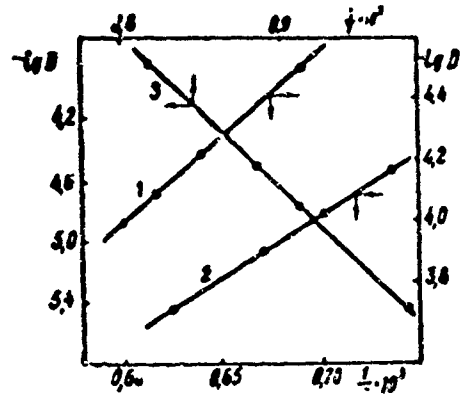

Figure 3. Temperature functions of diffusion coefficients: 1, 2 -- iron and nickel in copper; 3 -- copper in aluminum.

TABLE 1

Diffusional Characteristics in the Process of Dissolution of Metals

(a)

Элемент	(b) Растворитель	(c) D_0, $см^2/сек$	(d) E, $кдж/моль$
Cu	Al—Cu	$6,6 \cdot 10^{3}$	177
(e) Тоже	Zn	$3,3 \cdot 10^{-5}$	8,2
—.—	Cd	$2,7 \cdot 10^{-5}$	5,8
—.—	Sn	$5,4 \cdot 10^{-5}$	6,1
—.—	Sb	$2,23 \cdot 10^{-4}$	11,0
—.—	Pb	$4,1 \cdot 10^{-4}$	9,6
—.—	Bi	$1,14 \cdot 10^{-4}$	11,6
Fe	Cu	$0,57 \cdot 10^{-2}$	50,0
Ni	Cu	$4,70 \cdot 10^{-3}$	41,8

LEGEND: a) Element; b) Solvent; c) cm^2/sec; d) Kilojoules/mole; e) Also.

Therefore, the function in Fig. 4 is to a certain extent similar to the rule of chemical kinetics which holds that the energy of activation of a process decreases linearly with increase in its heat effect. Moreover, in most cases /3/ the activation energy of self-diffusion considerably exceeds the E of diffusion. The process of migration in solids /7/ is characterized by values of E comprising a significant (0.4 - 0.7) proportion of the heat of sublimation ΔH. In molten metals E proves to be smaller by an order of magnitude /4/. But in this case as well a correlation is revealed (Cf. Fig. 4) between the activation energy of diffusion and the heat of vaporization. With increase in the latter E also rises, amounting to however only a small proportion of ΔH.

A direct relationship between the saturation concentration and the heat of vaporization can be found from Fig. 4 by comparing the curves 1 and 2. As is known, such a relationship cannot be strictly substantiated thermodynamically and therefore the functions found are kinetic, are particular in character and justified evidently only for a certain group of alloys.

In the liquid phase, due to the appearance of a large free volume, the displacement of particles compared with solids is appreciably facilitated. For ready fluidity of the melts, a vacancy that is even substantially smaller in terms of the dimensions of the diffusing particles can serve as a site for the penetration of migrating atoms. Therefore, noteworthy is the fact of an increase in E and a decrease in $Д$ with rise in atomic number Z of the element (Table 2).

TABLE 2

Energy of Activation of Diffusion E, Compressibility β, and Atomic Volumes of the Solvent Elements

(a) Элемент	(b) Атомный №	(c) E, кдж/моль	(d) V, $см^3/г \cdot атом$	(e) $\beta \cdot 10^6$ $бар^{-1}$ адиабат.	(f) σ, $эрг/см^2$
Zn	30	8.2	9.16	1.9	754
Cd	48	5.8	13.00	2.5	630
Sn	50	6.1	16.30	2.7	581
Sb	51	11.0	18.39	—	274
Pb	82	9.6	18.30	2.9	431
Bi	83	11.6	21.33	3.7	346

LEGEND: a) Element; b) Atomic number; c) Kilojoules/mole; d) $cm^3/g \cdot atom$; e) bar^{-1}, adiabatic; f) erg/cm^2

The atomic volume of the solvent also increases in the same direction. In the physics of metals, moreover, it is known that the compressibility of elements with increase in Z rises. A similar relationship has been observed for the adiabatic compressibility β of molten metals /8/ as well. Nevertheless, See Table 2, it is possible to trace an unexpected parallel between β and E, i.e., the energy requirements in an elementary act of diffusion increase with increase in compressibility of melt.

Comparison of the diffusion coefficients of copper in solid /3/ and liquid metals does not provide a simple relationship linking the quantity $Д_ж$ $Д_{тв}$ and the relative change in volume $\Delta V : V$ in fusion. The value of $Д_ж \cdot Д_{тв}$ of the metal differs from 10^2 for Sb to 10^5 for Pb. $[Д_ж \cdot Д_{тв} = D_{liq} \cdot D_{sol}]$

In spite of an increase in the coordination number during melting and negative value of the ΔV for bismuth, $Д_ж$ also exceeds $Д_т$ by 2 orders of magnitude for several elements /3/.

The high surface tensions of melts σ /9/ of zinc, cadmium, and tin correspond to the smaller values of $Д_0$ (Table 1). And in contrast, smaller σ for antimony, lead, and bismuth correspond to a larger $Д_0$.

However, a simple relationship linking the volume of holes $V_д = 0.68\ (kT : \sigma)^{3/2}$ with the pre-exponential multiplier cannot be viewed yet as possible. Only a qualitative relationship can be traced out between the activation energy of diffusion and surface tension. High interparticle bonds of the melt with high value of σ as a rule correspond to lower energies E.

Analysis of diffusion in solid metals taking into account their compressibility, thermal expansion, heat of sublimation, and melting point $T_{пл}$ have led /7/ to an expression for $Д_0$ as a function of activation energy in the form

$$\ln Д_0 = A + B\frac{E}{T_{пл}}, \qquad (2)$$

where A and B = constants.

In other words, a linear relationship should hold between $\ln D_0$ and $E/T_{пл}$. In the derivation of equation (2) no special limitations were imposed characteristic of an anisotropic crystalline body. Therefore, we attempted to verify its application to molten metals.

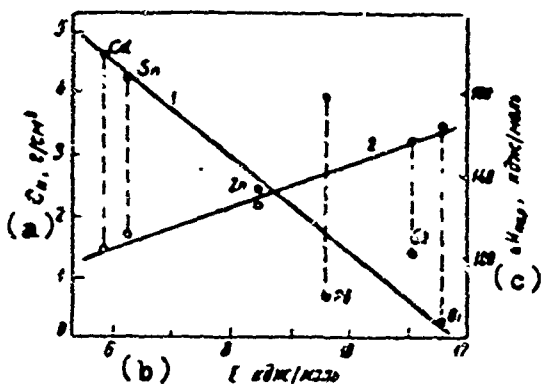

Figure 4. Relationship of energy of activation of the diffusion process with the value of the solubility of copper in the metals C_H at 700° (1) and the heat of vaporization of the elements ΔH_{vap} (2). LEGEND: a) g/cm^3; b) Kilojoules/mole; c) ΔH_{vap}, kilojoules/mole

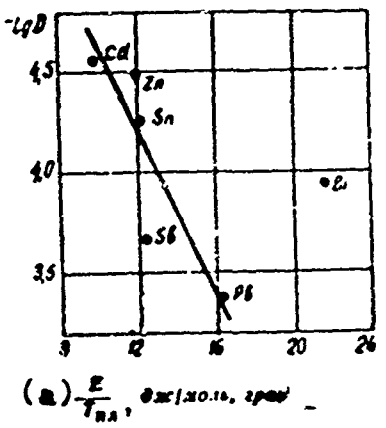

Figure 5. Pre-exponential quantity as a function of $E/T_{пл}$ for various metals.
LEGEND: a) joules/mole, deg.

Fig. 5 shows that in addition to bismuth all the measured values of $\ln D_0$ for the diffusion of copper in melts are satisfactorily described by equation (2). The exclusion of bismuth from the general function probably cannot be accounted for by the low melting point and the high E, since these variables were considered along with the volume of the solvent in the derivation of the formula used.

The application to liquid metals of the equation

$$D \cdot \eta = \frac{kT}{6\pi r}$$

encounters the limitations related to two facts. First, it is necessary to substitute in it the value of $\square$ (ln C/d ln a), i.e., the self-diffusion coefficient, and consequently, information is needed on the concentration dependence of activity. Secondly, at constant temperature, as was noted in /10/, the first member depends on characteristics of melt structure. Therefore, in distinction to the very dilute amalgams, our data on diffusion cannot be described by the simple Stokes-Einstein equation.

Conclusions.

1. The method of dissolution from an equally accessible surface was used to measure the dissolution rates and the diffusion coefficients of copper in liquid zinc, cadmium, tin, antimony, lead, and bismuth and also of iron and nickel in molten copper.

2. It was found that the energy of activation of the diffusion process in the metals studied ranged from 5.8 to 11.6 kilojoules/mole and are uniformly lowered with increase in copper solubility.

3. The diffusion coefficients are of the order of 10^{-5} cm^2/sec, and the values of the pre-exponential factors for iron and nickel in their diffusion in copper exceeds by 10-fold the corresponding values in the diffusion of copper in fusible metals.

4. The qualitative applicability of ideas developed for diffusion in the solid state is shown for liquid metals and an attempt is made to explain the results obtained from the vantage point of the hole structure of liquids.

LITERATURE

1. Shurygin, P. M., Boronenkov, V. N., Kryuk, V. I., Izv. VUZ Tsvetnaya metallurgiya, 3, 59 (1962).

2. Levich, V. G., Fiziko-khimicheskaya gidrodinamika (Physico-chemical Hydrodynamics), Moscow, Fizmatizdat, 1959.
3. Zait, V., Diffuziya v metallakh (Diffusion in Metals), Moscow, Foreign Literature Publishing House, 1958.
4. Ling Jang, G. Derge, Metallurg. Soc. Conferenco, 7, 503, (1961).
5. Shvidkovskiy, V. G., Nekotoryye voprosy vyazkosti rasplavlennykh metallov (Some Problems of the Viscosity of Molten Metals), Moscow, Gosizdat, 1955.

6. Khansen, M., Anderko, K., Struktury dvoinykh silavov (Structure of Binary Alloys), Moscow State Scientific-Technical Pub. House of Lit. on Ferrous and Nonferrous Metallurgy, 1962.
7. Gertsriken., S. D., Dekhtyar, I. Ya., Diffuziya v metallakh i splavakh v tverdoy faze (Diffusion in Metals and Alloys in the Solid State), Moscow, 1960.

8. Kudryavtsev., B. B., Primeneniye ul'traakusticheskikh metodov v praktike fiziko-khimicheskikh issledovaniy (Use of Ultrasonic Methods in the Practice of Physico-chemical Research), Moscow, 1962.
9. Darken, L. S., Gurri, R. V., Fizicheskaya khimiya metallov (Physical Chemistry of Metal), Metallurgizdat, 1960.
10. James, C. M., J. Chem. Phys., 23, 518 (1955).

Received by Editor
24 October 1962

ANODE POLARIZATION OF SILICON IN THE COPPER-SLAG SYSTEM

G. A. Toporishchev, O. A. Yesin and V. N. Kalugin

(Ural Polytechnic Institute, Chair of the Theory of Metallurgical Processes.)

The interaction between molten metals and slag in some cases is limited by the access of reagents to the interface surface. In the passage of direct current this limitation is shown in concentration polarization /1-3/ developing. This relationship has been studied chiefly for the cathodic process. Information on anode polarization is still limited /2/. In this connection, we investigated the change in electrode potential with current density and with time in the transition of silicon from liquid copper to molten slag.

The alloys were prepared from grade MOc copper and pure silicon (99.98% Si). Slags containing CaO, SiO_2, Al_2O_3, MgO, Na_2O, and B_2O_3 were prepared from oxides of the pure and of the analytical grades. The electrolytic cells are depicted schematically in Fig. 2. The construction a is a cylinder of molten magnesium 50-60 mm in diameter, and 70-80 mm in height, in which four vertical channels are drilled (20-25 mm in depth, and 4-5 mm in diameter and with inclined openings to these channels for tungsten current-lines. In the use of this cell, liquid alloys of Cu-Si of the same composition serve as the anode, cathode and reference electrode. In the assemblies *б* and *в* a magnesite or corundum crucible is placed in a graphite or alundum cylinder. In the bottom of the corundum crucible is an opening 0.5-2 mm in diameter. The arrangement of the electrodes and the current lines to it can be seen from Fig. 1. In cells of this type a tungsten wire (1-1.2 mm in diameter) serves as the cathode, bent in its

lower portion in the form of a circle (5-10 mm in diameter). Through its center passed the reference electrode made of platinum wire (0.5 mm in diameter). The depth of submersion of the electrode and its position was regulated by micrometric scew.

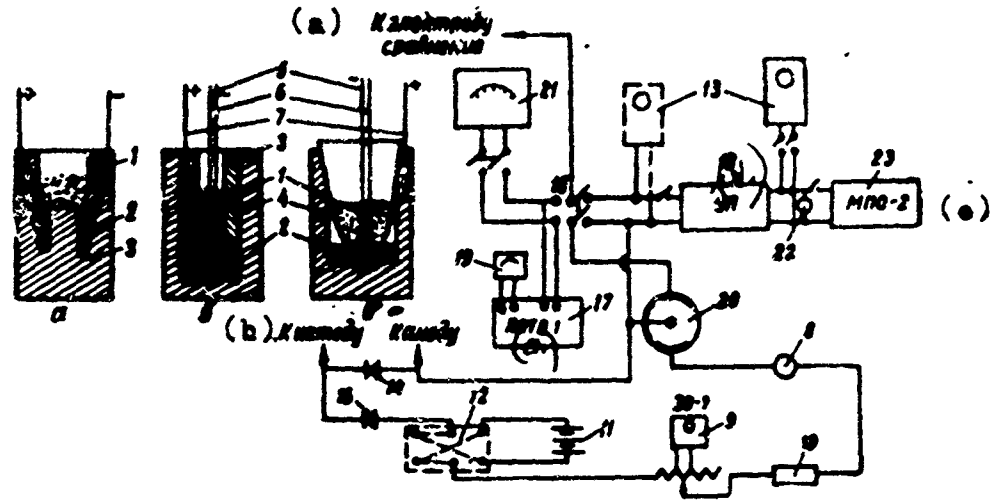

Figure 1. Diagram of measuring circuit and cell design: 1 -- oxide melt, 2 -- metallic alloy, 3 -- magnesite crucible, 4 -- graphite or corundum crucible, 5 -- platinum reference electrode, 6 -- tungsten wire cathode, 7 -- anode, 8 -- multi-limit ammeter, 9 -- EO-7 electronic oscillograph, 10 -- resistance magazine, 11 -- series of batteries, 12, 15 -- two-position switches, 13 -- cathode oscillograph with afterglow, 14 -- contacts of depolarization relay, 16 -- contacts of polarizing current relay, 17 -- PPTV-1 type potentiometer, 18 -- amplifying current attachment, 19 -- galvanometer with scale of $24 \cdot 10^{-9}$ amp/division, 20 -- commutator, 21 -- tube voltmeter, 22 -- milliammeter, 23 -- MPO-2 slave oscillograph. LEGEND: a) To reference electrode; b) To cathode, to anode; c) PPTV-1; d) Current amplifier; e) MPO-2 slave oscillograph.

The diagram of the measuring circuit is shown in Fig. 1. It permits recording of the volt-ampere curve by the commutator method and the recording on photographic film by means of the oscillograph--of change in polarization with time during the switching on and switching off of current.

Used as the commutator was a collector seated on the shaft of a small motor. The current from the anode was led to the face of the collector with the help of a spring plate. The reference electrode and the cathode were connected to brushes. In one revolution of the shaft four switchings elapsed, such that at 1400 rpm up to 186 current discharges per second was attained.

The nature of commutator performance is shown in Fig. 2 by the oscillograms of current and polarization period to record the current oscillogram a loop of the MPO-2 oscillograph was connected in series through the attachment of the R-1 type with the rheostat 10 (Cf. Fig. 1). The variation in anode potential was photo-

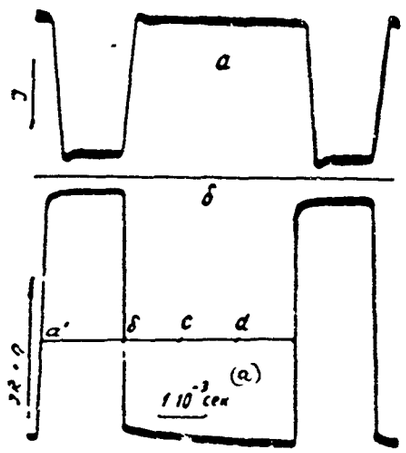

Figure 2. Oscillogram of current (δ) and anode polarization (b), of the Cu-Si alloy. C_{Si} = 0.13%, t = 1420°, I = 0.14 amp.
LEGEND: a) Second

graphed with the screen of the EO-7 oscillograph. At the moment the current was switched on (point a Fig. 2) a sharp jump in voltage was observed caused by the ohmic resistance, then a smooth increase in potential due to polarization of the electrode occurred. When the current was connected (point b' in Fig. 2) the ohmic voltage disappears rapidly, after which polarization of is gradually reduced.

Measurement of the values of the commutator was carried out in the interval of time from c to d. The neglected change in potential occurring from the moment the current was switched off to the beginning of measurement represented not more than 5-7%. The stability of the number of commutator switchings and the sharpness of the discharges were controlled during the experiments by the EO-7 electronic oscillograph in conjunction with the ZG-10 generator. To reduce interference and induction in the measuring circuit the reference electrode was grounded.

The experiments were conducted in vertical resistance furnaces, the heating element of which was a graphite tube. The temperature held constant by a manual or automatic control using the EPV-01 potentiometer. It was measured with a platinum-rhodium thermocouple and the optical OPPIR-17 pyrometer.

Before determination of polarization the system was conditioned with weak currents. Then successively increasing values of i were introduced and for each of these the variation in anode potential with time was established. The curves η - i were constructed from the polarization values established.

Initially, the behavior of the copper anode without silicon added was investigated. Used as electrolyte was slag containing 55% SiO_2, 10% MgO and 35% CaO. The polarization curves obtained (Figure 3, curve 1) closely adjoined the abscissae axis and had no maximum currents,

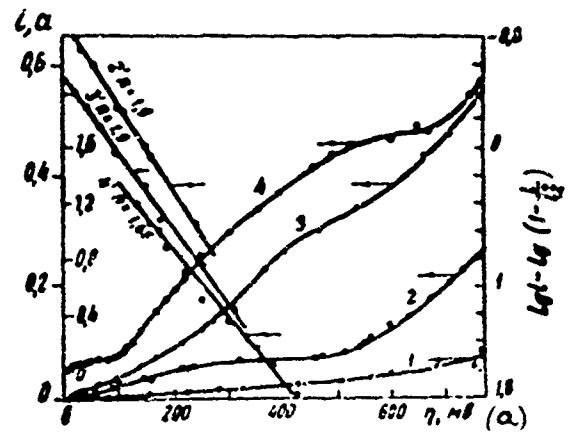

Figure 3. Anode polarization curves for pure copper at 1290° (1) and for the following Si content in it: 0.006% at 1240° (2 and 2'): 0.07% at 1230° (3 and 3'); 0.013% at 1430° (4 and 4'). Slag in experiments 3, 3', 4, and 4': 15% SiO_2, 45% CaO, 35% Al_2O_3, 5% B_2O_3; in experiments 1, 2, and 2': 55% SiO_2, 35% CaO, 10% MgO. The diameter of the alloy-slag interface in experiments 1, 2, 2' is 0.3 cm; in experiments 3, 3', 4, 4' is 0.2 cm. LEGEND: a) millivolts

nor inflection points. With the addition to copper of small amounts of silicon clearly pronounced limiting currents appear (cf Figure 3). They are probably caused by delayed diffusion of Si atoms in copper. This is attested to, in particular, by the proportionality between the limiting currents i^0 and the concentration observed at the given temperature:

C_{Si} in Cu, wgt %	0,006	0,07	0.1	0,006	0,02	0,23	0,005	0,07
Temperature, °C	1240	1240	1230	1300	1320	1330	1480	1480
i^0, amp/cm^2	0,5	5,4	7,2	0,95	4,0	26,2	3,4	38,0

Deviations from this function are caused by fluctuations in temperature, by error in the determination of the anode composition, and by the change of its surface during polarization.

The presence of limiting currents, the proportionality of their concentration of Si in copper, and also the slow decrease

and increase in potential with time (Fig. 2) indicates the diffusion nature of polarization.

The following reactions /See Note/ are possible on the copper-silicon anode:

$$Si \rightarrow Si^{4+} + 4e; \quad (1)$$

$$Si \rightarrow Si^{2+} + 2e. \quad (2)$$

(/NOTE/ Here, and below, the symbols of the ions are given schematically without accounting for their complexation.)

Diffusional polarization in this case is caused only by deviations at the electrode concentrations of atomic silicon /Si/ and the ions Si^{4+} and Si^{2+} from equilibrium values. Therefore, for the processes (1) and (2) it can be represented by the equation

$$\eta = \frac{RT}{nF} \ln \frac{(Si^{n+})}{(Si^{n+})_p} - \frac{RT}{nF} \ln \frac{[Si]}{[Si]_p},$$

where p = equilibrium composition.

The concentrations of Si on the surfaces of the copper-silicon alloy and the ions of Si in the near-anode layer of the slag vary with the current density in accordance with the expressions

$$[Si] = [Si]_p - ki = [Si]_p \left(1 - \frac{i}{i_2^0}\right)$$

and

$$(Si^{n+}) = (Si^{n+})_p + ki = (Si^{n+})_p \left(1 + \frac{i}{i_1^0}\right).$$

Hence,

$$\eta = \frac{0.0002}{n} \lg \left(1 + \frac{i}{i_1^0}\right) - \frac{0.0002}{n} \lg \left(1 - \frac{i}{i_2^0}\right). \quad (3)$$

Here the first term is caused by the accumulation of Si^{n+} ions at the anode, and the second--by the excess of Si atoms at the surface of the alloy, due to their rapid removal by diffusion within both phases. Since the concentrations of the ions $(Si^{4+})_p$ is high, then $i^0 \gg i$ and the first term in the process (1) can be neglected. Then

$$\eta_1 = -\frac{0.0002T}{4} \lg \left(1 - \frac{i}{i_2^0}\right). \quad (4)$$

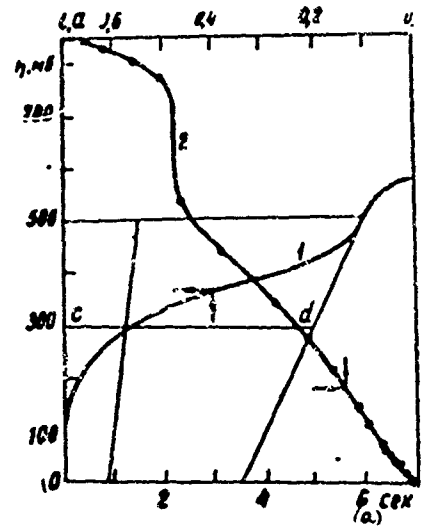

Figure 4. Change in anode polarization with time for C_{Si} = 0.08% and 1250° (1) and with current strength for C_{Si} = 0.11% and 1230° (2). Slag: 15% SiO_2, 35% CaO, 20% Al_2O_3, 10% Na_2O, 20% B_2O_3; τ = 4.95 seconds. LEGEND: a) Seconds

It is known that in melts the ions of the lower valency of the non-transitional metals can exist only at low concentrations /4/. Therefore, the value of $(Si^{2+})_4$ is low and for the process (2) $i^0 \ll 1$. This allows us to neglect unity in the first term of equation (3) and give it the form

$$\eta = \frac{0,0002}{2} \left| \frac{i}{i_1^0} - \frac{0.0002\,T}{2} \lg \left(1 - \frac{i}{i_2^0} \right) \right. . \qquad (5)$$

As Fig. 3 shows the experimental points on the polarization curve fall on straight lines plotted according to the coordinates

$$\eta - \left[\lg i - \lg \left(1 - \frac{i}{i_2^0} \right) \right] .$$

Their angular coefficients (0.16 - 0.21) are close to the required equations (5) at the experimental temperatures. In other words, the anodic dissolution of silicon under the conditions adopted occurs mainly in the form of bivalent ions. Their formation on the cathode was established earlier /3/, but only at high concentrations of silica ($>$30% SiO_2) in the slag.

We should note that in certain experiments (Cf. Fig. 3, curve 4) still another limiting current was observed at the outset of the polarization curve. However, its magnitude did not depend on the concentration of silicon in copper. Experimental points of this initial section of the curve are described by the

equation

$$\eta_1 = -\frac{0{,}0002\,T}{n}\lg\left(1-\frac{i}{i_n}\right).$$

At experimental temperatures the angular coefficients correspond in some cases to small n = 2.5 - 3.0, and in others--n = 0.95 - 1.3. The last value was attained only in the case when the measurements were conducted over a prolonged time in a cell made of molten magnesium.

Apparently, in the first case the anodic wave corresponds to the dissolution of boron $B \longrightarrow B^{3+} + 3e$, inasmuch as it has a higher electronegative potential as compared with Si. Boron appeared in the process of preparing the Cu - Si alloy, which was carried out under borate slag. Its presence in the metal was confirmed by chemical analysis.

In the second case, the wave probably corresponds to the oxidation of bivalent iron to trivalent. The source of the iron oxide was molten magnesium.

To confirm the valency with which silicon enters the slag, the change in polarization with time at a current density above the maximum was studied. Under these conditions, during a transitional time equal to τ the polarization curve can be represented /5/ either by the function

$$\eta = -\frac{0{,}0002\,T}{4}\ln\left(1-\frac{t^{\frac{1}{2}}}{\tau^{\frac{1}{2}}}\right),$$

corresponding to the equation (4), or by formula

$$\eta = -\frac{0{,}0002\,T}{2}\ln\left(1-\frac{t^{\frac{1}{2}}}{\tau^{\frac{1}{2}}}\right)+\ln t^{\frac{1}{2}},$$

corresponding to the expression (5).

One of the curves of the polarization increase with time for the alloy containing 0.08% Si is shown in Fig. 4. The points of this curve, in the coordinates

$$\eta - \left[\lg t^{\frac{1}{2}} - \lg\left(1-\frac{t^{\frac{1}{2}}}{\tau^{\frac{1}{2}}}\right)\right] \text{ и } \eta - \lg\left(1-\frac{t^{\frac{1}{2}}}{\tau^{\frac{1}{2}}}\right)$$

fall on a straight line only for case 1 (Fig. 5). The line has an angular coefficient of 0.17, which corresponds to a value of n = 2 at the experimental temperature. A similar result yields analysis of the quantity η as a function of i (Fig. 4, curve 2), for the alloy containing 0.11% Si obtained under the same conditions as was curve 1. Here the angular coefficient of the line in the coordinates η -- $\left[\lg i - \lg\left(1-\frac{i}{i_l}\right)\right]$ also yields n = 2.

From this it follows that the diffusion of Si^{2+} occurs at least at an order of magnitude higher more rapidly than Si^{4+}. Evidently, this is due to the lower charge and large size of the Si^{2+} cation, which in this respect is closer to the modifier-ions (for example, Ca^{2+}, Ba^{2+}).

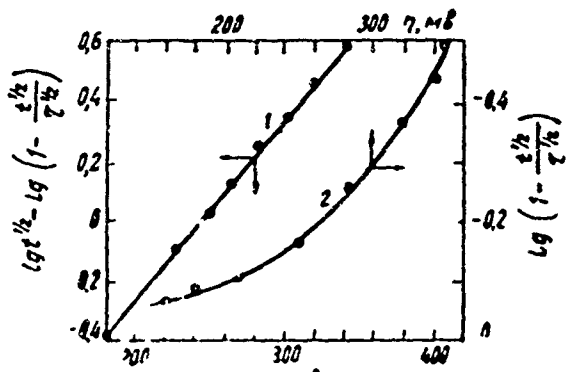

Figure 5. $Lgt^{\frac{1}{2}} - \lg\left(1-t^{\frac{1}{2}}/t_l^{\frac{1}{2}}\right)$ and $\lg\left(1-\frac{t^{\frac{1}{2}}}{\tau^{\frac{1}{2}}}\right)$ as functions of anode potential for alloys containing 0.08% Si at 1250°. Slag: 15% SiO_2, 35% CaO, 20% Al_2O_3, 20% B_2O_3, 10% Na_2O_3.

To determine the diffusion coefficients a method was used /5,6/ based on the fact that at a current density higher than the limiting value, after a certain interval of time a jump in potential is observed caused by the reduction in the concentration of the dissolving element down to zero. The transitional time can be found from the curve of increase in polarization with time (Cf. Fig. 4) and the diffusion coefficient calculated /7/ from the formula

$$Д = \frac{4 i^2 \tau}{\pi n C_0^2 F^2}.$$

Under the assumption that the surface of the liquid copper anode is a hemisphere /2/, values of D were obtained in the 1100-1350° temperature interval which are described by the equation

$$Д = 14{,}8 \cdot 10^{-4} \exp\left(\frac{-12\,000}{RT}\right).$$

Here the diffusion energy of activation is 12 kilocalories.

The values of D_{Si} in copper that were found afford an evaluation of the radius of the diffusing particle r_{Si} by means of the equation /8/

$$Д = \frac{kT}{\pi n \eta r_{Si}}. \qquad (6)$$

In it, n = 4 when the r_p of the solvent atoms is large and $r_p > r_{Si}$, and n = at $r_p < r_{Si}$. If $r_p = r_{Si}$, then

$$Д = \frac{kT}{2 r_{Si} \eta}. \qquad (7)$$

The dimensions of the diffusing particle calculated from the formulas (6) and (7) are obtained as equal to 0.9 AU at n = 4, 0.6 AU at n = 6, and 5.9 AU at $r_p = r_{Si}$ = 1.2 AU. The best agreement occurs for the case when $r_p > r_{Si}$. Then the radius of the diffusing particle calculated by equation (6) is close to that for the ion Si^{2+}. In other words, silicon diffuses probably in the form of an ion, but not as the atom. The data on copper viscosity is taken from the study /9/.

In conclusion, let us note that the use of the chronopotentiometric method for determination of the coefficient of diffusion of an element dissolved in liquid metal is possible only within a definite interval of its concentrations. The lower limit is 0.005 - 0.01% and is due to the difficulties related in determination of the true concentration, and also with its commensurability with the concentration for impurities present in the metal. The upper limit can be taken as 0.2 - 0.5% It is related to the need to use high current densities. This often leads to distortion of the initial section of the polarization curve on which appear "peaks" "surges" caused by changes in electrode surface with time and its local overheating.

Conclusions.

1. The commutator method at 1200-1500° for various cell constructions was used to establish that the anodic transition of silicon from copper to slag under the conditions studied is inhibited by its delayed diffusion in the metal.

2. It is shown that the anodic dissolution of silicon occurs chiefly in the form of the bivalent ion.

3. The coefficients of diffusion and the energy of activation are estimated for silicon in molten copper.

4. The limits of concentration of an element are found which are advisable to be used for the chronopotentiometric method of determining diffusion coefficients in liquid metals.

LITERATURE

1. Yesin, O. A., Toporishchev , G. A., Zh. fiz. khimii (Journal of Physical Chemistry), 31, No 2, 1957.
2. Musikhin, V. I., Yesin, O. A., DAN SSSR, Vol 145, No 2, 1962.
3. Yesin, O. A., Chechulin, V. A., Zh. fiz. khimii, 2, 1958.
4. Baimakov , Yu. V., Fizicheskaya khimiya rasplavlennykh soley i shlakov (Physical Chemistry of Molten Salts and Slags), Metallurgizdat, page 22, 1962.
5. Delakhey., P., Novyye pribory i metody v elektrokhimii (New Instruments and Methods in Electrochemistry), For. Lit. Pub. /House, 1957.
6. Sand, H., Phil. Mag., 1, 45 (1902).
7. Frumkin, A. N., Barotskiy, V. S., Ioffe, Z. A., Kabanov, B. N., Kinetika elektrodnykh protsessov (Kinetics of Electrode Processes), Moscow, 1957.
8. Yang, L., Gerge, G., Phys. Chem. Process Metallurgy, Pt. I, Metallurg. Soc. Conf., 7, N.Y.-London, p. 519, 1959.
9. Obrabotka tsvetnykh metallov i splavov, spravochnik (Processing of Nonferrous Metals and Alloys), Metallurgizdat, page 18, 1961.

Received by Editor
18 March 1963

EFFECT OF EXTENT OF ROASTING OF COPPER-ZINC CONCENTRATES ON THE RESULTS OF SMELTING OF CINDERS

V.I. Smirnov, A.P. Doroshkevich and Yu.A. Yablonskiy

(Ural Polytechnical Institute, Chair of Metallurgy of Heavy Non-Ferrous Metals.)

The sulfide ores of Ural copper deposits are characterized by the presence of zinc, the content of which in many cases exceeds the copper content. Due to mutual thin ingrowths in the ores of copper and zinc sulfides, when these ores are subjected to selective flotation copper concentrates are obtained with a significant zinc content. Smelting of such concentrates in reverberatory furnaces encounters great difficulties.

A method of preliminary roasting of copper-zinc concentrates introduced at one of the plants affords much improvement in the smelting results and increases the coefficient of complex utilization of the actual composition of the concentrates. Accordingly, it appears advisable to establish the rational extent of charge roasting which would assure the highest recovery of copper in the matte and of zinc in the slag.

Investigations were conducted with copper concentrates, whose composition is shown in Table 1. Copper in the sulfide concentrations is found mainly as chalcopyrite, zinc--as sphalerite, residual iron--as pyrite; in the Altyn-Topkinskiy concentrate copper is present in the form of chrysocolla.

The sulfide concentrations presented in Table 1 underwent granulation in a cup granulator and then the granules obtained, of the fractions - 1.6 + 0.63 mm, after natural drying were roasted in the laboratory furnace on a fluidized bed. As the result of the roasting of granules cinders were obtained with various sulfur contents (Table 2).

TABLE 1

Chemical Composition of Concentrates

(a) Наименование концентратов	(b) Содержание, % Cu	Zn	Fe	S	SiO_2	CaO	MgO	Al_2O_3
(c) Среднеуральский	11,2	13,0	28,7	38,2	2,8	0,4	0,3	1,3
(d) Бурибаевский	12,2	2,2	33,6	39,9	4,7	не обнаруж. (h)	0,3	0,6
(e) Пышминский	24,1	0,05	29,5	33,4	3,8	4,6	0,7	0,8
(f) Алтын-Топканский	16,4	0,2	11,9	0,8	40,7	0,4	1,3	—
(g) Гранулы из смеси концентратов	13,2	6,0	26,5	33,0	8,5	0,5	—	—

LEGEND: a) Concentrate; b) Content; c) Central Ural; d) Buribayevskiy; e) Pyshminskiy; f) Altyn-Topkanskiy; g) Granules of a concentrate mixture; h) Not detected.

Chemical Composition of Cinders TABLE 2

(a) Огарки		(b) Содержание, % Cu	Zn	$S_{общ}$ (c)	S_s
(d) Из среднеуральского концентрата	1	14,0	14,0	13,4	12,6
	2	14,3	14,4	12,4	11,7
	3	15,1	13,8	10,1	8,5
(e) Из бурибаевского концентрата	4	15,4	2,3	14,1	11,6
	5	16,2	2,4	9,5	7,8
	6	16,7	2,6	8,9	8,2
(f) Из пышминского концентрата	7	26,0	0,05	17,6	15,8
	8	27,2	0,06	13,9	12,0
	9	27,3	0,06	13,5	11,5

LEGEND: a) Cinders; b) Content; c) S_{tot}; d) From Central Ural concentrate: e) From Buribayevskiy concentrate; f) From Pyshminskiy concentrate.

TABLE 3

Elementary Composition of Cinders

(a) Огарок	(b) Содержание, % Cu	Zn	Fe	$S_{общ}$ (c)	S_s	SiO_2	CaO
1	15,3	7,8	30,1	12,0	10,5	10,0	0,4
2	14,9	8,1	29,0	16,0	14,4	9,6	0,5
3	14,3	7,9	28,1	20,0	18,6	9,7	0,5

LEGEND: a) Cinder; b) Content, %; c) S_{tot}

The cinders obtained were charged with fluxes (quartz and limestone) and converter slag and underwent smelting in corundum crucibles in a Kryptol furnace at 1350°. The fusion and residence of the melt in the furnace after this temperature was continued for 30-35 minutes. The purpose of the smeltings of the roasted concentrates in a given series of experiments was an orientational study of the influence that the extent of roasting of sulfide materials have on the distribution of the main metals--copper and zinc--between slag and matte.

The orientational smeltings conducted revealed that the smelting of fluxed cinders with low sulfur content (8.5 - 10.5% or 6 - % total sulfur in the charge) results in rich matte being produced (from 65 to 79% Cu). As a result, slag is produced with a high copper content. The deficiency of sulfur in the cinders not only results in rich matte, but also the formation of metallic copper in the bulk of the matte. Direct extraction of the copper in the matte in the smelting of such cinders amounts to 84 - 87%, in the best instance--92%, and the loss of copper with the slag is 6%, and in some cases as much as 11% of the total copper content in the cinders.

Smelting of cinders with a higher sulfur content affords production of matte containing 40 - 55% Cu, in addition, the direct extraction of copper in the matte is increased to 97%. Smelting permits the concentration in the slag of 80 - 95% of the Zn originally in the cinders. Thus, preliminary smelting of cinders showed the need for less extensive roasting of copper concentrates in order to obtain cinders containing more than 13% sulfur.

Since concentrates differing in composition are received at copper-smelting plants, subsequently work was conducted with a mixture of concentrates, consisting of 60% Ural-average, 10% Altyntopkanskiy, 15% Buribayuvskiy, and 15% Rushminskiy concentrates with 2% bentonite to the mixture to improve rolling and to achieve durable granules. The composition of the granules produced from this mixture is shown in Table 1.

The granules produced from the mixture of concentrates were roasted in a fluidized bed furnace and cinders of three types were obtained (Table 3). The cinders were studied as to the form in which copper, zinc, and iron (Table 4) appeared in them.

As can be seen, in the roasting of granules at temperatures of the order of 720 - 780° significant oxidation of sulfide minerals occurs. Up to 39 - 48% Cu of its total content in the cinders enters the oxidized form, including 12 - 18% present in the ferrite form, 21 - 26% as the free oxide, and 3 - 4.5% in the sulfate form.

For zinc at the temperatures indicated a higher extent of sulfate- and ferrite formation is characteristic than for copper: 20 - 21.5% of the total zinc content is present in the sulfate and

25 - 32% in the ferrite forms; 6 - 7% is present as the free oxide.

TABLE 4

Forms of Compounds of Copper, Zinc, and Iron in Cinders

(a) Огарок	(b) % меди от общего содержания в огарке в форме					(c) % цинка от общего содержания в огарке в форме					(d) % железа (от общего содержания) в виде магнетита
	сульфатной (e)	окисленной (f)	сульфидной (g)	ферритной (h)	остаток (i)	сульфатной (e)	окисленной (f)	сульфидной (g)	силикатной (j)	ферритной (h)	
1	2,8	26,2	51,1	18,9	1,0	20,3	6,9	40,5	0,8	31,5	51,2
2	4,6	21,3	60,5	13,0	0,6	20,4	6,2	48,7	1,5	23,2	40,1
3	3,9	23,5	61,6	11,4	0,6	21,4	5,9	45,3	2,4	25,0	33,9

LEGEND: a) Cinder; b) % copper of total content in cinder in form listed; c) % zinc of total content in cinder in form listed; d) % of iron (of total content) as the magnetite; e) Sulphate; f) Oxide; g) Sulfide; h) Ferrite; i) Residual; j) Silicate

A significant amount of iron in the cinders (34 - 51%) is in the magnetite form.

The cinders produced undergo smelting in order to study the effect of the roasting on the distribution of copper and zinc, between the matte and the slag. The composition of the slag from which the smelting was calculted, and the composition of the quartz, limestone, and converter slag used here are shown in Table 5.

The results of smelting of slags of the first type are shown in Table 6, and for slags of the second type -- in Table 7.

The results of laboratory experiments on smelting of roasted material allows us to recommend to a copper-smelting plant switching over to the smelting of pre-roasted concentrates on fluidized beds the most profitable sulfur content in the cinders, which would yield the most advantageous distribution of zinc between these smelting products and the maximum extraction of copper in the matte.

Even in previous studies /1,2/ it was established that the distribution of zinc in smelting of cinders depends on the extent of preliminary roasting of the material. Comparison of the results of smelting of cinders with sulfur content at 12, 16 and 20% (corresponding to 9.5%, 13.5% and 17.5% S_{tot} in the charge) leads to the conclusion that the most advantageous cinder has a sulfur content close to 16%. In smelting this cinder fully satisfactory slagging of zinc (80 - 84% of its content in the charge) is observed, a slag fully satisfactory in copper content is achieved, and the extraction of copper in the matte amounts to 94 - 95%. The matte in these series of smeltings was held at 38 - 42% Cu, which corresponds to an average composition of the matte at many copper-smelting plants.

TABLE 5

Chemical Composition (in %) of Estimated Slags, Fluxes, and Converter Slag

		FeO	SiO_2	CaO
(a)	Шлак 1	45,0	35,0	2 и 5
(b)	Шлак 2	41,0	32,0	2 и 5
(c)	Кварц	—	99,9	—
(d)	Известняк	0,4	8,0	49,9
(e)	Конвертерный шлак	56,2	23,8	0,8

LEGEND: Remark: Converter slag contains 2% Cu and 7% Zn.
a) Slag 1; b) Slag 2; c) Quartz; d) Limestone; e) Converter slag

In smelting cinders with total sulfur content close to 12% slags were produced with high copper content (0.94 - 1%), the extraction of which in the matte was reduced to 90 - 92%. Although here the extraction of zinc in the slag increased to 90 - 95%, but obviously this increase does not represent a great advantage compared to the decrease in the copper recovery in the matte.

Smelting of cinders with a 20% sulfur content reveals a significant decrease in the slagging of zinc and a noticeable impoverishment in the copper content of the matte produced. Additionally, when cinders with the sulfur content shown are produced less sulfur is available for sulfuric acid production.

To avoid difficulties in fuming of slags, smelting of roasted zinc charge must be carried out with sufficiently basic slags having a content of not less than 33 -35% SiO_2 and a limited CaO content. Experiments show that increasing the CaO content in slags more than 4 - 5% does not produce a substantial reduction in the copper loss in slags, while decreasing the CaO content down to 1 - 2% results in some increased copper content.

When we take literature data into account, in particular /2/, and the results of experimental smeltings, we conclude that in smelting roasted zinc charge the optimal level slag must contain 32 - 35% SiO_2, 4 - 5% CaO, 9.5 - 10.5% ZnO, 40 - 45% (FoO + Fe_3O_4).

LITERATURE

1. V. I. Smirnov, V. D. Mishin, Trudy Ural'skogo Politekhnicheskogo instituta imeni S. M. Kirova (Works of the polytechnic institute imeni S. M. Kirov), No 5, 1938.

TABLE 6

Results of Smelting of the First Type of Slag

(a) Огарок	(b) Состав штейна, %			(c) Состав шлака, %					(d) Распределение, %			
									(e) меди в		цинка в (f)	
	Cu	Zn	S	Cu	Zn	FeO	SiO_2	CaO	штейн (g)	шлак (h)	штейн (g)	шлак (h)
1	54,1	4,1	22,1	0,96	7,1	43,7	34,7	4,2	89,4	5,6	11,9	85,0
1	54,9	4,1	21,3	1 03	7,5	43,4	35,5	2,2	90,2	7,2	12,1	88,3
2	38,7	6,4	23,0	0,78	7,3	43,8	34,6	4,6	94,4	4,9	17,2	82,2
2	42,6	5,5	23,1	0,80	8,5	46,1	35,0	2,2	93,5	5,4	14,2	83,7
3	24,2	7,6	23,6	0,76	6.0	43,2	33,2	5,1	96,4	3,6	41,1	44,7
3	24,0	7,5	23,5	0,78	6,1	44,4	34,4	2,1	95,5	4,0	40,4	46,2

LEGEND: a) Cinder; b) Matte composition; c) Slag composition; d) Distribution; e) Copper in; f) Zinc in; g) Matte; h) Slag

TABLE 7

Results of Smelting of the Second Type of Slag

(a) Огарок	(b) Состав штейна, %			(c) Состав шлака, %					(d) Распределение, %			
									(e) меди в		цинка в (f)	
	Cu	Zn	S	Cu	Zn	FeO	SiO_2	CaO	штейн (g)	шлак (h)	штейн (g)	шлак (h)
1	58,1	4,1	22,3	0,94	8,2	41,1	32,0	4,9	91,2	6,2	—	95,5
1	60,1	3,3	21,7	0,96	8,5	42,3	32,1	2,3	92,0	6,2	—	96,0
2	41,9	6,0	21,5	0,77	8,6	40,0	32,7	4,9	94,0	4,7	20,2	78,5
2	40,0	6,3	21,9	0,78	8,5	41,1	32,7	2,1	93,8	5,0	—	83,5
3	24,2	7,5	22,5	0,72	7,8	41,2	31,0	4,7	94,5	4,4	37,2	63,6
3	26,6	7,0	22,3	0,74	6,8	40,8	31,7	1,9	95,2	4,6	31,8	54,5

LEGEND: As in Table 6

2. V. I. Smirnov, S. V. Berenov, Sbornik nauchno-issledovatel'skikh rabot Uralgintsvetmeta (Collection: Scientific Research of the Uralgintsvetmet), No. 1, 1935.

Received by Editor
25 March 1963

THEORY OF THREE-LAYER CONTINUOUS CONVERSION OF COPPER MATTES

Yu. Goletsi, Yu. Shmidl and F. Segnalek

(Chair of Non-Ferrous Metallurgy of the Vysshaye tekhnicheskoye uchebnoye zavedeniye /Higher Technical School/, city of Koshitse, Czechoslovak Socialist Republic.)

In the second half of the 19th century copper began to be produced from copper matte by blowing compressed air through a layer of the molten matte. From analogy with the process of purging pig iron this process was called conversion or the Bessemer process, from the name of the English metallurgist Bessemer, although he did not deal with the purging of copper mattes. The predecessor to the conversion process is the Mabuki process, under which even in the 16th century purging of molten matte /1/ was already being applied in Japan.

The first initiator of the method of purging copper matte, similar to the Bessemer process for pig iron, were the Russian engineers V. A. Semennikov, N. A. Iossa, and A. A. Auerbakh in 1966-1880 /3/. Conversion in Egil was carried out by I. Holloway and F. P. Mann in 1880 /4/. In the U.S. conversion was used at the Parro metallurgical plant in 1884 from whence it took the name of Parro conversion.

Over the past century the essential changes were not introduced into converter design. The discontinuity of the process causes substantial stoppages in performance, resulting in significant heat losses. Fluctuations in the temperature of the lining reduces its service, which means additional idle time during repair of linings. The hermetic sealing of the converter top has not been resolved, which hinders the use of heat and sulfur dioxide from the outgoing gases. The converter slag, due to its high content of useful metals, represents reversible material. The main

shortcoming of the existing converters is the imperfect system of blast feed, limiting productivity, and resulting in premature wear of the lining near the tuyeres and, furthermore, requiring much laborious physical work in cleaning the tuyeres, although in recent years experiments have been successfully made on mechanizing tuyere cleaning.

One of the ways of intensifying conversion is the use of oxygen-enriched air. However, under the presently existing design, the converter, even when oxygen-enriched air is used, would be unsuitable even for partial automatization. Therefore, for conversion it is necessary to build a new installation which would afford the possibility of carrying out a continuous process.

In our own research into an installation for continuous conversion we relied in part on the results of the investigations by D. A. Diomidovskiy /5,6/, who suggested that the process be carried out in two separate installations for the first and second periods. He undertook experimental studies in the installation described in the article /5/, using the technology that was the same for converters of existing design.

However, in addition to a new installation, to achieve continuous conversion it is necessary to create a new technology of the continuous production of converter copper in a single installation. The purpose of this article is to consider prerequisites for the continuous conversion of copper matte aimed at the production of crude copper in a single installation.

Thermodynamic analysis of the conversion of copper matte. Before beginning the analysis of the possbility of continuous conversion of copper matte, we present a survey of the theory of the existing process.

It is possible to assume the course of a whole series of reactions between oxygen, copper matte, flux, and their reaction products. Thermodynamic calculations of the reactions of copper matte conversion are given in article /7/ and here we only summarize their results.

The most negative free enthalpy values are found for reactions of the first period, in particular the reactions

$$FeS + 1{,}5O_2 = FeO + SO_2; \quad (1)$$

$$3FeS + 5O_2 = Fe_3O_4 + 3SO_2; \quad (2)$$

$$2FeS + 3O_2 + SiO_2 = 2FeO \cdot SiO_2 + 2SO_2. \quad (3)$$

Reaction (1) is part of reaction (3), therefore in what follows we will look only at reactions (2) and (3). The values of the free enthalpies of these reactions are the most negative.

Temperature affects their order. For instance, in spite of the presence of silica at 1150°, the formation of magnetite occurs predominantly. With increase in temperature the formation of magnetite is reduced and above 1450° it is theoretically precluded, since the value of the free enthalpy of reaction (3) at any concentrations of FeS in the bath will be significantly more negative. The theoretical yield obtained wholly corresponds to practical experiments. Prevention of magnetite appearing at low temperatures by addition of silica is impossible, since at these temperatures silica does not react rapidly enough with the ferrous oxide appearing on the fayalite.

In practical terms, copper mattes almost always contain magnetite and in conversion its further appearance is possible, therefore it is necessary to explain that it occurs with the mattes during conversion. It is obvious that it is either reduced by some one of the compounds presents to ferrous oxide, or enters the slag.

Based on analysis of the modes of magnetite reacting with sulfide it is possible to consider only the overall reaction

$$Fe_3O_4 + FeS + 5SiO_2 = 5(2FeO \cdot SiO_2) + SO_2. \qquad (4)$$

The negative value of free enthalpy of reaction (4) with increase in temperature is increased.

The value of the free enthalpy of the reaction of magnetite with Cu_2S is positive, therefore this reaction does not take place. The formation of metallic iron from the reaction

$$2FeO + FeS = 3Fe + SO_2 \qquad (5)$$

at conversion temperatures also is impossible. Other reactions between the sulfide and the oxide at conversion temperatures do not take place.

Let us now consider the reaction between cuprous sulfide, ferric sulfide, oxygen, and their products. These reactions are as follows:

$$Cu_2S+1{,}5O_2=Cu_2O+SO_2; \quad (6)$$
$$Cu_2O+FeS=Cu_2S+FeO; \quad (7)$$
$$2Cu_2O+2FeS+SiO_2=2Cu_2S+2FeO\cdot SiO_2; \quad (8)$$
$$2Cu_2O+Cu_2S=6Cu+SO_2. \quad (9)$$

The value of free enthalpy of reaction (6) at conversion temperatures is sufficiently negative to theoretically prove the possibility of this reaction occurring in the first period. The possibility of its occurrence is greater the lower the FeS concentration.

The Cu_2O formed can react either with FeS by reactions (7) and (8), or with Cu_2S by reaction (9). The value of free enthalpies of reactions (7) and (8) is more negative than the value of the free enthalpy of reaction (9), therefore at appreciable FeS concentrations its oxidation occurs chiefly.

During purging of copper matte two periods are distinguished. In the first period oxidation of FeS to FeO and Fe_2O takes place, and the slag formation of the FeO forming occurs simultaneously. In the second period the oxidation of Cu_2S occurs by the reaction

$$Cu_2S+O_2=2Cu+SO_2, \quad (10)$$

which is the composite of reactions (6) and (9).

Theoretical possibilities of the continuous conversion of copper matte. Careful thermodynamic analysis of the order of the reactions occurring under the existing methods of copper matte conversion and a study of the changes in their free enthalpy values as a function of temperature and concentration affords the possibility of finding the thermodynamic prerequisites on which to develop a technology for continuous conversion of copper mattes to produce crude copper in a single installation. The main problem is to establish conditions for the simultaneous occurrence of reactions in the first and second periods.

It follows from the foregoing that without lowering the ferric sulfide concentration in the copper matte to a low level, it is impossible to expect metallic copper to be formed. The problem consists in establishing such conditions so that simultaneously with the reactions (1), (2) and (3) the reaction (6) occurs, and such a quantity of Cu_2O is formed which would not wholly react according to equations (7) and (8), but react partially also according to reaction (9).

Change in the values of the free enthalpies of the reactions (1), (2), and (3) depending on the concentration of FeS and Cu_2S is shown in Fig. 1 /8/. With decrease in concentration of FeS the values of the free enthalpies of these reactions are reduced. Simultaneously, during the first period the concentration of Cu_2S is increased, therefore it is possible to obtain such a state of the system in which the free enthalpies of the reactions will become identical. This state, corresponding to the content of 0.002% FeS ($-\lg C_{FeS} = 4.38$), shown in Fig. 1 (.1 a).

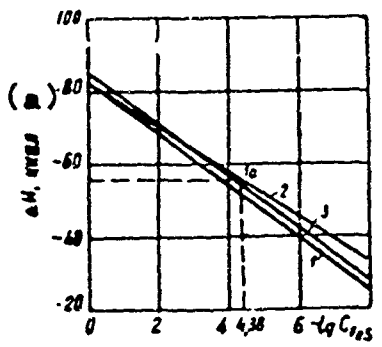

Figure 1. Value of the ΔH_T as a function of the concentration of FeS at 1250°. LEGEND: a) KCal.

From the viewpoint of thermodynamics continuous conversion of copper matte with the production of crude copper in a single installation can be carried out in the following way. In the bath of white matte copper matte is obtained and such a quantity of air which is capable of simultaneously oxidizing the ferrous sulfide supplied with its transition into slag, and cuprous sulfide with the production of converter copper. Here three components are present simultaneously in the bath: converter slag, matte and converter copper. To substantiate the possibility of continuous conversion it is necessary to investigate whether these three compounds can possibly be simultaneously present from the viewpoint of their specific gravity mutual solubility.

The specific gravity depends on temperature. In order to verify the possibility of the stratification of the 3 components, we present the specific gravities for the solid (20°) and molten (1200°) states for several slags and mattes.

The specific gravities of the converter slags are as follows /9/

At	20°	4,10	4,04	4,02	3,91	3,72
At	1200°	3,62	3.57	3,55	3,41	3,22.

The specific gravities of copper mattes as a function of copper content are as follows /9/:

copper content %	specific gravity/cm^3 at 20°	at 1200°
30	4,96	4,13
40	4,99	4,28
50	5,05	4,44
70	5,46	4,93
80	5,77	5,22

In this case the fact that for white matte the highest specific weight is achieved (Fig. 2) is favorable, which results in its improved separation from converter slag.

The specific gravity of converter copper (98.3% Cu) /9/ represents at 20° 8.61 g/cm^3, at 1200° -- 7.78 g/cm^3.

The literature presents various opinions on the solubility of Cu_2S and FeS in slag. Based on latest information it can be assumed that the solubility is limited to such an extent that from the viewpoint of practice one can disregard it. In the FeS - Cu_2S system when molten unlimited mutual solubility exists. Limited solubility is known to exist in the Cu - Cu_2S system. In the continuous conversion an independent layer of converter copper will begin to appear only after the sulfur content in the white matte is reduced to 17.9%, and in addition, the sulfur content in converter copper will amount to 1.8% S. It is true that in the literature it is mentioned /10/ that the Cu - Cu_2S diagram is not accurate and that the solubility of cuprous sulfide is less.

Based on verification of these specific gravities in the molten state and mutual solubilities, it can be concluded that the converter slag, the matte and converter copper will form three layers, will separate from each other.

As has already been indicated, producing converter copper occurs at a very insubstantial (of the order of 0.001%) FeS content. Hence, to realize continuous conversion of copper matte in a single installation it is necessary to undertake conversion in a white matte environment.

As the air sweeps through the level of the melt it encounters a relatively small amount of melt, which is the basis for the mechanism of continuous conversion.

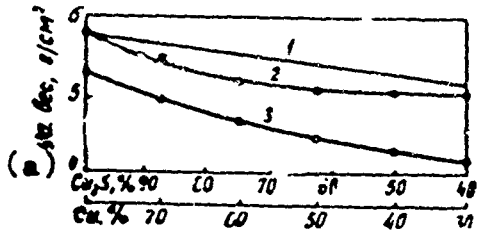

Figure 2. Specific gravities of copper mattes: 1 -- theoretical line; 2 -- for the solid state; 3 -- for the liquid state. LEGEND: a) Specific weight, g/cm^3

Reaction (6), oxidation of Cu_2S with the formation of metallic copper (9) is the chief reaction. The reaction of direct oxidation of ferrous sulfide with air oxygen is of low probability, since the possibility of these two compounds contacting is insubstantial; therefore, the chief oxidizer of FeS is Cu_2O according to reaction (7).

Part of the metallic copper formed, encountering FeS, can react with it according to the equation

$$2Cu+FeS=Cu_2S+Fe, \qquad (11)$$

and metallic iron will be oxidized by cuprous oxide

$$Fe+Cu_2O=2Cu+FeO. \qquad (12)$$

The FeO forming reacts with the present SiO_2 forming fayalite. Direct oxidation of metallic iron and copper by atmospheric oxygen, as true also for the oxidation of FeS, is doubtful.

Taking the law of effective masses into account, one should expect that the layer of metallic copper appears at a significantly higher FeS content in the matte than would be assumed based on the values of the free enthalpies of the reactions occurring during conversion.

Based on analysis of theoretical assumptions of continuous conversion of copper matte in the production of converter copper in a single installation the following technology can be presented /11/.

Initially, it is necessary to prepare the bath to consist of three layers: an upper thin layer of converter slag, a central

thickest layer of white matte, and a lower, also thin layer of converter copper. Preparation is achieved by charging in the continuous converter copper matte and purging air through it to the partial production of crude copper according to the formula conversion technology. After such diepersion continuous conversion commences, consisting of the steady addition to the bath of the original copper matte. The amount of copper matte and flux added should be in agreement with the amount of air blown through, which should be sufficient not only to oxidize the entering ferrous sulfide and to convert it into slag, but also to oxidize the resulting cuprous sulfide. With constant maintenance of the thickness of the separate layers continuous overflowing of the amounts of converter slag and converter copper formed take place.

Conclusions.

The method of conversion of copper matte used thus far has serious deficiencies, especially in that it is unsuitable for automation. To determine the possibility of eliminating these shortages a description has been given in the article of the theoretical analysis of prerequisites for the use of continuous conversion of copper mattes in the production of converter copper in a single installation and the technology of such a process has been suggested.

LITERATURE

1. Hentze, E., Sintern, Schmelzen und Verblassen sulfidischer Erze und Huttenprodukte, Berlin, 1929

2. Avetisyan., Kh. K., Metallurgiya chernoy medi (Metallurgy of Blister Copper), Moscow, 1954.
3. Diomidovskiy, D. A., Pechi tsvetnoy metallurgii (Furnaces Used in Non-Ferrous Metallurgy), Moscow, 1956.
4. Prost, Metallurgie des metaux autres que le fer. Paris, 1924.
5. Diomidovskiy, D. A. et al, Tsvetnyye metally (Non-Ferrous Metals), No 2, 27 (1959).
6. Holeczy, Y., Zprava zo studijneho pobylu v SSSR v ramci stuidijnej pracovnej cesty v dnoch, 26, 5-9, 6, 1960.

7. Schmiedl, Y., Holeczy, Y., Hutnicke listy, 1960, roc XV, c 7, str 529-537.
8. Vyskumna zprava. Nove sposoby spracovania medeneho kamienka Katedra kovohuthictva HF VST v Kosiciach, 1961.
9. Ioganaen, F., Vise, V., Problemy sovremennoy metallurgii (Problems of Modern Metallurgy), No 4, 40 (1958).

10. Radl, R., Fizicheskaya khimiya pirometallurgii medi (perevod s angliyskogo) (Physical Chemistry of Copper Pyrometallurgy (translated from English)), For. Lit. Publ. House, 1955.
11. Ceskoslovensky patent c. 104449.

Received by Editor
28 March 1963

ELECTRODEPOSITION OF SILVER FROM MOLTEN NITRATES

P. V. Polyakov

(Leningrad Polytechnical Institute, Chair of Electropyrometallurgy of Non-Ferrous Metals.)

Electrolytic winning of refractory metals--titanium, zirconium, tantalum, beryllium, and others--are gaining ever greater importance in the national economy. Accordingly, the study of phenomenon related to the electrocrystallization of metals in the electrolysis of molten salts is of great practical interest. No less important is the theoretical side of the question, dealing with the origin and development of the new phase at the cathode.

The requirement placed on the deposits obtained from melts differ, but generally, they lead to macrocrystalline deposits. As is known, the size of the crystal is determined by the ratio of the rates of formation of crystallization centers and their subsequent growth /1/.

Silver belongs to the group of metals that are the most convenient for investigation of the phenomenon of electrocrystallization from melts. Aten with co-workers /2/ were some of the first investigators of deposits of silver obtained from nitrate, halogenide, and sulfate melts. It was shown that the character of the deposits depends on the preliminary heat treatment of the silver cathode. These researchers established the dissolution of the silver along sections with increased temperature and its precipitation on colder sections of the unpolarized electrode. The crystals of silver formed in the electrolysis of melts as a rule were larger than those separated from aqueous solutions. The greatest polarization is observed in the separation of silver from chloride and iodide melts, the least -- from nitrate melts. Polarization increases with decrease in concentration of the silver ion and with decreasing

temperature. Dilution leads to a fine crystalline deposit being obtained.

K. M. Gorbunovaya /3/ also established the dissolution of silver in the zone of increased temperature. Increasing the concentration and temperature according to her data leads to the growth of large crystals only in nitrate melts, but not in chlorides. It was observed that frequently accretion of the separated metal onto the silver cathode occurs and the opinion was stated that high temperature, and the ability of atoms caused by it, facilitates the possibility of their access to sections having a minimum free energy, due to which compact deposits cannot be obtained.

T. Erdey-Gruz and R. F. Kardos /4/ determined the optimal conditions for the growth of a single crystal of silver, for which the best electrolyte is pure nitrate, whereas a single crystal cannot be grown from chlorides. It was established that the growth of crystals is accompanied by certain fluctuations from the regularities formulated by Kossell and Stranskiy; this is accounted for by the adsorption of melt anions along crystal edges. The function $i - \Delta\varphi$ is linear. In some cases an inflection is observed on the polarization curve corresponding to current densities most favorable for crystal growing.

S. Shternberg and D. I. Markhidan /5/ showed that in the electrolysis of molten AgCl chemical polarization is absent. At $D_k \approx 0.2$ amp/cm^2 they found a polarization minimum on the switching off curve.

The study /6/ is concerned with the growth of crystals in the electrocrystallization of silver from molten chlorides.

P. Drossbakh /7/ points to a high value of the surface energy of the electrode, influencing the formation of the electrolytic deposit in the precipitation of silver from chloride melts.

Some of the conditions determining whether compact silver deposits are obtained from molten nitrates are presented in a short report by S. Dbalik, I. Lindau, and F. Z. Sauerwald/ Zauerval'd/ /8/. It was established, in particular, that a positive effect is shown on production of compact deposits by reduced temperature, rotation of cathodes, and application of pulsating current, but also with the addition of salts having low electroconductivity.

The present study presents results of research on the determination of the number of crystalline silver seeds as a function of the electrolysis conditions of molten nitrates.

In the experiments a test tube of molybdenite glass was used, which was placed in an electric furnace with high thermal inertia. The temperature was measured to an accuracy of one degree by a high-temperature thermometer.

Used as cathodes were carefully buffed platinum end-cathodes with an area of $7 \cdot 10^{-4}$ cm^2 and 0.28 cm^2 in the form of wire soldered on the subface in tubes made of molybdenum glass.

The experiments were conducted with a soluble silver anode at constant current intensity using a circuit not fundamentally different from one used previously /9/. The constancy of current intensity with time was achieved by including in the circuit in series a cell of large ohmic resistance. The electrolyte was made of the re-crystallized salts KNO_3 and $NaNO_3$, chemically pure grade, and analytically pure $AgNO_3$.

Before being used the electrode was washed in concentrated nitric acid, then in boiling distilled water, and was thoroughly dried. The condition of the electrode surface was controlled under a microscope at a magnification of 450.

The electrode was kept in the melt for 10 minutes, and then, after being polarized by a current of given intensity, it was washed free of salts in boiling water and its surface with small crystals of silver appearing was examined under microscope.

Before a new experiment the deposit was dissolved in concentrated nitric acid, the electrode was washed and dried.

In the study of the influence of electrolysis conditions the micro-cathode was used in order to have within the field of sight the entire surface on which precipitation occurred.

Preliminary experiments with a large cathode showed that the number of crystallization centers at low concentrations depends in great measure on the surface energy of the faces of separate crystals of platinum constituting the cathode surface (Figure 1). The time required for polarization of the electrode to obtain crystal seeds accessible for observation under the microscope at a magnification of 450 was usually 30 seconds. For longer polarizations the number of crystal seeds was not increased, independent of current density, temperature, and concentration of silver.

In the determination of the number of crystal seeds not less than three experiments under identical conditions were conducted. In most, the results were in agreement. However, in certain cases, passivity of the electrode was found, resulting in a several-fold decrease in the number of the precipitating crystals. Used as electrolyte was a melt consisting of an equimolar mixture of KNO_3 and $NaNO_3$ with the addition of 0.005, 0.02, 0.06, and 0.4 mole $AgNO_3$ per 1 mole of the mixture. Several experiments were conducted with a melt of pure $AgNO_3$

The number of crystal seeds (per 1 cm^2) as a function of variation in current density, temperature, and concentration of silver ions, is presented in the table. At constant

concentrations and temperature the number of crystal seeds increases almost linearly with increase in the current density (Figures 2 and 3).

Number of Silver Crystallization Centers (per 1 cm^2) as a Function of Current Density, Concentration of $AgNO_3$ (molar %) and Temperature

$D_к$, $a/см^2$ (a)	240°	270°	300°	350°
$C_{AgNO_3} = 0{,}005$ м. д. (b)				
$1{,}2\cdot10^{-3}$	$6{,}7\cdot10^5$	$3{,}2\cdot10^5$	$0{,}7\cdot10^5$	$0{,}5\cdot10^5$
$2{,}4\cdot10^{-3}$	$17{,}2\cdot10^5$	$7{,}2\cdot10^5$	$1{,}9\cdot10^5$	$1{,}07\cdot10^5$
$3{,}6\cdot10^{-3}$	$25{,}0\cdot10^5$	—	—	—
$6{,}0\cdot10^{-3}$	$46{,}5\cdot10^5$	$28{,}6\cdot10^5$	$11{,}4\cdot10^5$	$3{,}6\cdot10^5$
$C_{AgNO_3} = 0{,}02$ м. д.				
$1{,}2\cdot10^{-3}$	$1{,}6\cdot10^5$	$0{,}58\cdot10^5$	$0{,}29\cdot10^5$	$0{,}14\cdot10^5$
$8{,}0\cdot10^{-3}$	$11{,}4\cdot10^5$	$6{,}9\cdot10^5$	$2{,}6\cdot10^5$	$0{,}86\cdot10^5$
$22\cdot10^{-3}$	—	—	$10{,}0\cdot10^5$	—
$34\cdot10^{-3}$	$64{,}3\cdot10^5$	$30{,}7\cdot10^5$	$17{,}2\cdot10^5$	$8{,}6\cdot10^5$
$C_{AgNO_3} = 0{,}06$ м. д.				
$3{,}2\cdot10^{-3}$	—	$0{,}13\cdot10$	$0{,}03\cdot10^5$	$0{,}03\cdot10^5$
$8{,}0\cdot10^{-3}$	$0{,}57\cdot10^5$	$0{,}27\cdot10^5$	$0{,}13\cdot10^5$	$0{,}11\cdot10^5$
$34\cdot10^{-3}$	$4{,}7\cdot10^5$	$2{,}85\cdot10^5$	$0{,}57\cdot10^5$	$0{,}57\cdot10^5$
$60\cdot10^{-3}$	$7{,}8\cdot10^5$	$4{,}70\cdot10^5$	$12{,}8\cdot10^5$	$1{,}28\cdot10^5$
$C_{A\ NO_3} = 0{,}40$ м. д.				
$8{,}0\cdot10^{-3}$	$0{,}11\cdot10^5$	$0{,}03\cdot10^5$	$0{,}03\cdot10^5$	$0{,}03\cdot10^5$
$60\cdot10^{-3}$	$0{,}86\cdot10^5$	$0{,}35\cdot10^5$	$0{,}22\cdot10^5$	—
$120\cdot10^{-3}$	$2{,}0\cdot10^5$	$1{,}4\cdot10^5$	$1{,}1\cdot10^5$	—
$240\cdot10^{-3}$	$3{,}6\cdot10^5$	$2{,}3\cdot10^5$	$2{,}7\cdot10^5$	—

LEGEND: a) amp/cm^2; b) molar fraction

For a pure silver nitrate melt the number of crystal seeds as a function of current density under otherwise constant conditions is not so distinctly pronounced.

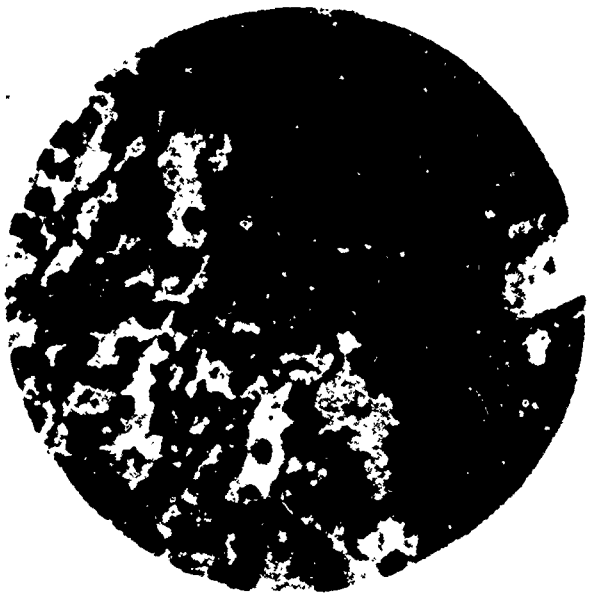

Figure 1. Formation of silver crystallization centers of the platinum cathode. Addition of $AgNO_3$ - 0.2 molar fraction, D_k - $8 \cdot 10^{-3}$ amp/cm^2, τ = 250°.

For example, within the range of current densities of $1 \cdot 10^{-3}$ - $60 \cdot 10^{-3}$ amp/cm^2 after 300° most frequently 1-2 crystals of silver grew, whereas increasing the current density to 240. 10^{-3} amp/cm^2 led to the formation of 6-10 crystals.

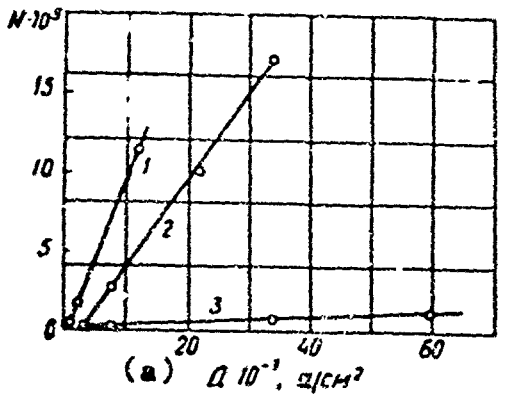

Figure 2. Number of silver crystallization centers (per 1 cm^2) as a function of current density at 300° and for the molar fractions of $AgNO_3$ listed: 0.005 (1); 0.02 (2); 0.06 (3). LEGEND: a) $D \cdot 10^{-3}$, amp/cm^2

At low $AgNO_3$ concentrations, reducing the temperature regularly led to increased number of crystallization centers, in which this effect was especially evident at low temperatures (Figure 4). Change in temperature has a relatively slight effect on the number of crystallization centers at high $AgNO_3$ concentrations (0.4 molar fraction) and in a melt of pure silver nitrate. The change in concentration of $AgNO_3$ decidedly affects the number of crystallization centers formed (Figure 5).

The data obtained allows us to make a comparison of the kinetics of crystal seed formation appearing in the electrolysis of molten nitrates with the kinetics of their formation in solutions of silver nitrate /10-13/.

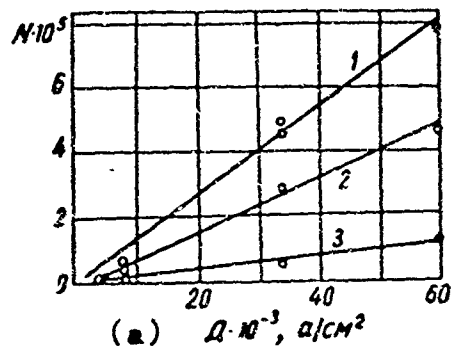

Figure 3. Number of silver crystallization centers (per 1 cm^2) as a function of current density for the molar fraction of 0.06 $AgNO_3$ and the temperatures: 1 -- 240°; 2 -- 270°; 3 -- 300°
LEGEND: a) $D \cdot 10^{-3}$, amp/cm^2

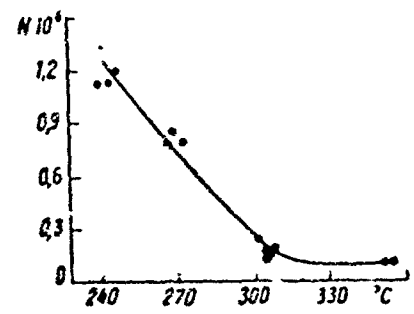

Figure 4. Number of silver crystallization centers as a function of temperature for the melt containing 0.02 mole $AgNO_3$. D_K = $8 \cdot 10^{-3}$ amp/cm^2

In both cases the dependence of the number of centers formed on the current density and concentration is identical in character. This similarity allows us to assume that in both aqueous solutions of $AgNO_3$, as well as in its melts, the process of crystal seed formation is based on the same phenomenon and differs only quantitatively. High temperature and the possibility of conducting electrolysis at very high concentrations allows us to vary the number of centers on the micro-cathode ($7 \cdot 10^{-4}$ cm^2), from a monocrystal obtained in the $AgNO_3$ melt to thousands in low-concentration melts.

The number of crystal centers formed as a function of the variation in current density is linear at constant concentration and temperature, but when the concentration or temperature is varied the slope of the linear function is changed (See Figures 2 and 3), exercising an equivalent influence on the kinetics of crystal seed formation. Increase in concentration or

temperature favors lowering the quantity of centers formed.

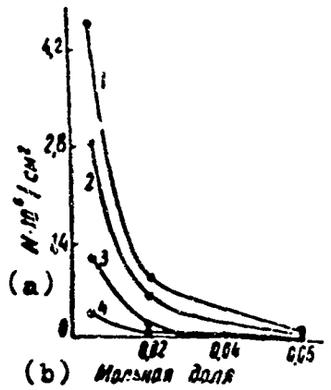

Figure 5. Number of crystallization centers as a function of $AgNO_3$ concentration at $D_K = 6 \cdot 10^{-3}$ amp/cm^2 and the temperatures: 1 -- 240°; 2 -- 270°; 3 -- 300°; and 4 -- 350°. LEGEND: a) $N \cdot 10^6$/cm^2; b) Molar fraction

A point of view exists on the process of silver crystallization on an indifferent cathode in the electrolysis of $AgNO_3$ solutions which holds that the process of ion-seed (or edge of crystal) passes through the stage of formation of an "intermediate phase" /9/. Similar ideas have been expressed by M. Le Blanc /15/ in his time, and also by V. Kohlschutter /14/, and analyzed by H. Fischer /16/.

Schottky /17/ believes that the cathode process does exist: the ion is a mobile atom adsorbed by the cathode's surface--surface diffusion of the atom to the position of lowest energy level (potential well). The assumption can be made that in melts at high temperatures such a process can exist, especially given a high concentration of cations in the melt. In this case the decrease in the number of crystal seeds with increase in temperature and ion concentration can be related to the increase in rate of surface diffusion of the adsorbed atoms of silver and the increasing probability of the formation of a smaller number of crystal seeds. However, this point of view requires experimental confirmation.

Conclusions.

1. Experiments are conducted on the electrolysis of the melts $KNO_3 + NaNO_3$ with various $AgNO_3$ concentrations. For the purpose of studying the kinetics of formation of crystal seeds

of silver on a platinum micro-cathode.

2. A linear dependence was established between the number of crystal seeds formed and current density at constant concentration and temperature. Increase in temperature and concentration results in a decrease in the slope of the linear function curve.

LITERATURE

1. Glazunow, A., J. Phys. Chem., 167, 399 (1933).
2. Aten, A. H., Hertog, H. I., Westenberg, L., Trans. Amer. Electrochem Soc., 47, 265 (1925).
3. Gorbunova, K. M., Izv. AN SSSR, otd. mat. i yest. nauk (News of Academy of Sciences USSR, Division of Math-Physical Sciences), 255 (1933).
4. Gruz-Erdey, T., Kardos, R. F., J. Phys. Chem., 178, 255 (1937).
5. Sternberg, S., Marchidan, D. I., J. Phys. Chem., 218, 250 (1961).
6. Ling Jang, Chien-yeh Chien, Hudson, R. G. J. Electrochem. Soc., 106, 632 (1959).
7. Dressbach, P., J. Electrochem., 56, 599 (1952).
8. Bolik, S., Lindau, I., Sauerwald, F., J. Phys. Chem., 218 141 (1961).
9. Samartsev, A. G., Evstrop'ev, K. S., Zh. fiz. khimii (Journal of Physical Chemistry), 5, 854 (1934).
10. Samartsev, A. G., Trudy 2-i konferentsii po korrozii metallov. Izv. AN SSSR (Works of the 2nd Conference on Corrosion of Metals, News Acad. Sci. USSR), Moscow, 1940.
11. Mikhailov, V. V. Uspekhi khimii (Advances in Chemistry), 18, 724 (1949).
12. Aten, A. H., Boerlage, L. M., Rec. Traw. Chim. Ray Bas. 39, 720 (1920) Cited by in the book by H. Fishcer Elektrolyische Abscheidung und Elektrokristallisation von Metallen. Berlin, 1954.
13. Vagramyan, A. T. Elektrossazhdeniye metallov (Electrodeposition of Metals), Published by the Acad. of Sciences USSR, Moscow, 1950.
14. Kohisehutter, V., Trans. Electrochem. Soc., USA, 45, 229 (1924).
15. Le Blanc, M., Abh. Bunsen Ges. Halle, 1910.
16. Fischer, H., J. Electrochem., 59, 612 (1955).
17. Schottky, W. F., J. Phys. Chem., 31, 40 (1962).

Received by Editor
25 January 1963

CRYSTALLOPTICAL AND THERMOGRAPHIC ANALYSES OF DEPOSITS OBTAINED IN THE PROCESSING OF NEPHELINIC ORE OBTAINED BY A HYDROCHEMICAL METHOD

M. N. Kazov, Z. T. Fateyev, V. D. Ponomarev, S. F. Akhmetov and Kh. N. Nurmagambetov

(Kazakh Polytechnical Institute, Chair of Metallurgy of Light and Rare Metals.)

Through investigation of the various technological operations in the hydrochemical method of processing nephelinic ores it was established that the structure of the deposits after leaching has a substantial effect on the results of subsequent operations.

For elucidation of the structure of these deposits they were studied with crystalloptical and thermographic methods.

The deposit after leaching (sodium-calcium hydrosilicate) were repeatedly examined under the MIN-8 microscope. By the crystalloptical method it was established that the sludge after leaching is monophase in most of its bulk and consists of right angled, very well formed crystals with lightly beveled edges. Their length fluctuates within the limits of 14 - 18 microns, or as the width varies within broader limits of 3 - 9 microns.

Fig. 1 presents a microphotograph of a post-leaching deposit of kiya-shaltyrskiye urtites obtained under laboratory conditions at 290°, a 30 minute exposure and operations lasting for 1.5 hours. The length of the rectangles is 14 - 18 microns, the width is 3 - 4 microns, the interference color is pale (white, grey), extinction is direct, elongation--negative. The indices of refraction are $N_p = 1.595$; $N_g = 1.632$. The compound described is determined as the sodium-calcium hydroxylate /1/. The ore mineral is found as individual grains.

A microphotograph of autoclaved slurry produced on an enlarged laboratory installation, is shown in Fig. 1 b.

In studying thermograms sodium-calcium hydrosilicate is obtained synthetically from calcium oxide and sodium silicate through autoclave treatment of the mixture with a caustic soda solution at 290° for 30 minutes (Fig. 2, curve 1). The curve has one endothermic effect at high 71°, corresponding to the separation of the water of constitution. The thermogram confirms the homogeniety of the deposit obtained, represented as the sodium-calcium hydrosilicate compound.

The curve 2 for the post-leaching deposits of kiya-shaltyrskiye urtites, after being leached on the enlarged laboratory installation, in mixtures with concentrated limestone buffer solution has two endoeffects: at 560°, corresponding to the precipitation out of water of constitution from sodium-calcium hydrosilicate (its value evidences the significant amount of this compound in the precipitate), and at a temperature of 864° /2/, corresponding to the decomposition of calcium carbonate. The presence of calcium carbonate is due to prolonged content of the resultant sodium-calcium hydrosilicate with air during filtration and rinsing (length of operation is 3 - 4 hours).

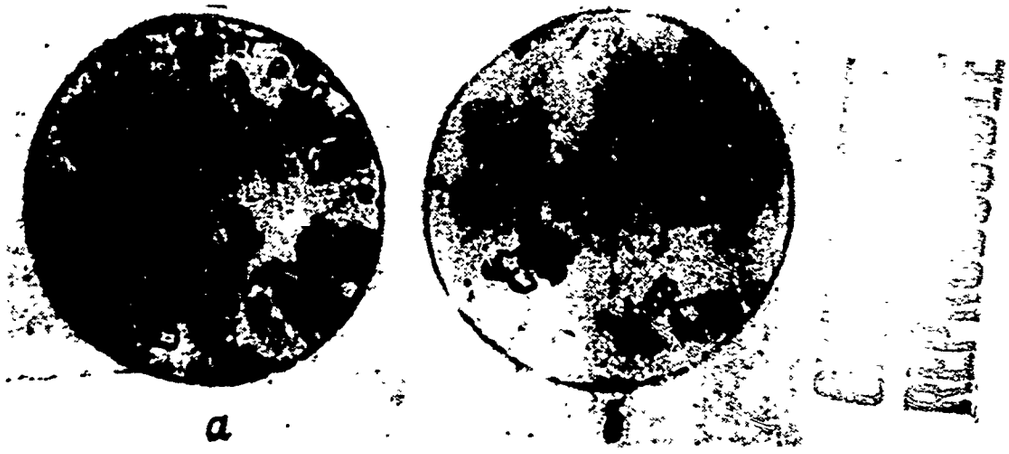

Figure 1. Microphotographs of the structure of the sodium-calcium hydrosilicate obtained by leaching of kiya-shaltyrskiye urtites. X 500.

The endoeffect corresponding to decomposition of calcium carbonate is absent in curve 1, since the duration of filtration and washing of the synthetically prepared deposits in the laboratory autoclave was reduced by 12 - 16-fold (down to 15 - 20 minutes).

As can be seen from the thermograms, the slurry after leaching is chiefy two-phase, although other impurities are present in small amounts. The use of these slurries after leaching for the

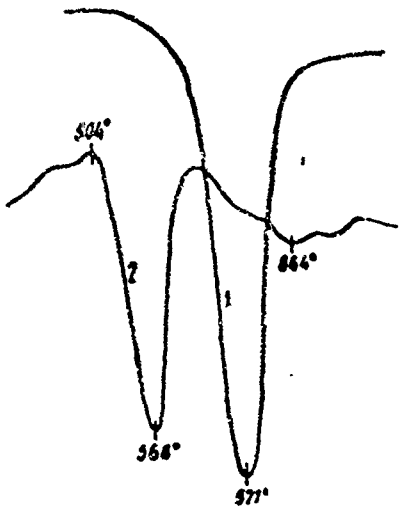

Figure 2. Thermogram of the precipitates obtained following leaching of synthetically produced sodium-calcium hydrosilicate (1) and kiya-shaltyrskiye urtites (2).

Figure 3. Microphotographs of the precipitate following regeneration of sodium oxide from the synthetically prepared sodium-calcium hydrosilicate (a), from the autoclaved slurry of kiya-shaltyrskiye urtites (b), and from the autoclaved slurry obtained from the large-scale laboratory apparatus (c). X 500.

causticization of soda solution showed that the finer precipitates which are obtained when all operations of leaching in the autoclave are carried out fairly rapidly, have the best causticizing capacity, since for the finer crystals the precipitate has a highly active surface. Moreover, one should note that the extent of causticization of the soda solution by the precipitate prepared in the laboratory autoclave is greater than by the precipitate of the enlarged laboratory autoclave due to its shorter contact with atmospheric carbon dioxide. The slurry in the enlarged laboratory installation was carbonized to a large extent and therefore its causticizing ability was less. These considerations are confirmed by crystallo-optical analysis of the precipitates after regeneration, in which calcium carbonate is present along with the main phase.

Deposits after regeneration. Regeneration of sodium oxide is carried out as is usually done with the hydrochemical method, i.e., the slurry following leaching is treated with a solution of caustic alkali at a Na_2O concentration of 60 g/li at 100° for 12 - 15 hours.

Under laboratory conditions regeneration was conducted in an autoclave, and when the enlarged installation was used -- in a mixture. Regeneration in the autoclave was conducted under the conditions of avoidance of contact of the pulp with atmospheric carbon dioxide, whereas this contact was established in the mixer. This accounts for the presence of a large quantity of calcium carbonate in the deposits (up to 50%), obtained after regeneration in mixers.

Presented in Fig. 3 a is a microphotograph of the deposit after regeneration with Na_2O from synthetically prepared sodium-calcium hydrosilicate. Regeneration was conducted in a laboratory autoclave with a caustic soda solution of Na_2O concentration of 59.7 g/li at 100° for 14 hours. The main bulk of the deposit consists of weakly anisotropic grains of calcium metasilicate /1,3/. The grains are almost perfectly spherical, with a diameter of 15 microns. The index of refraction is 1.582. Present in small amounts is the initial phase -- sodium-calcium hydrosilicate and calcium carbonate.

A microphotograph of the deposits after regeneration on the enlarged laboratory installation is shown in Fig. 3 C. Regeneration was performed in a tank with a mixture operating at a rotation rate of 150 rpm, the pulp volume being 40 liters. The concentration of the solution upon regeneration by Na_2O was 60 g/li, temperature = 95°, and duration - 16 hours.

Following regeneration the deposit consisted generally of three phases: carbonate (approximately 50%), calcium metasilicate (irregularly spherical grains with pale interference color, sometimes simply fog-like patches, approximately 40%), and sodium-cal-

cium hydrosilicate (about 10%). A microphotograph of the deposit confirms the earlier expressed assumptions that along with the regeneration of sodium oxide from sodium-calcium hydrosilicate, carbonization of the deposits due to atmospheric carbon dioxide occurs.

The practical absence of minerals evidences good leaching. Therefore, formation of carbonate in general should be related to prolonged contact of the slurry with the air. Carbonization of the deposit can possibly be explained by the high dispersion of the irregularly spherical grains of metasilicate (Cf. Fig. 3 c), since the adsorptive film of carbonate prevented their expansion.

In autoclave regeneration (Cf. Fig. 3 a, b), at 90 - 100° a small amount of carbonate is present in the precipitates. These deposits have greater causticizing ability than deposits obtained on an enlarged installation. Therefore, it follows that during regeneration and causticization that contact of pulp with air be excluded.

The thermogram of metasilicate obtained through regeneration of alkali from synthetic sodium-calcium hydrosilicate (Fig. 4, curve 1) revealed 2 exothermal effects at 164° and 817°.

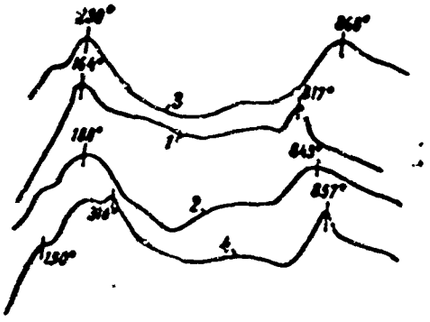

Figure 4. Thermograms of precipitates obtained by heating the sodium-calcium hydrosilicate.

Two exo-effects at approximately the same temperatures are observed on curve 2, obtained in the heating of a deposit corresponding to Fig. 3 b, only here the exo-effects are more blurred.

Corresponding to curves in 3 is the deposit (Fig. 3 c) obtained on an expanded laboratory installation. Here the exo-effects are shown at 230° and 860°.

Curve 4 is recorded during the heating of metasilicate obtained by the overflow of equimolar quantities of sodium silicate and calcium chloride with subsequent washing of the deposit until

the chlorine ions have completely disappeared. Crystalloptically, it proved to be amorphous.

On the thermograms two effects are generally observed: first, the more blurred (its onset coincides with the preceding effect and is continued to 310°), and the second, is the higher (temperature near 860°). In all cases a low-temperature exo-effect is observed at 170-230° with the exception of curve 4.

The absence of endo-effects suggests the thought that the water contained in the deposit is not crystallizational, but derives from obtaining of metasilicate chemically.

In investigations by E. Tilo et al /4/, in the study of the salts of low-molecular silicic acids, in particular calcium silicates, it is indicated that their hydrolysis leads to the formation not of crystal hydrates, but to "acidic" silicates. From the monosilicate $CaNa_2SiO_4$, whose structure has been determined by X-rays, these researchers obtained by the reaction of hydrolysis the calcium-sodium hydromonosilicate -- $CaNaOHSiO_3$ and the calcium dihydromonosilicate $Ca(OH)_2SiO_3$.

The last two compounds are none other than sodium-calcium hydrosilicate, which we obtained during leaching, and which have the composition of $2CaNaOHSiO_3$ or $Na_2O \cdot 2CaO \cdot 2SiO_2 \cdot H_2O$, and calcium metasilicate, obtained in the regeneration of $Ca(OH)_2SiO_3$ or $CaO \cdot SiO_2 \cdot H_2O$.

The authors present the following structural formula:

$$Ca^{2+} \quad 2Na^{+} \quad \left[\begin{array}{c} O \\ | \\ O^- - Si - O^- \\ | \\ O^- \end{array} \right]$$

and regard this compound as the neutral salt of tetrabasic-orthosilicic acid. Therefore, structural formulas of sodium-calcium hydrosilicate (we will retain the name earlier adopted by us) are

$$Ca^{2+} \quad Na^{+} \quad \left[\begin{array}{c} O^- \\ | \\ HO - Si - O^- \\ | \\ O^- \end{array} \right]$$

and for calcium metasilicate,

$$Ca^{2+} \quad \left[\begin{array}{c} OH \\ | \\ HO - Si - O^- \\ | \\ O^- \end{array} \right]$$

E. Tilo et al showed that calcium metasilicate CaH_2SiO_4 is stable toward water. This compound is the final product of the hydrolysis of $CaNa_2SiO_4$, occurring in two steps:

$$CaNa_2SiO_4 + H_2O \rightleftarrows CaNaSiO_4 + NaOH;$$
$$CaNaHSiO_4 + H_2O \rightleftarrows CaH_2SiO_4 + NaOH.$$

The second step of the hydrolysis continues for a longer period with large excess of water. The presence of alkali accelerates it by three-fold. Only at high concentrations of the ions Na^+ and OH^- in the liquid phase is hydrolysis accordingly retarded.

The process called by us regeneration is essentially the hydrolysis described above. And in our experiments regeneration occurs more completely and more rapidly not with water, but with caustic soda solutions of 60 g/li concentration, in terms of Na_2O.

The relatively small transition of silica into the solution can be explained by the fact that silica is bound in the acidic salt CaH_2SiO_4, whose solubility in water is low. Possibly, this silicate is partially decomposed in alkaline solution.

In explaining the exo-effect obtained in the thermograms of metasilicate at 170-230°, we made the suggestion that the system of metastable state is converted into the stable state with the liberation of excess energy.

The same authors speak of the appearance of an unstable phase of $CaNaHSiO_4$, yielding a roentgenogram of $CaNa_2SiO_4$, and only 180° is this unstable product converted into the stable phase of $CaNaHSiO_4$ with its characteristic lattice.

From crystalloptical analysis of the precipitates we have obtained after regeneration at 100° it is clear that in them remained a small amount of the initial phase of the sodium-calcium hydrosilicate, and the main bulk of the precipitate consists of calcium metasilicate. It can be suggested from analogy with the formation of the unstable phase of sodium-calcium hydrosilicate that calcium metasilicate is also in an unstable state, and then the exo-effect at 170-230° can be explained by the transition of the metasilicate to the stable state.

The second exo-effect at 820-860° can be explained by the transformation of calcium metasilicate to wollastonite /4/. This transformation is accompanied by bright glow and by intense compression of the compound. Between 750 and 800° the initial lattice of metasilicate is completely destroyed and the compound becomes amorphous.

Further formation of the crystal lattice of wollastonite is accompanied by liberation of energy, which corresponds to the second exo-effect on curves 1 and 4 of Figure 4.

The precipitates after causticization of the soda solution by sodium-calcium hydrosilicate. The precipitates are obtained as multiphase. Crystalloptical and thermographic analyses frequently cannot give a satisfactory explanation of the composition of the precipitates. However, qualitatively it is possible to assume the cause to be the at times incomplete regeneration of alkali from the precipitate and different extent of use of the precipitate calcium oxide.

Examined under the microscope were precipitates obtained in causticization of soda solution of 100 g/li concentration, for the extent of CaO use ranging from 35% to 60%, and for different degrees of regeneration.

In Figure 5a, b, is shown a microphotograph of the precipitate following causticization of a soda solution by autoclaved slurry. The

conditions of causticization are as follows: temperature = 100°, duration = 10 hours, soda solution concentration = 39.0 g/li of Na_2O. The extent of use of precipitate CaO is 47.4%.

The deposits consist of several phases, the chief of which is carbonate (cf Figure 5 6), represented by fine round or tabular (square) grains with high interference colors. They will form either small clusters or encompass another solid phase. The indices of the fraction are N_p = 1.486, N_d = 1.658. The calcium carbonate content in the precipitate is 50-60%.

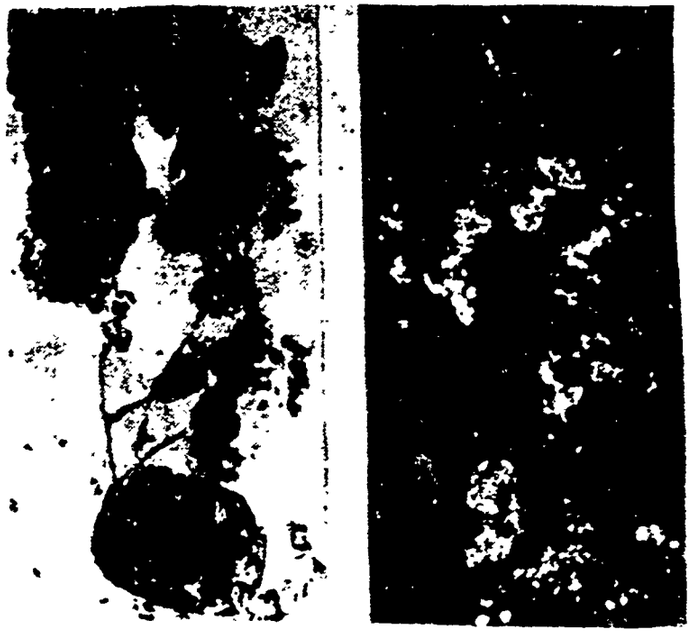

(a) (b)

FIGURE 5. Microphotographs of deposit obtained after treating autoclaved slurry with soda solution of 58.5 g/li Na_2O concentration.
a - Without analyzer;
b - With analyzer
6 600.

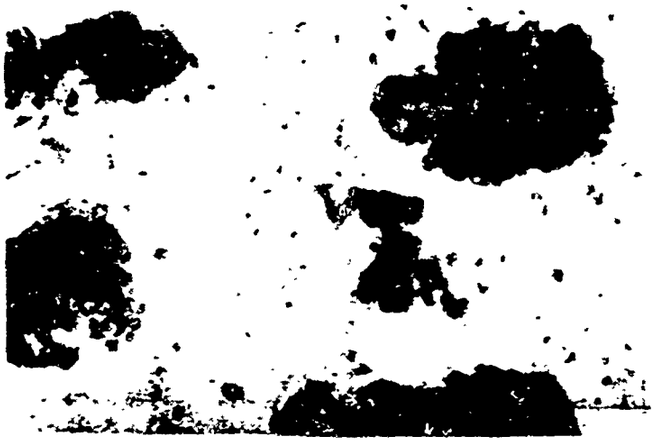

FIGURE 6. Microphotograph of deposit obtained after treatment of autoclaved slurry with soda solution of 39.0 g/li Na_2O concentration, X 500.

The second and third phases are hypothetically represented as undecomposed original sodium-calcium hydrosilicate and calcium hydrosilicate. The phases indicated are nuclei of zonal grains with carbonate growing along the periphery, which does not afford a possibility of determining their indices of refraction. Furthermore, the precipitate contains a small amount of silica (approximately 5%), which will form colorless isotropic grains of 15-30 microns in size, of irregular form with an index of refraction = 1.460.

Analysis of the microphotographs on Figures 5 and 6 and comparison of them with Figures 1 and 3 shows that the process of causticization probably occurs in parallel with regeneration, i.e., with the formation of calcium metasilicate.

Along with the fine grains of carbonate zonal formations are observed, suggestive of metasilicate., but covered by carbonate, which prevents further causticization and possibly, fuller regeneration of alkali from sodium-calcium hydrosilicate.

Conclusions

1. As the result of crystalloptical and thermographic analyses it has become possible to more fully explain the results obtained in the technological operations of regeneration and causticization.

2. It has been shown that the structures of sodium-calcium hydrosilicate varies as a function of length of preparation. To increase the activity of this compound the process must be conducted under conditions favoring minimal contact with atmospheric carbon dioxide.

LITERATURE

1. Pol'dman, M. M., Medvedkov, B. Ye., Ni, L. P., Ponomarev, V. D., Izv. AN Kaz. SSR. Seriya metallurgii, obogashcheniya i ogneuporov (News of the Academy of Sciences Kazakh SSR, Series on Metallurgy, Beneficiation and Refractories), No 5, 1961.
2. Berg, L. G., Vvedeniye v termografiyu (Introduction to Thermography), Published by Academy of Sciences USSR, 1961.
3. Astreyeva, O. M., Petrografiya vyazhushchikh veyshchestv (Petrography of Binding Materials), Gosstroyizdat, 1959.
4. Tilo, Ye., Funk, G., Vikhman, Ye. M., Fizicheskaya khimiya silikatov (Physical Chemistry of Silicates), Foreign Literature Publishing House, 1956.

Received by Editor
6 July 1962

PROBLEM OF OBTAINING PURE MAGNESIUM IN ELECTROLYTIC REFINING

U. D. Deyter and A. I. Belyayev

(Moscow Institute of Steel and Alloys, Chair of Pure Metals and Semi-Conductor Material)

Metallic magnesium, of a purity higher than the purity of magnesium obtained with the electrolytic method at present, is achieved by vacuum deposition. But this method has several shortcomings: periodicity of the process, complicated and expensive equipment, low utilization factor of equipment, and others. Moreover in deposition certain impurities are difficult to remove due to the nearness of the boiling points to that of magnesium (Zn, Ca chlorides).

These shortcomings are not present in the electrolytic method of metal refining, for instance in the production in this way of ultra-pure aluminum. A successful attempt to transfer this process to the metallurgy of magnesium has lately been made by O. A. Lebedev and K. D. Muzhzhavlev /1/. They applied it to produce high-purity magnesium, as well as for processing of the secondary metals. They used both a two-layer as well as a three-layer method for electrolytic refining of metallic magnesium. The metal obtained had approximately the same purity as magnesium purified by sublimation (residual content of impurities = 0.005% by weight).

The aim of this present study was to investigate the effect of electrolyte composition on the yield in terms of current in the electrolytic refining of magnesium and to find the electrolyte composition which gives the highest cathode yield on a current basis.

We used the three-layer method of electrolytic refining (laboratory electrolyzer used in studying this process is shown in Fig. 1). The interpolar distance l varied between 18 and 22 mm. The current intensity was constant in all the experiments and

was equal to 3.0 amperes. The actual current densities on the anode and cathode are difficult to determine. Division of the value of the current intensity by sections of the graphite cathode and anode metal (i.e., the broadened section in the bottom of the crucible) gives D_k = 1.70 amp/cm^2 and D_a = 0.61 amp/cm^2. The operating temperature of the electrolyte (the quantity used was 300 g) was 700° in all cases. Added to all electrolytes was 2% by weight of CaF_2. The salts used, in addition to KCl and KaF_2, were of the technically pure grade. Magnesium chloride (from the magnesiumthermy of titanium) was not free of moisture. Used in each experiment was approximately 20 grams of anode alloy containing 20% Cu. In experiments with electrolyte containing $BaCl_2$, due to the higher specific weight of these alloys the anode alloy contained 35% Cu. The batch of individual components corresponding to the electrolyte composition was loaded in the electrolyzer, and it was placed in a heated furnace. After the salts were melted anode alloy was added and the salt melt was dehydrated and cleaned as it was intensively mixed with an iron spatula.

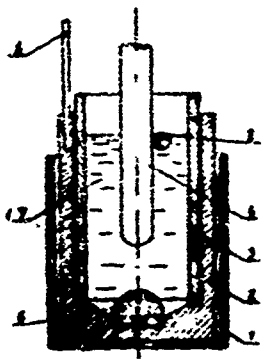

Figure 1. Diagram of the electrolyzer: 1 -- iron crucible; 2 -- graphite crucible; 3 -- corundum diaphragm; 4 -- graphite cathode; 5 -- iron anode current lead-in; 6 -- anode alloy; 7 -- electrolyte; 8 -- cathode metal

After gas evolution ceased the graphite cathode was lowered into the melt and upon attainment of the operating temperature electrolysis was begun. The cathode metal collected on the surface of the electrolyte in the form of little balls up to 5 mm in diamter. Upon completion of the experiment they were collected by the iron spatula into a large ball, which later on hardening of the metal was extracted from the still liquid electrolyte. The electrolyte and the remainder of the anode alloy congealed in the graphite crucible. This was then broken and the anode metal separated from the electrolyte. Part of the anode alloy remaining in the form of fine balls on the bottom of the crucible, in

spite of inclining the crucible bottom, was impossible to extricate. Therefore, calculation of the anode yield in terms of current by difference of the weight of the anode alloy before the experiment and after it gave overhigh values.

In order to determine approximately what values the anode yield actually attains in terms of current several experiments were carried out. Four hundred grams of an electrolyte were melted from separate salts in a corundum crucible (in weight percent): 50 $MgCl_2$, 12.5 KCl, 37.5 NaCl with the addition of 8 grams (to weight percent) of CaF_2; the melt was dehydrated as described above at a temperature of about 750°. When the slurry which was formed upon dehydration settled, the pure electrolyte (300 - 350 grams) was decanted to a second corundum crucible. An anode alloy in a graphite boat was placed into this crucible along with pure magnesium as the "cathode metal". A second batch of anode alloy was added to the graphite boat directly under the surface of the melt, in order to make possible the best comparison of it with pure magnesium (Fig. 2).

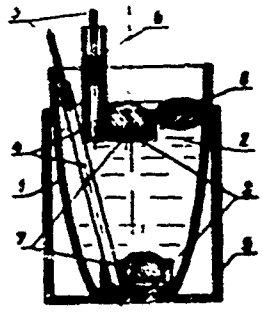

Figure 2. Diagram of the device used for determining chemical losses of magnesium: 1 -- corundum crucible; 2 -- electrolyte; 3 -- graphite boat; 4 -- carbon rod; 5 -- iron wire; 6 -- corundum tube (for protection of the copper rod from oxidation); 7 -- anode melt; 8 -- pure magnesium; 9 -- iron crucible

After sustaining the melt for 3 hours, the weight losses of magnesium and of the anode alloy were determined. The results are

presented in Fig. 3. As can be seen, loss of anode alloy exceeded by almost two-fold the loss of pure magnesium. Within the limits studied the electrolyte's temperature was not determining, and the loss of anode electrode depended little on its location in the electrolyte (on the surface or on the bottom of the crucible). The character of the magnesium losses can be apparently explained as due to the following causes: direct oxidation of the metal at the electrolyte surface by atmospheric oxygen and moisture; oxidation of magnesium chloride owing to absorption of atmospheric oxygen by the electrolyte according to the reaction

$$MgCl_2+H_2O \rightarrow MgOHCl+HCl;$$

subsequent reaction of magnesium hydroxychloride with magnesium

$$Mg+2MgOHCl \rightarrow 2MgO+MgCl_2+H_2;$$

formation of magnesium subchloride by the reaction

$$Mg+MgCl_2 \rightarrow 2MgCl(Mg_2Cl_2).$$

R. A. Sandler /2/ calculated the value of the standard heat formation of magnesium subchloride MgCl, H^0_{298} = - 62.9 kilocalories/mole. Following method described by O. K. Kubaschevskii /Kubashevskiy/ and E. Ewans /3/, the value of the standard enthalpy of MgCl S^0_{298} was calculated as equal to 17.3 kilocalories/mole - deg.

The values of the free energy of the reaction of MgCl formation calculated on the basis of these data to the first approximation of Ulikh remained positive within a broad temperature range (25 - 1105%). This means that the formation of magnesium subchloride under these conditions is thermodynamically of low probability (Table 1).

But actually it is possible to assume that the formation of MgCl occurs directly on the surface of the metal in very small amounts until the equilibrium constant reaches a value which M. G. Bakun and Ye. A. Ukshe /4/ calculated as equal to approximately $40 \cdot 10^{-4}$. The magnesium chloride thus formed is carried away by diffusion and circulation of the electrolytes from the surface of the metal, undergoing a disproportionation reaction:

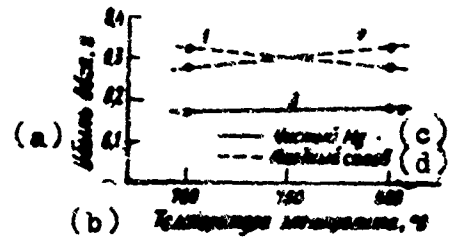

FIGURE 3. Chemical losses as a function of electrolyte temperature: anode alloy on bottom of crucible (1) or directly on electrolyte surface (2); pure magnesium (3). Duration of experiment = three hours.
LEGEND: a) Weight loss, grams; b) Electrolyte temperature; c) Pure magnesium; d) Anode alloy

$$MgCl \longrightarrow 0{,}5Mg+0{,}5MgCl_2.$$

This permits us to explain the appearance of "dark streams" and of some fine particles spreading from the regulus of magnesium and giving "the impression of some sputtering of the metal," of which writes A. I. Zhurin /5/ in conducting experiments on the electrolysis of magnesium.

It is possible to assume that the formation of magnesium subchloride under the influence of the electrolytic potential in electrolysis is increased. Weight losses of the anode alloy and of pure magnesium differing greatly from each other are obviously caused by the formation on the anode alloy surface of galvanic short-circuiting elements (in which copper is the cathode) that favor dissolution of magnesium.

The weight losses found give for the strength of the current used in electrolysis (3 amperes) a decrease in the cathode yield in terms of the current of 4% and an increase in the anode yield in terms of the current of 8%. Of course, it is impossible to transfer these values directly to experiments in electrolytic refining, but they in any case give us an idea of the extent of chemical losses of magnesium. Since mechanical losses of the anode metal are actually absent, then we can assume that the anode yield in terms of current in our experiment is 105 - 115%.

The experiments in electrolytic refining of magnesium using electrolytes based on alloys of the $MgCl_2$ - KCl - NaCl system in order to find the optimal content of $MgCl_2$ and the optimal KCl: (KCl + NaCl) ratio in the electrolytes were conducted. Then the possibility of increasing the cathode yield in terms of current by increasing the specific gravity of the salt melt by adding calcium chloride or barium chloride was studied.

TABLE 1

Temperature Dependence of Free Energy Z_T^0 of the Reaction $Mg + MgCl_2 \rightleftarrows 2MgCl$

(a) Температура		(b) Z_T°, ккал
°K	°C	
298	25	+25,98
923	650	+22,59
987	714	+22,39
1378	1105	+22,25

LEGEND: a) Temperature; b) Z_T°, kcal

Results of the first series of experiments are presented in Fig. 4. As can be seen, the content of $MgCl_2$ and KCl:(KCl + NaCl) ratio in the electrolyte have a decisive influence on the cathode yield in terms of current. For a content of approximately 45 weight % of $MgCl_2$ the value of the current-based yield in KCl-3 electrolyte /KCl:(KCl + NaCl) = 0/ reaches a maximum value (96 - 97%). With an increase in $MgCl_2$ concentration η_{T_K} is lowered sharply. The curve of the yield in terms of current for the electrolyte with higher KCl:(KCl + NaCl) ratios are lower on the curve, but rise with increase in $MgCl_2$ content of 45 weight %. However, their slope is more gradual. Maxima have also been noted for these, corresponding to definite concentrations of $MgCl_2$ which are the higher the higher the KCl content in the electrolyte. But absolute values of the maxima do not exceed 92%.

In Fig. 5 are plotted the lines of equal cathode yields in terms of current for the melts of the $MgCl_2$-KCl-NaCl system, constructed on the basis of the results obtained. From Fig. 5 we can easily see the favorable influence on the yield in terms of current of alloys free of KCl with a content of 45 weight % $MgCl_2$; it is also clear that with increased $MgCl_2$ content in the electrodes above 50 weight %, the KCl content must also be augmented, so that it is possible to achieve in each case a maximum yield in terms of

current, but simultaneously its absolute value is reduced.

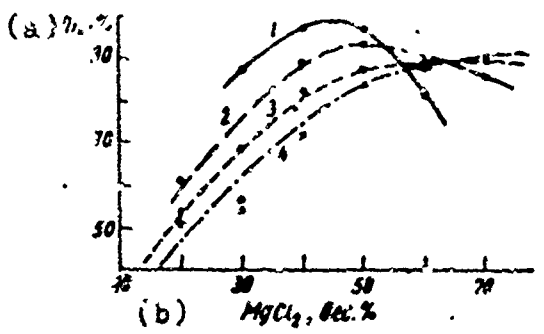

FIGURE 4. Cathode current-based yield as a function of $MgCl_2$ content in electrolytes of the $MgCl_2$-KCl-NaCl system. Weight ratios of KCl : (KCl + NaCl):1 - 0; 2 - 0.25; 3 - 0.5; 4 - 0.75 LEGEND: a) η_{T_k} ; b) $MgCl_2$, weight percent

The effect of the KCl:(KCl + NaCl) ratio in the electrolyte on the current-based cathode yield that was found is accounted for by the following. Both KCl as well as NaCl form in the solid phase compounds with magnesium chloride. This means that both chlorides in the molten state with magnesium chloride yield complexes, i.e., lower the activity of $MgCl_2$, and here the complexes with KCl are more stable than complexes with NaCl /6, page 77/. This is due to the fact that the compounds $KCl \cdot MgCl_2$ and $2KCl \cdot MgCl_2$ are dystectics /7, pages 349, 362/ and that the compounds $NaCl \cdot MgCl_2$ and $2NaCl \cdot MgCl_2$ melt incoherently /7, pages 499, 501/.

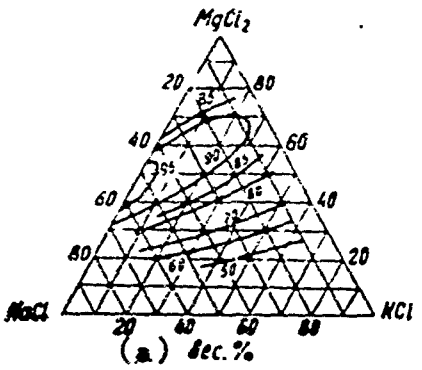

FIGURE 5. Lines of equal cathode current-based yields (%) in the $MgCl_2$- KCl-NaCl system.
LEGEND: a) Weight percent

In order to better represent the effect of complexes of KCl with $MgCl_2$ on the current-based cathode yield an attempt is made to graphically represent η_{T_K} as a function of the content of "free" $MgCl_2$ in the electrolyte (Fig. 6). Taken as the content of "free" $MgCl_2$ was the difference between the KCl and the $MgCl_2$ concentrations in the electrolyte in mol. %, i.e., $MgCl_2$ free = $MgCl_2$ abs - KCl.

In Fig. 6 it is clear that independently of the KCl:(KCl + NaCl) ratio in the electrolyte the cathode yield maxima in terms of current are reached for a "free" $MgCl_2$ content in the electrolyte within the limits of 25 - 40 mole %. This graph of course does not quite accurately reflect the true experimental situation. Thus, for instance, the negative values for the "free" $MgCl_2$ content are impossible (they occurred at high concentrations of KCl and low concentrations of $MgCl_2$ in the electrolyte).

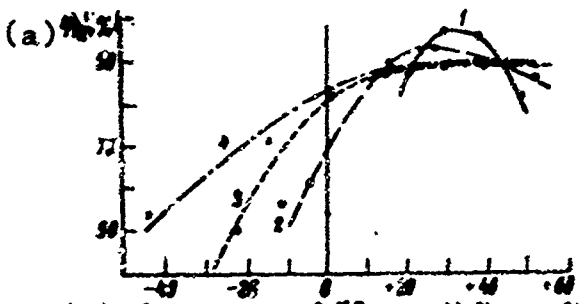

FIGURE 6. Cathode current-based yield as a function of "free" $MgCl_2$ content in electrolytes of the $MgCl_2$-KCl-NaCl system. Weight ratios of KCl: (KCl + NaCl); 1 - 0; 2 - 0.25; 3 - 0.5; 4 - 0.75.
LEGEND: a) η_{T_K}; b) Content of "free" $MgCl_2$, mole-%

With the addition of $CaCl_2$ to the electrolyte a few experiments were carried out, since a more substantial increase in the specific weight of the electrolyte can be achieved with barium chloride. The results of the experiments are presented in Fig. 7 a. The comparison curves shown in this figure gives us the cathode yield in terms of current, which was attained in these electrolytes, but without the addition of $CaCl_2$.

It is clear from the curves (Fig. 6) that at given ratios of other electrolyte components $CaCl_2$ significantly increases the cathode yield in terms of current. The effect of $CaCl_2$ can be explained as follows: $CaCl_2$ forms in the solid phase a compound with KCl, $CaCl_2 \cdot KCl$ (dystectic) with melting point of 754°. With $MgCl_2$

and NaCl, calcium chloride does not produce compounds in the solid phase /7, page 179/. Due to the higher melting point of the $CaCl_2 \cdot KCl$ compound compared to the compounds $KCl \cdot MgCl_2$ (488°) and $2\,KCl \cdot MgCl_2$ (433) it can be assumed that in the melt complexes of $CaCl_2$ with KCl are more stable than complexes of $MgCl_2$ with KCl. Therefore, the $CaCl_2$ introduced into the electrolyte, forming complexes with KCl reduces the amount of complexes of $MgCl_2$ with KCl in the electrolyte and thus accounts for an increase in the content of "free" $MgCl_2$. This latter content approaches the optimal value, since that in addition with the increased specific weight of the salt solution a rise in cathode yield based on current.

The effect of 10% $BaCl_2$ in electrolytes containing 40 weight percent $MgCl_2$ on the current-based cathode yield as a function of the weight ratio KCl: (KCl + NaCl) shown in Figure 7 b. As we can see, addition of $BaCl_2$ at the given $MgCl_2$ content results in an increase in the cathode current-based yield compared to the $BaCl_2$-free starting melts only when the weight ratio KCl: (KCl + NaCl) is higher than 0.3.

The main reason for such an effect of $BaCl_2$ on the current-based yield is apparent in the following description. Whereas in the system NaCl - $BaCl_2$ there is no chemical compound /7, pages 119-121/, $BaCl_2$ forms with KCl in the solid phase the compound $2\,KCl \cdot BaCl_2$ (dystectic, with melting point of 660°) /7, 113 and 114/. As also for the case of $CaCl_2$, it can be assumed that complexes of $BaCl_2$ with KCl_2 in the melt are stabler than complexes of KCl with $MgCl_2$. Therefore, the addition of $BaCl_2$ to melts with a high KCl: (KCl + NaCl) ratio also increases the content of "free" $MgCl_2$, which in addition to increasing the specific gravity of the electrolyte, also leads to the positive effect of $BaCl_2$ on the current-based cathode yield.

For electrolytes with low KCl concentrations, or those free of KCl, complexes of $MgCl_2$ with KCl are few and not at all present, so that almost all the $MgCl_2$ is in the free state.

Little data /7, page 117/ is on the $BaCl_2$-$MgCl_2$ system. Both chlorides form in the solid phase a compound containing approximately 40 mole-% $BaCl_2$ (which corresponds to $3\,MgCl_2 \cdot 2\,BaCl_2$), which decomposes at 590°, but due to the relatively high decomposition temperature $BaCl_2$ is more capable of forming in the melt complexes with $MgCl_2$ than is NaCl ($NaCl \cdot MgCl_2$ decomposes at 465° and $2\,NaCl \cdot MgCl_2$ at 415°).

Therefore, the addition of the $BaCl_2$ to melts with low KCl: (KCl + NaCl) ratio leads to a reduction in the content of "free" $MgCl_2$, in which the concentration of the latter leaves the optimal region and the current-based cathode yield is diminished. With increased KCl content in the melts complexes of $MgCl_2$ with $BaCl_2$ are formed to a lesser extent, because of complexes of $BaCl_2$ with KCl are stabler due to the different behavior during fusion of the corresponding compounds $2\,KCl \cdot BaCl_2$ (dystectic) and $3\,MgCl_2 \cdot 2\,BaCl_2$

(this melts incoherently).

Figure 7c shows the effect of 20% Ba Cl_2 on the current-based cathode yield as a function of the weight ratio KCl: (KCl + Na Cl) in melts with a constant composition of 40 weight percent Mg Cl_2. In contrast to the behavior of the curve in Figure 7b, here the negative effect of Ba Cl_2 in the electrolyte free of KCl or with low KCl content is not observed. Since complexes of Ba Cl_2 with Mg Cl_2 in the melt are not stable, then it can be assumed that compared to melts lean in magnesium chloride content (Figure 7b), complexation between Ba Cl_2 and Mg Cl_2 does not increase sharply, in spite of the higher Ba Cl_2 content. Moreover, in the original melts (See Figure 7c) the content of "free" Mg Cl_2 is greater and the increase in the specific gravity of the melts here is very significant, such that the negative influence of Ba Cl_2 is not observed. The positive effect of Ba Cl_2 in electrolytes with a higher KCl: (KCl + Na Cl) ratio (0.5-0.75) of course, is preserved. In this region of the curve the absolute values of the η_T is somewhat lower than the corresponding electrolytes in Figure 7b. This is due to the fact that here the addition of Ba Cl_2 is responsible for such a decided elevation in the content of "free" Mg Cl_2 that it departs from the optimal region.

To determine the optimal working temperature for electrolytes several experiments were conducted using the electrolyte number 12: 40 weight percent Mg Cl_2 60 weight percent Na Cl + 2% Ca F_2 and the electrolyte No 16:50 weight percent Mg Cl_2, 50 weight percent Ba Cl_2 + 2% Ca F_2. In experiments with the electrolyte No 16 previously dehydrated salt melt was used (dehydration at 700° using an anode alloy, separation of the pure melt from the slurry and metal by decanting). This made it possible to determine more or less precisely the actual anode current-based yield in electrolysis.

The results of these experiments are shown in Figure 7. In accordance with the electrolysis experiments on magnesium /9, page 231/, a working temperature of approximately 680° proved to be the best.

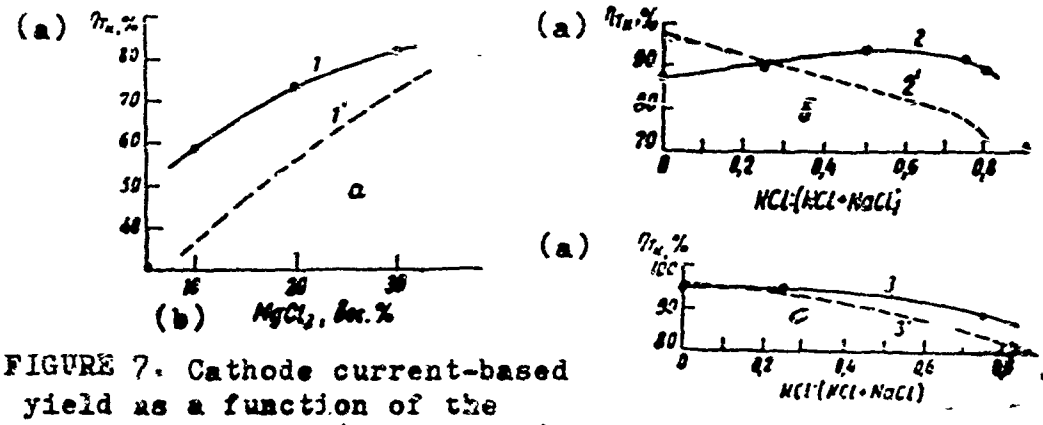

FIGURE 7. Cathode current-based yield as a function of the weight ratio KCl:(KCl + NaCl) in electrolytes of the follow-

(continued next page)

ing systems (weight %): a - 10$CaCl_2$-40$MgCl_2$-KCl-NaCl (1); b - 10$BaCl_2$-40$MgCl_2$-KCl-NaCl (2); c - 20$BaCl_2$-40$MgCl_2$-KCl-NaCl (3). 1', 2', 3' - Comparison curves. LEGEND: a) η_{T_k} ; b) $MgCl_2$, wt. %.

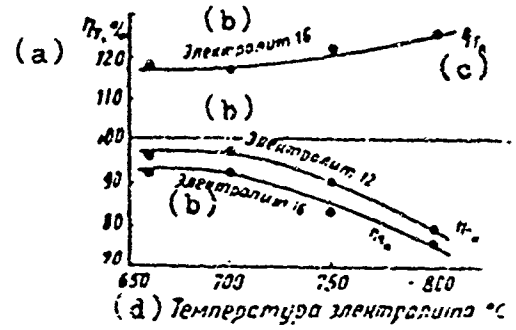

FIGURE 8. Cathode and anode current-based yield as the function of electrolyte temperature. LEGEND: a) η_T; b) Electrolyte; c) η_{T_k} ; d) Electrolyte temperature °C.

Some samples of the cathode metal the composition of the impurity Al, Fe, Cu, and Si (Table 2) were determined by chemical analysis. In not a single case was it possible to detect silicon.

Comparison with the composition of the original metal (magnesium of grade MG 1) showed that the composition of aluminum and copper is not diminished, but the iron impurity is significantly reduced. It must be noted that the amount of cathode metal obtained in the experiment was very moderate, which made determination of aluminum difficult, very far from precise determination. Moreover, as the experiments of O. A. Lebedev and K. E. Muzhzhavlev /1/ have shown, the content of impurities in the cathode metal, especially the Al content, depends strongly on the anode density of the current and increases with the latter. Since in our experiments a relatively high anode current density was used, the relatively low frequency of the cathode metal becomes understandable. We must add here that salts that were chemically not pure were used for the electrolytes, which also affected the purity of the resulting cathode magnesium, although some purification of the salt melt occurred in the dehydration from the anode alloy.

Further, it can be assumed that a certain portion of the very fine drops of anode alloy forming in dehydration were swept along by the circulating electrolyte to the cathode metal and contaminated it. This is especially clearly seen in experiments with the electrolyte No 32. The use of a lighter anode alloy containing 20% Cu here resulted in an impurity content in the cathode metal twice as high as that obtained when an anode alloy containing 35% Cu was used (See Table 2).

Nonetheless, in experiments we conducted the total purity of purity of magnesium following electrolytic refining is 100-200% higher than the original.

TABLE 2

Purity of Cathode Magnesium.

№ электролита (a)	Состав электролита, (b) вес. % $BaCl_2$	$MgCl_2$	KCl	NaCl	Cu в анодном сплаве, вес. % (c)	Среднее значение $\eta_{T_к}$, % (d)	Содержание примесей, вес. % (e) Al	Fe	Cu	Si	Итого (f)
12	—	40	—	60	20	96,83	0,020	0,006	0,030	—	0,056
30	10	40	25	25	35	94,00	0,023	0,013	0,011	—	0,047
32	10	40	—	50	20	89,20	0,035	0,019	0,029	—	0,083
—	10	40	—	50	35	87,43	0,022	0,007	0,012	—	0,041
38	20	40	30	10	35	88,50	(g) следы	0,010	0,015	—	0,025
40	20	40	—	40	35	84,87	0,016	0,006	0,013	—	0,035
43	30	40	—	30	35	95,65	0,020	0,019	следы (g)	—	0,039
Исходный металл—магний марки МГ1 (ГОСТ 804-56) (h)							0,020	0,040	0,01	0,01	0,080

LEGEND: a) Electrolyte No; b) Electrolyte composition, weight %; c) Cu in anode alloy, weight %; d) Mean value of $\eta_{T_к}$, %; e) Content of impurities, weight %; f) Total; g) Traces; h) Original metal-magnesium of MG 1 grade (GOST 804-56).

Conclusions

1. The highest current-based cathode yield in the electrolytic refining of magnesium was obtained for a cathode current density of 1.70 ampires/cm^2, using an electrolyte based on melts of the system $MgCl_2$ - KCl-NaCl, in which the content of "free" $MgCl_{2\,ads}$ - KCl is 25-40 mole %. The current-based yield is the higher the lower the KCl:(KCl + NaCl) ratio in the electrolyte.

2. Additions to the electrolyte of $CaCl_2$ and $BaCl_2$, besides increasing the specific gravity of the electrolyte, have a positive influence on the current-based yield, especially in melts rich in potassium chloride. The presence of $BaCl_2$ in electrolytes free of KCl can lead to a certain decrease in the current-based cathode yield.

3. The optimal working temperature of the process of electrolytic refining of magnesium is approximately 680°.

LITERATURE

1. Lebedev, O. A., Muzhzhavlev, K. D., Izv. VUZ, Tsvetnaya metallurgiya (News of the Higher Education Institutions, Non-Ferrous Metallurgy), No 6, 80 (1960); No 2; 72 (1962).

2. Sandler, R. A., Tr. VAMI (Works of the All-Union Aluminum and Magnesium Inst.) No 47, Leningrad, p 106, 1961.
3. Kubaschewski, O., Ewans, E., Metallurgical Thermochemistry. N.Y.-Paris, 193, 1958.
4. Bukun, N. G., Ukshe, E. A., DAN SSSR, Vol.128, No 6, 1217 (1959).
5. Zhurin, A. I., Metallurg (Metallurgist) 10, 487 (1935).

6. Delimarskiy, Yu. K., Markov, B. F., Elektrokhimiya rasplavlennykh soley (Electrochemistry of Molten Salts), Metallurgizdat, Moscow, 1960.
7. Spravochnik po plavkosti solevykh sistem (Handbook on Fusibility of Salt Systems), Vol 1, Acad. Sci. USSR Publ. House, Moscow-Leningrad, 1961.
8. Strelets, Kh. L., et al., Metallurgiya magniya (Metallurgy of Magnesium), Metallurgizdat, Moscow, 1960.

Received
29 December 1962

EXTRACTION OF VANADIUM FROM CONVERTER SLAG BY THE METHOD OF CHLORINATION IN THE MELT

S. A. Amirov, V. V. Pechkovskiy, R. Kh. Kurmayev

(Permsk Polytechnical Institute, Chair of the Technology of Inorganic Compounds)

The existing method of recovery of a vanadium from converter slag by the method of oxidative roasting with sylvinite has several shortcomings, mainly: the rotary furnaces used for roasting are cumbersome and of low productivity; the processes of leaching, filtration, and precipitation are periodic, laborious, and involve manual labor; the vanadium pentoxide obtained is contaminated with impurities and cannot be used without refining not only to obtain ductile metallic vanadium, but also as raw material for chemical production; the extent of vanadium recovery is relatively low; such value components as titanium, chromium, and others are irretrievably lost to waste.

Therefore, the need of investigating the methods of slag processing which would permit not only an increase in the recovery of vanadium, but also allow the complex use of the raw material is evident.

Considering the complicated composition of slag and its elemental content, readily forming volatile chlorides, the chlorination method is the most advisable to use.

Most metals in the groups IV and V of the periodic system will form volatile chlorides with low boiling point or sublimation. This property has already been used for extraction of many of these metals. For vanadium-containing materials the chlorination method was first applied by Khote in 1885 for processing vanadinites. The chlorination of Kufinskiye and other concentrates has been studied by Krafil'nikov. M.N. Sobolev /1/ presents data on the chlorination of slag in hydrochloric acid solution to dry chlorine. The highest extraction of the vanadium (94.9%) has been reached by this researcher

in the chlorination of uncalcined slag with carbine at 800°. Pokornyy /2/ has studied the chlorination of lead-zinc vanadites. Block and Ferrante /2/ produced vanadium chloride from the chemically pure pentoxide in the presence of gas black. Research on chlorination of ferrovanadium with subsequent purification of the crude chloride has been conducted by Tayzek and Ingleud /2/, Gropfhianu and Tribunescu /3/. Of interest also is the work of Capley and Roddy /Kaple and Roddi/ /4/ on the preparation of the vanadium pentoxide of high purity by the chlorination of "red cake". Erlich and Seifert /5/ have dealt with the chlorination of vanadium-containing materials using hydrogen chloride. As to the most recent work one should note research on the chlorination of converter slag in a fixed layer /6,7/ which shows the possibility of practically complete recovery of vanadium. Fowley,Wood, and Hawk /2/ believe that reduction of the corresponding vanadium chloride by magnesium is the basis on which the process of producing high purity vanadium on an industrial scale must be developed. Several years ago a semi-industrial production line of ductile vanadium by reduction from VCl_2, which was produced by chlorination of ferrovanadium containing 80% V /8/ was carried out in Great Britain.

In considering the chlorination process, we must dwell on methods of separating the chlorides formed. It is known from the literature /9-11/, that the vanadium chlorides VCl_4 and $VOCl_3$, which are liquids, are unlimited in miscibility both among themselves, as well as with the chlorides $TiCl_4$, CCl_4, $FeCl_2$, $AlCl_3$, and $POCl_3$ and probably can be divided by the methods of distillation and rectification. VCl_3, a crystal under ordinary conditions, is obtained by the thermal decomposition of the vanadium tetrachloride.

From a survey of the literature it follows that the chlorination method is very promising for the recovery of vanadium and that the ductile vanadium and its pentoxide obtained through this process are of high purity. However, until recently no rational technology of vanadium recovery and also of other components from converter slag has been proposed with indices higher than the existing technology.

Many others have tried to produce raw material for vanadium production by the chlorination of expensive ferrovanadium. In the chlorination the low-intensity and expensive process of the fixed layer charge was used, here almost all the iron was calcined together with the vanadium chlorides, contaminating the latter. If one would consider that the iron content in the slags is three-four times higher than that of the vanadium, then it is obvious that such a process is of very low efficiency. The same is true for the "fluidized layer" process, which is in fact in this case technologically difficult to carry out /7/.

These shortcomings can be solved by applying the method of chlorination of material in the melt of chlorides of alkali metals.

We know from the literature /12/ that the chlorides of iron will form with the chlorides of alkali metals low-volatility compounds of the $MeFeCl_4$. The vapor pressure of the tetrachlorferrate of alkali metal is many times lower compared to the vapor pressure of binary chlorides.

The method of chlorination in the melts found wide application in the production of magnesium and titanium and successfully competes with the method of chlorination of briquetted charge. This process is technologically easy to carry out and is of high productivity.

The aim of this report is study of the conditions of chlorination of converter slag in the medium of molten chlorides of alkali metals.

Used as raw material for the experiments was converter slag from the Chusovskiy Metallurgical Plant, obtained in the processing of iron-ore concentrates of the Kachkaranskiy deposit, whose composition is as follows (in weight %): 11.07 V_2O_5; 6.0 TiO_2; 51.6 FeO; 2.2 Fe_{metal}; 3.8 MnO; 20.7 SiO_2; 2.5 Cr_2O_3; 1.5 Al_2O_3; 1.2 CaO; 0.8 MgO.

Petrographic analysis revealed that the vein mineralogical constituentes of slag include spinellide, fayalite, and chrystoballite. Vanadium is contained in spinellide (Fe, Mn) O·$(V,Ti,Cr,Al,Fe)_2O_3$, and is also observed often in concretions with another mineral phase -- fayalite $(Fe,Mn,Ca,Mg)_2SiO_4$ and is present in the slag as grains of laminar and prismatic form of light-yellow color. Chrystoballite is present in small amount and will form colorless laminar grains. Approximately 3% is hematite and glass. The grains of glass are russet-colored, indicating the presence in it of ferrous oxide. Individual prismatic crystals are observed in transmitted light, of clear cleavage and red interference color of the first order ($N_{aver} \approx 1.767$), which can be grouped as metasilicates of the (Fe, Mn, Ca, Mg)SiO_3 type. The changes in the standard isobaro-isothermal potential for reactions of chlorination of the main constituentes of the slag have been calculated for the 600-1000° temperature range, which is shown in Table 1 and Figure 1. Ferrous chloride and vanadium trioxide are appreciably capable of being chlorinated without a reducing agent. Under these conditions the formation of a vanadium trichloride is the most probable -- a compound which is practically involatile. Therefore, the separation of the vanadium in the form of its volatile chlorides (VCl_4 and $VOCl_3$) under these conditions is of low probability. In the presence of a reducing agent chlorination of the oxides of the vanadium and iron with the formation of the lower chlorides has thermodynamic advantages when compared with Ti_2O_3 and SiO_2. Even though the chlorination of the last-named compounds in the presence of a reducing agent is also characterized by high enough negative values of ΔH, still the decisive factor which determines the practical extent of chlorination of the various oxides and the possibility of the formation of given vanadium chlorides is the kinetics of the processes occuring.

In chlorination in the melt the kind of processes occurring at the interfaces and the rate of removal of the chlorides formed from the melt are of great significance.

TABLE 1

Reactions of Chlorination of Oxides in Melts

№ реакции (a)	(b) Реакция	№ реакции	(b) Реакция
1	$\frac{1}{3}V_2O_3+Cl_2=\frac{2}{3}VCl_3+\frac{1}{2}O_2$	12	$FeO+Cl_2+\frac{1}{2}C=FeCl_2+\frac{1}{2}CO_2$
2	$\frac{1}{3}V_2O_3+Cl_2+C=\frac{2}{3}VCl_3+CO$	13	$\frac{2}{3}FeO+Cl_2=\frac{2}{3}FeCl_3+\frac{1}{3}O_2$
3	$\frac{1}{3}V_2O_3+Cl_2+\frac{1}{2}C=\frac{2}{3}VCl_3+\frac{1}{2}CO_2$	14	$\frac{2}{3}FeO+Cl_2+\frac{2}{3}C=\frac{2}{3}FeCl_3+\frac{2}{3}CO$
4	$\frac{1}{4}V_2O_3+Cl_2=\frac{1}{2}VCl_4+\frac{3}{8}O_2$	15	$\frac{2}{3}FeO+Cl_2+\frac{1}{3}C=\frac{2}{3}FeCl_3+\frac{1}{3}CO_2$
5	$\frac{1}{4}V_2O_3+Cl_2+\frac{3}{4}C=\frac{1}{2}VCl_4+\frac{3}{4}CO$	16	$\frac{1}{4}Ti_2O_3+Cl_2=\frac{1}{2}TiCl_4+\frac{3}{8}O_2$
6	$\frac{1}{4}V_2O_3+Cl_2+\frac{3}{8}C=\frac{1}{2}VCl_4+\frac{3}{8}CO_2$	17	$\frac{1}{4}Ti_2O_3+Cl_2+\frac{3}{4}C=\frac{1}{2}TiCl_4+\frac{3}{4}CO$
7	$\frac{1}{3}V_2O_3+Cl_2+\frac{2}{3}VOCl_3+\frac{1}{6}O_2$	18	$\frac{1}{4}Ti_2O_3+Cl_2+\frac{3}{8}C=\frac{1}{2}TiCl_4+\frac{3}{8}CO_2$
8	$\frac{1}{3}V_2O_3+Cl_2+\frac{1}{3}C=\frac{2}{3}VOCl_3+\frac{1}{3}CO$	19	$\frac{1}{2}SiO_2+Cl_2=\frac{1}{2}SiCl_4+\frac{1}{2}O_2$
9	$\frac{1}{3}V_2O_3+Cl_2+\frac{1}{6}C=\frac{2}{3}VOCl_3+\frac{1}{6}CO_2$	20	$\frac{1}{2}SiO_2+Cl_2+C=\frac{1}{2}SiCl_4+CO$
10	$FeO+Cl_2=FeCl_2+\frac{1}{2}O_2$	21	$\frac{1}{2}SiO_2+Cl_2+\frac{1}{2}C=\frac{1}{2}SiCl_4+\frac{1}{2}CO_2$
11	$FeO+Cl_2+C=FeCl_2+CO$		

LEGEND: a) Reaction No; b) Reaction

KCl, NaCl of chemical purity grade were used in the experiments. Petroleum coke of coarseness <50 microns was calcined without access to air at 800° for about 10 hours. The content in the coke of carbon was 97.1%, volatile -- 0.38%, and ash -- 2.5%. The granulometric composition of the slag used was: -85 microns -- 97.4%; 85 microns -- 1.2%; 100 microns -- 1.1%; 160 microns -- 0.2%.

The diagram of the installation for chlorination of slag is shown in Figure 2. Chlorination was conducted in a quartz test tube of 30mm diameter and 250mm long closed by a rubber cork, and prevented from chloride fumes by a teflon film. Passing through the cork was a quartz bubbling tube with internal diameter = 5mm, and

the thermocouple jacket. The bubbling tube was lowered to the bottom of the reaction vessel in such a manner that the chlorine entering for exit from the tube was broken up against the bottom of the vessel into small bubbles.

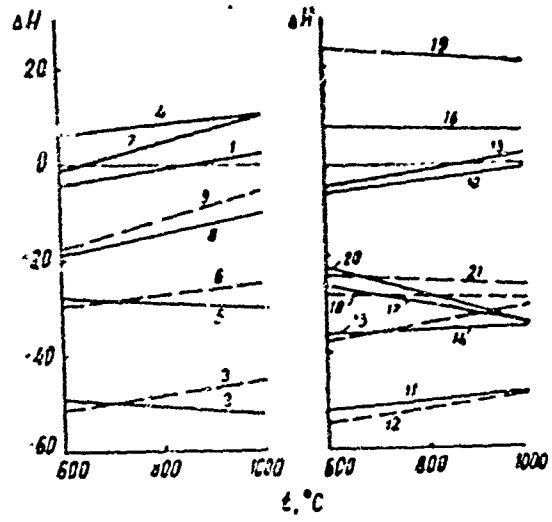

FIGURE 1. Changes in standard isobaric-isothermal as a function of temperature for reactions of chlorination of the oxides of vanadium, iron, titanium, and silicon. Numbers under the curves correspond to reaction numbers in Table 1.

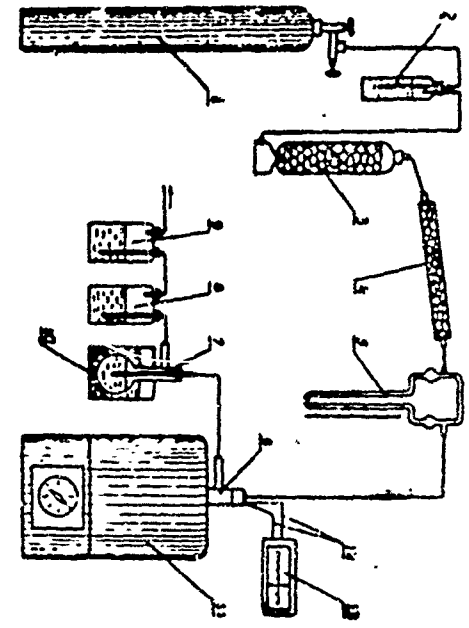

FIGURE 2. Diagram of setup for chlorination: 1-chlorine cylinder; 2-vessel with concentrated H_2SO_4; 3-column with silicagel; 4-$CaCl_2$ tube; 5-Rheometer (filled with

(Legend continued below)

A mixture of 55 grams KCl and 45 grams NaCl was loaded into a quartz test tube, which mixture was then melted and heated at 700° for 30 minutes to remove moisture. Then 3 grams of slag was added and the test tube was sealed with a cork. The chlorine was supplied at the rate of 10 liters/hour.

After the experiment the melt was poured out, ground to powder in a hand mill and analyzed for V, Ti, Fe, and Si. The vanadium and titanium were determined with sulfuric acid and photocolorimetric methods, iron was analyzed with a mercurometric method, and silicon -- a sulfuric acid method /13/.

concentrated H_2SO_4); 6-Quartz reaction test-tube; 7-Absorbing flask containing 25% H_2SO_4; 8-Absorbing vessel containing 10% H_2SO_4; 9-Absorbing vessel containing 3% H_2SO_4; 10-Beaker filled with supersaturated NaCl solution; 11-Furnace; 12-Chromel-alumel thermocouple; 13-Millivoltmeter

The results of the experiments showed that vanadium trioxide and ferrous oxide are chlorinated at 700° without a reducing agent and have appreciable yields of volatile chlorides, which confirms the thermodynamic probability of these reactions taking place. When chlorination is continued for 120 minutes the recovery of a vanadium amounts to 11.0%, and iron--3.4%. Oxides of titanium and silicon, as should have been expected, under these conditions are practically not chlorinated at all. With increase in temperature up to 1000° the recovery of a vanadium and iron is lower still, while that of titanium and silicon remain unchanged.

The degree of vanadium and titanium extraction as a function of duration of experiment at 700° in the presence of a reducing agent is shown in Figure 3.

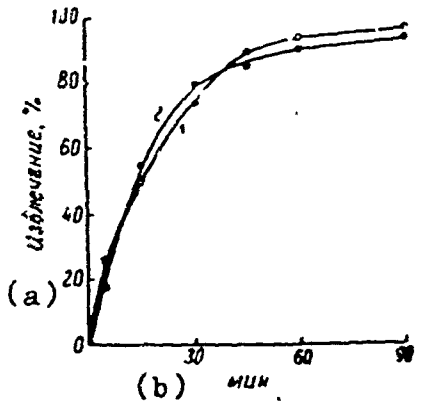

FIGURE 3. Extent of recovery of vanadium (1) and of titanium (2) as a function of duration of experiment at 700°.
LEGEND: a) Recovery, %; b) Minutes

The carbon content was 40% of the charge weight. When the experiment lasted 90 minutes the extent of the vanadium recovery was 97.6%, titanium -- 95.8%, and silicon -- 66.5%. The greater part of the iron (80.0%) remained in the melt.

After 1-3 experiments the absorbing solutions were poured out and the quantity of vanadium and titanium in them was determined. On balance the deficiency in vanadium was 4.1%, in titanium -- 5.7%.

When the temperature was increased to 800°, as we can see Figure 4, the extent of vanadium and titanium extraction increases.

At higher temperatures experiments could not be completed, since sinturing of slag particles with the test tube walls is observed.

The extent of recovery of vanadium for 30 minutes at 700° and the consumption of chlorine at the rate of 10 liters/hour amounted to, as related to particle size, as follows: - 150 microns -- 74.3%, + 250 - 500 microns -- 72.3%, and + 500 - 750 microns-- 56.2%. Consequently, at particle dimensions above 500 microns the extent of vanadium recovery drops sharply. This reduction is determined not only by the increase in surface contact of particles with the gas, but also by the settling of the largest particles on the bottom of the test tube, therefore, it is necessary to apply a slag of thin consistency (- 150 microns).

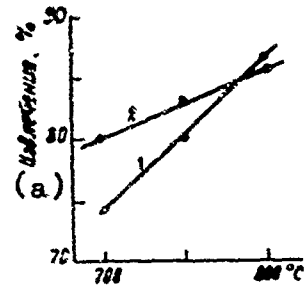

FIGURE 4. Extent of recovery of vanadium (1) and of titanium (2) as function of temperature. Duration of experiment = 30 minutes. LEGEND: a) Recovery

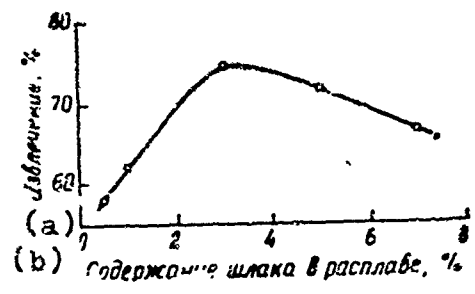

FIGURE 5. Effect of slag content in melt on extent of recovery at 700°. Duration of experiment = 30 minutes. LEGEND: a) Recovery; b) Slag content in melt

The greatest recovery of vanadium was achieved at a slag content in the melt of 3-4% (Figure 5). At higher slag content the extent of recovery is decreased as the result of increase viscosity of the suspension.

The optimal amount of coke with which the highest recovery of the vanadium and titanium is achieved averages close to 30% of charge weight (Table 2). Further increase in the coke content does not affect recovery of vanadium and titanium and only slightly increases the extraction of iron and silicon. The consumption of carbon was taken above the stoichiometric amount by several fold due to the possibility of coke being removed from the chlorination zone.

TABLE 2

Extent of Recovery of Slag Constituents as a Function of Coke Content in the Charge Heated for 30 Minutes at 700°, and at a Chlorine Supply Rate of 10 liters/hour

LEGEND: a) Coke content in charge; b) Extent of recovery

(a) Содержание угля в шихте, %	(b) Степень извлечения, %			
	V	Ti	Fe	Si
14	18,5	24,4	5,3	1,9
25	73,2	75,8	6,4	4,3
35	74,4	80,5	9,6	44,1
40	74,3	80,0	11,8	45,6
45	74,2	81,0	11,4	48,7

Increase in chlorine consumed significantly steps up the extent of vanadium extraction. Thus, after 30 minutes at 700° and a carbon content in the charge of 40% a chlorine feed rate of 5 liters/hour results in a 61.4% recovery of the vanadium, at a chlorine rate of 10 liters/hour -- 74.3%, and at 15 liters/hour -- 81.5%. Taking into consideration that in all these experiments a chlorine excess above the stoichiometric amount was present, this influence can be explained by the improvement in the intensity of mixing of the suspension, agitation of the melt, which promoted breaking up of the gas bubbles and improved the homogeneity of the suspension. When the chlorine was diluted with nitrogen /See Note/ at a constant gas mixture feed rate of 10 liters/hour the vanadium recovery was reduced.

(/NOTE/ The nitrogen was freed of oxygen following a method described in the report /14/.)

Thus, if for pure chlorine the extraction of vanadium was 74.3%, then for a chlorine content of 75 and 50%, the recovery was, respectively, 68.9% and 61.8%. The extent of chlorine use here amounted to, respectively, 6.20 and 30%.

The absorption of chlorine by the melt, which should increase with higher partial pressure of chlorine plays an essential role in the mechanism of similar processes. Absorption in the KCl-NaCl system can be determined even by a small, but appreciable solubility of chlorine, which is according to the data of Yu. M. Ryabukhin /15/ (Moles/$cm^3 \cdot 10^7$): KCl -- 10.40 at 848°; NaCl -- 2.21 at 847°, and KCl-NaCl mixture (1:1) -- 7.0 at 850°.

For a melt of an equimolar mixture of KCl and NaCl the deviation of the solubility of chlorine from the additive value is insubstantial.

Based on the concept of the absorption of gases by a liquid, the resulting dependence of the extent of quality in use on its concentration gaseous phase can be accounted for by the increase in the total surface of absorption during the experimental period with dilution of chlorine, i. e. the specific interface surface per unit chlorine weight rises. The absorption of chlorine can possibly explained also as due to the effect of the melt composition on the extent of vanadium recovery. Experiments show that for 30 minutes at 700°, a coke content in the charge of 40% and a chlorine feed rate of 10 liters/hour results in a 72.6% recovery of vanadium at a 40% KCl content in the mixture, 74.3% -- at 55% KCl, and 82.2% -- at 70% KCl. The increase in vanadium recovery with increased KCl content in the melt can be explained by the fact that the solubility of chlorine in molten KCl is higher than in molten NaCl. To a certain extent the viscosity of the melt can also have some effect, since the viscosity of molten KCl is somewhat lower than that of molten NaCl /16/. Given constancy of temperature and invariability of the mechanism of reaction, depending on the composition of the melt, and increase in the actual viscosity of the medium lowers the

diffusion coefficient, resulting in a retardation in mass transfer and to reduced chlorination rate. The analyses of the vanadium chlorides formed conducted by the method of infrared absorption spectra of the molecules on the IKS-12 instrument revealed that the vanadium chloride compound formed is present practically speaking only as the hydroxytrichloride.

In conclusion, it is necessary to note that in the present report it is explained only the fundamental possibility of recovering vanadium from converters slag by chlorination of the melt. This method, however, has certain defects, related to the high iron content in slags, which can necessitate frequent replenishment of the melt, and also is related with the need to separate the mixture of components $VOCl_3$-$TiCl_4$ forming, which have a low boiling point difference.

Further research is projected to be pursued in the following areas: study of the methods of separating iron from slags and the possibility of regenerating chlorine and iron; study of the nature of the interactions of slag components with the melt; separation of the $VOCl_3$ - $TiCl_4$ mixture; and the production of vanadium trichloride from VOC_3.

CONCLUSIONS

1. The possibility is shown of practically complete recovery of vanadium and titanium from converter slag by chlorination in a medium of molten chlorides of alkaline metals.

2. The extent of vanadium and titanium recovery is established as functions of duration of experiment, temperature, presence of reducing agent, and also of slag particle size, rate and concentration of chlorine fed into the gaseous mixture, and melt composition.

3. The optimal conditions for chlorination of slag in the laboratory experiments were determined: temperature -- 700-800°; duration of process -- 90 minutes; and carbon content in the charge -- 30%. Here, the recovery of vanadium amounted to 97-98%; titanium -- 95-96%; silicon -- 66-67%; and iron -- 20%.

4. It has been established that in the chlorination of the melt approximately 80% of the iron remains in the melt.

LITERATURE

1. Sobolev, M. N., Izvlecheniye vanadiya i titana iz ural'skikh titanomagnetitov (Recovery of Vanadium and Titanium from Ural Titanomagnetites), Joint Scie.-Technical Publ. House, 1936.

2. Izvlecheniye i ochistka redkikh metallov. Perevod s angl. (Extraction and Purification of Rare Metals, translated from English), ed. by O. P. Kolchin, Atomizdat, 1960.
3. Gropsianu, Z., Tribunescu, P., Rev. chim. No. 7-8, 3 (1955).
4. Capley, R. E., Roddy, I. W., J. Less-Common Metals, v. 2, No. 1, 1960.
5. Erlich, P., Seifert, H. I., J. Anorgan. und Allgem. Chem., No. 5-6, 301 (1959).
6. Amirova, S. A., Pechkovskiy, V. V., Prokhorova, V. G., Polotnyanshchikova, M. I., NDVSh, Khimiya i khimicheskaya tekhnologiya (Chemistry and Chemical Technology), No 2, 398 (1959).

7. Amirova, S. A., Pechkovskiy, V. V., Prokhorova, V. G., Zueva, N. D., Uchenye zapiski Permskogo Gosuniversiteta (Scientific Notes of Permsk State Univ.), Vol XVII, No 173 (1960).
8. Rostoker, U., Metallurgiya vanadiya (per. s angl.) (Metallurgy of Vanadium), translated from English, Moscow, 1959.
9. Morozov, I. S., Toptygin, D. Ya., Zh. neorgan. khimii (Journal of Inorganic Chemistry), Vol 1, No 11, 1959.
10. Nisel'son, L. A., Sokolova, T. D., Zh. neorgan. khimii, Vol IV, No 7, 1645 (1961).
11. Markov, B. F., Voitovich, B. A., Barabanova, A. S., Ukr. khim zh. (Ukrainian Chemical Journal), No 5, 580 (1961).
12. Korshunov, B. G., Morozov, I. S., Ionov, V. I., Zorina, M. A., Izv. VUZ, Tsvetnaya metallurgiya, No 5, 67 (1960).

13. Gillebrand, V. F., Lendel', G. Ye., Brait, G. A., Gofman, D. I., Practicheskoye rukovodstvo po neorganicheskomu analizu (Practical Handbook on Inorganic Analysis), Goskhimizdat, Moscow, 1957.

14. Karyakin, Yu. V., Angelov, I. I., Chistyye khimicheskiye reaktivy (Pure Chemical Reagents), Goskhimizdat, 1955.

15. Ryabukhin, Yu. M., Zh. neorgan. khimii (Journal of Inorganic Chemistry), Vol VII, No 5, 1101 (1962).
16. Strelets, Kh. L., Taits, A. Yu., Tulyanitskiy, B. S., Metallurgiya magniya (Metallurgy of Magnesium), Metallurgizdat, Moscow, 1960.

Received by Editor
17 December 1962

ELECTRODEPOSITION OF BISMUTH FROM PERCHLORATE SOLUTIONS

V. M. Kochegarov, Ye. A. Zyablov

(Taganrog Radio Engineering Institute, Chair of Chemistry)

Bismuth films obtained by an electrochemical method can be of much interest in the radio engineering industry for use as electrical contact on semi-conductor surfaces. Several studies /1-5/ deal with the electrochemical isolation of bismuth from its solutions, although the technology and conditions of the electrolysis of obtaining high-quality bismuth film cannot be considered as sufficiently advanced. Accordingly, studies in this area are of both practical and theoretical interest.

The present article presents results of an investigation of the electrodeposition of bismuth from perchlorate solutions. Cathode polarization and current-based bismuth yield was studied as a function of concentration of metal, temperature of solution, and current density.

Solutions (1-5) were investigated with bismuth perchlorate concentrations (in moles/liter) of 0.01, 0.05, 0.1, 0.25, and 0.38, as well as free perchloric acid present at a 2 moles/liter concentration in each of these solutions.

Bismuth perchlorate was obtained by dissolving freshly prepared bismuth hydroxide in hydrochloric acid followed by gentle heating. All the chemical reagents were of the chemically pure grade, and the solutions were prepared with deionized water. Then the corresponding solutions with the same concentration of $HClO_4$ (2 moles/liter) were prepared from a solution of elevated bismuth concentration (about 0.4 mole/liter) by dilution. The amount of solution in the glass electrolyzer was always the same (200 ml). Copper disks 5 cm^2 served as cathodes. Rods of metallic bismuth were used as anodes. Quantitative determination of bismuth in the solution was done by the weight method /6/.

Polarization curves were recorded for the indicated solution by the compensational method /7/ at 20, 40, and 50° using a thermostat with an accuracy of ±0.5°. The reference electrode was a saturated

calomel electrode. The values of the electrode potentials were calculated on the hydrogen scale.

After recording polarization curves for all the solutions electrolysis was carried out and the current-based yields were measured in solutions 3, 4, and 5 at three temperatures.

In the figure are displayed the polarization curves recorded for five solutions at a temperature of 20°.

As we can see from the figure, the stationary electrode potential of bismuth in the solutions investigated is in a range of potential values close to those calculated [8]. Appreciable polarization is observed on the polarization curves even in relatively highly concentrated solution. When the current density in these solutions with low metal concentration is increased, diffusion effects begin to be manifest, which lead to the appearance of a limiting current and to a very decided shift in the electrode potential in the region of the electronegative values, i.e., the appearance of concentration polarization. At low current densities, polarization is almost totally independent of the concentration of the metal and in all solutions is practically identical. Thus, the independence of polarization from metal concentration indicates that it is not caused by diffusion effects.

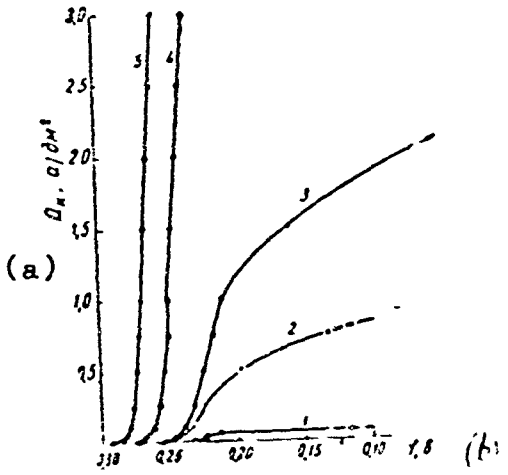

FIGURE. Cathode polarization curves for solutions 1-5 at 20°.
LEGEND: a) amp/decimeter^2; b) Volt

In the literature [5] it has already been observed that the precipitation of bismuth from perchlorate solutions is limited by crystallization polarization. It appears to us that polarization in the precipitation of bismuth is caused by a peculiarity of the chemical bond in the bismuth crystal. Due to the complicated structure of bismuth [9, 10] covalent bonds appear along with the metallic in the crystal. The appearance of a covalent bond apparently hampers the formation of a bismuth

crystal, which then requires an additional energy of activation expressed in increased electrode potential.

As experiments have shown, the yield of bismuth in terms of current within wide current density ranges (from 0.5 to 5 amp/cm^2) at three temperatures was practically equal to 100% (varied from 99.5 to 100%) which is confirmed by the shape and position of the polarization curve. These yields are located in regions of electropositive potential values. The temperature of the solution also does not change the current-based yield. However, the conditions of electrolysis diversely affect quality of the precipitate. At low current densities the precipitates are produced loose and non-uniform on the cathode surface. Extremely high current densities lead to the formation of dendrite-like and loose deposits. It has been found that the most optimal conditions leading to the precipitation of the uniform, semi-brilliant, and compact deposits include current density equal to 2-3 amp/cm^2 and a solution temperature of 20°. Precipitates obtained under these conditions are of high quality and good cohesion with cathode surface. They are also readily obtained on the semi-conductor surfaces. With the sedimentation on the surface on p-germanium and p-silicon an ohmic contact will be formed. On surfaces of p-germanium and p-silicon bismuth films will form rectifying contacts. These studies will be presented in a separate article.

Conclusions

1. Cathode polarization is observed in the separation of bismuth from perchlorate solutions. A suggestion is made as to the cause of crystallization polarization in the separation of bismuth.

2. The composition of the solution and electrolysis conditions are recommended for obtaining bismuth film on semi-conductor surfaces. The solution composition (in grams/liter) is: 70 - 100 $Bi(ClO_4)_3$ 200 $HClO_4$; D_k = 2-3 amp/cm^2, solution temperature = 20°; soluble anodes (bismuth rods).

LITERATURE

1. Billiter, Zh., Osnovy gal'vanotekhniki (Fundamentals of Electrolytic Metallurgy), Metallurgizdat, Moscow, 1941.
2. Drozdov, B. V., Gidroelektrometallurgiya tsvetnykh metallov (Hydroelectrometallurgy of Non-Ferrous Metals), ONTI, Leningrad-Moscow, p 310, 1938.
3. Kalaner, L. I., Noveyshiye dostizheniya gal'vanostegii (Advances in Electroplating), published by Khar'kov State University, p 154, 1951.
4. Levin, A. I., Zh. prikl. khimii (Journal of Applied Chemistry), Vol XVII, No 11-12, 1944.
5. Loshkarev, M. A., Dubyago, E. I., Trudy chetvertogo soveshchaniya po elektrokhimii (Works of the 4th Conference on Electrochemistry), Moscow, p 467, 1959.
6. Mukhina, Z. S., Nikitina, E. I., et al, Metody analiza metallov i splavov (Methods of Analysis of Metals and Alloys), Oborongiz, Moscow, 1959.
7. Vagramyan, A. T., Solov'eva, Z. A., Metody issledovaniya protsessov elektroosazhdeniya metallov (Methods of Investigating Electrodeposition of Metals), published by Acad. of Sciences, USSR, Moscow, 1955.
8. Latimer, V., Okislitel'nye sostoyaniya elementov i ikh potentsaly v vodnykh rastvorakh (Oxidation States of Elements and their Potentials in Aqueous Solutions), For. Lit. Publ. House, Moscow, 1954.
9. Krebs., Poluprovodnikovye veshchestva. Sbornik statei (Semi-Conductor Compounds, Comp. of Art.), For. Lit. Publ. House, Moscow, 1960.
10. Mooser, E., Pearson, W. B., J. Electronics, 1, 629 (1956).

Received by Editor
9 February 1963

ADSORPTION OF GASES ON URANIUM MIXED OXIDES

V. G. Vlasov, V. M. Zhukovskiy, A. G. Lebedev, V. N. Shalaginov

(Ural Polytechnical Institute)

Reactions of indirect reduction of metal oxides include as the intermediate links acts of adsorption of the reducing agent gas and desorption of its oxidation product /1-3/. Therefore, of much interest is a comparison of data on the sorbability of gases on the surface of oxides and the kinetic characteristics of the reduction of the latter.

In this report a study is made of the adsorption of the gases H_2, CO, NH_3, N_2, CO_2, H_2O on uranium mixed oxide. The results are compared with data on the reduction kinetics of this oxide.

Uranium mixed oxide used in the investigation had a specific surface of 2.5 m^2/g and a density of 8.34 g/cm^3. The chemical composition precisely corresponded to the formula U_3O_8. The quantity of impurities from spectral analysis amounted (in %): K - $1.4 \cdot 10^{-2}$; Na - $1.2 \cdot 10^{-2}$; Ca - $1.0 \cdot 10^{-2}$; Mn - $1.1 \cdot 10^{-4}$; Fe - $1.6 \cdot 10^{-3}$; Si - $3.1 \cdot 10^{-3}$; Cu - $2.8 \cdot 10^{-4}$; Al - $1.3 \cdot 10^{-3}$; Ni $< 2 \cdot 10^{-3}$; Cr $< 1 \cdot 10^{-3}$.

The original salt used in obtaining this oxide was uranyl nitrate $UO_2(NO_3)_2 \cdot 6H_2O$. It underwent oxalate and peroxide purifications /4,5/ as the results of which uranium peroxide $UO_4 \cdot n H_2O$ was produced. Then, by decomposition of the peroxide in a stream of oxygen at 350° for four hours followed by heat treatment for an hour at 400° uranium trioxide was obtained /6/. This compound was reduced with hydrogen at 800° to uranium dioxide. Finally, the dioxide was oxidized in air at 550° for five hours down to uranium mixed oxide.

The equipment for measuring the adsorption of gases is similar to that described in the report /7/. It has the following main characteristics: the volume of the working part of the system, depending on the gas pressure, varies within the limits of 30 - 36 cm^3. The volume of the reaction vessel is 22.8 cm^3. Gas is admitted into the reaction space by means of a gas burette with an 0.02 cm^3

scale division. The gas pressure is measured by a U-shaped closed manometer to an accuracy of +0.5mm Hg. An electric tubular oven is used in heating. The temperature was held to a precision of + 2°.

Hydrogen was obtained in the Kipp apparatus; gaseous nitrogen -- by evaporation of liquid nitrogen. These gases were freed from traces of oxygen by passage through a column containing activated copper. Traces of moisture were trapped in a liquid nitrogen-cooled trap. Carbon monoxide was prepared by decomposition of formic acid with concentrated sulfuric acid /8/. Ammonia and carbon dioxide were taken directly from cylinders. Before being admitted into the reaction space the last three gases were cleaned through schemes recommended by Brauer /6/.

The portion of uranium mixed oxide in each experiment amounted to 38.4 grams, which corresponded to a total oxide surface of $96m^2$. After preliminary evacuation to high vacuum (residual pressure 10^{-3} - 10^{-4} mm Hg) of the oxide sample-containing reaction section, heated to 200-250°, the adsorption vessel was cooled to room temperature and a certain quantity of gas admitted into it.

The gas pressure at the moment of attainment of adsorptive equilibrium was measured by the manometer. Then the temperature was increased to the next level set for the experiment and a new measurement was made. After measurements throughout the entire temperature range of interest the adsorption vessel was again cooled to room temperature. It must be noted that the gas pressure here established always precisely coincided with the pressure existing at the initial equilibrium at room temperature. Hence, equilibrium was reached from two sides, evidencing the presence of true thermodynamic equilibrium. Then a new portion of gas was added to the system and the experiment was repeated. The quantity of gas adsorbed was calculated in micro-moles per square meter of surface oxidized.

The adsorption of the water vapor was determined by a weight method in a device used for kinetic studies, monotypical with that described in the reports /9, 10/. It is clear from Figure 1 that the adsorbability of hydrogen is low. Present on the isobars of hydrogen adsorption are minima lying approximately at +50°. Below +50° increase in temperature is accompanied by decrease in hydrogen adsorbability, while for temperatures above 50° -- increase. It follows from this data that at low temperatures adsorption of hydrogen on the surfaces of uranium mixed oxides occurs with the evolution of heat, but at temperatures above +50° -- with absorption.

The adsorbability of carbon monoxide on uranium mixed oxide (Figure 2) is an order of magnitude near the adsorbability of hydrogen. A difference consists in the fact that with increase in temperature, a continuous, although small, decrease in the amount of carbon monoxide adsorbed is also found.

Comparison of the data of adsorbability of water vapor and carbon dioxide on uranium mixed oxide (Figures 3 and 2b) shows that water vapor

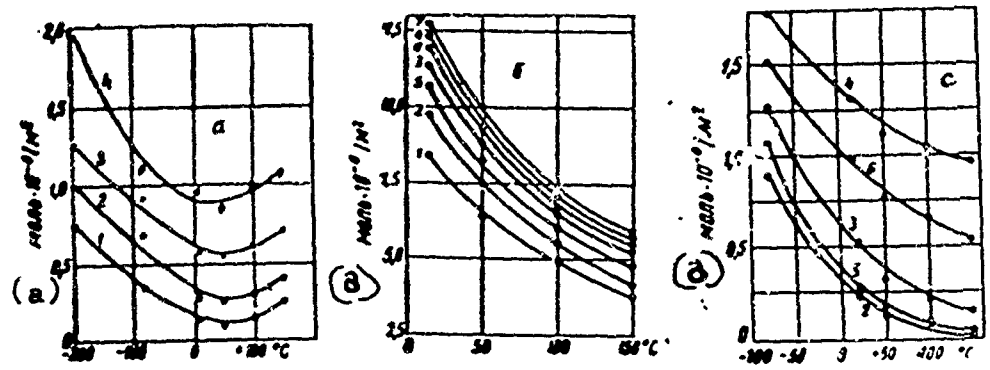

FIGURE 1. Adsorption isobars of hydrogen (a), ammonia (b) and nitrogen (c). Pressure (mm Hg): 1 - 50; 2 - 100; 3 - 200; 4 - 300; 5 - 150; 6 - 250; 7 - 350. LEGEND: a) Mole·$10^{-6}/m^2$.

is sorbed in significantly large amounts compared with carbon dioxide. If at the pressure P_{CO_2} = 50 mm Hg and 200°, the adsorbability of CO_2 on U_3O_8 becomes so low that it was difficult to measure while the adsorbability of steam continued to remain extraordinarily high even at P_{H_2O} = 10 mm Hg and temperatures of 200-500°.

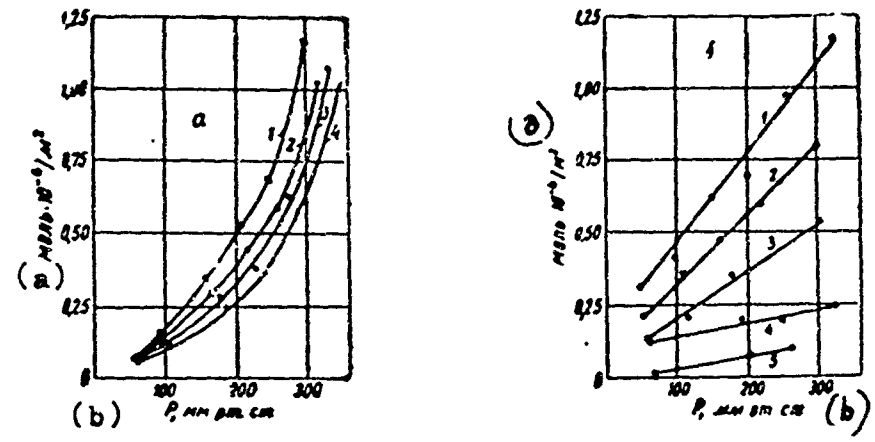

FIGURE 2. Adsorption isotherms of carbon monoxide (a), and carbon dioxide (b). 1 - 20°; 2 - 50°; 3 - 100°; 4 - 150°; 5 - 200°.

The results of studying adsorption of ammonia are shown in Figure 1b. Ammonia is adsorbed in amounts approximately 1 order of magnitude larger than for hydrogen and carbon monoxide. Its adsorbability increases with increasing pressure and decreasing temperature.

Under the conditions studied nitrogen was adsorbed on uranium mixed oxide in relatively small amounts (cf Figure 1c). The adsorbability of nitrogen in order of magnitude is comparable with the adsorbability of hydrogen, but in contrast to the latter, it steadily decreases with increase in temperature and at P_{N_2} : 100 mm Hg, and a temperature above 150° it becomes so small that the method we adopted does not permit its detection. This last fact is in good agreement with the experimental data on the kinetics of the reduction of uranium oxides by hydrogen and by a nitrogen-hydrogen mixture. It is shown in the report /11/ that the reduction of the nitrogen-hydrogen mixture practically speaking is not distinguished from reduction by pure hydrogen. Nitrogen here plays only the role of an inert diluent, having no effect on the mechanism of reduction.

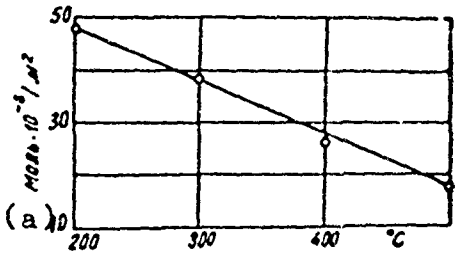

FIGURE 3. Adsorption isobar of hydrogen vapor at P_{H_2O} = 10 mm Hg. LEGEND: a) Mole·$10^{-6}/m^2$.

Comparison of results of investigating the adsorption of hydrogen and carbon monoxide on uranium mixed oxides shows that the adsorbability of these gases in relation to U_3O_8 is close to one another.

Therefore, if one were to consider this factor only, one could expect similar kinetic features in the reduction of uranium mixed oxide by hydrogen and carbon monoxide, the more so, since thermodynamically the reducing ability of these gases relative to U_3O_8 are also very close to each other /12/.

However, we must consider the following facts. As a result of a chemical act of reduction molecules of water vapor or carbon dioxide will be formed, which are retained for some time by the adsorptional centers of the surface oxidized and thereby temporarily leave the reactive arena of the active surface. It was earlier shown that the adsorbability of water vapor is considerably higher than that of carbon dioxide. Hence, we can expect that the inhibiting effect of carbon dioxide is low, and that water vapor must significantly hamper the reduction of uranium mixed oxides.

In previous experiments we established that the reduction of U_3O_8 by carbon monoxide begins to occur at a marked rate already at 250°, while at 450° the final product of composition $UO_{2.06}$ is produced in 50 minutes

of reduction. At the same time the reduction of U_3O_8 by hydrogen only commences at 450° and the furthest reduced product is of the composition $UO_{2.8}$, although it was obtained at 700° [12].

The inhibiting effect of steam is also revealed in the report [13]. The inhibitory effect of the reaction product on the rate of uranium mixed oxide reduction under conditions in which the system is far from equilibrium, is in good agreement with both representations of the adsorptionally catalytic theory of reduction [1, 2]. Being adsorbed on the active centers located chiefly at surface defects of the crystal lattice, the water vapor blocks the centers and thus impedes access of the reducing agent to the reactive surface.

The significant adsorbability of water vapor on uranium mixed oxides established in our work, especially at low temperatures, is correlated with the results of kinetic studies: the inhibitory action of water vapor is the greater the lower the reduction temperature.

Data on the adsorbability of nitrogen and ammonia are also in agreement with the results of kinetic research on the reduction of uranium mixed oxide by ammonia [14].

In this report the assumption was made that the slowest stage, limiting the reduction of U_3O_8 as a whole is one of the stages of the decomposition of ammonia on the surfaces of the reduced oxide, namely -- the desorption of nitrogen in the gas stage. The adsorbability of nitrogen on uranium mixed oxide at the reduction temperatures is vanishingly small, whereas the adsorbability of ammonia is very significant. As a result of the acts of adsorption and dissociation of ammonia on the oxide surfaces atomic hydrogen and nitrogen appear, retained by the adsorptional centers of the surface layer of the oxide. Hydrogen is apparently localized near the oxygen ions. As far as the nature of the adsorptional centers on which nitrogen is sorbed is concerned, it is still vague. In all probability the role of these centers may be fulfilled both by ions of the metal (U^{6+}), as well as by oxygen ions.

Interaction between the adsorbed hydrogen and oxygen of the oxide is accompanied by the transition of hexavalent uranium to quadrivalent. The rate of this transition is proportional to the concentration of the electrons in the lattice of the reduced oxide, as well as in the field of the U^{6+} ions present in the surface layer and capable of sharing in the reaction. The concentration of free electrons depends mainly on the progress of the reaction:

$$O^{2-} + H_{adsorbed} = OH^- + e;$$
$$OH^- + H_{adsorbed} = H_2O_{adsorbed} + e,$$

i.e., it is determined by the number of oxygen centers reacting with hydrogen. We can also expect that nitrogen adsorbed on the centers will hinder their reaction with hydrogen. More precisely, only those

oxygen ions which are free of nitrogen will enter into reaction with the adsorbed hydrogen. Therefore, the number of centers O^{2-} and OH^{-} capable of interacting with hydrogen, and consequently, also the concentration of the free electrons are evidently determined by the rate of desorption of nitrogen from the surface of the uranium mixed oxide.

On the other hand, adsorption of nitrogen on the metal ions can impede the reduction reaction, reducing the number of U^{6+} capable of participating in the reaction. The last quantity, in its turn, is also determined by the rate of desorption of nitrogen from the oxide surface. And since this state is slowest, then it also determines the overall rate of reduction.

CONCLUSIONS

1. Adsorbability of hydrogen, carbon monoxide, ammonia, nitrogen, carbon dioxide, and water vapor on uranium mixed oxide is studied at elevated temperatures.
2. A correlation is established between the data of adsorbability of gases and the results of studies made of the kinetics of uranium mixed oxide reduction by hydrogen, a nitrogen-hydrogen mixture, ammonia, and carbon monoxide.

LITERATURE

1. Chufarov, G. I., Tatiyevskaya, E. P., Problemy metallurgiya (Problems of Metallurgy), Academy of Sciences USSR Publishing House, Moscow, 15, 1953.
2. Chufarov, G. I., Tatiyevskaya, E. P., Fiziko-khimicheskiy osnovy proizvodstva chuguna (Physico-Chemical Fundamentals in Pig Iron Production), Metallurgizdat, Sverdlovsk, 21, 1956.
3. Yesin, O. A., Gel'd, P. V., Fizicheskaya khimiya pirometallurgicheskikh protsessov (Physical Chemistry of Pyrometallurgical Processes). p 1, Metallurgizdat, Sverdlovsk, 1962.
4. Galkin, N. P., Maiorov, A. A. Veryatin, U. D., Tekhnologiya pererabotki kontsentratov urana (Technology of Uranium Concentrates Processing), Atomizdat, Moscow, 1960.
5. Shevchenko, V. B., Sudarikov, B. N., Tekhnologiya urana (Technology of Uranium), Atomizdat, Moscow, 1961.
6. Brauer, G., Rukovodstvo po preparativnoy neorganicheskoy khimii (Handbook on Preparative Inorganic Chemistry), For. Literature Publishing House, Moscow, 1956.
7. Tatiyevskaya, E. P., Chufarov, G. I., Izv. AN SSSR, OTN (News of Acad. of Sci. USSR, Div. Tech. Sci.) 7, 1005 (1946).
8. Karyakin, Yu. V., Angelov, I. I., Chistyye khimicheskiy preparaty (Pure Chemical Reagents), Goskhimizdat, Moscow, 1955.

9. Strekalovskiy, V. N., Vlasov, V. G., Zh. prikl. khimii, 34, No 1, 32 (1961).
10. Vlasov, V. G., Shalaginov, V. N., Zh. prikl. khimii 34, No 1, 20 (1961).
11. Vlasov, V. G., Zhukovskiy, V. M., Kinetika i kataliz (Kinetics and Catalysis), 3, 6 (1962).
12. Galkin, N. P., Maiorov, A. A., Veryatin, U. D., Sudarikov, B. N., Nikolaev, N. S., Shishkov, N. D., Krutikov, A. B., Khimiya i tekhnologiya ftoristykh soyedineniy urana (Chemistry and Technology of Fluoride Compounds of Uranium), Atomizdat, Moscow, 1960.
13. Strekalovskiy, V. N., Vlasov, V. G., Zh. prikl. khimii 34, No 1, 38 (1961).
14. Vlasov, Zhukovskiy, V. M., Zh. prikl. khimii , 36, No 1, 42 (1963).

Received by Editor
21 January 1963

ELECTROCONDUCTIVITY IN THE UO_3 - C SYSTEM

Ye. V. Tkachenko, A. D. Neuymin, V. G. Valasov
and V. N. Strekalovskiy

(Ural Polytechnical Institute)

Use of the measurement of electroconductivity for controlling chemical reactions in oxide systems is not new. For example, it has been used in studying the oxidation of metals /1/, their dissociation /2,3/, their reduction by gaseous /4,5/ and solid reducing agents /6/. The advantage of the method is its high sensitivity to small structural changes arising due to external factors: temperature, pressure, and ongoing chemical processes.

In the measurement of electroconductivity of the oxide-carbon mixture it is necessary to select for investigation the temperature range in which the electroconductivity of carbon will be constant. It is known that the electrical conductivity of the several forms of carbon increases to a temperature of 300° and remains approximately constant to 600°, in then decreases /6,7/. Therefore, if one were to study the reaction of a metal oxide with carbon within the temperature range of, for instance, 400 - 500°, then the method of measuring electroconductivity can be applied with sufficient accuracy /6/. This feature is of special importance due to the fact that elucidation of the mechanism of one of the most complicated reduction processes -- reduction of metal oxides at low temperatures -- suffers from insufficient experimental data and, chiefly, limited numbers of research methods.

In this report the measurement of electroconductivity is used to study the process of reduction of uranium trioxide UO_3 by solid carbon. Kinetic and roentgenographic studies of this process are described in our reports /8,9/, from which it follows that an appreciable interaction of uranium trioxide with

acetylene black is observed at approximately 400°, and reaction with graphite -- close to 430°; the formation of uranium mixed oxide U_3O_8 begins at an oxygen content corresponding to the composition $UO_{2.91}$. The temperature at the onset of noticeable dissociation of UO_3 in vacuum is within the limits of 420 - 430° /10,11/ and, thus, it is very close to the temperatures of beginning reaction of UO_3 with carbon, determined by us kinetically. Therefore, of greatest interest for research is the role of dissociation in reduction. Also of interest is the question of the onset of formation of the U_3O_8 phase, since for uranium oxides apparently the method of electroconductivity measurement can be more sensitive than, for instance, the roentgenographic method.

Uranium trioxide was prepared by heat treatment of uranium peroxide /12/. Its specific gravity is 5.95 g/cm^3, and its specific surface $\approx$13 m^2/g. X-ray phase analysis has revealed that the resulting UO_3 is amorphous. Used as the reducing agent was spectrally pure graphite from the Kudinovskiy Electrocarbon Plant and acetylene black, previously treated as described in the studies /8,9/. Tablets 10 mm in diameter and 3-4 mm in height are prepared from a thoroughly ground mixture of U_2O_3 and carbon prepared by pressing under a pressure of 2500 kg/cm^2. In order to insure the reliability of the electrical contacts, films of powdered silver are pressed on the faces of the tablets, then they are placed in a special cell (Figure 1) and secured between platinum sheets which are in contact with platinum leads. Electrical conductivity is measured by means of an alternating current bridge at a frequency of 3000 cps with an electronic oscillograph serving as a null-instrument. The bridge circuit is similar to that described in the study /13/. Heating is carried out at a rate of $\approx$ 250 deg/hour in an electric furnace. The temperature is sustained to a precision of $\pm$ 3°. The experiments are carried out in vacuum with continuous evacuation (residual pressure = 10^{-3} mm Hg).

Since the amount of carbon will strongly affect the value of the electrical conductivity of the oxide-carbon mixture, the experiments were conducted with a reducing agent content of 4.5 and 1.4 weight percentage, which corresponds to the stoichiometric amount of carbon required to reduce UO_3 to UO_2 and to U_3O_8, respectively. It should be noted that at a reducing agent content of 20% "bridgelets" were formed and the experiments were not subject to control by means of the method described. Phase X-ray analysis was conducted using the Debye-Sherrer method. Powder diagrams were obtained with copper radiation under tube operating conditions of 14 milliamps, 30 kv, in RKD chambers of 57.3 mm diameter.

It is known that UO_3 is a n-type semiconductor /13, 14/. The electrical conductivity of the semi-conductor oxides varies not only with temperature, but also depends on their structure and chemical composition. Therefore, according to the change in the electrical conductivity of the samples, it is possible to control

the state of the oxidized semiconductor effectively in its reaction with the reducing agent.

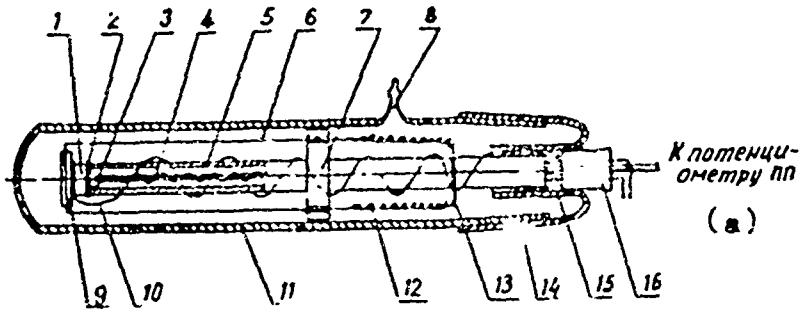

FIGURE 1. Diagram of the cell for measuring electrical resistance. 1 - Tablet of original sample; 2 - Platinum sheets; 3 - Thermocouple soldering; 4 - Two-channel alundum tube containing thermocouple; 5 - Alundum rod; 6 - Cylinder of heat resistant alloy; 7 - Screen made of asbestos-cement; 8 - Outlet to vacuum pump; 9 - Alundum tube; 10 - Platinum current leads; 11 - Quartz test tube; 12 - Steel springs; 13 - Spring holder; 14 - Quartz test tube; 15 - Bitumin; 16 - Rubber stopper. LEGEND: a) To potentiometer.

Figure 2 presents the results, in the coordinates lg - 1/T, based on temperature variation of electrical conductivity of both pure UO_3 (curve 4) as well as of its mixtures with carbon black (curves 1, 3) and graphite (curve 2), clearly showing that for all the functions characteristic breaks exist in the temperature region of 420-450° and 500°. This means that about 300° variation in the composition of the oxide can be recorded by this method and that the presence of carbon does not alter the general characteristic picture, since the electrical conductivity of carbon in the 300-600° interval, as has already been pointed out, remains practically unchanged.

The experimental results were supplemented by data on the dissociation kinetics of UO_3 and the reducing agent (UO_3 + C), obtained under identical conditions, but were also supplemented by data of X-ray phase analysis of a large number of intermediate products whose composition lies between UO_3 and $UO_{2.67}$ (U_3O_8). From comparison of all the data it follows that in the 430-460° region the onset of the formation of the new phase is observed at an overall composition of $UO_{2.91}$.

Thus, from 300° (where the electrical conductivity of carbon ceases to change) to 430-460° (cf Figure 2) the variation in electrical conductivity is determined mainly by changes in the UO_3-based (UO_3-p) solid solution; here, the chemical composition of the solution changes to $UO_{2.92}$. It also follows from Figure 2 that independently of the process type (dissociation, reduction)

the material of the reducing agent (graphite, carbon black) and its quantity (1.4 and 4.5%), the onset of formation of the new phase U_3O_8 is observed in the 430-460° region in the intermediate product of overall composition $UO_{2.91}$. Obviously, up to 400° it is specifically the temperature that determines changes in the process in question, where the main role is evidently played by the acts of crystallochemical transformation in the oxide.

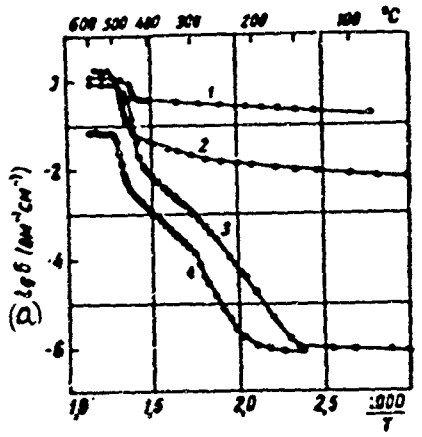

FIGURE 2. Specific electrical resistance of UO_3 and of the mixture UO_3 + C as a function of temperature: 1 - UO_3 + 4.5% carbon black; 2 - UO_3 + 4.5% graphite; 3 - UO_3 + 1.4% carbon black; 4 - UO_3. LEGEND: a) lg G ($ohm^{-1}cm^{-1}$).

The concurrence of the slopes of the curves 3 and 4 in Figure 2 (UO_3 and UO_3 + 1.4% C) up to 400° allows us to assume that in the reduction of UO_3 by solid carbon the loss of oxide oxygen is initially due mainly to its dissociation. Actually, the dissociation of UO_3, as was shown by the method of electrical resistance measurements, begins at 250-300°. Here, carbon plays the role of inert diluent of good conductance and its appreciable reaction with the gaseous medium is not observed in any case up to 400°. Also not occurring is the interaction of carbon with the oxide directly in the solid phase. As to the fact that carbon plays the role of inert diluent up to a certain point, evidence is found as follows: the less carbon in the mixture (curves 1, 3) the less the electrical conductivity of UO_3 (curve 4) differs from that of UO_3 + C (curves 1, 3). Here, over some area dissociation of the oxide is possible along with its carbothermic reduction, a phenomenon which has been noted in the literature for the example of manganese oxides /15/.

It is characteristic that in the dissociation of UO_3, the formation of U_3O_8 begins at 450°, whereas in the reduction of UO_3 by carbon black, the formation of U_3O_8 begins at $\approx$ 425°, and when the reducing agent is graphite -- at 450°. Thus, at temperatures above 400° the role of the reducing agent becomes manifest, which

follows from a comparison of the rates of dissociation of UO_3 /10/ with its reduction by carbon black /8/, graphite /9/, wood and sugar coal /16/. Moreover, it must be said that the mechanism of reduction of powdered and briquetted mixtures can be dissimilar, although the qualitative relationship of the rates of dissociation and reduction (at identical temperatures) will probably remain unchanged.

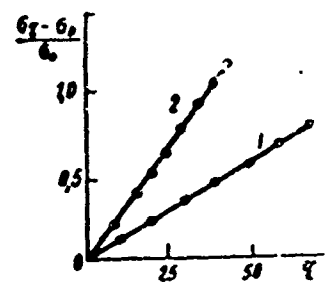

FIGURE 3. Relative change in electrical conductivity of the mixture UO_3 + C at 400° as a function of treatment time. σ_β = specific electrical conductivity of the mixture UO_3 + C at moment temperature of 400° is attained. σ_τ = specific electroconductivity of the mixture UO_3 + C at given moment of time τ. 1 - UO_3 + 4.5% graphite; 2 - UO_3 + 4.5% carbon black.

Above 450° two phases co-exist: U_3O_8 and UO_{3-p} (cf Figure 2). A certain increase in the temperature coefficient of electrical conductivity is due to an increase in the amount of the more electroconductive phase U_3O_8 compared with UO_{3-p} /17, 18/. Finally, about 500°, when the conversion of UO_3 to U_3O_8 was mainly completed, a variation in the temperature dependence of electrical conductivity of U_3O_8 itself was observed /3, 17, 18/. Thus, the method of measuring electrical conductivity succeeded in confirming the conclusion, based previously on kinetic and X-ray data /8/, which states that there is a lower limit to the homogeneity of the uranium trioxide-based solid solution.

The above noted dependence between the rate of oxide reduction on activity of a solid reducing agent has also been confirmed in our case by way of other data. As we can see in Figure 3, the relative increase in the electrical conductivity with time at 400° for the UO_3 - carbon black mixture is greater than for the UO_3 - graphite mixture (the amount of reducing agent is identical).

Data on the increase in electrical conductivity with time at the several temperatures for the UO_3 - graphite mixture (Figure 4) show that the intensity in variation of electrical conductivity at the several temperatures (tangent of the slope of the lines) can serve as the characteristic rate in our case of the overall process,

confirming a similar conclusion found earlier by V. P. Yelyutin, Yu. A. Pavlov, and others using the example of the reduction of vanadium oxides with solid carbon /6/.

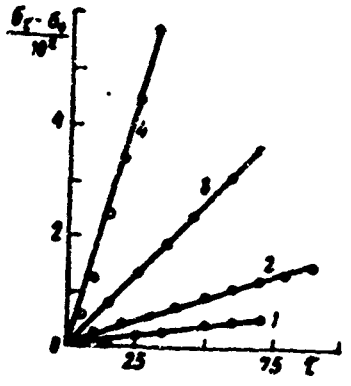

FIGURE 4. Change in electrical conductivity of the mixture UO_3 + 4.5% graphite at several temperatures as a function of the time of treatment: 1 - 350°; 2 - 375°; 3 - 400°; 4 - 425°

CONCLUSIONS

1. The method of measuring electrical conductivity, which is simple and under certain conditions convenient, has been used to corroborate the boundary limit to the existence of a uranium trioxide-based solid solution, determined earlier by kinetic and X-ray methods /8, 9/, and also has shown that the rate of the overall process can be characterized by the rate of change in electrical conductivity. With the aid of this method it has been possible to obtain data affording ideas on the role of dissociation in the reduction process.

LITERATURE

1. Shreyder, A. K., Zavodskaya laboratoriya (Plant Laboratory), 10, 1207 (1956).
2. Murat, M., Eyrand, C., Comptes Rendus, 254, No. 17, 3084 (1962).
3. Tkachenko, Ye. V., Neuymin, A. D., Vlasov, V. G., Strekalovskiy, V. N., Fizika metallov i metallovedeniye (Physics of Metals and Metallurgy), Vol 16, No 2 (1963).
4. Yelyutin, V. P., Pavlov, Yu. A., Shulepov, V. I., Myakisheva, T. G., Zh. fiz. khimii (Journal of Physical Chemistry), 36, 7, 1524 (1962).

5. Strekalovskiy, V. N., Neuymin, A. D., Bessanov, A. F., Zh. fiz. khimii, 36, 6, 1355 (1962).
6. Yelyutin, V. P., Pavlov, Yu. A., Surovoy, Yu. N., Shulepov, V. I., Izv. VUZ, Chernaya metallurgiya, No 7, 16 (1961).
7. Tekhnika vysokikh temperatur (High Temperature Techniques), ed. Campbell, For. Lit. Publ. House, Moscow, 1959.
8. Tkachenko, Ye. V., Vlasov, V. G., Fizika metallov i metallovedeniya, 15, 2, 239 (1963).
9. Vlasov, V. G., Tkachenko, Ye. V., Izv. Sibirskogo otdeleniya AN SSSR (News of the Sibirian Branch of the Academy of Sciences USSR), in press.
10. Vlasov, V. G., Lebedev, A. G., Zh. prikl. khimii, Vol 34, No 9, 1739 (1961).
11. Kats, D. Zh., Rabinovich, Ye., Khimiya urana (Chemistry of Uranium), part one, Foreign Literature Publishing House, Moscow, 1954.
12. Brauer, G., Rukovodstvo po preparativnoy neorgan khimii, 1956.
13. Pal'guen, S. F., Volchenkova, Z. S., Khimiya i tekhnologiya pedkikh elementov Tr. in-ta khimii, UFAN (Chemistry and Technology of Rare Elements, Transactions of the Institute of Chemistry, UFA Affiliate of the Academy of Sciences USSR), No 2, 183 (1958).
14. Willardson, R. K., Moody, I. W., Goering, H. L., J. Inorg. Nucl. Chem., 6, No 1, 19 (1958).
15. Kozlov, V. A., Vlasov, V. G., Zh. prikl. khimii, Vol 32, No 3, 523 (1959).
16. Vlasov, V. G., Kozlov, V. A., Zh. prikl. khimii, Vol 33, No 4, 760 (1960).
17. Zhukovskiy, V. M., Vlasov, V. G., Lebedev, A. G., Fizika metallov i metallovedeniya, Vol 14, No 3, 475 (1962).
18. Zhukovskiy, V. M., Vlasov, V. G., Lebedev, A. G., Fizika metallov i metallovedeniya, 14, No 2, 319 (1962).

Received by Editor
29 December 1962

DETERMINATION OF THE ORIENTATION OF TUNGSTEN CRYSTALS BY ETCHING FIGURES

A. I. Pekarev

(Institute of Metallurgy of the Academy of Sciences USSR)

The conventional method of determining the orientation of single crystals is based on reciprocal X ray photographs of cut sections or surfaces of monocrystals in the Laue chamber on standard equipment. Determination of the orientation of separate grains, the deformation bands, and elements of deformation (traces of glide and twinning planes) on semi-crystalline material is possible only with the use of unique sharp-focus X ray tubes. Therefore, both optical and electron microscopy are used in determining orientations in micro-volumes along with roentgenography.

The metallographic method consists in the following. The polished section of the metal sample is subject to special etching (chemical, electrolytic, vacuum) to display etching figures (EF), whose form depends on the method of etching the crystal lattice and on the orientation of the crystal with respect to the section surface. G. M. Fomin /1/ determined the predominant orientation of grains in zones of transformer steel. Each grain was categorized by etching form in one of four groups. In a given case approximate sorting of the grains was quite satisfactory to establish texture. For accurate determination of each grain is possible after measurement of the angles between the elements of EF in corresponding to geometric transformations.

In etching metals (molybdenum, tungsten, etc), crystallized in body-centered cubic (B-CC) form the etching figures were limited to the planes {110} with the closest packing of atoms and are trihedral and tetrahedral angles cut off by the section surface from a rhombododecahedron.

Within each separately situated EF, from the center to the apices of the angles run rays which are ribs having the directions (111) of solid angles. D. N. Vasilkovskiy /2/ developed in detail a method of nomographic determination of orientation by the angles between the

rib directions. To manifest such ribs in tungsten microstructure it is necessary to deeply etch the section with an aqueous solution of potassium ferricyanide and alkali.

Electrolytic etching of tungsten in a 2-10% alkali solution affords clear EF on the section surface, although the rays within the etching figure are almost indistinguishible and here a method of determining orientation from the size of the EF is needed. The method proposed by Kostron /3/ is applicable only for metals crystallizing in face-centered cubics (FCC) for which the EF are limited to the planes of the $\{100\}$ system.

The methods suggested for determining orientation in F-C C metals from the size of the EF involves the use of stereographic projection to simplify the mathematical analysis.

Each side of a triangular etching figure ABC (Figure 1) is the axis of a zone to which the plane $\{100\}$ and the section plane belong. The problem reduces to finding the plane parallel to the section surface in which there would lie three zonal axes forming sides of the triangle.

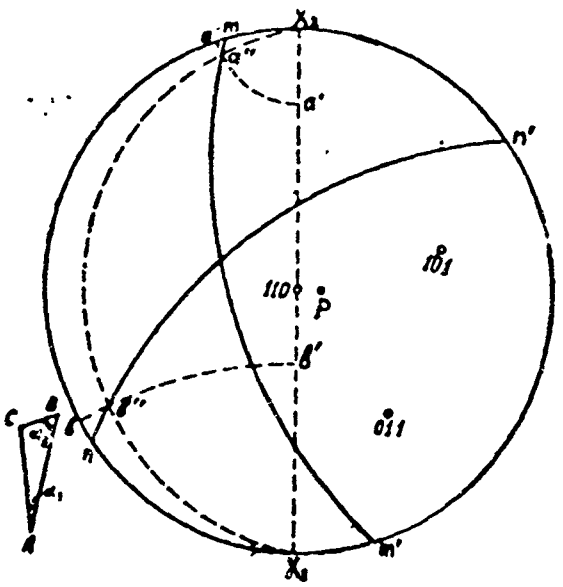

FIGURE 1. Determination of orientation for the triangular etching figure. Solid lines - traces of $\{100\}$, - - - - - parallels and trace of the plane sought for

All faces belong to the $\{100\}$ system. We take one of the EF as (110) and on a standard stereographic projection for the (110) plane draw the traces mm' nn' of the two other faces (101) and (011) of the etching figure.

The two sides AC and BC of the triangle in Figure 1 lie under the angles α_1, α_2 to an arbitrarily selected base side AB lying in the plane $(1\bar{1}0)$. We superimpose the base side with the axis X_1 X_2 of the stereographic sphere and the angles α_1, α_2 are laid off, respectively, from the poles X_2 and X_1. Then the directions of the

sides AC and BC must lie somewhere on the parallels aa' and bb' of the Woulfe network.

The great circle found on tracing paper following the traces mm' and nn' are superimposed on the Woulfe network (See Figure 1) and we rotate the great circle around the center until the points of interception a' and b' of the traces of the planes (101) and (011) with the latitudes aa' and bb' will not appear on the same meridian X_1 b' a' X_2. The resulting meridian is the projection of the slide plane, but the pole of the plane sought for is .P. Transferring the tracing paper onto the standard stereographic projection of the (110) plane we determine the orientation of the section surface. The direction of the side to the triangle is determined by the points a", b", X_1.

If EF is of the quadrangular form ABCD (S2), then the traces nn' and mm' of the two planes (011) and $(0\bar{1}1)$ adjoining the plane (110) are plotted on the standard stereographic projection of the (110) plane. The three planes (110) will form the tetrahedral angle of the EF. Two angles (more suitably, acute angles) adjacent to the same side BC are measured in the quadrangle, under which are traced the parallels cc' and bb' (See Figure 2) onto the Woulfe network.

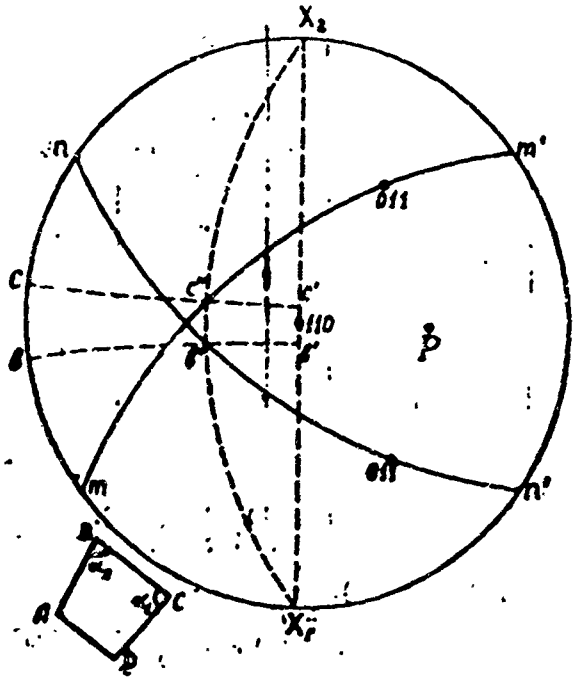

FIGURE 2. Determination of the orientation for the quadrangular etching figure. The solid lines - traces of the {100} ,- - parallels and trace of plane sought for.

The order of determination of the orientation of the section surface is similar to the case of the triangular EF. The meridian

X_1 b" c" X_2 is the trace of the plane sought for.

It is apparent that the square form of the EF has a surface with the indices {100}, but the surface with equilateral triangles is oriented at {111}. Shown in Figure 3 are the possible forms of EF. The dash line indicates the boundary between orientations with the triangular and quadrangular EF and the region close to (110), where the etching figures appear only after much work and are of irregular oval or broken-line form.

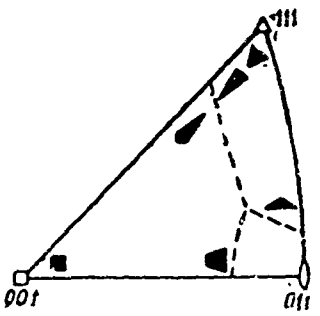

FIGURE 3. Forms of etching figures as a function of orientation on the stereographic triangle.

The angles between the sides of the EF can be measured to an accuracy of 2-4° in a photograph of microstructure or directly with the mettalomicroscope used for reading angles by the rotary table (using a MIM-8 type microscope). When the Woulfe network is used, of 20 cm in diameter, the accuracy of the geometric construction is close to 1-2°. The total error in determining the orientation of the section plane usually does not exceed 4°.

Figure 4 presents a photograph of the microstructure of two samples of cast tungsten with triangular and quadrangular forms of EF. The tungsten section underwent electropolishing and electro-etching in 10% Na OH at a current density of 1.5 and 0.05 amp/cm^2. Presented in the table are the results of orientation determinations from Figures 1, 2, and 4. The direction of the glide line can be determined by the angle between the glide line and the already known orientation of any side of the etching figure.

TABLE

Results of Determination of Orientations

(a) № рисунка	(b) Сторона ФТ	(c) Грань ФТ	(d) Угол между сторонами, *град*	(e) Ориентировка стороны: точка на схеме (g)	(e) Ориентировка стороны: ближайшая плоскость (h)	(f) Ориентировка шлифа: ближайшая плоскость (h)	(f) Ориентировка шлифа: угол к ней, *град* (i)
1 и 4*а*	*CA* *AB* *BC*	101 110 011	19 59	*a″* X_1 *e″*	111 221 122	551	3
2 и 4*б*	*AB* *BC* *СД*	011 110 011	81 84	*e″* X_1 *c″*	711 001 711	010	7

LEGEND: a) Figure number; b) Side of etching figure; c) Face of etching figure; d) Angle between sides, degrees; e) Orientation of side; f) Orientation of section; g) Point on diagram; h) Nearest-lying plane; i) Angle of nearest-lying plane to section, degrees

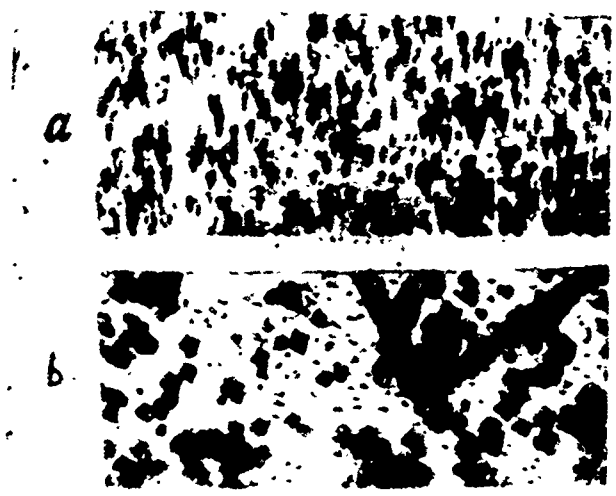

FIGURE 4. Triangular (a) and quadrangular (b) etching figures on a section of cast tungsten, X 250.

LITERATURE

1. Fomin, G. M., Tr. Moskovskogo instituta stali (Works of the Moscow Institute of Steel), No 10, 149 (1938).
2. Vasil'kovskiy, D. N., Nekatoryye voprosy katodnoy elektroniki (Some Problems in Cathode Electronics), Publ. by Cent. Asiatic State Univ., Tashkent, 29, 1959.
3. Kostron, V. H., Z. Metallkunde, 41, 10, 370 (1950).

Received by Editor
15 April 1963

THERMAL FATIGUE OF CERTAIN TITANIC ALLOYS

N. M. Pultsin, N. S. Samoylov and V. B. Pokrovskaya

(Military-Aircraft Engineering Academy)

Parts operating under the condition of alternating heating and cooling must have requisite resistance to thermal fatigue, i.e., against destruction of their material through repeated changes in its thermal state during performance. During non-uniform heating and heterogeneity of bulk changes, thermal stresses arise in the material leading to a breakdown in its solidity.

Various materials functioning under identical conditions develop dissimilar resistance to thermal fatigue. This is accounted for by many factors, including the physical properties of thermal expansion and thermal conductivity. For example, titanium and its alloys differ significantly from other metallic materials in the values of their thermal conductivity and thermal expansion. The thermal conductivity of titanium is 0.037 calories/cm·sec·deg, approximately 100-115% less than for steel, while the coefficient of thermal expansion is $8.3 \cdot 10^{-6}$ per degree -- almost 50% lower than for steel.

Such difference in the fundamental physical properties is responsible for a substantial change in the value and distribution of thermal stresses in cyclic heatings and coolings of titanic alloys and leads to such destruction of these materials from thermal fatigue which is essentially different from the breakdown of steels and other alloys.

In this report an investigation is made of thermal fatigue of certain titanic alloys. The investigations were conducted on an original device /1,2/, developed with the participation of one of the authors. Used as samples were square sheet plates 120 × 120 × 1.5 mm in size. Heating by the use of induction method, using a loop-shaped inductor. During the course of the tests, the inducator was placed on one side of a rigidly secured

sheet sample. The heating zone was in the form of an ellipse and on the inductor's side was characterized by somewhat greater area than on the opposite side.

The thermal cycle in the various experiments was characterized by upper temperatures of 800°, 900°, 1000°, and lower - near 20°. Cooling was carried out by a stream of tap water. The heating was continued at an average rate of 200° per second and lasted 4-5 seconds and cooling -- -160° per second and lasting for 5-6 seconds.

In the tests a determination was made of the number of "heating-cooling" cycles until the moment that the first fissure, 0.10-0.15 mm in length, appeared in the material. Also investigated were the kinetics of fissure development. Here an ultrasonic method of detecting moments of origin and used in studying fissure enlargement /2/ was used.

A study was made of microstructure and the microhardness of the titanic alloys was determined in that zone of the sample which underwent cyclic temperature variations. Together with the titanic alloys, OT-4 and VT-14, for comparison the resistance to thermal fatigue of the nickel alloy EI-435 was examined.

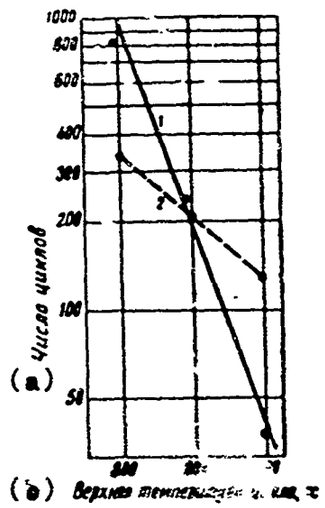

FIGURE 1. Number of "heating-cooling" cycles before cracks appear as a function of the value of the upper cycle temperature when the titanic alloy OT4 (1) and the nickel alloy EI435 (2) is tested for thermal fatigue. LEGEND: a) Number of cycles; b) Upper cycle temperature, ° C

Alloy OT-4. Fig. 1 presents a graph of changes in the number of "heating-cooling" cycles before the appearance of a thermal fatigue crack as a function of the value of the upper cycle temperature in samples of sheet titanium alloy OT-4 1.5 mm in thickness. As can be seen from the graph plotted in semi-

logarithmic coordinates, with increases in the upper cycle temperature the number of cycles before the appearance of cracks drops sharply, evidencing a significant lowering of the thermal resistance of the OT-4 alloy with increase in upper cycle temperature.

In addition to the titanic alloy OT-4, thermal fatigue of the nickel alloy EI-435 was also tested. The number of "heating-cooling" cycles until sample breakdown at the upper cycle temperatures of 900 and 800° amounted to, respectively, for the OT-4 alloy to 241 cycles and 804 cycles, and for the EI-435 alloy -- 206 and 345 cycles.

Hence, the thermal resistance of the titanic alloy OT-4 at the upper cycle temperature studied is significantly higher than that of the nickel alloy EI-435, especially at a low upper cycle temperature. This is accounted for by the low coefficient of thermal expansion of titanium.

On the other hand, if we were to compare the rate at which the number of cycles were reduced up to breakdown with increase in the upper cycle temperature (Cf. Fig. 1), then we would see that at high temperatures (1000°) the nickel alloy proves to be more thermally resistant than the titanic, which can be explained by the high peak-resistance of nickel alloys.

The ultrasonic defectoscope was used to investigate the kinetics of growth of the thermal-fatigue cracks. Shown in Fig. 2 is the variation in the length of the thermal fatigue crack as a function of the number of "heating-cooling" cycles at various upper temperatures of the cycle. From analysis of the graphs presented it follows that each curve has two sections--a curvilinear and a rectilinear. The curvilinear section corresponds to the slow, but accelerating development of thermal fatigue cracks. This acceleration takes place the more rapidly the higher the upper cycle temperature.

The rectilinear section corresponds to a constant rate of crack formation. With higher upper temperature cycle the rate of thermal fatigue crack formation increases in straight-line proportionality (Fig. 3).

Alloy VT-14. Investigation of the thermal fatigue of VT-14 alloy was conducted on sheet samples 120 X 120 X 2 mm in size. The tests were carried out at 3 upper cycle temperatures of 800, 850 and 900°. Here it was found that even a very large number of heat-shift cycles does not cause in this alloy the development of visible thermal fatigue cracks. However, as will be shown below, for cycles with 900° as the upper temperature micro-fissues appear, extending into the surface altered layer appearing as the result of saturation by oxygen of titanium during the cyclic heatings.

Metallographic studies and determination of micro-hardness. Metallographic studies were conducted on samples tested for thermal fatigue and determination of micro-hardness was made. For this

sheet samples were cut along the major axis of an elliptical patch and subjected to polishing, buffing, and etching. Investigations revealed that as the result of testing for thermal fatigue substantial variation in the physical structure of the alloy in the heating zone appeared.

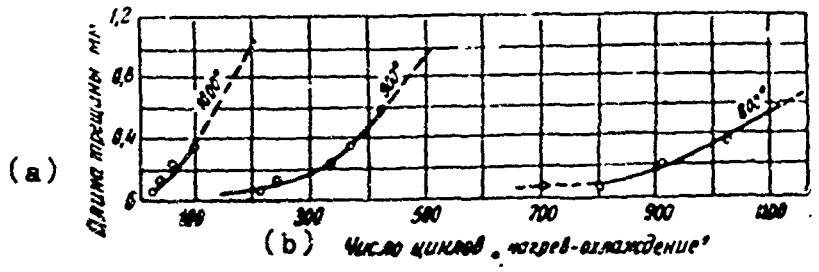

FIGURE 2. Length of thermal fatigue cracks as a function of number of cycles at various upper cycle temperatures in the testing of the titanic alloy OT4.
LEGEND: a) Length of fissure, mm; b) Number of "heating-cooling" cycles

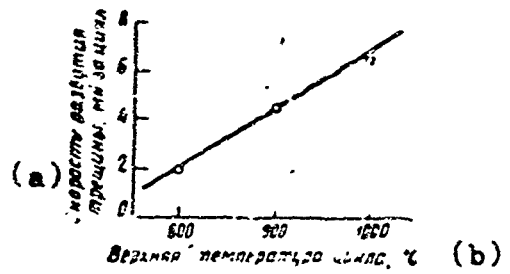

FIGURE 3. Change in rate of thermal fatigue crack formation in the OT4 alloy as a function of upper cycle temperature.
LEGEND: a) Rate of crack formation, microns per cycle; b) Upper cycle temperature, ° C

The original structure of the OT-4 alloy is two-phase fine-grained with the clearly pronounced striation characteristic of sheet material undergoing significant deformation in the process of being rolled. The structure of the OT-4 alloy in the heating zone following testing for thermal fatigue was essentially altered. Along the edges of the patch where the heating temperature was not high some coarsening of the grains

took place, the structure was maintained as equiaxial two-phase (Fig. 4, a). Such a variation in structure took place as the result of recrystallization of the alloy at low heating temperatures.

The structure in the high-temperature zone of the patch is needle-shaped, in which the needles become coarser with increase in heating temperature. The appearance of the needle-like structure is due to the high rate of cooling of the metal against a background of local heating during the process of testing for thermal fatigue, and the coarsening of the grains -- by the sizeable growth of the crystallites of the solid beta-solution at high temperatures. The presence of the coarse-needle-shaped structure in the heating zone (together with the effect of thermal stresses) can favor the rise of thermal fatigue cracks.

As the result of heating to high temperature (1000°) the formation of a modified layer (Figure 5) saturated in oxygen occurs, in which the solid solution of this layer has a structure elongated and arbitrarily oriented grains. It must be noted that the thickness in structure of this layer are identical both on the inductor side as well as on the opposite side of the sheet sample tested.

The testing of the OT 4 alloy for thermal fatigue at an upper cycle temperature of 900° leads to structural changes less clearly pronounced than at 1000°.

The change in the micro-hardness of the hardness of the material along the axis of the heating patch is in accordance with structural transformations. Thus, for example, for a sample of the OT 4 alloy tested for thermal fatigue at an upper cycle temperature of 900°, the micro-hardness in the central zone of the patch exceeds 400 kg/mm^2 while its value in the surrounding material is about 270 kg/mm^2. In the central zone of a patch of sample of the same alloy tested at an upper cycle temperature of 1000°, the micro-hardness is about 350 kg/mm^2, ie, 50 kg/mm^2 lower than at 900°.

The original structure of the VT 14 alloy is also two-phase, but with a less pronounced striation. The structure in the heating zone depends little on temperature and remains almost unchanged from the edge to the center of the heating patch.

Shown in Figure 6 are microphotographs of the structure of the VT 14 alloy in the zone of the heating patch (upper cycle temperature = 900°). This structure, in spite of the high heating temperature, is fine-grain with weakly pronounced acicularity. It is possible that this is precisely what accounts for the high resistance of the VT 14 alloy to thermal fatigue.

A surface layer with a characteristic structure (Figure 7) and increased hardness has been found for a sample of the VT 14 alloy tested for thermal fatigue at an upper cycle temperature of 900° for a protracted period (397 heat-cycle). Thermal fatigue cracks appeared in this layer, extending right through the layer, but not entering the zone of the underlying material.

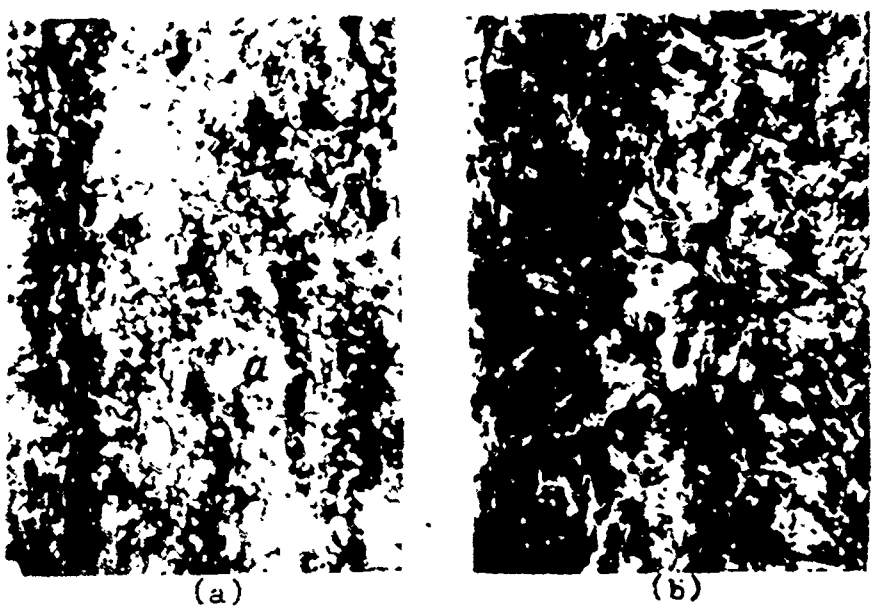

FIGURE 4. Microstructure of the OT4 alloy in the zone of the heating patch when testing for thermal fatigue. a - at edge of patch, b - in middle of patch, X 450, upper cycle temperature = 1000°.

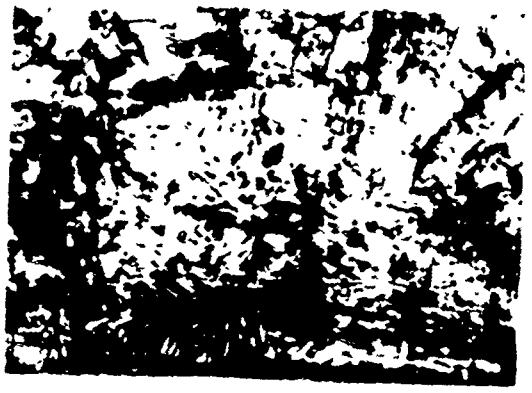

FIGURE 5. Microstructure of the OT4 alloy in the center of the heating patch showing a zone of surface modified layer, X 450, upper cycle temperature = 1000°.

FIGURE 6. Microstructure of the VT14 alloy in the heating patch zone, X 450, upper cycle temperature = 900°.

FIGURE 7. Microstructure of the edge of a sample of the VT14 alloy tested for thermal fatigue at an upper cycle temperature of 900°. Visible is the oxygen-saturated modified layer and cracks in it, X 450.

CONCLUSIONS

1. A study has been carried out of thermal fatigue of the titanic alloys OT 4 and VT 14 and of the nickel alloy EI 435. It has been established that the heat resistance of titanic alloys at upper cycle temperatures up to 900° is higher than for the nickel alloy EI 435.

2. The formation of thermal-fatigue cracks at various upper cycle temperatures has been investigated and it has been shown that the growth rate of these cracks increases with temperature.

3. As the result of investigation of the microstructure and micro-hardness in the zone of the heating patch it has been found that when testing for thermal fatigue substantial change in the structure and increase in the micro-hardness of titanic alloys appears, where the structure becomes needle-shaped. The suggestion was made that formation of the coarsely acicular structure favors the genesis and development in the material of thermal fatigue cracks.

4. It has been observed that when an alloy is subjected to prolonged testing a surface layer saturated with oxygen can appear, so fragile that thermal fatigue cracks will form in it. However, these cracks in the VT 14 alloy do not depart beyond the limit of the layer and do not penetrate the underlying material.

LITERATURE

1. Stroyev, S. S., Samoylov, N. S.. Sb. statey Termostoikost' zharoprochnykh splavov (Collection of Articles: Thermal Stability of Heat-Resistant Alloys), ed. N. M. Sklyarov, Oborongiz, Moscow, 1962.

2. Stroyev, S. S., Samoylov N. S., Pavlov, V. Ya., Byull. izobreteniy (Invention Bulletin), No 21, 1961; Description of Invention in Author's Certificate No 142457.

Received by Editor
23 January 1963

GALVANIC COPPER-PLATING OF TITANIUM AND ITS ALLOYS

V. V. Usov, V. I. Liner

(Moscow Institute of Steel and Alloys,
Chair of Corrosion and Protection of Metals)

The chief advantage of titanium and its alloys over other structural materials lies in the combination of high mechanical properties and corrosional resistance with low specific gravity. Titanium has the highest specific strength among technical materials. And the strength of titanic alloys is not reduced even during heating up to 400-500°, especially important for modern technology. Titanium exhibits high corrosional resistance in an air atmosphere, sea water, and in several strong chemical reagents.

With an increase in the areas of technical use of titanium the need arose to deposit galvanic coatings on titanium alloys, which partly or completely eliminates certain shortcomings specific to titanium. These shortcomings include low heat and electrical conductivity; difficulty in soldering; burrs arising in friction and adhering to tools; energetic reaction with oxygen and nitrogen, especially at elevated temperatures.

Galvanic copper-plating of titanium lowers the transitional resistance, increases electro- and thermoconductivity, improves the conditions of low-temperature soldering. The copper coat can serve also as a technological lubricant in the cold treatment of titanium by pressure and protect the surface of articles from scraping and burrs, significantly improving surface quality. Other galvanic coatings can be applied on the copper layer by usual methods.

The indicated ways of using titanium with copper plating can be recommended only for titanium articles used at temperatures lower than that of the formation of intermetallic compounds of titanium with copper since the brittleness of the diffusion layer leads to lowered strength of the adhesion of copper with the underlying metal.

In the copper plating of titanium difficulties appear like those which occur in the galvanic plating of aluminum and magnesium. A dense oxide film responsible for the high corrosive stability of titanium prevents the durable adhesion of the galvanic deposit with the substratum. When this film is removed by mechanical means or in aggressive media rapid repeated oxidation takes place. Activation of the titanium surface before deposition of the galvanic layer is therefore the central problem in this technology.

Many variants of the preliminary preparation of the surface of titanium under galvanic plating have been proposed. Their essential content amounts to removing the oxidized film and preventing its formation by intermediate layers consisting of fluorides /1/, hydrides /2,3/, or by layers of copper /4/ and zinc /5/. Of the methods for preparing the titanium surface enumerated the one I make most application consists in prolonged etching in concentrated acids -- sulfuric and hydrochloric /6/. Several metals, most often chromium, have been deposited on the hydride layer formed in etching. Of the other methods of surface preparation one should note the contact zincing of titanium for subsequent nickel-plating /7/ and copper-plating /8/. In the last case it is recommended that the titanium be previously anodized in a solution of sulfuric acid. The thickness of the copper layer is 1-2 microns. When the thickness of the coat had increased peeling of the copper is observed directly in the course of electrolysis.

Earlier, in searching for a method to prepare the surface and to activate titanium before copper plating, positive results were achieved after etching titanium in mixtures of fluoric and nitric acids in a 1:3 ratio and activation in a mixture of 800 ml ethylene glycol, 200 ml/liter (40%) of hydrofluoric acid, and 100 g/l of zinc fluoride /9,10/. A compact dark-grey film of 0.1 - 0.3 mm/cm^2 thickness was formed here on the titanium surface (the thickness of the film is of the same order of magnitude as for a galvanized treatment of aluminum). Electron diffraction and spectral analyses made it possible to establish that the film is a zinc hydride: the layer underlying the surface consists of the titanium hydrides Ti H - $Ti H_2$, and the upper layer -- metallic zinc.

The conditions of activation (temperature, concentration of hydrofuoric acid, and duration of treatment) determine the composition of the film and the reasons in which durably adhering copper deposits are attained. In determining the optimal activation conditions (See Note) the concentration of HF was varied from 90 to 60 grams/liter with a 5 grams/liter interval. At each concentration the increment in film weight and the percentage content of hydrogen were determined as functions of temperature and duration of treatment. The film increment was determined by weighing before and after etching in concentrated hydrochloric acid. The hydrogen content

percentage was determined by a spectral method, which gives an averaged value of 40 - 50 microns in depth.

(/NOTE/ Participating in the experimental part of the study were the technicians: E. L. Troshina, V. V. Ul'yanova, and V. P. Kuzenkova.)

The increment in film weight depends to a great extent on the solution temperature; as the temperature rose from 14 to 30° the increment increased from 0.1 to 0.3 milligrams/cm^2 (Figure 1). Duration of treatment led to a slight increase in film thickness, while the concentration of HF has almost no effect on film thickness. The percentage content of hydrogen in the film increased with increasing temperature from 16 to 20° and then dropped sharply (See Figure 1 b). Increase in HF content results in a relative increase in the hydrogen content.

Confirmation of the durability of the copper plate adhesion, 50 microns thick, depending on the activation conditions, revealed that the region in which durably adhering copper deposits were achieved is reduced with decreased concentration of HF and with increased temperature. Consequently, the conditions for obtaining platings of satisfactory adhesion are in direct dependents on the hydrogen content in the surface layer. We often observe that on films without a dark sublayer no satisfactory adhesion of the copper plate was obtained. The optimal conditions for preparing the titanium surface for copper plating are as follows: temperature -- 18 - 20°, concentration of HF -- 90 - 75 grams/liter, and duration of treatment -- not less than 1-2 minutes.

The solution of the activation bath contained about 95 grams/liter HF after the preparation and is formulated on the basis of 5 decimeter^2 of titanium per liter. As the processing continues the HF concentration in the bath falls off and titanium fluoride and water becomes accumulated, which is carried off by the samples, therefore the bath must be corrected with concentrated hydrofluoric acid. The total working capacity of the activation bath under laboratory conditions was 50 decimeter^2/liter.

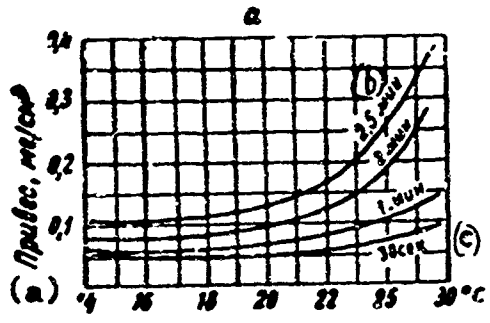

FIGURE 1a. Effect of temperature of activation solution on the film increment in weight. HF concentration: 75-80 g/li. LEGEND: a) Weight increment, mg/cm^2; b) Minutes; c) Seconds.

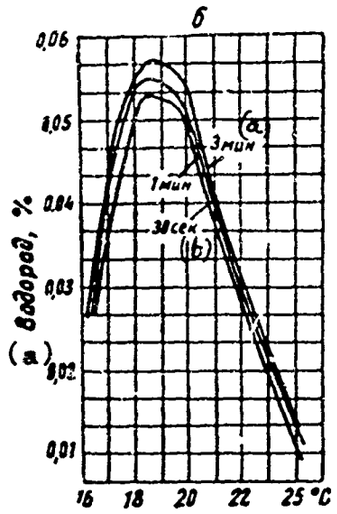

FIGURE 1b. Effect of temperature of activation solution on percentage content of hydrogen in the zinc-hydride film. HF concentration: 75-80 g/li. LEGEND: a) Minutes; b) seconds.

It was noted that the purity of the zinc fluoride affected in some way the formation of the hydride sublayer, but we have not yet explained the role of the purity in zinc fluoride.

Copper plating of titanium was initially carried out in a cyanide electrolyte containing Seignette's salt. Direct copper plating in sulfate for hydrofluoroboride electrolyte does not insure lasting adhesion of the plating with the substratum, probably due to contact precipitation of copper on the film. The cyanide copper plating conditions were found to be the following: current density -- 2 amp/decimeter^2 (10 seconds), and then 1 amp/decimeter^2 (10 minutes), electrolyte temperature -- 40°. Copper was deposited from the electrolyte sulfate over the copper precipitated in the cyanide electrolyte. To achieve lasting copper deposits it is important to watch the content of free cyanide. A deficiency in cyanide leads apparently to contact precipitation of copper, but an excess -- to dissolution of the zinc deposit. The optimal free cyanide content is 7.5 - 9.5 grams/liter.

In testing the possibility of replacing cyanide we concentrated on pyrophosphate electrolytes, which are not poisonous, are simple in composition, have high dispersibility, high value for permissible current densities, and a current-based yield approaching 100%. Pyrophosphate electrolytes varied in composition were tested;

positive results were achieved in copper plating of titanium from two consecutive baths each with a different $P_2O_7^{4-}$: Cu ratio /11, 12/.

Used as the preliminary bath was an electrolyte of the following composition: 10 grams/liter Cu; 350 grams/liter $P_2O_7^{4-}{}_{tot}$; $P_2O_7^{4-}$: Cu not less than 35; 25 grams/liter $K_2C_2O_4$; pH = 9. The copper plating conditions were as follows: Room temperature, initial current density -- 1 amp/decimeter^2 (10 seconds), and then 0.1-0.3 amp/decimeter^2. The electrolyte was prepared from potassium pyrophosphate of high solubility compared to sodium pyrophosphate. The thickness of the copper layer in the preliminary copper-plating bath was 0.5 microns against a total thickness of 100 microns. The electrolyte in the subsequent copper-plating bath was of the following optimal composition (in grams/liter): 30 Cu; 210 $P_2O_7^{4-}{}_{tot}$; 20 KNO_3; 25 $K_2C_2O_4$; 15 ml/liter NH_4OH (25%); pH = 8.2 - 8.8. The electrolyte temperature was 55 - 60°; current density = 1.3 amp/decimeter^2. The anode to cathode surface ratio was 3:1. If high dispersibility is not required copper plating is possible in the sulfate electrolyte after preliminary copper plating in the first pyrophosphate electrolyte. The copper plating electrolytes did not contain SO_4^{2-} and were corrected with oxalic acid or sodium hydroxide, since in the SO_4^{2-} containing electrolytes at pH > 9 copper salts are precipitated. The presence of SO_4^{2-} has practically no effect on the current-based copper yield (Figure 2).

The minimum $P_2O_7^{4-}$: Cu ratio in the preliminary copper-plating bath was equal to 35; when this value is decreased no strong adhesion of copper with substrate could be achieved. Study of the cathode process in the preliminary copper-plating bath revealed that the increased content of free potassium pyrophosphate (Figure 3) or the decrease in copper content (Figure 4) results in a significant shift in the discharge potential of copper toward the side of negative values. Comparison of the stationary copper potentials with the discharge potentials points to the high polarization with which copper ions are discharged in these electrolytes (Figure 5).

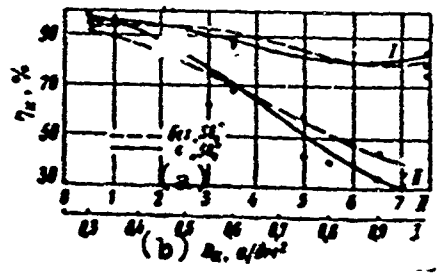

FIGURE 2. Effect of current density on cathode current-based yield in preliminary copper-plating bath and in the working bath. LEGEND: a) --- without SO_4, _____ with SO_4; b) D_K, amp/decimeter^2.

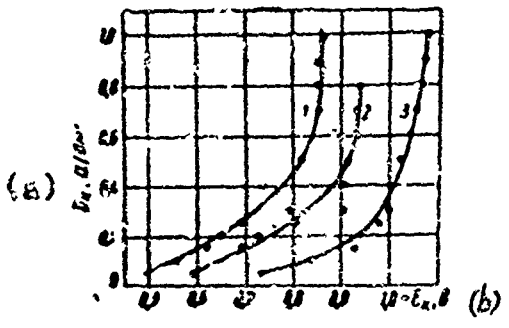

FIGURE 3. Effect of concentration of $K_4P_2O_7$ free of 0.1 N (1), 1 N (2) and 6 N (3) on cathode polarization of copper. Cu content = 0.25 N. LEGEND: a) D_k amp/dec^2; b) Volt.

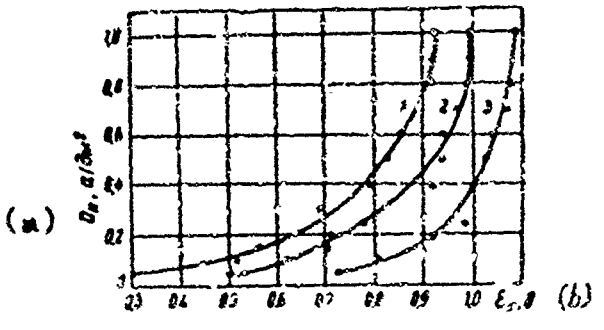

FIGURE 4. Effect of Cu concentration of 1 N (1), 0.4 N (2), 0.1 N (3) on cathode polarization at a content of 5 N $K_4P_2O_7$ free. LEGEND: a) D_k amp/dec^2; b) Volt.

The low copper content in the electrolyte used in the preliminary copper-plating bath and the significant concentration of pyrophosphate (6.8 N) leads to an increase in cathode polarization, which compared to the working copper-plating bath at a current density of 0.3 amp/decimeter^2 is 450 millivolts higher (Figure 6). The more negative value of the discharge potential of the copper ions in the first bath and its approximation to the discharge potential of the copper from the cyanide electrolyte, apparently, insures adhesion of the copper to the titanium due to prevention of contact precipitation of copper on the zinc hydride film. Adding potassium oxalate (25 grams/liter) to the electrolyte leads to a significant lowering of the anode potential, promoting better dissolution of the copper anodes (Figure 7). The dispersive power of the pyrophosphate electrolytes is sufficiently high and approaches that of cyanide baths.

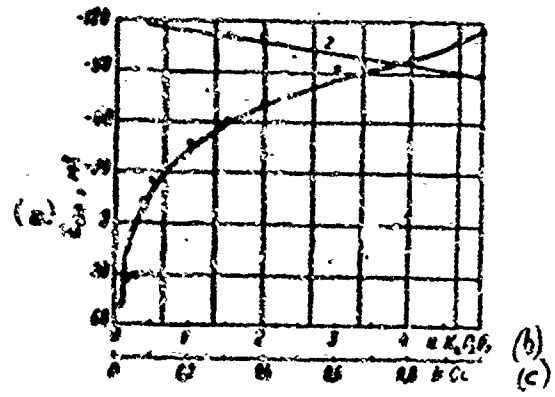

FIGURE 5. Effect of $CuK_4P_2O_7$ free concentrations on the stationary potential of copper in the preliminary copper-plating bath at a constant content of 0.25 N Cu (1); 5 N $K_4P_2O_7$ free (2).
LEGEND: a) Millivolts; b) Normal, $K_4P_2O_7$; c) Normal Cl.

These pyrophosphate electrolytes can also be used in preparing titanium by etching in concentrated acids.

At the present, it can be assumed as widely accepted that heat treatment improves the adhesion of galvanic platings with titanium-based alloys. Heat treatment can fulfill the role of controlling adhesion quality. Peeling after heating testifies to the unsatisfactory preparation of the surface.

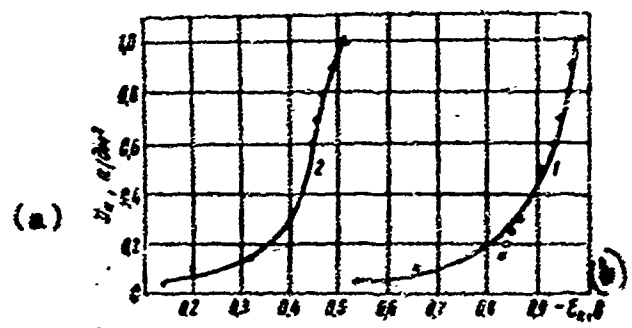

FIGURE 6. Effect of current density on cathode polarization in preliminary (1) and working (2) copper-plating baths.
LEGEND: a) amp/decimeter^2; b) Volt

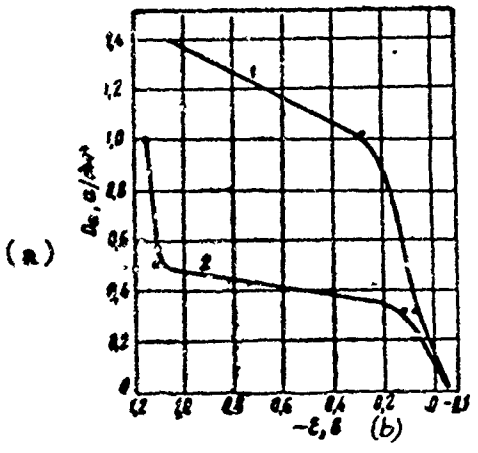

FIGURE 7. Effect of current density on anode polarization in preliminary copper-plating bath: 1 - with addition of 25 g/liter $K_2C_2O_4$; 2 - without adding $K_2C_2O_4$.
LEGEND: a) amp/decimeter^2; b) Volt

The durability of the copper adhesion with titanium without annealing is inadequate, and when a sheet material is bent flaking is observed. Raising the temperature from 200 - 400° markedly improves adhesion. Temperatures of 400-500° with duration of treatment not less than 20-10 minutes can be regarded as optimal for annealing. The durability of the adhesion of copper and titanium discovered by the method of notching the ends and bending sites at an angle of 90° heated to 500°, and also by a specially developed method of cementing plated samples of a definite shape with epoxide cements followed by subsequent rupture on an Amsler machine. In the last case the durability of the adhesion amounts to 120-140 kg/cm^2 before annealing, and after annealing at 200° (30 minutes) to 180-200 kg/cm^2, and under optimal annealing conditions exceeds 350-400 kg/cm^2 (in the last instance the breakdown occurs along the cementing line). After heat treatment the samples undergo repeated bending, notching at the bend site, and also low-temperature soldering.

Increasing the annealing temperature above 550° worsens the adhesion due to the appearance of a brittle layer of intermetallides and to differences in the coefficients of thermal expansion of titanium and copper. The thickness of diffusion layer in heating at 550° (30 minutes) is 0.3 micron, at 750° -- 1.5 microns, and at 800° the layer grows suddenly and unevenly, while at 850° four phases appear further and fusion of the plating commences, evidently due to the formation of an eutectic /See Note/ (Figure 9). The durability of the adhesion of copper to titanium after annealing at 650° is only 100 kg/cm^2.

(/NOTE/ The metallographic investigations were conducted by E. R. M Sizova under the supervision of L. I. Stoklitskiy.)

FIGURE 8. Uniformity of the distribution of copper platings in cyanide and pyrophosphate electrolytes, measured in the Hull cell: 1 - cyanide bath; 2 - preliminary copper-plating bath; 3 - working bath.
LEGEND: a) Deposition of Cu, microns; b) Distance between anode and cathode.

The technology proposed gives good results for deformed titanium after rolling and traction (for sheet, wire, and tubular material). The surface of titanium following hot pressing and stamping requires before activation more severe etching or mechanical working.

The testing of the technology of copper plating for titanium alloys reveals that the copper plates on alloys of titanium with aluminum, manganese, and tin (VT-5, VT-5-1, OT-4-1) have strong adhesion with the substratum. Two phase alloys of titanium with molybdenum, chromium, (VT-3-1, VT-8, and VT-14) produce on the platings after annealing (500 -- 10 minutes) scalings in the form of swellings. It is apparent that the conditions of etching and activation of the surfaces of these titanium alloys calls for special investigation.

(a)

(b)

(c)

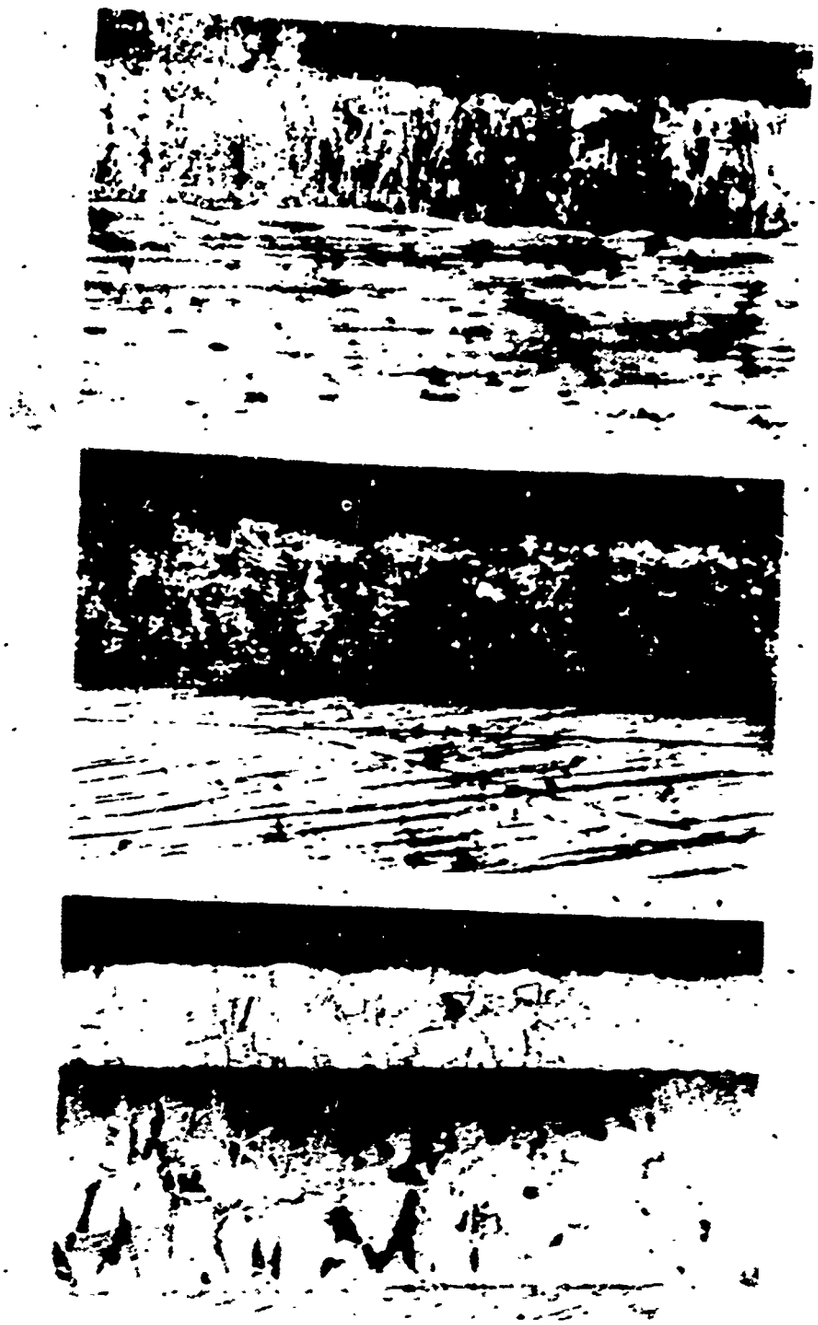

FIGURE 9. Microphotographs of sections of VT-1 titanium with galvanic copper plating before and after heat treatment: a - original state, X 200; b - heat treatment at 500° for ten minutes, X 200; c - heat treatment at 850° for five minutes, X 250.

LITERATURE

1. Brenner, 43rd Ann. Techn. proc. Amer. Electroplaters' Soc. 1956.
2. Burdina, S. M., Samartsev, A. G., Zh. prikl. khimii, 33, No 5, 1141 (1960).
3. J. Electrochem. Soc., v. 106, No. 4, 1959.
4. Missel, Metal Finish, v. 55, No. 9, 1957.
5. Richaud, Rev. Metallurgie, Oct, 1957.
6. Burdina, S. M., Samartsev, A. G., Zh. prikl. khimii, Vol 34, No 2, 1961
7. Smolenskaya, G. N., Kudryavtsev, N. T., Metallovedeniye i termicheskaya obrabotka metallov (Metallography and Heat Treatment of Metals), No 11, 1960.
8. Ginberg, A. M., Gorina, A. P., Peredovoy nauchno-tekhnicheskoy i proizvodstvennyy opyt (Advanced Scientific-Technical and Production Experience), No 21, 1960.
9. Layner, V. I., Sukhacheva, S. V., Izv. VUZ, Tsvetnaya metallurgiya, No 1, 1961.
10. Layner, V. I., Stoklitskiy, L. I., Syagina, V. V., Aviatsionnaya promyshlennost' (Aviation Industry), No 3, 1962.
11. Serota, Metal Finish, April 1960.
12. Passal, Plating, June 1939.

Received by Editor
18 March 1963

EFFECT OF MAGNESIUM AND CALCIUM ON THE CORROSIONAL RESISTANCE OF NICKEL IN A FLUORINE ATMOSPHERE AT 700-850°

A. V. Kurdyumov, V. N. Goloborodov, M. A. Stepanov

(Moscow Institute of Steel and Alloys,
Chair of the Technology of Casting Processes)

According to literature data nickel is the stablest metal in a fluorine atmosphere at 500-600 /1,2/. Under these conditions a yellowish-green film of fluoride, protecting nickel from intensive attack, will be formed on nickel surfaces. When the temperature is increased above 600-700 the protective properties of the fluoride film are reduced and corrosional attack of nickel increases sharply. It is assumed that to improve the corrosional stability of metals including nickel, it is necessary to alloy it by such metals as exhibit higher affinity to fluoride than the alloyed metal, and produce dense fluoride films which are melted and vaporized at higher temperatures than the fluoride of the basis metal. Magnesium and calcium are alloying elements suitable for nickel. Several physical-chemical properties of the fluorides of these elements are presented in Table 1 /3-5/.

Physico-Chemical Properties of Fluoride — TABLE 1

(a) Свойство, размерность	NiF_2	MgF_2	CaF_2
Температура плавления, °С (b)	Сублимирует при (f) t>1000°	1225	1418
Температура кипения, °С (c)	—	2260	2500
Параметры элементарной ячейки, Å (d)	a=4,710 c=3,118	a=4,64 c=3,06	a=5,45 —
Свободная энергия образования, ккал-на г-атом фтора при 27° (e)	—73	—125	—138

LEGEND: a) Property, dimension; b) Melting point; c) Boiling point; d) Elementary cell parameters, AU; e) Free energy of formation, kcal per g-atom of fluorine at 27°; f) Sublimates at t > 1000°.

Alloys were prepared (Table 2) to verify this assumption.

Due to the large difference in the physical-chemical properties of nickel, magnesium, and calcium, and also in view of the intensive absorption of hydrogen, melting of these alloys presents certain difficulties. Adding magnesium and calcium to nickel is accompanied by a large thermal effect that leads to intensive heating of the melt and promotes contamination by its oxide and gas inclusions. To avoid gas absorption the alloy melting was conducted under flux in magnesite or aluminum crucibles in a high-frequency furnace.

The starting materials in alloy preparation were the following: Nickel electrolyte, distilled calcium, and the Ni - Mg alloy (50% Mg).

TABLE 2

Properties of Alloys Investigated

(a) № сплава	Химический состав по шихте, % (b)			(c) Твердость, кг/мм²	(d) Условия получения сплава
	Mg	Ca	Ni		
1	—	—	100	71	Тигель магнезитовый. Флюс стекло. Раскисление не производилось (e)
2	—	1,5	ост.	61	Тигель магнезитовый. Флюс CaF_2+MgF_2 (50 вес. %) (f)
3	—	2,5	—.—	84	—.—
4	—	4,0	—.—	121	—.—
5	1,5	—	—.—	130	Тигель алундовый. Флюс CaF_2+MgF_2 (50 вес. %)
6	2,5	—	—.—	139	—.— (g)
7	6,0	—	—.—	260	Тигель магнезитовый. Флюс CaF_2+MgF_2 (f)
11	2,5	2,5	—.—	116	—.—
12	1,5	1,5	—.—	93	—.— (g)
27	—	—	100	60	Тигель алундовый. Флюс CaF_2+MgF_2 (50 вес. % Раскислитель—магний (h)
28	—	—	100	63	Тигель алундовый. Флюс CaF_2+MgF_2. Без раскисления (i) (g)
31	6,0	—	ост.	248	Тигель алундовый. Флюс CaF_2+MgF_2 (50 вес. %)
40	6,0	—	ост.	253	Тигель магнезитовый. Флюс CaF_2+MgF_2 (f)

LEGEND: a) Alloy No; b) Chemical composition in charge, %; c) Hardness, kg/mm^2; d) Conditions of alloy production; e) Magnesite crucible, glass flux, deoxidation not done; f) Magnesite crucible, flux: $CaF_2 + MgF_2$ (50 weight percent); g) Alundum crucible, flux: $CaF_2 + MgF_2$ (50 weight percent); i) Deoxidation not done; (h) Deoxidizer - Magnesium

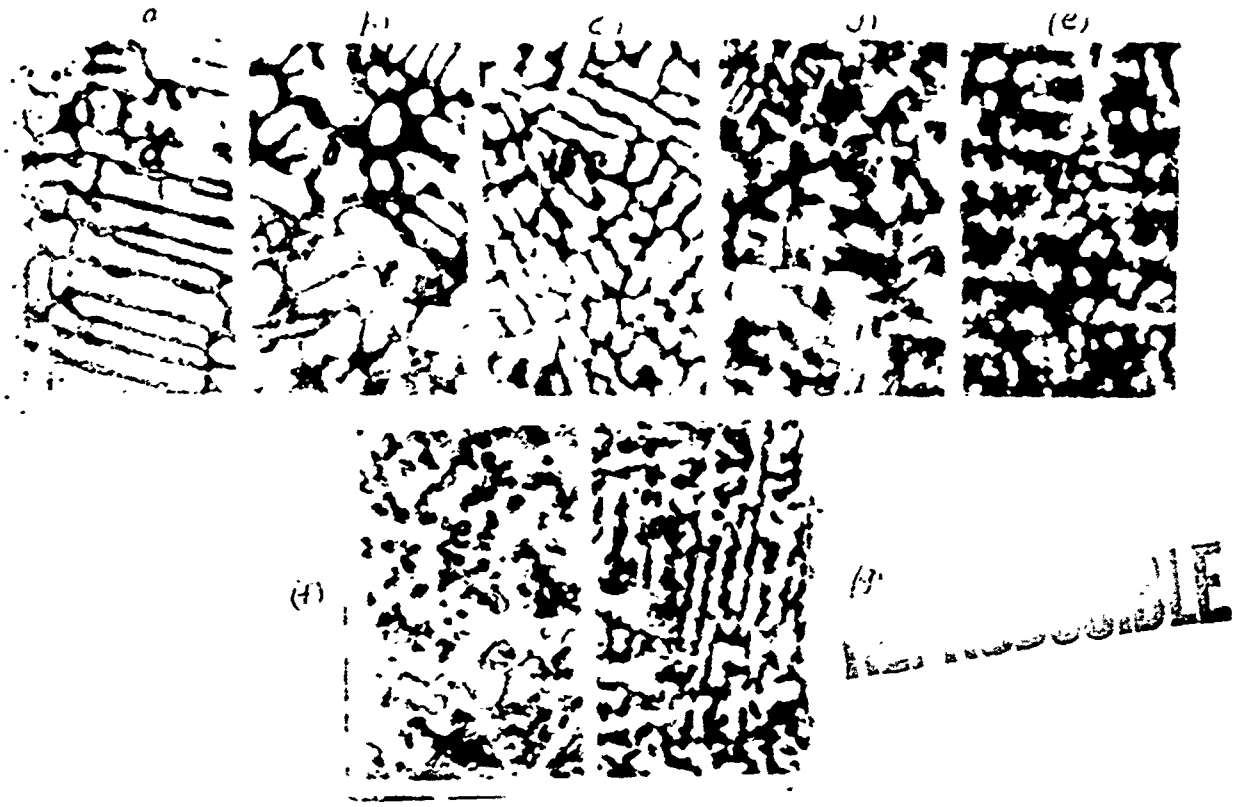

FIGURE 1. Microstructure of alloys of nickel with calcium and magnesium in the cast state. Etchant HNO_3 (1:1), X 200. a - Ni + 2.5% Ca; b - Ni + 4.0% Ca; c - Ni + 1.5% Mg; d - Ni + 2.5% Mg; e - Ni + 6.0% Mg; f - Ni + 1.5% Ca + 1.5% Mg; g - Ni + 2.5% Ca + 2.5% Mg

Used as flux was the powdered alloy of magnesium and calcium fluorides (50% Ca F_2 + 50% Mg F_2). The nickel-magnesium alloy was prepared by dissolving nickel in molten magnesium at 800-850° under a layer of VIZ flux consisting of an alloy of the chloride salts of magnesium, potassium, sodium, calcium fluoride, and magnesium oxide /6/.

Melting was carried out in the following order. Nickel was loaded into a cold crucible, the surface of the nickel being sprinkled with flux. The nickel was melted; the Ni - Mg alloy or pure calcium was added to the melt.

To reduce the losses of the alloying elements the melting was intensively mixed with a quartz rod. In the preparation of alloys with magnesium and calcium, calcium was introduced last. After thorough mixing the melt was poured into a metallic casting mold. Vacuum oil was used to lubricate the casting mold. The ingots produced were cleaned of oxide films and burrs and were cut into samples for testing.

The hardness of the alloys in the cast state was determined by use of a Brinell press with a ball diameter of 10mm and a 3000 kg load

(See Table 2). We can see with increased calcium and magnesium content the hardness of the alloys rises. The hardness increases especially rapidly in alloys containing magnesium.

The microstructure of cast alloys is shown in Figure 1.

In the Ni-Ca alloys, after etching with dilute nitric acid (1:1) nickel-rich solid solution dendrites are clearly evident, along the boundaries of which the eutectic will be demarcated. Within in the calcium content the eutectic content will be increased (Figure 1 a, b).

The microstructure of Ni-Mg alloys, analogous to the microstructure of Ni-Ca alloys, is represented by nickel-rich solid solution dendrites. Between them a eutectic will be delimited, one constituent of which is Ni_2Mg. The solid solution dendrites in the Ni-Mg alloys are more branched than in the Ni-Ca alloys. The amount of eutectic for the same percentage of alloying additions is the larger, and its structure is the finer (Figure 1 c,d,e) /than the Ni-Ca alloys/.

The Ni-Mg-Ca alloys show the same microstructure as the binary alloys. In terms of the quantity of eutectic they occupy a midposition between the binary alloys of nickel with calcium and magnesium (Figure 1, f,g).

Corrosional tests were conducted in reactors consisting of steel pipes lined with molten alloy of fluorides of calcium and magnesium, or enameled with an alloy of fluorides. For certain experiments nickel pipes served as the reactor.

Samples consisting of small cubes with 10-12mm edges and surface-cleaned with emery paper were weighed and placed in a horizontal tubular reactor on a nickel support, where they were kept at the given temperature in a fluorine atmosphere for a certain interval of time. The reactor was placed in a tubular detachable furnace with a nichrome heater. A 5-7 mm gap was left between the reactor wall and the furnace wall to warn of local overheating. The temperature was measured by means of a chromel-alumel thermocouple placed inside the reactor in a nickel case. The temperature set was maintained automatically by means of the ERM-47 instrument.

The consumption of gas was recorded with a diaphragm manometer and was 30-40 grams/hour. Fluorine was produced by electrolysis of potassium trifluoride and was cleaned free of hydrogen fluoride on the sodium chloride granules. After purification the gas contained 92-95% F, 4-6% HF, 1-2% N, and inert impurities.

Before the tests were begun the reactor was swept through with fluorine for 10-12 minutes. The electric heater was turned on when the entering gas flow became constant; the temperature was raised to the level chosen and maintained for the entire experiment (5-10 hours). The samples-containing reactor was cooled to room temperature as fluorine was fed in continuously. The samples underwent examination, weighing and metallographic analysis (determination of the thickness of the layer attacked). Usual formulas were used in calculating the weight index of the corrosion weight /7/. Estimation of the corrosion

rate from the weight increased was hampered by the crumbling of the corrosion products, and by weight losses due to their incomplete removal from the surface of the samples before weighing.

The results of the test are presented in Table 3 and Figures 2-5. As we can see from Table 3, the values of the corrosion rate under the same testing conditions fluctuated within broad intervals.

re

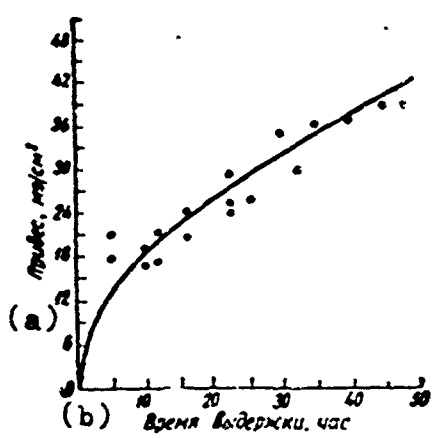

FIGURE 2. Change in weight of samples of the alloy Ni + 6% Mg as a function of time of fluorine exposure at 750°.
LEGEND: a) Weight increment, mg/cm^2;
b) Exposure time, hours

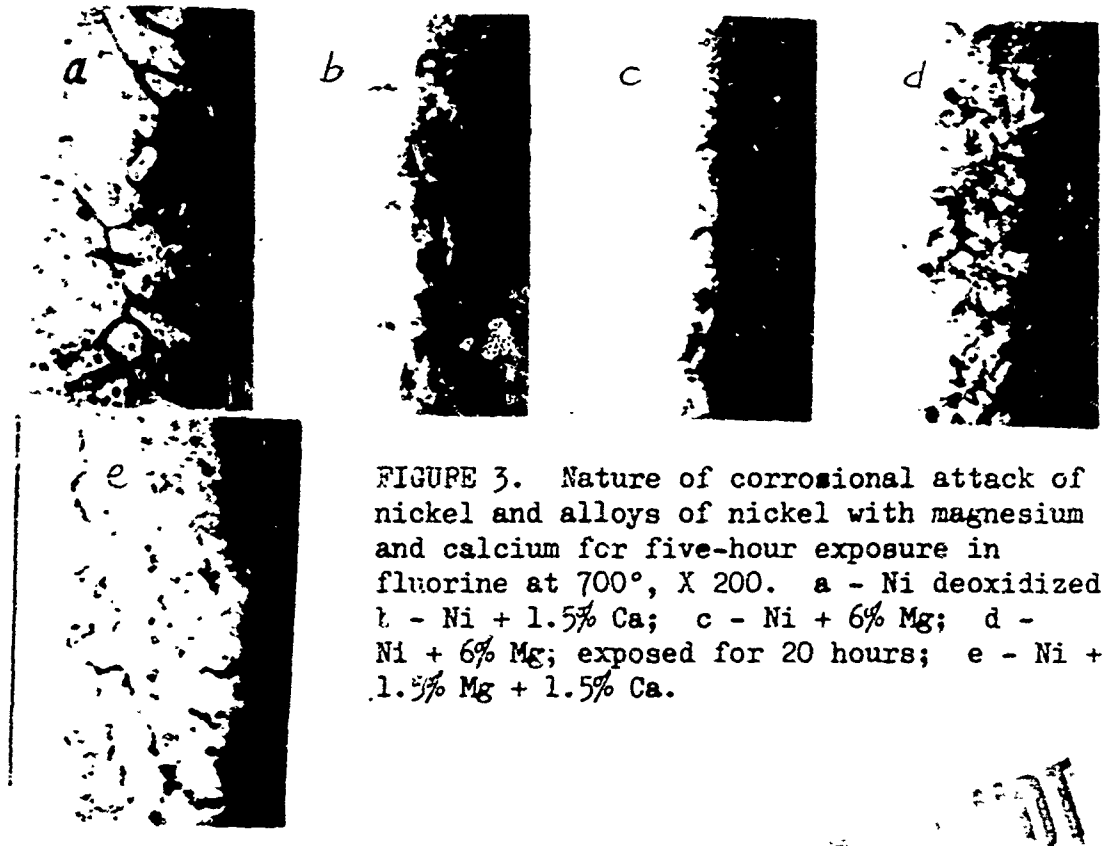

FIGURE 3. Nature of corrosional attack of nickel and alloys of nickel with magnesium and calcium for five-hour exposure in fluorine at 700°, X 200. a - Ni deoxidized; b - Ni + 1.5% Ca; c - Ni + 6% Mg; d - Ni + 6% Mg; exposed for 20 hours; e - Ni + 1.5% Mg + 1.5% Ca.

TABLE 3

Corrosional Resistance of Alloys in Fluorine at Different Temperatures

(a) Сплав №	(b) Условия опыта: температура, °С (f)	время выдержки, час (g)	Весовой показатель коррозии, $г/м^2 \cdot$ час (c): K^+	K^-	(d) Толщина разрушенного слоя, мм	(e) Материал реактора
1	2	3	4	5	6	7
(a1)	700	7	6,5—11,0	10,0—17,1	—	Фториды (h)
	750	4,5	17,0	26,2—43,6	—	Эмаль (i)
	800	4	7,4	11,4	0,081	Фториды
	"	8	11,8	17,8	0,185	Эмаль
2	700	5	44,0			Эмаль
		12	Образец полностью разрушился (k)			Фториды
3	700	5	52,0	(l) —		Эмаль
		12	Полностью разрушился			Фториды
4	700	5	Очень сильное разруш.			Эмаль
		12	Полностью разрушился (m)			Фториды
5	700	7,5	51,0—62,0	—	—	Эмаль
	750	7,5	0,8—1,68	—	—	—"—
	800	8	26,0—41,0	—	—	—"—
6	700	7,5	7,3—11,6	—	—	Эмаль
	750	5,0	5,2	—	—	—"—
	"	10	3,9—193,0	—	—	—"—
	800	4	21,8	—	—	Фториды
7	700	2,5	14—29,0	—	—	Фториды
	"	5	14,3	—	—	Никель (j)
	"	11	7,6—30,2	—	—	Эмаль
	750	7,5	0,8—6,9	—	—	—"—
	"	10	—	65,0	—	—"—
	"	14	3,8—7,0	—	—	Никель
	800	5	3,4—6,0	—	—	Фториды
	"	8	6,3—6,7	—	—	Эмаль
	"	4,5	65—71	—	—	Никель
	"	6	15,0	—	—	—"—
11	700	5	—	22,5	0,2—0,4	Эмаль
		12	—	8,2	—	Фториды
12	700	5	—	9,0	0,081—0,185	Эмаль
		20	—	22,5	—	—"—
27	700	5	6,2	9,55	0,14—0,157	Никель
	750	5	8,2	12,6	0,175—0,263	—"—
	800	4,5	66,0	101,6	0,1575	—"—
	850	5	28,6	—	0,157—0,263	—"—
28	700	5	5,0	7,7	0,0875—0,105	Никель
	750	5	10,3	15,8	0,105	—"—
	800	4,5	100	154	0,140	—"—
	850	5	61,3	—	0,175—0,21	—"—

TABLE 3 (Cont'd)

Corrosional Resistance of Alloys in Fluorine at Different Temperatures

1	2	3	4	5	6	7
31	700	5	14,3	—	0,044	Никель (i)
	750	5	47,7	—	0,074	—.—
	800	4,5	65,0	—	0,074	—.—
	850	5	60,8	—	0,111	—.—
40	700	5	32,6—67,6	—	0,03	Никель (i)
		5	36,0—42,0	—	0,074	—.—
		10	17,3—19,4	—	0,111	—.—
		12	17,7	—	—	—.—
	750	16	15,2	—	—	—.—
		22	11,7	—	0,185	—.—
		26	10,1	—	—	—.—
		30	11,2	—	—	—.—
		32	9,4	—	—	—.—
		35	10,3	—	0,259	—.—
		40	9,1	—	—	—.—
		45	8,6	—	—	—.—
		50	10,0	—	0,296	—.—
	800	4,5	45,0—71,0	—	0,111	—.—
	850	5	64,5—96,3	—	0,111	—.—
	900	5	3[illegible]—577	—	1,1—2,0	—.—

LEGEND: a) Alloy No; b) Conditions of experiment; c) Weight index of corrosion, $g/m^2 \cdot hr$; d) Thickness of attacked layer, mm; e) Material of reactor; f) Temperature; g) Exposure time, hours; h) Fluorides; i) Enamel; j) Nickel; k) Sample wholly destroyed; l) Wholly destroyed; m) Very intense destruction, Wholly destroyed.

The cause of such behavior of the material can be both corrosion of the substratum and the reactor as well as the stresses appearing in the forming fluoride film. The higher these stresses, the more severely the film will be cracked, the greater the fluoride loss, and the still greater distortion that can appear in estimation of the corrosion rates. Particularly, one should take note of the brittleness of the nickel fluoride, whose particles break away during the time the sample is exposed at room temperature. The criteria of Pilling and Bedworts for nickel fluoride forming on the film is about 3.35. This gives us reason to assume that the continuity of the film is disturbed as the result of internal stresses developing.

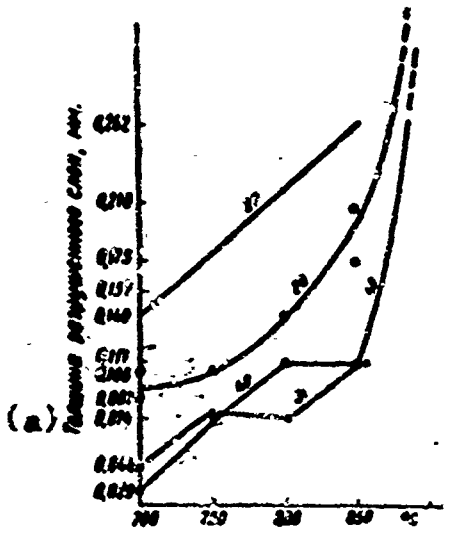

FIGURE 4. Effect of temperature on thickness of attacked layer of alloy for five-hour exposure in fluorine. Figures above the curves denote alloy number (See Table 2). LEGEND: a) Thickness of attacked layer, mm

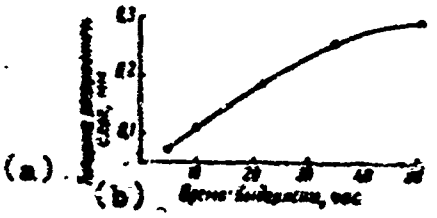

FIGURE 5. Effect of time of fluorine exposure on thickness of attacked layer in the alloy Ni + 6% Mg at 750°. LEGEND: a) Thickness of attacked layer, mm; b) Duration of exposure, hours

When comparing the corrosion rate of nickel and its alloys with magnesium and calcium based on the weight index it is possible to see that the stability Ni-Mg alloys in several experiments exceeds the stability of nickel. In addition, a dense, hard-to-remove fluoride film of grey or greyish-green forms on the surface of the samples of Ni-Mg alloys. The Ni-Ca and Ni-Ca-Mg alloys are unstable under similar testing conditions.

Additional data on the stability of the material is given by metallographic investigation.

Study of microsections reveals that almost all the alloys investigated after corrosion testing exhibit along the edges of the sample sharply delimited layers different from the main metal in structure and etchibility. The microstructure of such layers is a conglomerate of grains of unattacked metal (alpha-solid solution) and fluorides of attacked eutectic. In most cases, independent of the thickness of such a layer, grains of the alpha-solid solution are found almost at the very surface of the sample (See Figure 3). This fact evidently promotes tight adhesion of the corrosion products with the metal surface.

In the Ni-Ca alloys the thickness of the attacked layer is significantly greater than in the Ni-Mg alloys. With increased calcium content and with increased exposure and heating temperature the width of the attacked layer is increased. In Ni-Mg alloys the thickness of the attacked layer changes little with variation in magnesium content. The melting conditions have some effect on the corrosion rate of the Ni-Mg alloys. When melting is carried out in alundum crucibles attack of the alloys proceeds more slowly than when melting is carried out in crucibles made of unmelted magnesite.

Just as for the Ni-Ca alloys, increase in heating temperature and duration of treatment in testing is accompanied by increased width of the layer attacked (See Figures 4,5). The corrosion rate however with increase in exposure time becomes less directly proportional (See Figure 2). The size of the corrosion foci are indirect dependence on temperature. The higher the temperature, the coarser the eutectic and the larger the grains of the alpha-solid solution, the more extensive will be the corrosion foci.

Preliminary exposure of the samples of Ni-Mg samples in fluorine at 600-650°, as specially conducted experiments showed, promotes a slow down in the corrosion rate at higher temperatures.

Breakdown of the cast nickel takes place due to broadening of the boundaries between the grains and their pulverization in the layer adjoining the sample surface (See Figure 3). In addition, formation of a solid fluoride film takes place. However, due to brittleness, when the section is prepared the film separates from the metal and does not become part of the thickness of the attacked layer as determined under the microscope. With increase in temperature or increase of time of exposure in fluorine the width of the layer containing the broadened grain boundaries is increased.

It must be noted that oxygen present in nickel as the eutectic Ni + Ni O has no appreciable affect on the corrosion rate (See Table 3).

When the results of the corrosional resistance of nickel and its alloys with magnesium and calcium obtained by weighing, and external appearance are compared, along with measurement of the thickness of the attacked layer, it can be seen that the most resistant are alloys of nickel with magnesium.

Such behavior of the Ni-Mg alloys can be explained by the fact that the small radius of the magnesium ion (0.65 AU) is favored by its rapid diffusion toward the reaction centers. In as much as the energy of formation of magnesium fluoride is higher than the energy of formation of nickel fluoride, it can be assumed that the film on the surface consists almost wholly of dense magnesium fluoride quite markedly inhibiting the diffusion of fluorine to the reaction centers. The buildup of the layer of fluorides with increased duration of treatment occurs evidently due to diffusion of the magnesium ions through the film formed, which is also impeded in view of the relatively small dimensions of the elementary cell of magnesium fluorides (a = 4.64, c = 3.06 AU).

Of the alloys of nickel with magnesium the one with the best corrosional resistance in fluorine at 700-750° is the alloy containing 6% Mg. This alloy is interesting both from the technological as well as the economic point of view -- it is simpler to cast and cheaper than pure nickel.

We must note that the assumption of the increase in nickel resistance by means of its alloying with calcium is not completely justified. The alloys containing calcium appeared in all cases to be less resistant than pure nickel.

CONCLUSIONS

1. The hardness, corrosional resistance in fluorine at 700-850°, and the microstructure of nickel and its alloys with magnesium (to 6 weight percent) and with calcium (to 4 weight percent) in the cast state have been studied.

2. It was established that the alloying of nickel with calcium worsens its corrosional stability. Alloying with magnesium not only does not diminish, but in several cases favors increase in nickel resistance. The reason for the increased resistance of nickel under these conditions can be found in the formation of a denser, stronger, and harder to remove film of magnesium fluoride.

3. Alloys of nickel with magnesium can be successfully fused in fluorine-containing gaseous media at elevated temperatures.

LITERATURE

1. Landay, Rosen, Ind. Engng. Chem., 39, 281 (1947).
2. Martinj, Steindler, Vogel, Richard C., Chem. Abstrs., v. 51, No 17, 1957.
3. Ryss, I. G., Khimiya ftora i ego neorganicheskikh soyedineniy (Chemistry of Fluorine and Its Inorganic Compounds), Goskhimizdat, Moscow, 1956.
4. Ftor i ego soyedineniya (Fluorine and Its Compounds, Vol 1, ed. J. Simons, For. Lit. Publ. House, Moscow, 1953.
5. Chemik, No 21, 1959 (Pol'sk).
6. Alttman, M. B., Lebedev, A. A., Polyanskiy, A. P., Chukhrov, M. V., Plavka i lit'ye legkikh splavov (Melting and Casting of Light Alloys), Metallurgizdat, 1956.
7. Zhuk, N. P., Korroziya i zashchita metallov (Corrocion and Protection of Metals), Mashgiz, 1957.

Received by Editor
22 April 1963

REVIEW OF THE BOOK BY N. A. DORONIN, KAL'TSIY

A. F. Alabyshev, A. G. Moratchevskiy

In recent years several small monographs have appeared dealing with the properties and technology of the production of sodium, potassium, lithium, beryllium, and several other metals, whose role in modern industry is ever mounting . One of these is the recently published book by N. A. Doronin, Kal'tsiy, /Calcium/ (Gosatomizdat, 1962), in which the properties and technology of the production of metallic calcium are described in detail. The rise in calcium production in the last decade is bound up with the growth of the production of infusible rare metals) Zi, Ti, Ta, Th, U, etc), and also with production of high-quality steels. In the monograph reviewed the technological processes of producing metallic calcium are described in detail, both for the electrolysis method, as well as for methods based on metallothermy or thermal dissociation of calcium carbide. Described in close detail, both as to theoretical fundamentals, as well as in technology, is an important industrial method of producing calcium -- electrolysis of $Ca\ Cl_2$ with a liquid copper cathode followed by vacuum distillation of the calcium from the alloy.

The book presents information on natural calcium carbonates and their calcining (Chapters I and II), the physical and chemical properties of metallic calcium are described, in addition to which compounds with oxygen, carbon, nitrogen, and the most important salts -- $Ca\ Cl_2$, $Ca\ F_2$, and others (Chapter III). Since the main raw material in electrolysis is $Ca\ Cl_2$, N. A. Doronin has described in detail the production of water-free calcium chloride (Chapter IV), and also has given the physico-chemical properties of the most useful electrolyte $Ca\ Cl_2$ - KCl (Chapter V). The last divisions of the book are concerned with the theory and technology of calcium production, mainly in baths fitted with a "liquid cathode" (Chapters VI and VII), vacuum distillation of calcium from a copper-calcium alloy (Chapter VIII), the production of calcium by means of metallic reducing agents, and by means of the thermal dissociation of calcium carbide (Chapters IX-XI). Examined in Chapters XII, XIII, and XIV, are: production of high purity calcium by distillation methods, rules for storing calcium and calcium alloys,

information on vacuum pumps used in industry.

Much of the information is technological in nature, dealing directly with the process of producing calcium by electrolysis, the first book on the subject to be published in such detail /See Note/ and its issuance undoubtedly should be welcomed.

(/NOTE/ These problems have been examined more briefly in the first monograph by N. A. Doronin, Metallurgiya kal'tsiya /Metallurgy of Calcium/, Gosatomizdat, Moscow, 1959.)

However, the book is not free of several shortcomings reducing its worth. Quite unsuccessful in style of presentation are those pages of the book where the author writes in the popular vein, and frequently becomes out of date and even incorrect in his treatment of such important concepts of physical chemistry as the notion of the voltage series (pages 28 and 29), equivalent electroconductivity (page 69), decomposition voltages (page 75), current-based and energy-based yields (page 75), pressure of saturated vapor and the Clapeyron-Clausius equation (page 107), the Rayleigh law and the vapor pressure above alloys (page 110), chemical affinity (pages 125 and 126), and the equation of the chemical reaction isotherm (page 128). As an illustration we can present the following statements: "If the copper-calcium alloy is heated to a temperature of 1500° C, then its content of calcium will boil and be vaporized..." (Page 110). On page 128 we can read: "For high temperatures at total pressure up to one atmosphere we can equate without large error the original activity of the gaseous section of the reaction to its original partial pressure." A list of such errors in the style of presentation can be enumerated at length. It also does not follow, in presenting the Nernst equation or the equation of the chemical reaction isotherm, to cite the book by Kh. L. Strel'ts et al, Metallurgiya magniya (Metallurgy of Magnesium).

Of course, it is difficult in very brief form to present the most general propositions of thermodynamics or electrochemistry, and this is reflected in parts of the book by N. A. Doronin. However, all these general questions must be assumed to be known to the reader, and then the exposition could have been presented more rigorously and clearly.

There is entirely no need in a special monograph intended for engineering technicians to make such a footnote as the following (page 125): "We understand as free energy the portion of the heat effect of a reaction which in the ideal case can be wholly transformed into work." This is of the more illogically done on page 125 since the term "free energy" has already been used by the author tens of times in previous pages. Incidentally, the change in free energy is represented on page 15 by ΔF_T^0, on page 27 as ΔF^0, on page 31 as ΔZ^0, and on page 25 again as F^0.

It is pointed out on page 39 that the reaction $Ca + Cl_2 = Ca Cl_2$ is accompanied by the evolution of 190 kcal/mole of heat, while on page 62 the heat of formation of $Ca Cl_2$ is presented as 155 kcal. On page

39 it is stated that the melting point of $CaCl_2$ is 772°, and on page 62 (Table 20) we see it given as 722°, for some reason. On page 62 the melting point of KCl is given incorrectly. Often the terms and expressions used in calculating equilibrium, in discussing the phase diagrams are often poorly chosen. One should not write "mixture of crystals" under Figure 38 (89), since in all cases there is present only the crystals of one specific type -- the solid phase alone. The compound $KCl \cdot CaCl_2$ is a coherently melting compound, therefore one should not write that it decomposes at temperatures above 754° (page 64). One should use in place of the imprecise terms "stable" and "unstable" chemical compound (page 86) the widely accepted term -- coherently melting and incoherently melting compound.

On page 74, he uses unnecessarily such various terms, employed synonymously, as "decomposition voltage", "emf of polarization", "decomposition potential", "standard emf". This is a completely unnecessary proliferation of terms. And kcal/mole, and not cal/mole should designate the ordinate axis for Figures 52 and 53 (pages 127 and 129), and no figures are given at all for Figures 65 b (page 160). The stoichiometric coefficient is omitted entirely on page 35 in describing the reaction of formation of carbide. The assertion of the author that C^{4-} ions participate in carbidothermic production stands as unproven.

It is much to be regretted that no references to the literature are given in the text, the exception being only in several cases where the last names of authors referred to are given. The list of studies used at the end of the book is far from exhaustive. No list of errors is included in the book, but this does not mean that there are none (on page 186 alone we noted three).

The book by N. A. Doronin, Kal'tsiy, is a valuable and necessary monograph on the technology of producing metallic calcium, the problems it considers is of interest not only for workers in the calcium industry, but also for a broad range of electrochemists and technologists. However, it is a pity that Gosatomizdat han published it without responsible scientific editing.

CSO-1500-S

-END-

DISTRIBUTION LIST

DEPARTMENT OF DEFENSE	NR. COPIES
HEADQUARTERS USAF	
AFNINDE	1
OTHER AGENCIES	
CIA	5
DIA	4
AID	2
NASA (ATSS-T)	1
OTS	2
NSA	6
ARMY (FSTC)	3
NAVY	3
NAFEC	1

MAJOR AIR COMMANDS	NR. COPIES
DDC	20
AFSC	
TDBTL	5
TDBDP	12
TDGS	1
TDBMT	10
TDT	2
TDEWP	2
TDEPR	2
TDEPF	2